Future Climate Scenarios for Norway based on linear empirical downscaling and inferred directly from AOGCM results.

R.E. Benestad

DNMI, January 22, 2001

Klima: 23/00

Contents

1 Introduction **1**

2 Results **3**
2.1 Evaluation of past climate variability 3
2.1.1 Annual mean surface temperature 4
2.1.2 Sea level pressure 4
2.2 Scenarios directly inferred from AOGCM results 7
2.2.1 Annual mean surface temperature scenarios 7
2.2.2 Seasonal global surface temperature scenarios from various climate models 7
2.2.3 Global precipitation scenarios 12
2.2.4 Temperature scenarios from direct interpolation of global GCM results 14
2.2.6 Sea level pressure 14
2.2.5 Local warming trends estimated from simple interpolation of ECHAM GSDIO results 16
2.2.7 Summary on the AOGCM scenarios 18

3 Evaluation of the empirical downscaling methods **19**
3.1 Introduction 19
3.2 "Regional" downscaling models 22

4 Test results **24**
4.0.1 An illustration of the EOF methods using a 2-DOF example 25
4.0.2 Comparing the common EOF method with the conventional approach when calibration predictors are different to the prediction predictors 26
4.0.3 Testing the common EOF method for zero anomalies. . . 28
4.0.4 Comparing the common EOF method with the conventional approach using model data for calibration and verification 28
4.0.5 Comparison between correlation skill scores of the common EOF and projection methods. 31
4.0.6 The influence of predictor domain size for downscaled trends derived from models calibrated with AOGCM T(2m). 32
4.0.7 The influence of predictor domain size for downscaled trends derived from models calibrated with AOGCM SLP. 33
4.2.1 Test of stationarity for linear relationship between large and small scales 36
4.1 Skill scores for common EOF downscaling models 36
4.2 Non-stationarity tests 36
4.1.1 Downscaling temperature prediction scores for various locations in Norway 37
4.1.2 Downscaling precipitation prediction scores for various locations in Norway 38
4.1.3 ANOVA statistics associated with the projection of model EOFs onto observed modes: ECHAM4 GSDIO and *Benestad* (2000a) data. 39

4.1.4 The variance associated with the 4 leading common EOFs of the combined ECHAM4 GSDIO and *Benestad* (2000a) data. 40
4.2.2 Test of stationarity for linear relationship between large and small scales 40

5 Temperature scenarios based on empirical downscaling of AOGCM results 43
5.1 Downscaling by common EOFs based on ECHAM4 GSDIO integrations 43
5.1.1 The influence of predictor domain size for downscaled January T(2m) scenarios 44
5.1.2 The influence of predictor domain size for downscaled April T(2m) scenarios 45
5.1.3 The influence of predictor domain size for downscaled July T(2m) scenarios 46
5.1.4 The influence of predictor domain size for downscaled October T(2m) scenarios 47
5.1.5 Downscaling by of ECHAM4 GSDIO common EOFs based on scan T(2m) 48
5.1.6 Trend estimate uncertainties associated with common EOFs downscaling of local temperature based on scan T(2m) fields 48
5.1.7 Evaluation of the spatial correlation during months when the downscaled trends suggest cooling 50
5.2 Downscaled ECHAM4 GSDIO scenarios based on predictors other than the T(2m) field 55
5.2.1 The influence of predictor domain size for downscaled January SLP scenarios 56
5.2.2 The influence of predictor domain size for downscaled April SLP scenarios 57
5.2.3 The influence of predictor domain size for downscaled July SLP scenarios 57
5.2.4 The influence of predictor domain size for downscaled October SLP scenarios 58
5.2.5 Downscaling of ECHAM4 GSDIO scenarios by common EOFs based on *Benestad* (2000b) Scandinavian SLP . . . 58
5.2.6 Downscaling by ECHAM4 GSDIO common EOFs based on 850hPa temperature scenarios natl. 61
5.2.7 Downscaling of ECHAM4 GSDIO by common EOFs based on 500 and 700 hPa geopotential height field. 63
5.2.8 Downscaling ECHAM4 GSDIO by common EOFs based on 500-700hPa thickness scenarios. 64
5.3 Downscaled scenarios based on other global climate model scenarios 67
5.3.1 Downscaling by common EOFs based on NCAR-CSM *scan* T(2m) scenarios. 67
5.3.2 Downscaling by common EOFs based on NCAR-CSM *scan* SLP scenarios. 68
5.3.3 Downscaling by common EOFs based on HadCM3 T(2m) scenarios. 69

5.3.4 Downscaling by common EOFs based on HadCM3 *nordic* and *scan* SLP scenarios. 70
5.3.5 Downscaling by common EOFs based on HadCM2 T(2m) scenarios. 71
5.3.6 Downscaling by common EOFs based on HadCM2 *scan* SLP scenarios. 72
5.3.7 Downscaling by common EOFs based on CCCma T(2m) scenarios. 73
5.3.8 Downscaling by common EOFs based on CCCma *scan* SLP scenarios. 74
5.3.9 Downscaling by common EOFs based on CSIRO T(2m) scenarios. 75
5.3.10 Downscaling by common EOFs based on *scan* CSIRO SLP scenarios. 75
5.3.11 Downscaling by common EOFs based on CCSR/NIES T(2m) scenarios. 76
5.3.12 Downscaling by common EOFs based on *scan* CCSR/NIES SLP scenarios. 76
5.3.13 Downscaling by common EOFs based on ECHAM3 T(2m) scenarios. 77
5.3.14 Downscaling by common EOFs based on *scan* ECHAM3 SLP scenarios. 78
5.3.15 Downscaling by common EOFs based on ECHAM4 GSA T(2m) scenarios. 79
5.3.16 Downscaling by common EOFs based on *scan* ECHAM4-GSA SLP scenarios. 79
5.3.17 Downscaling by common EOFs based on GFDL surface temperature scenarios. 80
5.3.18 Downscaling by common EOFs based on *scan* GFDL surface pressure scenarios. 80
5.3.19 Downscaling by common EOFs based on NCAR-DOE surface temperature scenarios. 81
5.3.20 Downscaling by common EOFs based on *scan* NCAR-DOE surface pressure scenarios. 82

6 Precipitation scenarios based on SLP **86**
6.1 ECHAM4/OPYC3 GSDIO 86
6.1.1 The influence of predictor domain size for downscaled ECHAM4 GSDIO SLP rainfall scenarios 89
6.1.2 Downscaling precipitation by common EOFs based on *Benestad* (2000b) Scandinavian ECHAM4 GSDIO SLP . 90
6.1.3 Downscaling of ECHAM4 GSDIO by common EOFs based on NCEP 700hPa geopotential height. 91
6.2 A super-ensemble scenario based on 33 estimations and 15 global climate model scenarios 92
6.2.1 F-statistics and P-value for the regression between SLP and precipitation. 95
6.2.2 Scenarios based on step-wise screening CCA of various AOGCMs scenarios 95

6.2.3 Downscaling of HadCM3 by common EOFs based on *Benestad* (2000b) SLP. 96
6.2.4 Downscaling NCAR-CSM by common EOFs based on *Benestad* (2000b) SLP. 97
6.2.5 Downscaling HadCM2 by common EOFs based on *Benestad* (2000b) SLP. 98
6.2.6 Downscaling HadCM2 by common EOFs based on *Benestad* (2000b) SLP. 99
6.2.7 Downscaling HadCM2 by common EOFs based on *Benestad* (2000b) SLP. 100
6.2.8 Downscaling HadCM2 by common EOFs based on *Benestad* (2000b) SLP. 101
6.2.9 Downscaling CCCma by common EOFs based on *Benestad* (2000b) SLP. 102
6.2.10 Downscaling CCCma by common EOFs based on *Benestad* (2000b) SLP. 103
6.2.11 Downscaling CCCma by common EOFs based on *Benestad* (2000b) SLP. 104
6.2.12 Downscaling CSIRO by common EOFs based on *Benestad* (2000b) SLP. 105
6.2.13 Downscaling ECHAM3 by common EOFs based on *Benestad* (2000b) SLP. 106
6.2.14 Downscaling ECHAM4 GSA by common EOFs based on *Benestad* (2000b) SLP. 107
6.2.15 Downscaling GFDL by common EOFs based on *Benestad* (2000b) SLP. 108

7 Climate scenarios based on several AOGCMs 111
7.1 An objective comparison of AOGCM model skill 111
7.1.1 Details on the box-plot scenarios. 115

8 Summary 117
8.1 Discussion 118
8.2 Conclusions 119

1 Introduction

Since *Arrhenius* (1896) proposed that atmospheric CO_2 has warming effect on Earth's surface, there has been a gradual accumulation of the carbon dioxide concentrations in the atmosphere (*IPCC*, 1995). Most of this long-term increase in the atmospheric CO_2 concentrations is believed to be a bi-product of an increasing anthropogenic energy consumption. This build-up leads to a perturbation in the energy balance between the incoming solar radiation and the infrared radiation emitted from Earth's atmosphere causing a climate change. This climate change issue has not been just an academical one, but has prompted for political actions and has lead to international meetings such as the "Earth Summit" in Rio de Janeiro in 1992 and an international political conference on climate change in Kyoto in 1997 and the Hague 2000. There are concerns about the effects of such an energy imbalance on our climate, and internationally coordinated efforts, such as the establishment of Intergovernmental Panel on Climate Change (*IPCC*, 1995), have been made to investigate the possible outcomes of such a climate change.

Although it is still not possible to predict the exact evolution of weather and climate, it is generally agreed that the global climate is warming up[1]. However, it is important to be able to quantify this change and have an idea of which implications a global warming will have for regional climates. In order to do this, it is necessary to have credible scenarios.

The most recent global coupled atmosphere-ocean general circulation models (AOGCMs) tend to give a realistic description of the large-scale climatic features, such as the mean circulation patterns (i.e. the Hadley Cell and westerlies in the mid-latitudes), the coupled ocean-atmosphere processes in the tropics associated El Niño Southern Oscillation (ENSO), and the shifts in the air masses often referred to as the North Atlantic Oscillation (NAO). The oceanic components of these climate models give a rough picture of the ocean currents and thermodynamics, but some scientists do not believe that these yet give an adequate description of ocean circulation patterns, which are believed to be important for regional climates. The oceans and the atmosphere interact with sea-ice, which often is represented by a simplified scheme in the AOGCMs. Furthermore, the model topography has till now been crude, and features such as the Norwegian mountain ranges have not been represented realistically in these models (see Figure 1). It is then no surprise that the most recent AOGCM cannot give a good detailed description of regional climatic features. Analytical results from *Grotch & MacCracken* (1991) may suggest that the global climate models cannot give a good description of features smaller than sub-continental scales.

Despite the caveats about the grid scale representation of climate, it is nevertheless important to evaluate the model against observations. *Hanssen-Bauer* (2000) compared model grid point temperature climatology of the GSDIO period 1961-1990 with the observations and found a good correspondence when the selected stations were taken from the same altitude as the model topography.

[1] There are some people who still are sceptical to the view that there is a global warming going on, however, these only represent a few individuals from the research communities. Since climate change affects economy and politics, there has been a high level of lobbying against actions to reduce greenhouse gas emissions from various interest groups and there have been politically motivated efforts to discredit the enhanced greenhouse warming theory.

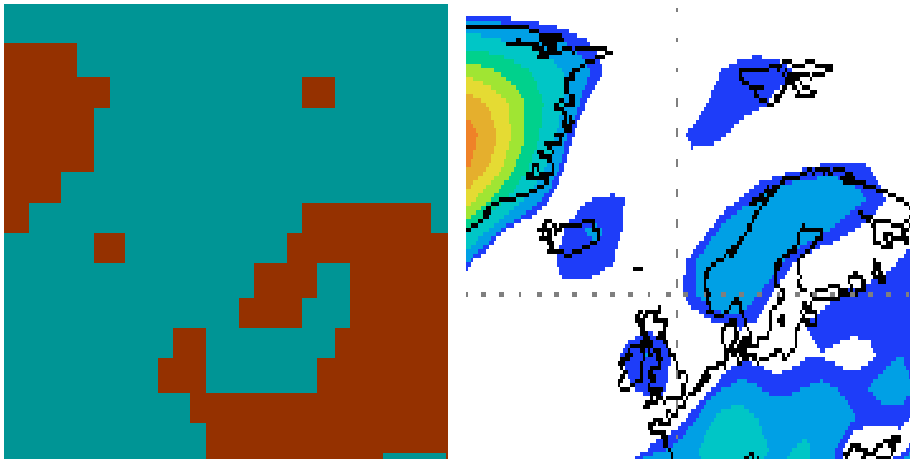

Figure 1: The land-sea mask for the Nordic countries used in the ECHAM4 model (left) and the ECHAM4 model topography (right). Note that Denmark is not present in the model. [The figures were obtained from the IPCC Web site].

It may be possible to use the AOGCMs to describe local climate characteristics if the local climate is affected by large-scale features. Moreover, there may be information in large-scale climate anomalies that can be used to infer local climate variability, however, this requires extra knowledge about how the gross atmospheric circulation affects the local climate variables. So-called downscaling models, based on either physical considerations (nested dynamical models used in dynamical downscaling) or empirical studies (empirical or statistical downscaling) can be used to relate the large scale climatic patterns to local scales. Here, we will focus on the empirical downscaling approach. It is important to note that the empirical models assume that the historical relations between large-scale and local climate anomalies also will be true for the future. On the one hand, it is important that the local scenarios[2] do not depart substantially from the AOGCM results, but on the other hand there are also large geographical differences in the local climate. Maritime climate along the coasts differs substantially from alpine climate, and significant differences between AOGCM and downscaled results are therefore expected for some regions as the model grid boxes may cover both climatic types. For instance, the west side of the mountain range in Norway has a much wetter climate than the eastern side, and the temperature variations in Karasjok (northern Norway) are much greater than for temperatures at Oksøy lighthouse in the south. The differences between the AOGCM results and the downscaled results must therefore be justified in terms of the observed geographical differences in the local climate types.

Benestad (1999c) conducted a pilot study on future local climate scenarios based on empirical downscaling of a transient climate change integration from Max-Planck-Institute (the GHG run, which does not include the effects of aerosols). A number of test results based on various predictor fields gave diverg-

[2]The mean temperatures of the stations in the area covered by the model grid box.

ing results, ranging from cooling to warming, and sensitivity experiments indicated a great deal of uncertainty associated with the downscaling itself. Some of uncertainty was attributed to the mismatch between simulated and observed spatial climate structures (EOFs). *Benestad* (2001) proposed a new empirical downscaling approach based on *common* EOFs (*Flury*, 1988; *Sengupta & Boyle*, 1993; *Barnett*, 1999), which aims to reduce this uncertainty factor. Whereas the conventional downscaled future climate scenarios based on the SLP fields suggested no warming as a result of changes in the large-scale atmospheric circulation pattern (*Benestad*, 1999c, Table 11), the test results based on the common EOF method gave a scatter within a range of 0.05 and 0.50°C/decade for the SLP predictor fields (*Benestad*, 1999a). These new downscaled results were affected by the choice of predictor domain (area), which records are included as predictands, and type of model. Some of this scatter may also be attributed to sampling fluctuations, and it is impossible to say *a priori* which choice is the most appropriate. *Benestad* (1999a) suggested an ensemble prediction solution (*Palmer* et al., 1998).

Results from 15 state-of-the-art AOGCMs from the IPCC web site as well as NCAR (*Benestad*, 2000b) will be used for making "consensus local climate scenarios": Max-Planck-Institute's (MPI) ECHAM4/ OPYC3 GSDIO, MPI ECHAM4/OPYC3 GSDO (GSA), KRFZ ECHAM3/LSG GSDO, UK Meteorological Office (UKMO) HadCM3 (GSA+ozone, but without flux correction, (*Gordon* et al., 2000)), UKMO 4 × HadCM2 (*Cullen*, 1993) (GSA), Australian CSIRO AOGCM (*Gordon & O'Farrell*, 1997) (GSA), 3 × Canadian CCCma (*McFarlane* et al., 1992; *Boer* et al., 1998a,b; *Flato* et al., 2000) (GSA), GFDL CGCM (GSA), NCAR CSM (*Meehl* et al. (2000), GSA, b006), and Center for Climate Research Studies (CCSR/NIES CGCM (*Emori* et al., 1999)). All these transient climate integrations are based on estimates for historical CO_2 and sulphate concentrations up to 1990 and the IPCC IS92a scenario beyond 1990.

It is important to note that flux correction schemes may bias the model solutions towards the present climate state. For instance, the Atlantic thermohaline circulation is sensitive to commonly used flux adjustment schemes (*Tziperman*, 2000). The model primarily used in the *RegClim* project is the ECHAM4/OPYC3, which uses such a flux correction scheme.

2 Results

2.1 Evaluation of past climate variability

Before applying the downscaling models to the AOGCM results, it is important to examine the global model data and check whether these are realistic. One may compare our observational records with the AOGCM reconstruction in order to assess the AOGCM's credibility. *Benestad* (1999c) compared the historical temperature and precipitation trends of *Hanssen-Bauer & Nordli* (1998) and *Hanssen-Bauer & Førland* (1998) with simulated "past" climate (1860-1990) and found significant model biases in the seasonality of these trends: ECHAM4 indicates strongest winter time warming in most of Norway while the observational record suggests that the clearest warming trend took place during spring. The most significant precipitation trends were found in autumn, which was consistent with the model results for southern Norway.

Here we will look at the magnitude of the past climate trends predicted by the ECHAM4 AOGCM and the associated geographical patterns on a global scale. These are compared with the best available observations (NCEP reanalysis II).

2.1.1 Annual mean surface temperature

Figure 2 shows a comparison between the NCEP re-analysis (a) and corresponding data from the ECHAM4 GSDIO integration (b) of the 2-meter temperature differences between 1979 to 1998 and 1950-1969. It is evident that the AOGCM temperature changes are of similar magnitude as those observed, however, the two maps indicate large regional differences. The observations suggest strongest warming in the Arctic east of Greenland and over Antarctica, whereas the GSDIO results suggest that the strongest warming in the northern hemisphere has taken place over the Labrador Sea and Hudson Bay. In contrast, the observations indicate a slight cooling over the Labrador Sea and Hudson Bay.

The arctic warming seen in the observations may be related to the melting of the sea-ice in this region (*Vinnikov* et al., 1999; *Johannessen* et al., 1999), but some of these differences may also be explained in terms of decadal variability, involving the NAO or possibly the Arctic Oscillation (AO) (*Thompson & Wallace*, 1998) it if really exists. The NAO is difficult to predict, and if these natural variations are chaotic, then one cannot expect the models to reproduce them. Hence the regional differences may not necessarily be an indication of model shortcomings.

2.1.2 Sea level pressure

The comparison between 20-year SLP differences centered on 1980 and 1960, shown in Figure 3 suggests that the SLP has undergone long-term changes, but much less so in the model results. It appears from this study that ECHAM4 has underestimated the long-term variance in the SLP.

The NCEP reanalysis II suggests 8hPa drop in the 20-year mean SLP near the Antarctic[3], but also strengthening over the Himalayas and the African continent with a magnitude up to 4hPa. Furthermore, the reanalysis indicates a long-term drop in the Arctic pressure. The implication of these changes is a strengthening of the meridional SLP gradient in the high latitudes and a strengthening of the zonal wind. The SLP drop over the Arctic is consistent with a observed strengthening of the NAO since 1970.

The differences between the best available observations and the model reconstruction of the past illustrate the difficulties associated with making detailed future climate scenarios. Once again, these differences should not be taken as a proof of model shortcomings at this stage, as much of these discrepancies may be accounted for by natural variability of chaotic nature and may therefore be unpredictable. Thus, even with a perfect model, one must expect to see large regional differences between the real world and model results. In section 2.2.2, we see that there are substantial regional differences between four members of an ensemble integration subject to identical forcing but different initial conditions. The trick is to extract the climate change signal from all this noise, which may possibly be done if one looks at long time scales and large scale behaviour.

[3]This is the region where the quality of the NCEP reanalysis is most questionable

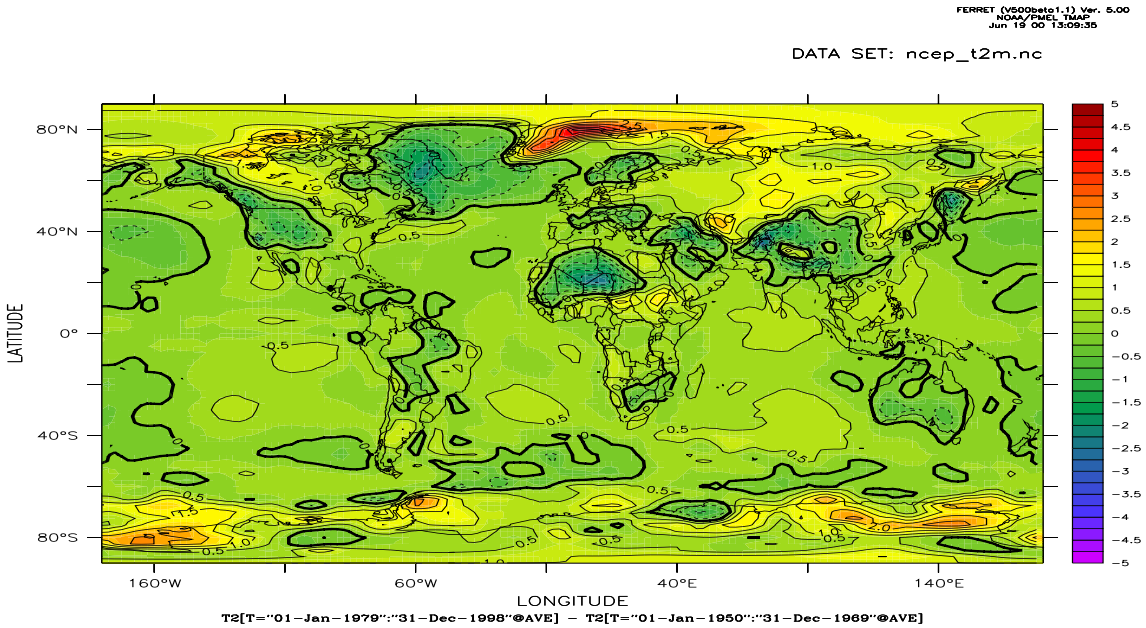

a

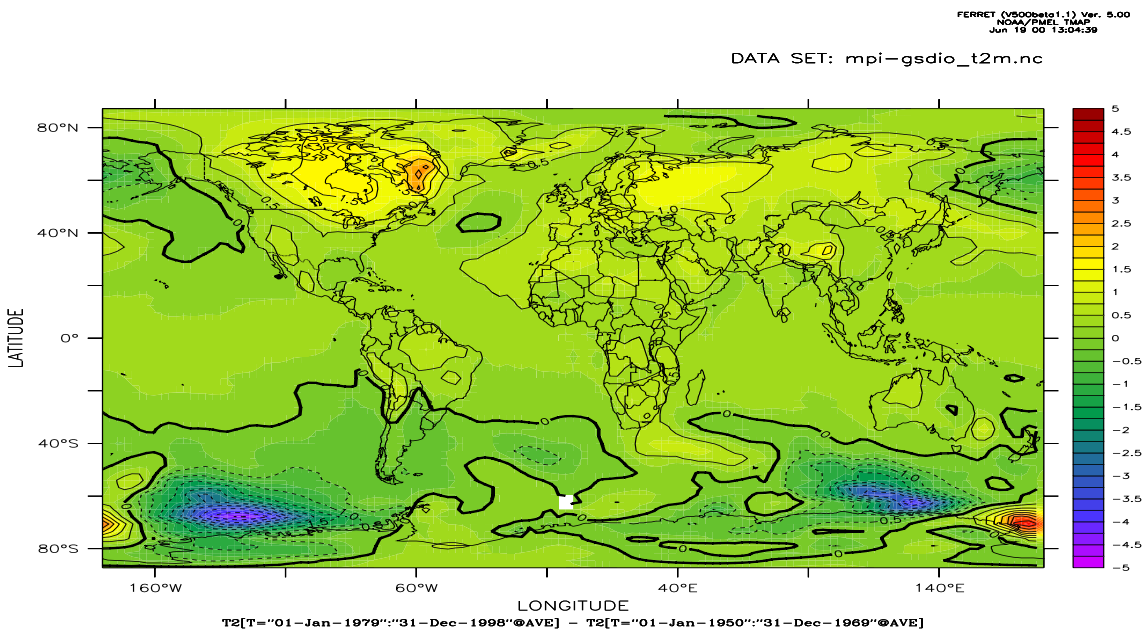

b

Figure 2: Estimated temperature change between two 20-year periods (including all seasons) centered on 1980 and 1960 for the NCEP 2-meter temperatures (a) and ECHAM4 GSDIO (b).

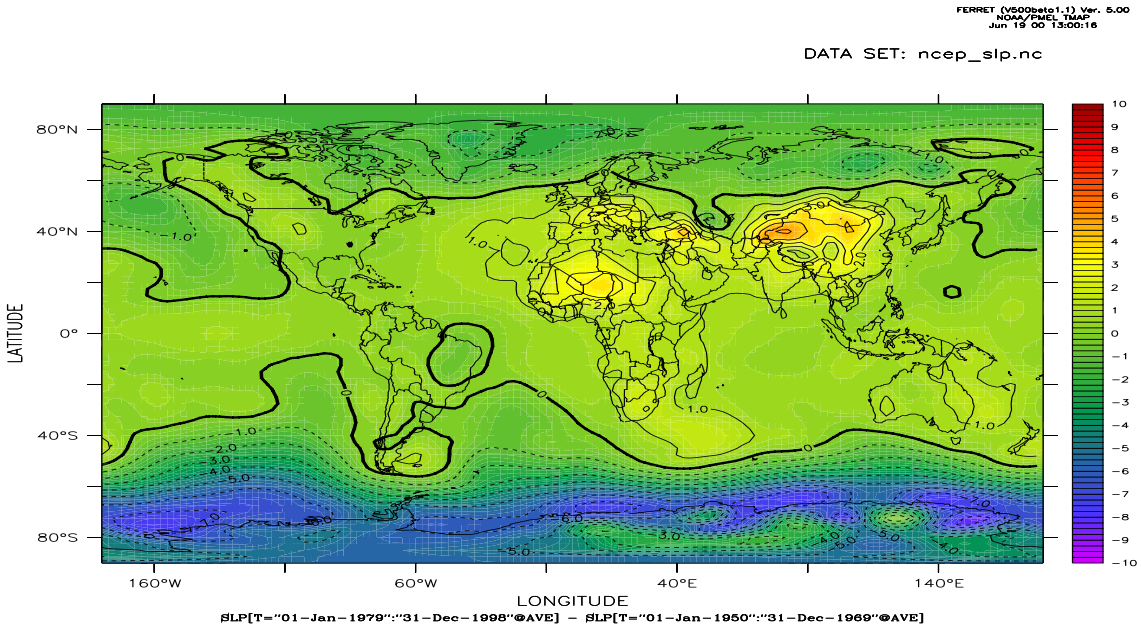

a

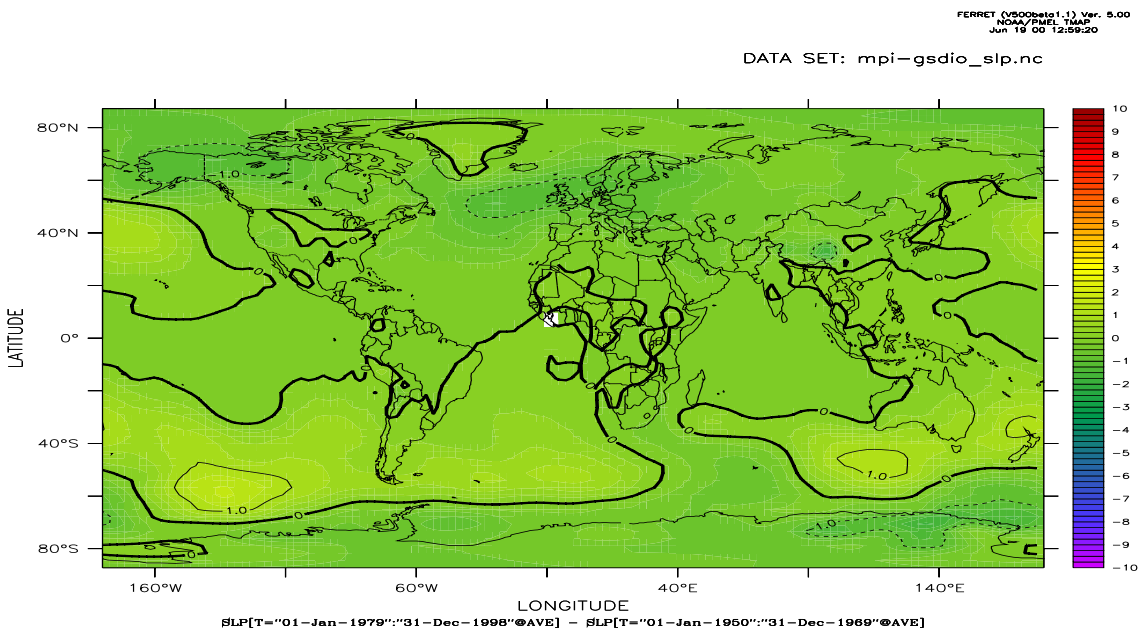

b

Figure 3: Estimated SLP change between two 20-year periods (including all seasons) centered on 1980 and 1960 for the NCEP 2-meter temperatures (a) and ECHAM4 GSDIO (b).

2.2 Scenarios directly inferred from AOGCM results

2.2.1 Annual mean surface temperature scenarios

The "climatic outlook" for the future based on the ECHAM4 GSDIO results are shown in Figure 4. The ECHAM4 GSDIO scenario (a) indicates an Arctic warming in addition to a rapid warming over a small region in the Antarctic[4], and is more in line with the historical NCEP data than the simulation of the past climate. One may therefore wonder whether the model response is lagging behind the real world for instance due to biased forcing during the model spin-up. Alternatively, the differences may also be due to natural variability. By comparing the results in Figure 4 to similar analysis on different time slices, it may be possible to say whether these differences are temporal fluctuations or whether they reflect the long-term trends. A similar analysis carried on the two time slices 01/01/1980-31/12/2009 (model dates) and 01/01/2020-31/12/2049 indicated similar patterns apart from the strong localized warming in the Southern Ocean (160-60°W, 80-60°S). The mean temperature difference between the time slices 01/01/1980-31/12/1999 and 01/01/2030-31/12/2049 exhibit a similar "hot spot" over the Barents Sea (40°E, 80°N) and cooling south of Australia, but the rest of the Arctic is also substantially warmer than compared to Figure 4. The warm spot in the Southern Ocean (160-60°W, 80-60°S) is present in the difference analysis between the time slices 01/01/1980-31/12/1999 and 01/01/2000-31/12/2049, suggesting that this feature is an ephemeral warm anomaly which is not part of the long-term trend but was present between 01/01/2000 and 01/01/2030.

The projected SLP change indicates a strengthening of the NAO as the Azores high pressure system becomes stronger and the Icelandic low is deepened. The dipole-like patterns near the regions where the storm tracks are located may imply geographical shifts in the positioning of these tracks (although, the storm tracks are probably more appropriately identified by high-frequency, less than 10 days, variance). Whereas the "storm track" over the North Atlantic is shifted northwards, the low-pressure region over the North Pacific is displaced equatorward. The meridional pressure gradient over the Southern Ocean is increased further by the poleward displacement of the low-pressure region.

In conclusion, there are important regional differences between the observations and the simulation of the past climate. There may also be a discrepancy in the timing of climate change, which may be a result of various model spin-up strategies.

2.2.2 Seasonal global surface temperature scenarios from various climate models

Figure 5 shows a comparison between the global mean 1990-2050 temperature estimates from various transient climate integrations. The scenarios start at different levels. *Machenhauer* et al. (1998) observed that the MPI ECHAM4 integrations may indicate too warm temperatures due to a warm bias in the model spin-up.

Although the fastest warming trends described by the models have comparable magnitude, there are important differences between the geographical

[4]The polar regions in the map are stretched, giving the impression that the Antarctic continent is larger than it really is.

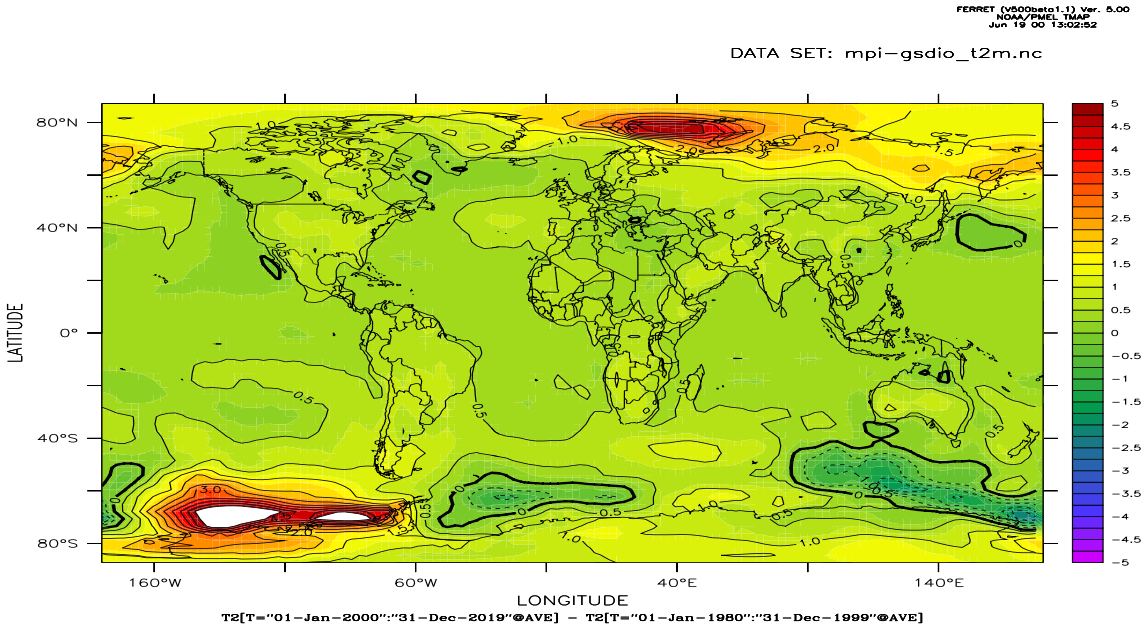

a

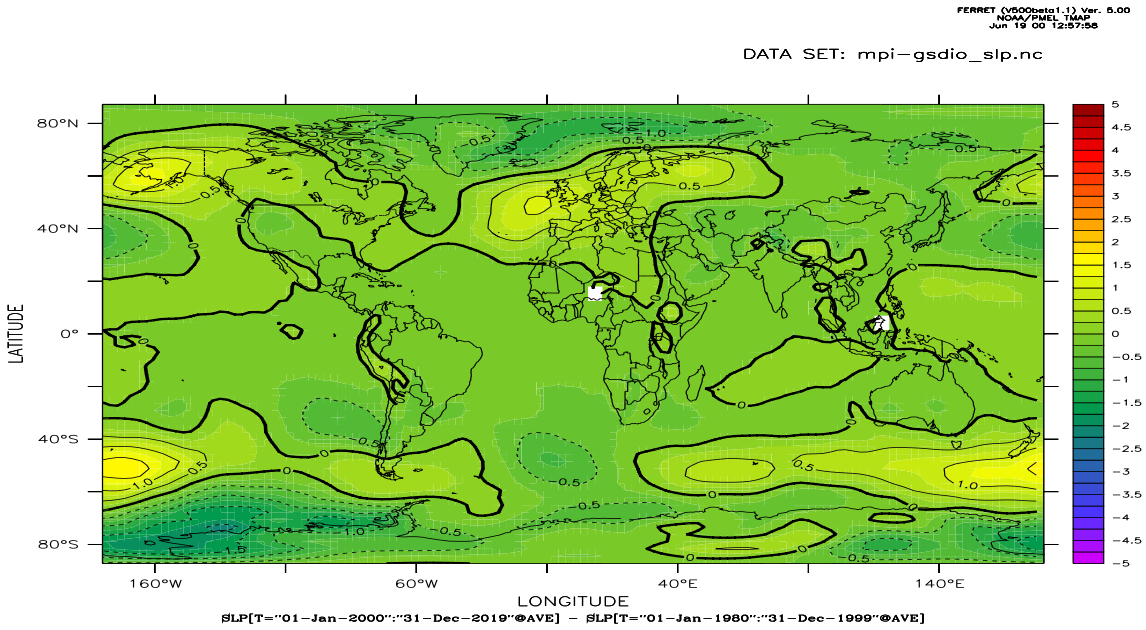

b

Figure 4: The geographical distribution of ECHAM4 GSDIO projected mean temperature (a) and SLP (b) change for the 20-year periods centered at 2010 and 1990.

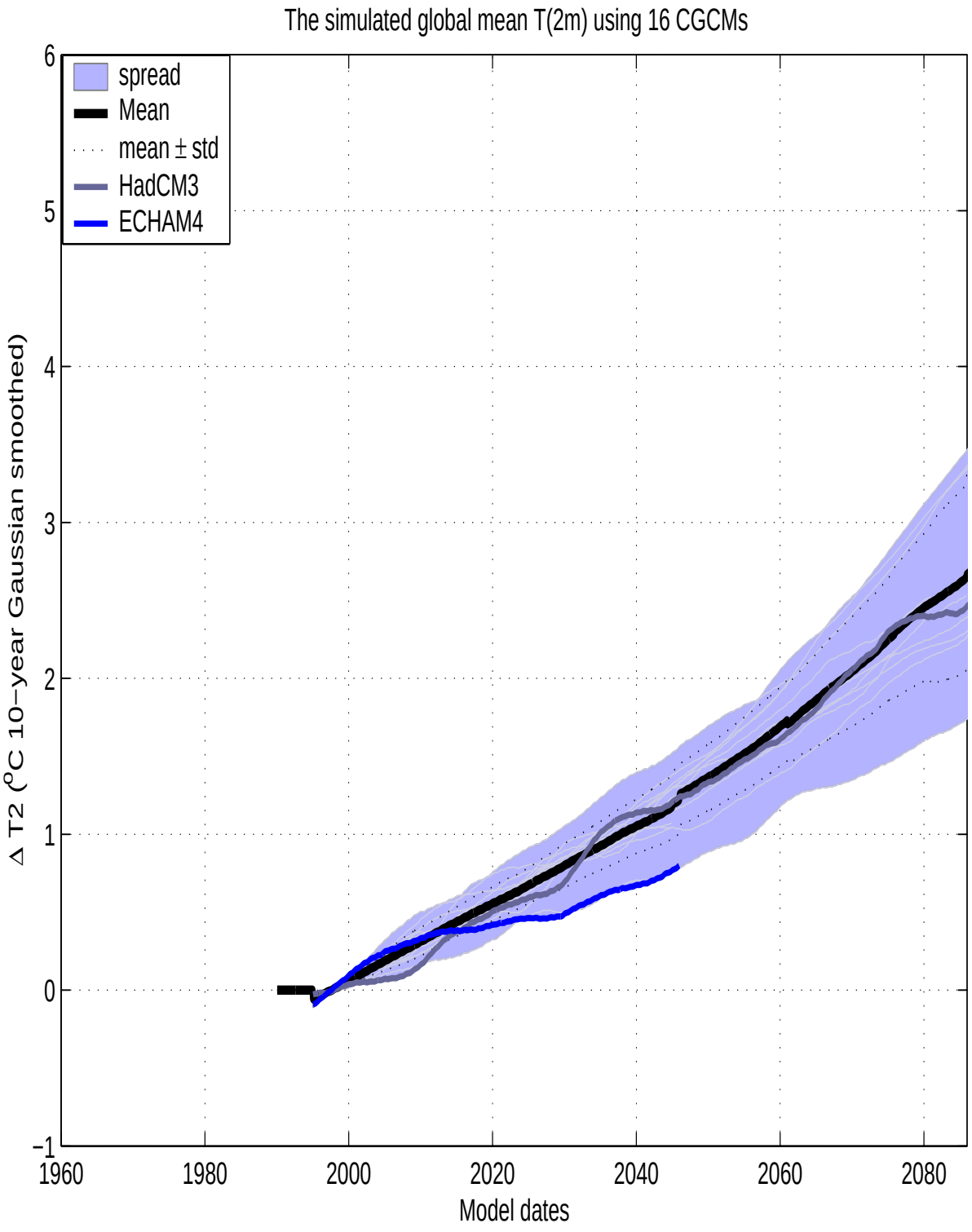

Figure 5: The global mean surface temperatures from 16 different AOGCM scenarios. The curves fro HadCM3 and ECHAM4-GSDIO are shown as black and blue curves. All the scenarios shown here, EXCEPT for the ECHAM4 GSDIO run were based on the GSA forcing (Sulphur and direct effect of aerosols).

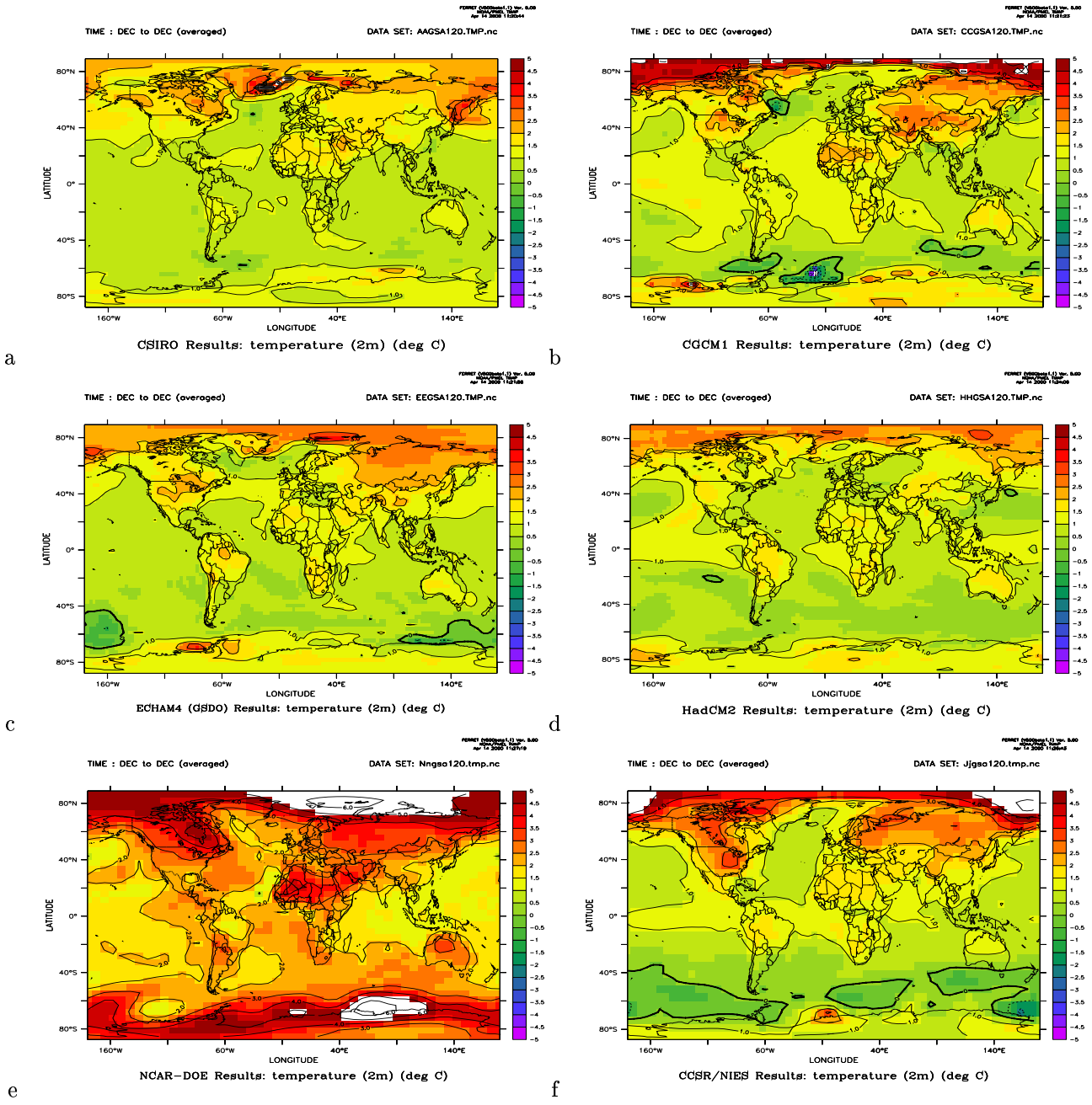

Figure 6: *A comparison between (2011 to 2030) - (1961 to 1990) GSA 2-meter temperature scenarios for a) GFDL, b) Canadian CCCma, c) ECHAM4, d) HadCM2, e) NCAR-DOE, f) Japanese CCSR/NIES.*

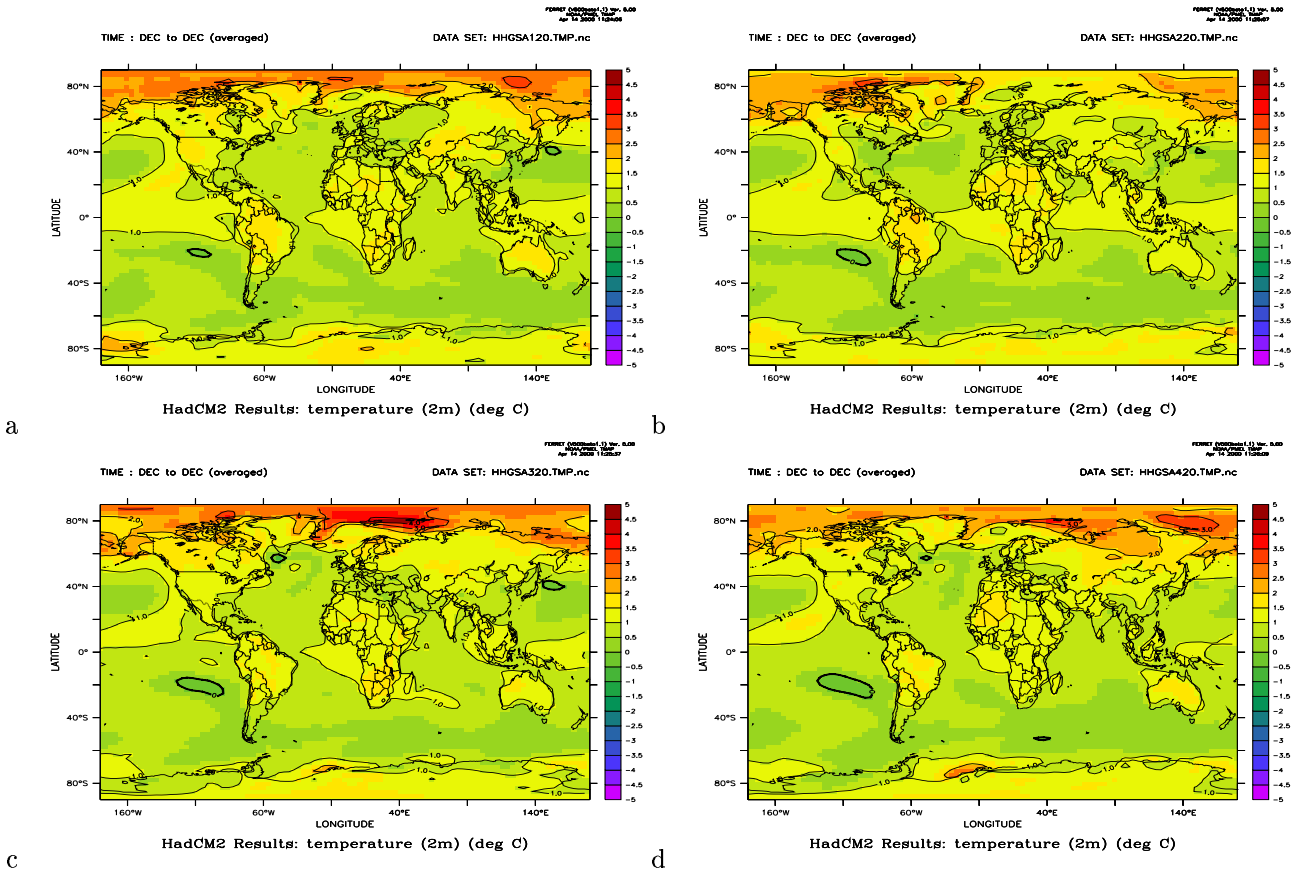

Figure 7: *Four members from an ensemble with the HadCM2 (GSA 2011-2030).*

Model	y-res	x-res	FA	Country
CSIRO (GSA)	32	64		Australia (*Gordon & O'Farrell*, 1997)
CCCma (GSA)	48	96		Canada (*Flato* et al., 2000)
ECHAM4/OPYC3 (GSDIO)	64	128	yes	Germany (*Roeckner* et al., 1992; *Oberhuber*, 1993)
ECHAM4/OPYC3 (GSA)	64	128	yes	Germany (*Roeckner* et al., 1996; *Oberhuber*, 1993)
ECHAM3/LSG (GSA)	64	128	yes	Germany
HadCM2 (GSA)	73	96	yes	UK (*Cullen*, 1993)
HadCM3 (GSA+ozone)	73	96	no	UK (*Gordon* et al., 2000)
NCAR-DOE (GSA)	40	48	no	USA
GFDL-19 (GSA)	40	48		USA (*Delworth* et al., 1999)
CCSR/NIES (GSA)	32	64		Japan (*Emori* et al., 1999)
NCAR-CSM (GSA)			no	USA (*Meehl* et al., 2000)

Table 1: Resolution of GCMs. 'The abbreviation 'FA' stands for 'flux adjusted'

warming pattern described by the different models. A comparison between a selection of the GCM (GSA: greenhouse gases and direct effect of aerosol, but no indirect effect) scenarios is given in Figure 6, which shows the global temperature difference between two 30-year periods centered around 2020 and 1980 respectively. These plots may be interpreted as different global warming scenarios, and it is evident that there are disagreements about the temperature changes over different parts of the world.

The Australian CSIRO model (a), the Canadian CGCM1 (b), the German ECHAM4/OPYC3 (c), the British HadCM2 (d)(only one arbitrary member of the ensemble), an old American NCAR-DOE model[5](e), and the Japanese CCSR/NIES (f) all indicate strongest warming in the polar regions. The American model suggests strongest warming, with greatest change over the Arctic and Antarctica as well as over Canada, Siberia, and northern Africa. The warming projected by the HadCM2 model, on the other hand, is relatively weak over the continents. The results from ECHAM4/OPYC3 GSDO (GSA) (c) suggest stronger warming than the chosen HadCM2 member (d) over the continents and the Barents Sea.

Not all of these discrepancies are necessarily due to different model representation of the climate processes, since different ensemble members of the HadCM2 model in Figure 7 show a great deal of uncertainty associated with poorly known initial conditions (The ensemble members have different initial conditions, but the same forcing), with high uncertainties associated with the climate over the Barents Sea. Whereas one member (b) shows weak warming over the Barents Sea region (less than 2°C) another run indicates dramatic changes in the same region (up to 4 °C). All the HadCM2 runs generally indicate less warming over the continents than the ECHAM4/OPYC3 model.

One conclusion that may be drawn from these results is that the spin-up process is important for the description of the local climatic evolution. The differences between the ensemble members seen in Figure 7 may be regarded as a result of the non-linear chaotic behaviour of climate, and hence part of the unpredictable natural variability. It is also evident that these natural fluctuations contaminate the climate change analysis, even for 20-year long time slices, if the climate change signal is defined as a function of the long-term external forcing (eg increased concentrations CO_2, water vapour, or aerosols). In this respect, Figure 7 illustrates that a length of 20 years is too short for making time slice scenarios.

2.2.3 Global precipitation scenarios

Figure 8 shows the global distribution of projected mean 1980-2020 precipitation changes associated with a global warming. All models suggest little change in the mid-latitudes, but there are some models which suggest dramatic changes in the tropics. One member of the Canadian model ensemble (b) indicates an east-west shift of the Pacific rain patterns so that the scenario resembles a permanent El Niño state. The ECHAM4 model (c) predicts a northward shift of the intertropical convergence zone (ITCZ) over the Indian ocean and wetter conditions over the tropical Pacific. The HadCM2 model (d) indicates in general more rainfall in the tropics, whereas the NCAR-DOE (e) model points to

[5]The NCAR-DOE model is not regarded as a good model and is not the "official" NCAR model (Kristjànsson, private communications)

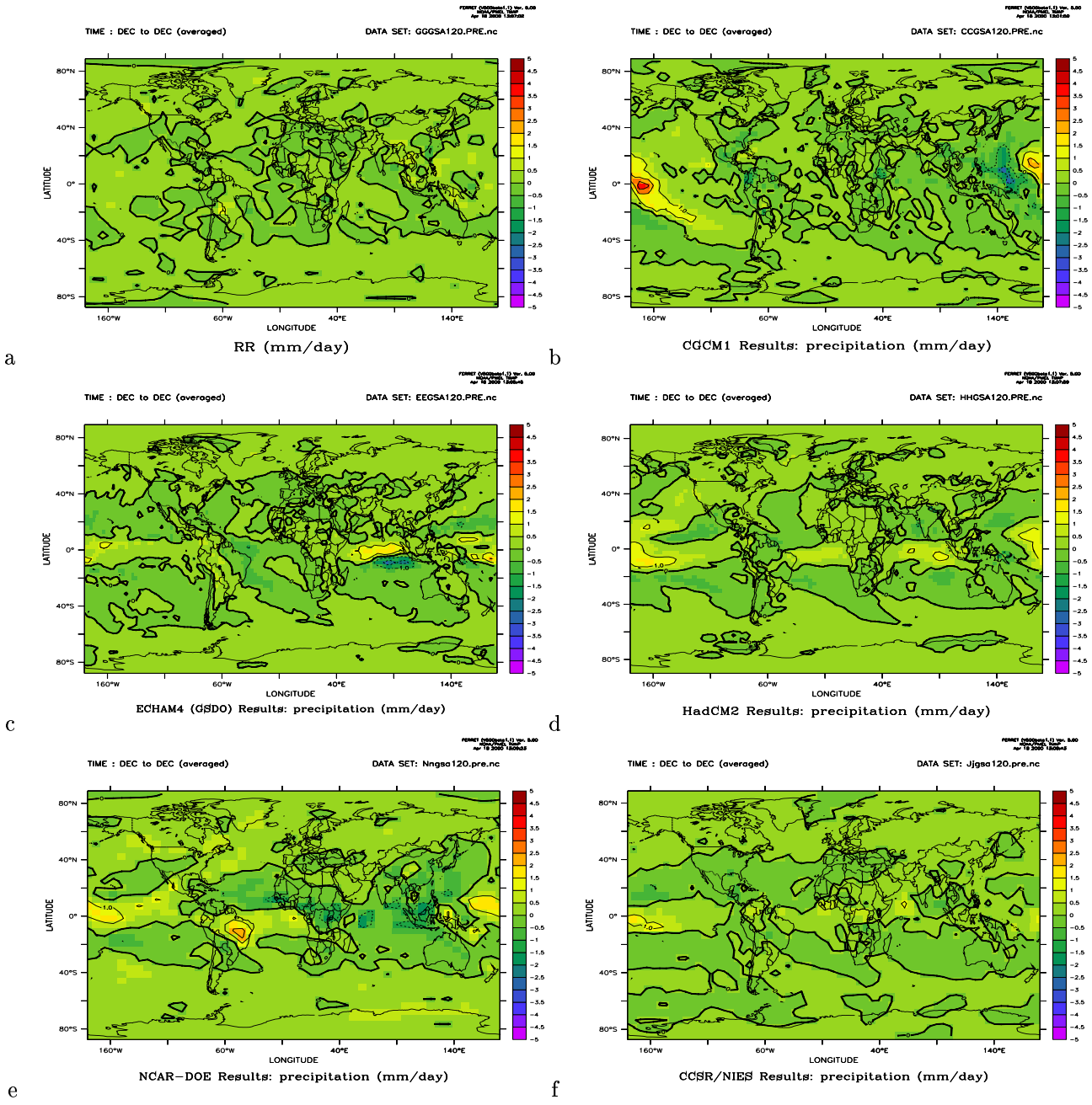

Figure 8: *A comparison between (2011 to 2030) - (1961 to 1990) GSA precipitation scenarios for a) GFDL, b) Canadian, c) ECHAM4, d) HadCM2, e) NCAR-DOE, f) Japan.*

enhanced precipitation over Brazil and eastern tropical Pacific. All the models seem to agree on slightly dryer conditions in the sub-tropics. There is not much signal in the mid-latitudes. It is interesting to note the lack of a strong signal along the storm tracks over the Pacific and Atlantic oceans. Statistical significance tests were not applied to these results as only the mean changes between 1980 and 2020 were obtained from the IPCC web site.

2.2.4 Temperature scenarios from direct interpolation of global GCM results

Figure 9 shows ECHAM4/OPYC3 GSDIO 2-meter temperature time series for a number of locations in Norway and their respective best-fit linear trend 1960-2050. The results indicate systematic warming for all of the locations, and a staggering winter warming rate of 1.18°C/decade over Svalbard consistent with Figure 6c (The GSDIO is a different experiment to the GSA/GSDO).

It is generally not recommended to take grid box values or interpolated values between the grid points as a representation of the local climate (*Grotch & MacCracken*, 1991), so the remainder of this report will therefore focus on downscaling large-scale climatic features (circulation pattern and temperature distributions) to infer local climate variability.

Empirical downscaling of AOGCM results frequently involve preprocessing by applying an empirical orthogonal function (EOF, or principal component analysis[6]) analysis to the data, and it is common to use EOFs to reduce the number of freedom and simplify regressional analysis by restricting the data to a few orthogonal vectors. Thus, using a few leading EOFs has the effect of filtering the data and discarding small-scale variability (noise). Ideally, these climatic trends ought to be unaffected by the preprocessing. Table 2 shows estimates of long-term linear trends interpolated to a number of climate station locations in Norway, for the model years 1980-2050 and after the AOGCM data have been filtered through the 10 leading EOFs. It is evident from the results in Table 2 that the the climatic trends *are* affected by the EOF filtering, and furthermore, the results vary with the region (spatial domain) over which the EOF analysis is applied.

2.2.6 Sea level pressure

Figure 10 shows maps of the best-fit scenario long-term (60 year) linear SLP trends in the ECHAM4 GSDIO (left) and the HadCM3 (right) for four different seasons (from the top: January, April, July, and October means). These trends are typically weak ($<$ 10hPa) compared with the interannual variability, and generally not statistically significant. The differences between the two model results may therefore partly be due to sampling fluctuations. It is also possible that any long-term variability in the SLP, and hence the trend estimates, is part of a low non-deterministic ("chaotic") process such as the NAO. Differences between the two model results should therefore not be interpreted as model misrepresentation of the SLP field in one or both models.

The GSDIO scenario suggest a strengthening of the NAO during January, whereas the HadCM3 describes a lowering in the SLP over the British isles. For April, the GSDIO results indicate the development of a tri-pole wave train with

[6]For further references, see *Wilks* (1995), *North* et al. (1982) or *Benestad* (1999d).

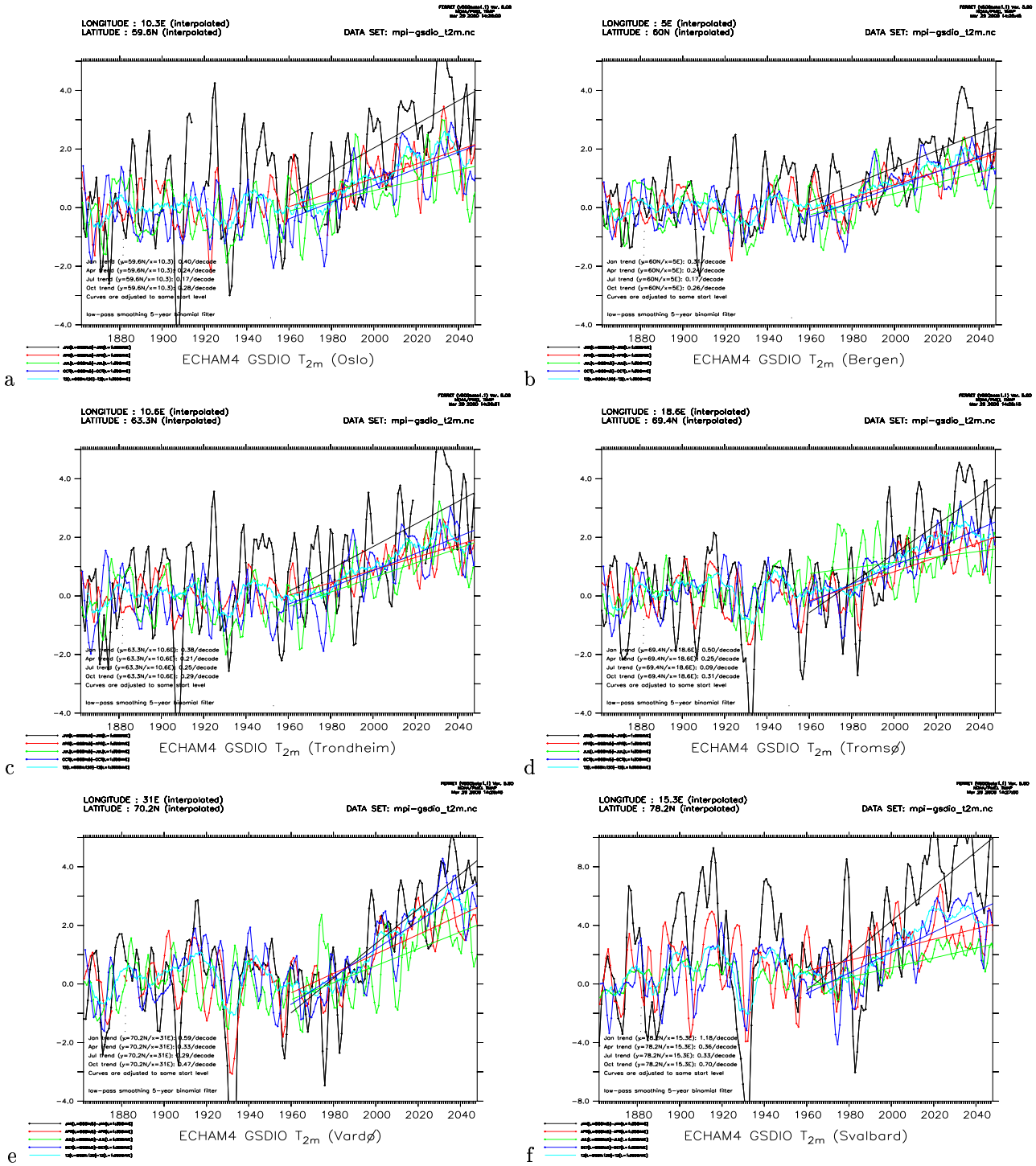

Figure 9: *Seasonal temperature development for 6 locations in Norway: a) Oslo, b)Bergen, c) Trondheim, d) Tromsø, e) Vardø, and f) Svalbard lufthavn. These scenarios are estimated from 'unintelligent interpolation' of ECHAM4 GSDIO results. Black=January, Red=April, Green=July, Blue=October, Cyan=Annual mean. The trends were estimated using the application Ferret (*S.Hankin & Denham, *1994) and a go-tool supplied with this package (this tool introduced wholes in the data for unknown reasons).*

2.2.5 Local warming trends estimated from simple interpolation of ECHAM GSDIO results

	scan				*nordic*				*natl*			
	Jan	Apr	Jul	Oct	Jan	Apr	Jul	Oct	Jan	Apr	Jul	Oct
FLISA	28	13	7	11	31	12	2	9	22	18	4	17
RØROS	25	12	9	10	30	10	4	7	21	16	5	17
ØSTRE TOTEN	27	12	6	10	30	12	2	8	21	17	4	16
FOKSTUA	23	12	8	10	27	11	2	7	19	14	4	16
DOMBÅS	23	12	8	9	26	11	2	7	19	14	3	16
ÅS	27	12	6	10	27	13	3	9	20	17	5	15
OSLO - BLINDER	27	12	6	10	28	13	3	9	20	17	4	15
NESBYEN - SKOG	25	12	6	10	27	12	2	8	19	16	3	15
FERDER FYR	26	12	6	10	26	12	4	9	19	17	5	14
GVARV	24	12	6	10	25	13	3	9	17	16	4	14
DALEN I TELEMA	23	12	5	10	23	13	3	8	16	15	3	14
TVEITSUND	23	12	6	10	23	13	3	9	16	15	4	13
OKSØY FYR	20	12	6	10	19	12	6	9	14	14	6	13
LISTA FYR	19	12	5	9	18	12	5	8	13	13	5	12
SIRDAL - TJØR	21	12	5	9	20	13	4	8	14	14	4	12
SAUDA	22	12	5	9	22	13	2	7	15	14	2	12
UTSIRA FYR	19	12	6	8	19	12	5	7	13	13	3	11
BERGEN	21	12	7	8	22	12	3	7	14	13	2	12
HELLISØY FYR	19	12	8	7	20	11	5	6	14	13	3	11
LÆRDAL - TØN	22	12	7	9	25	12	2	7	17	14	2	14
LEIKANGER	22	12	7	8	24	12	3	7	16	14	3	13
OPPSTRYN	21	12	8	9	24	11	3	7	17	13	3	14
KRÅKENES FYR	19	11	10	7	20	10	7	6	14	11	5	11
TAFJORD	21	12	9	9	23	10	4	7	17	13	4	14
ONA II	19	12	10	8	21	10	6	6	15	12	6	13
VÆRNES	23	12	11	10	27	9	7	7	19	14	7	16
ØRLAND III	21	12	11	9	24	9	7	7	17	12	7	15
VALLERSUND	21	12	11	9	24	9	7	7	17	12	7	15
LEKA	21	12	15	10	24	8	13	7	18	11	10	14
MAJAVATN III	26	13	13	11	31	9	10	7	24	14	8	16
MYKEN	21	12	13	11	23	9	12	8	20	11	8	13
GLOMFJORD	24	13	11	11	28	9	9	7	24	12	7	14
BODØ VI	24	13	11	12	27	10	10	8	24	12	7	13
SKROVA FYR	22	13	10	12	23	10	10	8	23	11	7	12
RØST II	19	12	13	11	21	9	12	8	19	10	8	12
SKOMVÆR FYR	19	12	14	11	20	9	13	8	18	10	8	12
DIVIDALEN	36	15	15	16	37	12	15	11	36	14	8	16
TROMSØ	29	15	13	16	29	13	13	11	30	13	7	14
LOPPA	30	15	11	17	29	14	12	13	30	14	7	15
SUOLOVUOPMI	36	14	14	18	36	13	16	14	36	15	9	17
SIHCAJAVRI	40	13	15	18	42	12	17	13	41	15	9	18
BANAK	33	16	13	19	32	15	16	16	33	15	10	17
SLETNES FYR					28	18	17	22	31	17	14	18
KARASJOK	36	15	15	20	36	14	18	16	37	16	11	18
MAKKAUR FYR					29	17	19	23	31	17	15	19
VARDØ					29	17	20	24	31	17	16	19

Table 2: Linear warming trends (×0.01°C/dec) for a number of locations in Norway where there are climate observation stations. These values have been estimated directly from the AOGCM results after AOGCM T(2m) had been filtered through the 10 leading EOFs estimated over the 0°W-30°E, 55°N-75°N (*scan*), 20°W-40°E, 50°N-75°N (*nordic*) and 90°W-40°E, 40°N-75°N (*natl*) domains (Fig 19) using the entire 1860-2050 record, and the interpolation used a 2-dimensional cubic spline method. The linear trends were estimated using a least-squares fit over the 1980 to 2049 period.

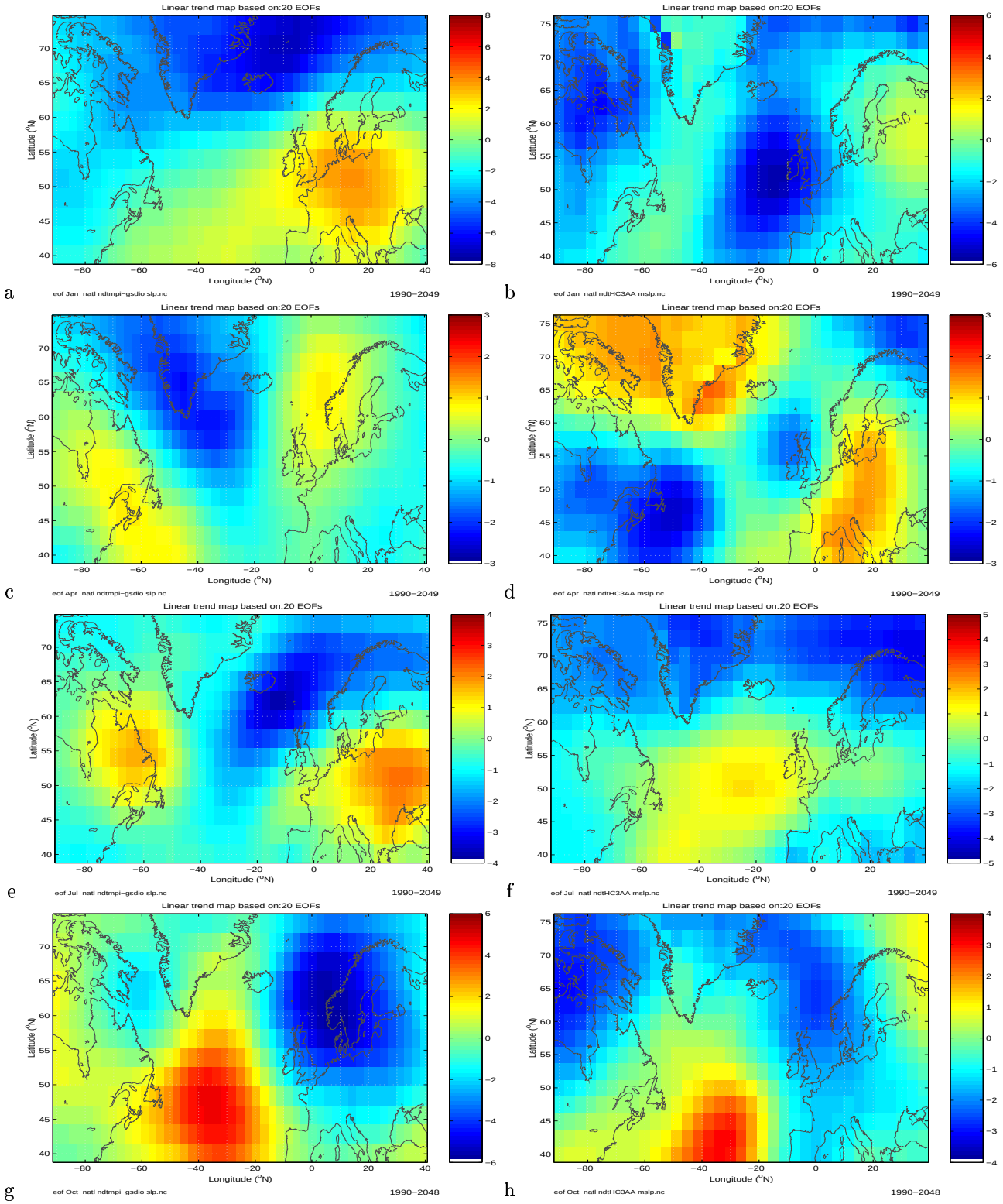

Figure 10: *Least squares best-fit linear SLP trend for January (a,b), April (c,d), July (e,f) and October (g,h) from the ECHAM4/OPYC3 GSDIO (left) and HadCM3 (right) experiments.*

maxima over the northwestern Atlantic, south of Greenland, and Norway. The HadCM3 scenario, in contrast, suggest opposite anomalies over the northwestern Atlantic and strengthening of the SLP in the vicinity of Greenland. The July SLP trends are also different, but the GSDIO integration appears to have a preference for wave train structures with 3 maxima. Only the October SLP trends from the two integrations show some resemblance, with a strengthening of the Azores SLP and weakening of the SLP over the Norwegian Sea, but this may be coincidental.

2.2.7 Summary on the AOGCM scenarios

Figures 6, 7 and 8 demonstrate that the results from an arbitrarily chosen AOGCM model cannot be taken as the prediction of the future climatic evolution since the various regional scenarios tend to differ among the various model experiments. Scenarios should therefore not be based on just one AOGCM, but all available models which convincingly demonstrate that they realistically reproduce the present-day climate. Here, a number of AOGCMs[7] will be used for making climate scenarios, but we will also go into more depth with the ECHAM4/OPYC3 GSDIO results, as this model has been chosen as the main AOGCM model for the RegClim project.

The results in figure 10 provide a good demonstration of why downscaled scenarios based on these fields should not be interpreted as a prediction of true future local climate changes. If both the ECHAM4 GSDIO and the HadCM3 scenarios both represent an equally probable climate outlook, then the downscaled scenarios from these must be interpreted as just possible climatic trends with equal chance of occurring.

It is important to stress that these scenarios do not attempt to *predict* the true future climate, but merely represent one realization of a number of possible outcomes. More reliable scenarios should be based on an ensemble of various AOGCM models (*Palmer* et al., 1998), in addition to different methodologies adopted for downscaling.

[7] *Benestad* (2000b) identified the identified HadCM3, HadCM2, ECHAM4, and NCAR CSM (*Meehl* et al., 2000) as the models which gave the best description of the present-day climate.

	1880	1890	1900	1910	1920	1930	1940	1950	1960	1970	1980
DB93			| ←			→ |		| ←			→ |
			9.3	year					12	year	
H99			→ |	→							
	inter	annual			decadal						
DH99			| ←				→ |				
				weak	assoc.	$T(2m)$					
F99						→ |					
			NAO	strong							
M98			←		→ |		←	→ |	→		
			NAO	north		NAO	south				
T99			| ←	→ |	| ←			→			
			weak	3.3yr		quasi-	biennial	clear			
			strong	4.4yr		quasi-	decadal	weak			

Table 3: Overview over NAO character. The abbreviation DB93 denotes *Deser & Blackmon* (1993), H99 is *Higuchi* et al. (1999), DH99 *Deliang & Hellström* (1999), F99 *Fu* et al. (1999), M98 *Mächel* et al. (1998), and T99 represents *Tourre* et al. (1999).

3 Evaluation of the empirical downscaling methods

3.1 Introduction

Local climate variations in parts of Norway are strongly influenced by the large-scale circulation associated with the North Atlantic Oscillation (NAO) (*Kapala* et al., 1998; *Benestad*, 2000c, 1998). A high NAO index (NAOI, the standardised pressure difference between the Azores/Lisbon/Gibraltar and Iceland) describes situations where the Azores high is strengthened and the low-pressure system over Iceland is deeper than normal. These conditions result in increased mean westerly winds over the North Sea and Norwegian Sea, and stronger advection of maritime air over Norway. Empirical downscaling therefore often involves a regression of the local climate variable onto the NAOI. It is for this reason of strong interest to gain a better understanding of the NAO, and one key question is whether the climate models can make skillful predictions of the NAO evolution.

Past studies of the NAO have suggested that it is a complex phenomenon associated with a range of time-scales and that the ocean plays a role. *Higuchi* et al. (1999) argued that the NAO is influenced by the North Atlantic SST, which implies that AOGCMs with unrealistic representation of the ocean will not produce reliable predictions of the NAO. The SST field is influenced by the ocean surface currents, which can be narrow and involve sharp gradients. *Deser & Blackmon* (1993) described the warming trend in SST along the Gulf stream between 1920-1950, and associated this warming to the reduction in the sub-tropical high. The climate variability involved a quasi-decadal oscillation

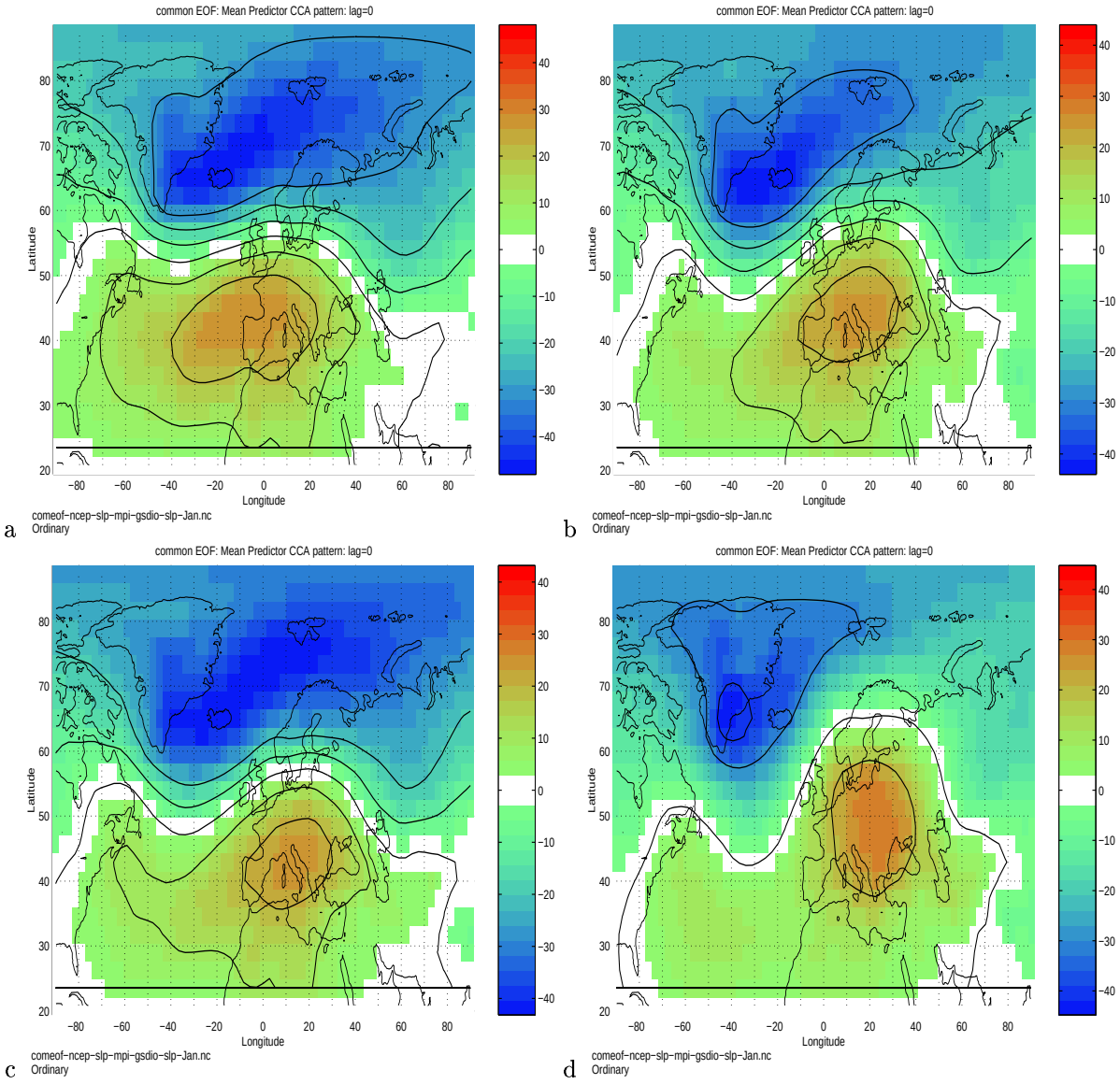

Figure 11: SLP predictor patterns which have highest correlation with the January temperature in a) southern Norway, b) Western Norway, c) middle Norway (Trøndelag), and d) northern Norway.

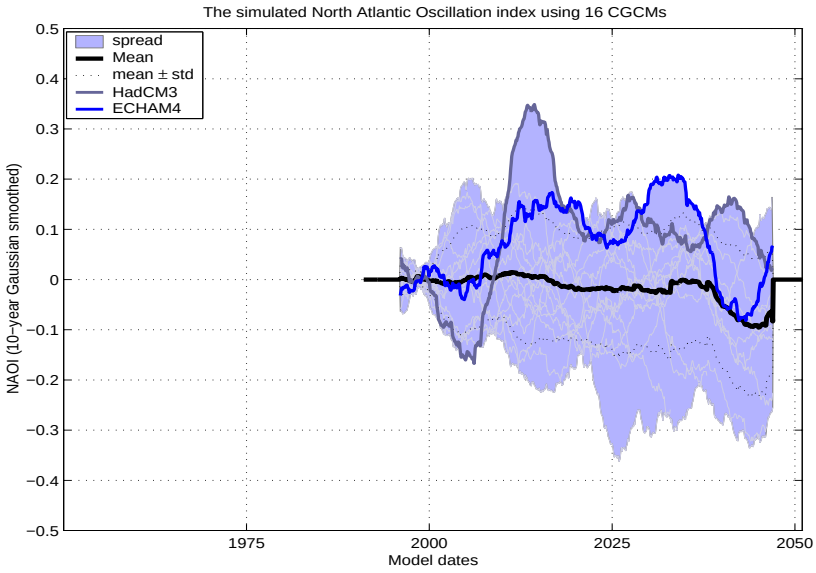

Figure 12: Estimated NAO index from 16 different AOGCM scenarios. The curves fro HadCM3 and ECHAM4-GSDIO are shown as black and blue curves. All the scenarios shown here, EXCEPT for the ECHAM4 GSDIO run were based on the GSA forcing (Sulphur and direct effect of aerosols).

of around 9 years for the 1900-1944 period, but with a preferred time scale of around 12 years for 1945-1988. According to *Higuchi* et al. (1999), the NAO was strongly influenced by an interannual modulation prior to 1900, but during 1910-1925, there was a gradual shift from interannual to decadal time scales.

Deliang & Hellström (1999) has found that the strength of association between the NAO and local Swedish temperature varies in space and time. There is a weaker correlation between the NAO and temperature further north. The correlation is strongest in March and weakest in July. The correlation between annual mean NAOI and temperature was strong before 1905, but dropped between 1905 and 1940. The strength of association was strong for all but the northernmost regions after the 1950s. A spectral cross-spectral analysis between the annual mean NAOI and mean temperature over 6 Swedish regions suggests common peaks at 2.3 and 3.5 - 12.5 years.

Fu et al. (1999) studied the abrupt warming over the northern hemisphere in the early 1920s, which had strongest effect during winter and at high latitudes. The warming was detected first close to the equator, and the Arctic surface air temperature lead the SST. Before the warming, an enhancement of the North Atlantic high and deepening of the Icelandic low had already taken place, but a further strengthening of the NAO was evident during the warming. The westerlies *weakened* in the 1930s. Large increase in the tropical cyclone activity was seen in the early 1920s, and may possibly be associated with the abrupt warming.

Hanssen-Bauer & Førland (1998) analysed the temperature trends in Svalbard and tried to relate these to changes in the large-scale circulation, but could not explain the "early 20th century warming" (from 1910 to 1930) in terms of

changes in the 1873-1993 SLP measured at 70°N-10°E, 80°N-10°E 70°N-20°E, and 80°N-20°E.

Mächel et al. (1998) found a northerly excursion of the Icelandic low in 1900-1930, followed by a southerly displacement for the 3 subsequent decades. After 1980, the centre of action migrated northward again. The Icelandic low-pressure system reached lowest readings during 1880s, but was then subject to strong fluctuations that lasted up to the late 1920s. The 1930-1960 period was characterised by short-term fluctuations, but a long spell of a strong NAO phase was observed in 1920-1930. The Icelandic low was weakened from 1976 until the late 1980s, after which it experienced a rapid strengthening.

Tourre et al. (1999) found a weakening in the 3.5-year spectral peak between 1900 and 1930, but the 4.4-year time scale was more prominent. The quasi-biennial signal was clearly present in 1920-1955, but quasi-decadal time scales (11.4 years) was less evident. *Stephenson* et al. (2000) argued that the NAOI could be described by an stochastic *ARIMA(p,d,q)* process, implying that the long-term NAO evolution may not be predictable.

Table 3 gives a summary of these empirical NAO studies. Although the NAOI can account for a large part of the local climate variability over parts of Norway, the index is defined somewhat arbitrary and it may not even be the best predictor that we have. Figure 11 shows the best predictor patterns for different parts of Norway according to a a canonical correlation analysis (CCA). It is evident that climatic fluctuations in the southern part of Norway are closely related to the NAO during January (a), but western Norwegian temperature variations are affected by a more southerly flow (b), and the meridional component of the geostrophic wind becomes increasingly important further north (d). For this reason, the approach to downscaling in this study is to use gridded fields rather than indices as predictors. Figure 12 shows low-pass filtered AOGCM estimates of the NAO index from 1990 to 2005. This figure illustrates the large inter-model variations in the simulated atmospheric circulation and its evolution.

3.2 "Regional" downscaling models

Benestad (1999c) reported improved skill for empirical models which only include a limited number of predictands within a small region. The reason is that step-wise regression approaches will identify different optimal predictor patterns for different parts of Norway. Figure 11 shows the different large-scale SLP patterns associated with the local January temperature in different parts of Norway and the inclusion of too many predictors may lead to an over-fit. Here, we will adopt similar "regional" models, and the empirical downscaling of the global climate scenarios was based on "regional" climate models relating the local climates within the same "climate" region (*Hanssen-Bauer & Nordli*, 1998; *Hanssen-Bauer & Førland*, 1998). There are two exceptions, as Røros and Kjøremsgrende (in Dombås) (*Hanssen-Bauer & Nordli* (1998) region 1, but close to the border with region 3) were grouped together with Værnes (*Hanssen-Bauer & Nordli* (1998) region 3) and Vardø ((*Hanssen-Bauer & Nordli*, 1998) region 6) was grouped together with Karasjok (*Hanssen-Bauer & Nordli* (1998) region 5). Figure 13 shows four maps indicating the climate station data used in four different "regional" downscale models.

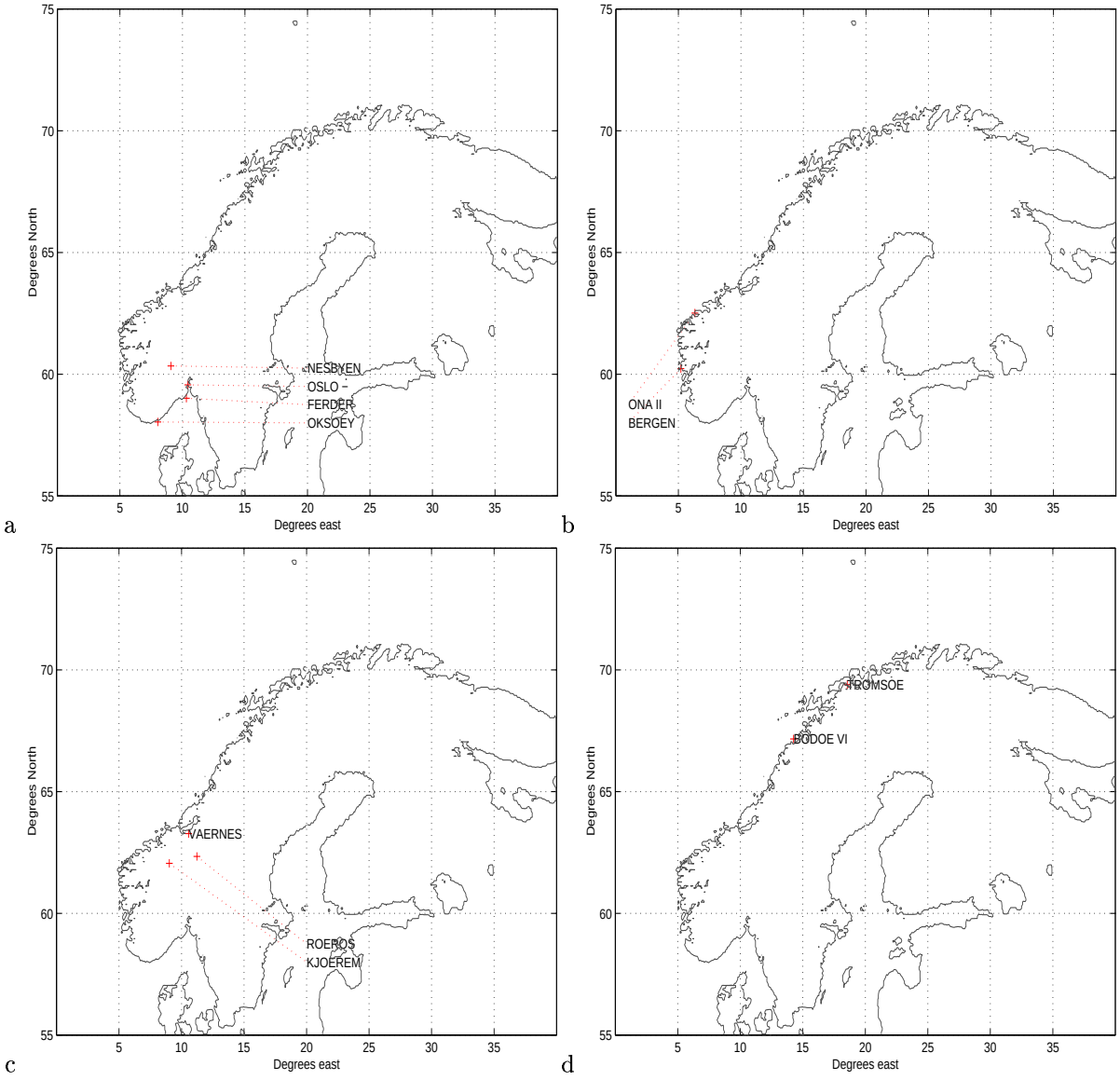

Figure 13: Maps showing the various location for the regional empirical models.

The station group shown in Figure 13a will henceforth be denoted the southern Norway group, and the corresponding empirical model SNorway. The panels b to d likewise define the western Norwegian group, mid-Norwegian group, and north-western Norwegian group, and the regional empirical models: WNorway, MNorway, NWNorway, and NNorway (the latter stations, Karasjok and Vardø, are not shown) respectively.

Only the 10 leading EOFs were considered in the downscaling studies. Tests comparing the effect of using pools of 10 and higher order EOFs (20 and 40 for the projection and common EOF methods respectively) from which the predictors were selected suggested that the higher order modes often are responsible for nonsensical results (no trend). The higher orders represent smaller scales than do the leading 10, and therefore would introduce more details in the predictor anomalies. As the downscaling extracts information from large-scale patterns, the omission of the small scale (often noisy) details contained in the higher order modes is justified. The purpose of downscaling is to infer local climate change from large-scale anomalies, but by reducing the predictor domain, the small-scale features become increasingly important.

The EOF analysis was applied to each calendar month separately, and the downscaling for the January months was derived using predictors based on EOFs calculated using (sub-sampling) the January fields only. Thus, the downscaled results discussed here were obtained with *stratified* models only.

It is important to test the downscaling methods thoroughly before applying these to make local climate scenarios that potentially may be used for making political decisions. Although the methods have been evaluated by *Benestad* (1998), *Benestad* (1999b), *Benestad* et al. (2000), and *Benestad* (1999a), we will make further tests which are more specific for their use in downscaling of global climate scenarios. The conventional "projection" (or regression *Benestad* (1999c), or using "Perfect Prog" *Schubert* (1998) and *von Storch* et al. (1993)) type approach[8] is compared more systematically and thoroughly with the common EOF approach here than in the earlier studies.

4 Test results

Since the empirical downscaling described here is based on EOF analysis, it is important to know how this type of transform affects the results. Here, a simplification is adopted, where the degrees of freedom is reduced to a minimum. This way, the two downscaling approaches can be compared in a simplified framework and serve as a model for the more complicated analysis when many degrees of freedom are involved. Furthermore, by limiting the system to two degrees of freedom, one has much greater control over the analysis, and it is easier to make clear cut experiments.

The empirical downscaling is based on the common EOF method (*Flury*, 1988; *Sengupta & Boyle*, 1993; *Barnett*, 1999) as proposed by *Benestad* (1999a). Concerns, however, have been raised regarding whether the common EOF method yields good predictions when the results from imperfect models with systematic biases are used as predictors (U. Ulbrich, personal communications). The issue is essentially a non-stationarity problem for ordinary EOF analysis, as the

[8]It is rarely stated explicitly in the literature how the authors have arrived from EOFs in the model climate "world" to corresponding patterns as seen in the observations.

4.0.1 An illustration of the EOF methods using a 2-DOF example

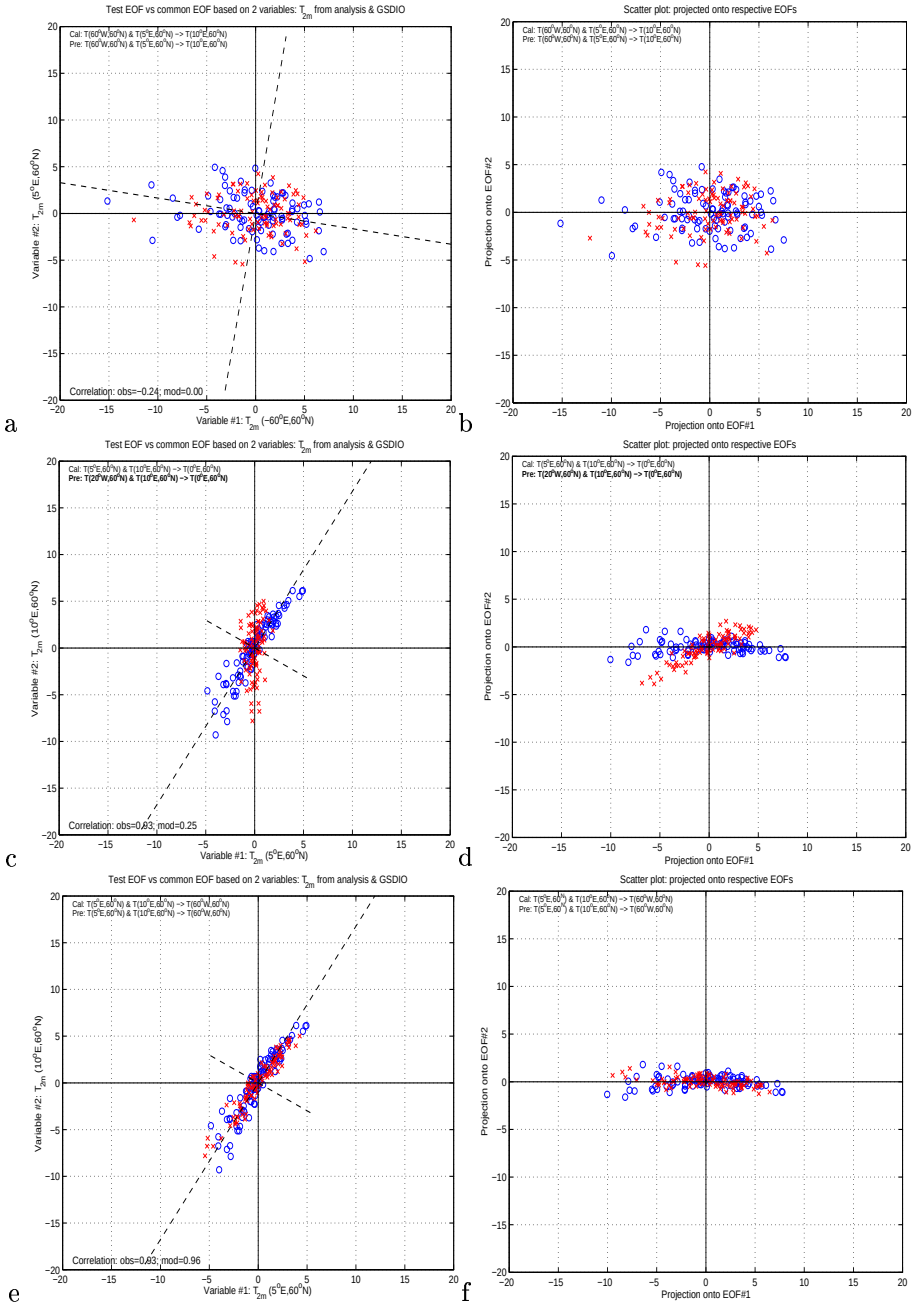

Figure 14: a) Scatter plots for two temperature series from observations (circles) and model integration (crosses) for which the EOFs are similar (similar relationship between the two series). b) The time series projected onto EOF of the "observations". c) Two time series where the EOF differ, and d) the projection onto EOF of the observations. e) and f) Similar to a) and b).

4.0.2 Comparing the common EOF method with the conventional approach when calibration predictors are different to the prediction predictors

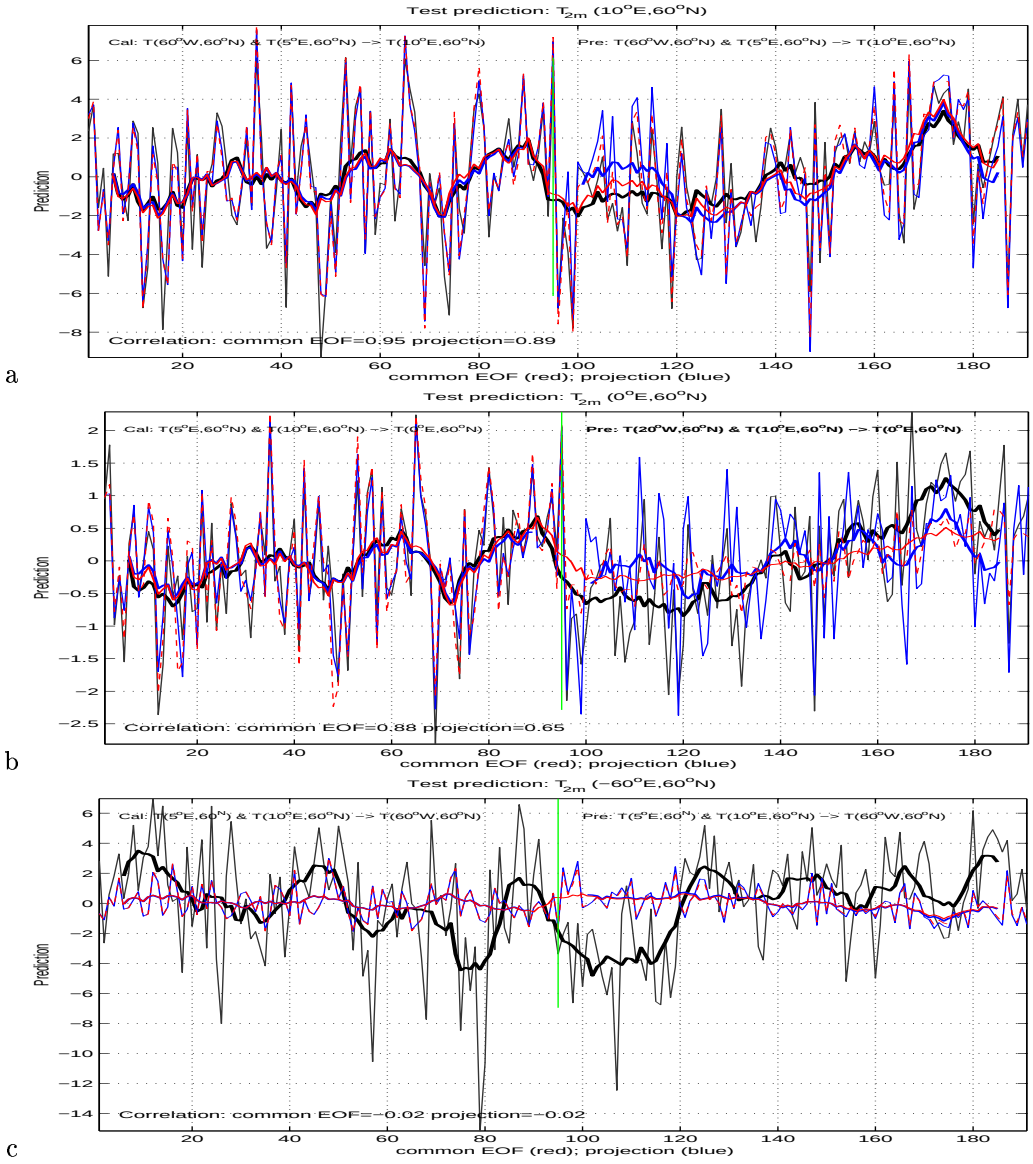

Figure 15: a) Test predictions using common EOFs (red) and conventional (blue) projection approach based on a test case where the "observed" and "future" EOFs are similar and b) using the differing model and observed EOFs shown in Figure 14d. The "truth" is shown as black curve. The common EOF method in this case boils down to an EOF analysis for a non-stationary data record. Panel c) shows the situation for similar observed and model EOFs, but where the predictand is unrelated to these.

observed and modeled fields may not be similar.

The EOF analysis seeks solutions which maximize the variance both in spatial and temporal domain. This transform is illustrated in Figure 14, where panels *a* and *c* show the scatter plots between two T(2m) time series: "observed" (circles) and "modeled" by (crosses). The analysis shown is similar to the two-dimensional PCA in *Wilks* (1995), p 376-386. The leading EOF is an eigenvector, or a the best-fit line that minimizes the squared mean distance between the data points and a best-fit straight line[9] (Figure 14, left panels, dashed lines). This line describes a coherent structure which accounts for maximum variance. When expressing the data in terms of their EOFs, the data are projected onto these eigenvectors, and these projections are often referred to as the principal components, PC. In data space, the EOF decomposition may be regarded as a rotation that aligns the data with the EOF basis functions (Figure 14, right panels). One could also regard the EOF transform as a process that "moves" all redundant (correlated) information about the series to the leading PC. The PCs describe the time evolution of the data in terms of their EOFs.

The EOFs shown in this report have been estimated from a subsample of the data to avoid temporal autocorrelation[10] (*North* et al., 1982; *Sengupta & Boyle*, 1993), and the PCs have then been calculated according to $\mathbf{V}^T = (\mathbf{\Sigma}^T\mathbf{\Sigma})^{-1}\mathbf{\Sigma}^T\mathbf{U}^T\mathbf{X}$, where $\mathbf{X}$ represents the data field (anomalies), $\mathbf{U}$ the spatial patterns (EOFs), $\mathbf{\Sigma}$ is a diagonal matrix holding the eigenvalues, and $\mathbf{V}$ represents the PCs. When all the EOFs are well resolved then they are mutually orthogonal ($\mathbf{U}^T\mathbf{U} = \mathbf{I}$) and any spatial anomaly pattern will therefore be a unique combination of EOFs.

The simple 2-D EOFs can be used in a study of the performance of the common EOF method contra the conventional projection approach. In this set of prediction studies, EOFs were estimated from two temperature time series taken from various grid boxes (locations) of a climate model integration (ECHAM4 GSDIO). The EOFs were used as *predictors* and a third series was used as the *predictand*. Only the first half of the series was used for model development whereas the latter half (i.e. the independent data) was used for model evaluation. A least-squares fit was used for model development. In the case of the conventional approach, the "simulated" series were projected onto the "observed" EOFs (Figure 14, right panels).

Figure 15 shows predictions based on the 3 different cases shown in Figure 14: where *i)* the EOFs of the "observations" are similar to those in the "future simulations" (a), *ii)* the EOFs of the "observations" are different to those in the "future simulations" (b), and *iii)* the EOFs of the "observations" are similar to those in the "future simulations", but unrelated to the predictand (c). The way the "observed" and "simulated" EOFs were determined was by selecting temperature series from different locations, and to ensure different EOFs in the "observations" and "simulations", the predictor series were constructed by taking temperature from different locations over the "observation" and "simulation" periods respectively. The labels given in the upper left and right corners of Figure 15 indicate which two locations were included in the predictors for the calibration and evaluation periods respectively, and at which location the temperature was predicted.

[9] Differs from least-squares fit, which minimises the *errors in y*.

[10] Temporal serial correlation is especially undesirable in association with common principal component analysis.

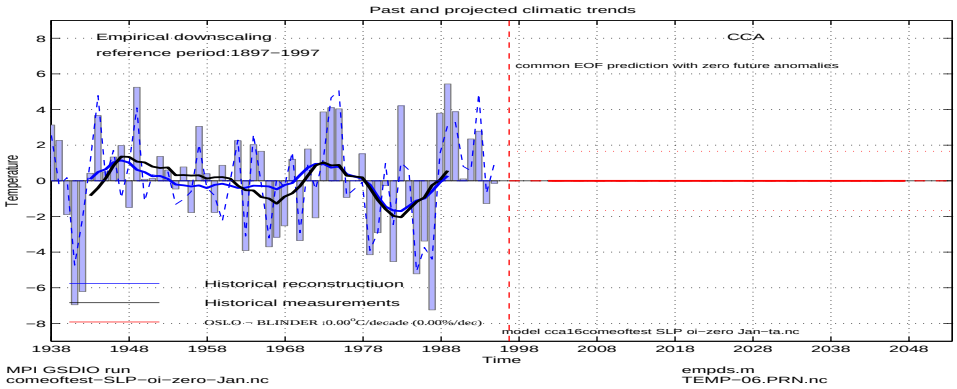

Figure 16: Test of the common EOF method using zero-anomaly fields for the independent data. The expected results are zero, in agreement with the predictions.

The "skill of prediction" is taken to be the correlation between the prediction and the predictand over the independent evaluation period, and the correlation scores are shown in the lower left corners of Figure 15. It appears from these correlation scores that the common EOF method is slightly superior to the conventional method.

Both the common EOF and the conventional methods perform well when the EOFs of the "simulation" are similar to those of the "observation" intervals (Figure 15a). If however, the data are non-stationary so that the EOFs are not similar between the two intervals ((Figure 15b), then the conventional model will nevertheless yield a prediction with strong fluctuations, but fails to reproduce the long-term trend. The common EOF method, by comparison, gives only a weak signal also associated with a weak long-term trend. The higher scores of the common EOF method may be attributed to the correlated long-term trends and the fact that the common EOF method was not "fooled" by the non-stationarity. Both approaches produced, as expected, near-zero signal for the case of low correlation between the predictors and predictand (Figure 15c)

4.0.3 Testing the common EOF method for zero anomalies.

It is expected that zero anomalies will produce zero weighting for the PCs. Figure 16 shows the test result of the common EOF method using SLP and where the model data has been set to zero before computing the common EOFs. The test predictions are indicated by the red curve, which is indeed constantly zero according to the expectations. There may be problems with the common EOF method if the modes are not clearly resolved and where the EOFs are not normal as the anomalous patterns may no longer be represented by a unique combination of spatial modes. It is therefore important to always test the empirical model results before trusting the downscaled scenarios.

4.0.4 Comparing the common EOF method with the conventional approach using model data for calibration and verification

Figures 17 and 18 show the results from a series of tests based on the common EOF method (upper panels) and the conventional downscaling method

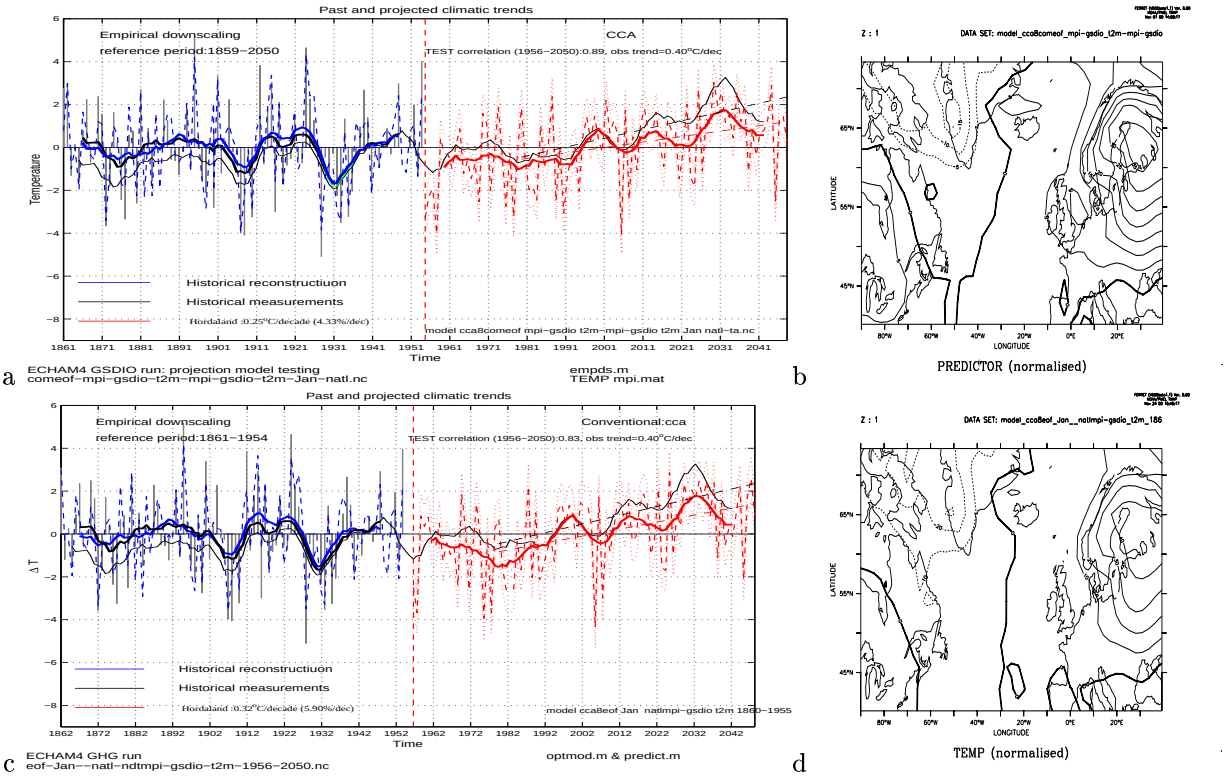

Figure 17: Comparison between a common EOF CCA downscaling model (upper) and a corresponding conventional model (lower) described in *Benestad* (1999c). Both models were calibrated with North Atlantic ECHAM4 GSDIO T(2m) as predictors and model grid point T(2m) at 60°N,6°E as predictands. The left hand panels show the grid point value (black), the prediction of the dependent data (blue), and the prediction of independent ("future") temperature (red).

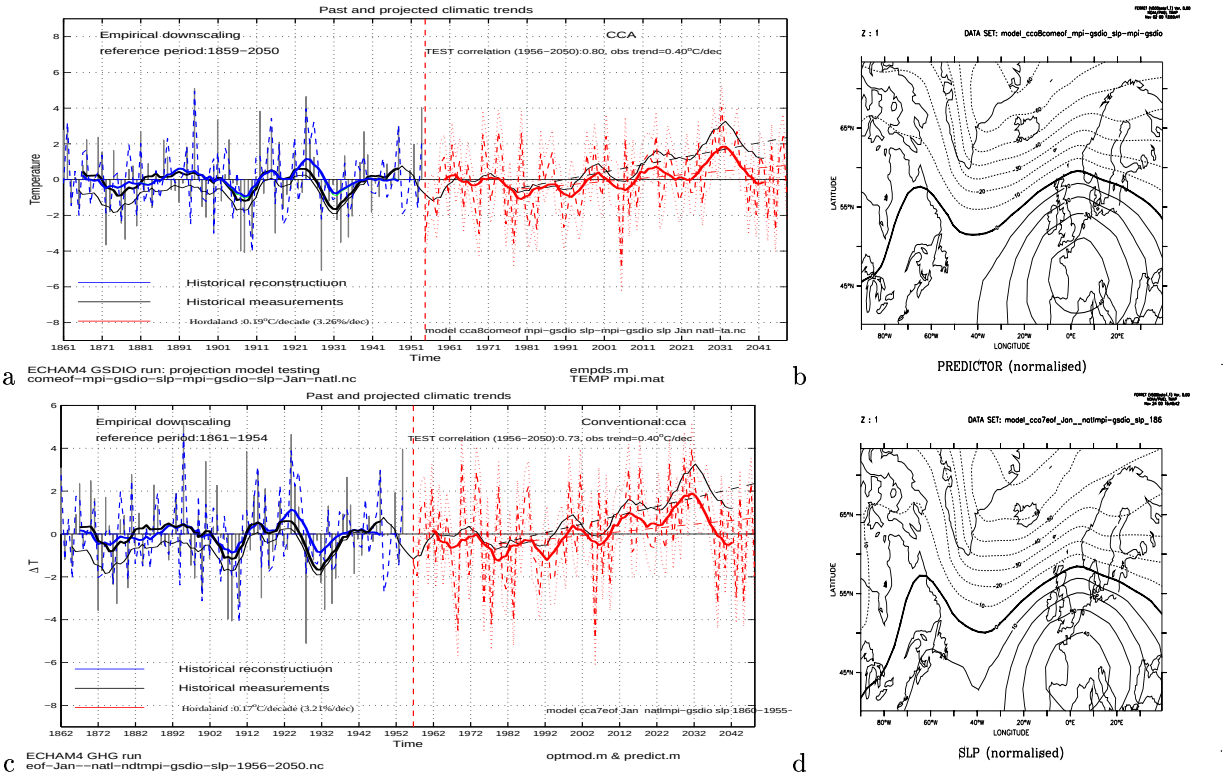

Figure 18: Comparison between a common EOF CCA downscaling model (upper) and a corresponding conventional model (lower) described in *Benestad* (1999c). Both models were calibrated with North Atlantic ECHAM4 GSDIO SLP as predictors and model grid point T(2m) at 60°N,6°E as predictands. The left hand panels show the grid point value (black), the prediction of the dependent data (blue), and the prediction of independent ("future") temperature (red).

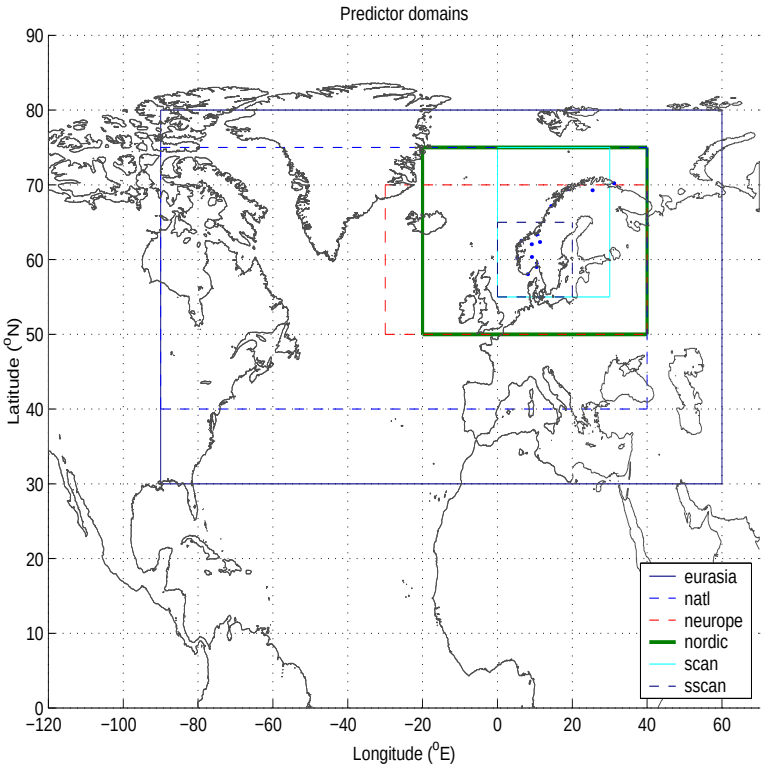

Figure 19: Map showing the various predictor domains

4.0.5 Comparison between correlation skill scores of the common EOF and projection methods.

	T(2m)				SLP			
Location	Jan	Apr	Jul	Oct	Jan	Apr	Jul	Oct
commonEOF								
"Hordaland"	89	83	86	83	80	63	50	55
"Telemark"	89	87	86	85	79	62	46	49
"Møre & R."	87	80	89	79	78	55	61	49
"N. Trøndelag"	91	85	69	75	84	62	31	48
"N. Sweden"	91	85	88	72	78	52	71	47
projection								
"Hordaland"	83	66	86	79	73	59	67	54
"Telemark"	86	72	86	84	71	57	70	55
"Møre & R."	82	57	85	81	69	51	74	48
"N. Trøndelag"	87	65	65	82	69	58	30	51
"N. Sweden"	83	63	85	86	48	48	70	49

Table 4: Pearson correlation skill-scores (%) associated with downscaled scenarios using the domain *natl* (90°W-40°E, 40°N-75°N). The scores were computed for the evaluation period 1956-2050. The downscaling models were calibrated with the ECHAM4 GSDIO T(2m) and SLP fields and 5 different grid-point values between 1860-1955.

4.0.6 The influence of predictor domain size for downscaled trends derived from models calibrated with AOGCM T(2m).

Location	natl	nord	scan	GP	natl	nord	scan	GP
commonEOF								
	January				*April*			
"Hordaland"	0.25	0.27	0.30	**0.40**	0.16	0.21	0.21	**0.20**
"Telemark"	0.33	0.34	0.38	**0.43**	0.20	0.23	0.22	**0.19**
"Møre & R."	0.31	0.38	0.42	**0.44**	0.12	0.18	0.22	**0.19**
"N. Trøndelag"	0.26	0.34	0.40	**0.35**	0.12	0.16	0.22	**0.21**
"N. Sweden"	0.44	0.55	0.64	**0.53**	0.14	0.17	0.25	**0.22**
	July				*October*			
"Hordaland"	0.00	0.06	0.10	**0.05**	0.16	0.20	0.12	**0.14**
"Telemark"	0.01	0.08	0.10	**0.08**	0.22	0.23	0.15	**0.16**
"Møre & R."	-0.04	0.08	0.12	**0.13**	0.21	0.24	0.13	**0.18**
"N. Trøndelag"	-0.01	0.07	0.22	**0.32**	0.12	0.19	0.16	**0.19**
"N. Sweden"	-0.08	0.13	0.19	**0.19**	0.19	0.26	0.20	**0.22**
projection								
	January				*April*			
"Hordaland"	0.32	0.14	0.09	**0.40**	-0.04	0.01	0.07	**0.20**
"Telemark"	0.47	0.22	0.13	**0.43**	-0.05	0.05	0.09	**0.19**
"Møre & R."	0.50	0.24	0.15	**0.44**	-0.06	0.02	0.09	**0.19**
"N. Trøndelag"	0.41	0.23	0.18	**0.35**	-0.06	0.02	0.09	**0.21**
"N Sweden"	0.73	0.42	0.39	**0.53**	-0.09	0.04	0.16	**0.22**
	July				*October*			
"Hordaland"	-0.09	-0.01	0.01	**0.05**	0.20	0.05	-0.05	**0.14**
"Telemark"	-0.07	-0.01	0.01	**0.08**	0.26	0.09	-0.01	**0.16**
"Møre & R."	-0.18	0.04	0.09	**0.13**	0.26	0.03	-0.01	**0.18**
"N. Trøndelag"	-0.18	0.04	0.01	**0.32**	0.21	0.03	0.03	**0.19**
"N Sweden"	-0.25	0.09	0.23	**0.19**	0.30	0.08	0.15	**0.22**

Table 5: Downscaled scenario trends (°C/decade) using the domains: *natl* (90°W-40°E, 40°N-75°N), *nord* (20°W-40°E, 50°N-75°N), and *scan* (0°W-30°E, 55°N-75°N). The downscaling models were calibrated with the ECHAM4 GSDIO T(2m) field and 5 different grid-point values between 1860-1955, and the downscaling prediction was done for 1956-2050. Because model grid point values were used as predictand, the downscaled results could be evaluated directly against a "truth" (GP).

4.0.7 The influence of predictor domain size for downscaled trends derived from models calibrated with AOGCM SLP.

Location	natl	nord	scan	GP	natl	nord	scan	GP
commonEOF								
	January				*April*			
"Hordaland"	0.19	0.23	0.22	**0.40**	0.05	0.02	0.02	**0.20**
"Telemark"	0.25	0.30	0.28	**0.43**	0.05	0.02	0.02	**0.19**
"Møre & R."	0.26	0.32	0.30	**0.44**	0.05	0.02	0.02	**0.19**
"N. Trøndelag"	0.22	0.27	0.26	**0.35**	0.05	0.02	0.03	**0.21**
"N. Sweden"	0.37	0.44	0.41	**0.53**	0.06	0.02	0.03	**0.22**
	July				*October*			
"Hordaland"	-0.06	-0.12	-0.13	**0.05**	-0.05	-0.03	-0.01	**0.14**
"Telemark"	-0.06	-0.13	-0.13	**0.08**	-0.05	-0.04	-0.02	**0.16**
"Møre & R."	-0.05	-0.13	-0.15	**0.13**	-0.06	-0.04	-0.02	**0.18**
"N. Trøndelag"	-0.02	-0.02	-0.03	**0.32**	-0.06	-0.03	0.00	**0.19**
"N. Sweden"	-0.04	-0.10	-0.14	**0.19**	-0.08	-0.07	-0.02	**0.22**
projection								
	January				*April*			
"Hordaland"	0.17	0.21	0.25	**0.40**	0.05	0.03	-0.03	**0.20**
"Telemark"	0.22	0.29	0.31	**0.43**	0.04	0.03	-0.05	**0.19**
"Møre & R."	0.21	0.29	0.38	**0.44**	0.05	0.02	-0.04	**0.19**
"N. Trøndelag"	0.16	0.25	0.34	**0.35**	0.05	0.03	-0.03	**0.21**
"N Sweden"	0.25	0.42	0.47	**0.53**	0.06	0.00	-0.04	**0.22**
	July				*October*			
"Hordaland"	-0.07	-0.23	-0.23	**0.05**	0.01	-0.08	-0.12	**0.14**
"Telemark"	-0.08	-0.26	-0.25	**0.08**	0.03	-0.08	-0.11	**0.16**
"Møre & R."	-0.04	-0.31	-0.41	**0.13**	0.01	-0.09	-0.12	**0.18**
"N. Trøndelag"	0.00	-0.12	-0.14	**0.32**	0.02	-0.11	-0.18	**0.19**
"N Sweden"	-0.02	0.00	-0.53	**0.19**	0.02	0.00	-0.23	**0.22**

Table 6: Downscaled scenario trends (°C/decade) using the domains: *natl* (90°W-40°E, 40°N-75°N), *nord* (20°W-40°E, 50°N-75°N), and *scan* (0°W-30°E, 55°N-75°N). The downscaling models were calibrated with the ECHAM4 GSDIO SLP field and 5 different grid-point values between 1860-1955, and the downscaling prediction was done for 1956-2050. Because model grid point values were used as predictand, the downscaled results could be evaluated directly against a "truth" (GP).

(*Benestad*, 1999c) (lower panels), using SLP and T(2m) as predictors respectively. These tests were made using model temperature from a few grid points as predictands and large-scale field from the same model results as predictors, adopting a similar strategy as described by *Murphy* (2000).

The left hand panels of Figure 18 and 17 show the predicted time series for the Norwegian west coast (red showing the prediction of the independent data and blue for the dependent data) and the true "observed" grid point values (black). The right panels show the predictor patterns.

The empirical model strategy adopted here is different to the empirical modeling described in *Hanssen-Bauer* (2000), whose regression model was calibrated on *historical observations* instead of the *GSDIO* results. The calibration data used in this study were also *detrended* before being used for model training, and the calibration period was 1860 to 1955, and the subsequent data (1956-2050) were used for model validation.

The test results of the common EOF method based on T(2m) obtained slightly higher scores than the conventional model for most of the months (Table 4, colons 2-5), except for 3 grid points during October ("Møre & Romsdal", "N. Trøndelag", and "N. Sweden").

A corresponding comparison for the SLP-based models suggests that the common EOF method achieves lower correlation scores for 3 grids ("Hordaland", "Telemark" and "Møre & Romsdal") in July and at 4 locations ("Telemark", "N. Trøndelag", "Møre & Romsdal", and "N. Sweden") in October (Table 4, columns 8-9).

The two sets of EOFs for the conventional approach were estimated for the non-overlapping data intervals 1860-1955 and 1956-2050, where both the calibration and the prediction predictors were computed over the same spatial domain.

As the model simulations appear to become more uncertain with lower spatial scales (*Grotch & MacCracken*, 1991), one may argue that the predictor domains ought to be sufficiently extensive so that the largest scales are captured. On the other hand, the larger the domain sizes, the higher demand on the realism of the model results as well as the observational data quality.

A set sensitivity test was carried out in order to see how sensible the downscaling results are to differences in the predictor domain size (see Fig 19 for the different domains). It is rarely stated explicitly in the literature why a particular domain size has been chosen (eg *von Storch* et al. (1993), *Murphy* (1999), *Goodess & Palutikof* (1998), *Zorita* et al. (1995), *Kidson & Thompson* (1998), *Crane & Hewitson* (1998), *Zorita & von Storch* (1999), *Schubert* (1998), and *Benestad* (1999c)) and if so (*Heyen* et al., 1996), it is rarely supported by analysis that demonstrates that the chosen size is the optimal one. Often, the reader must assume that the predictor domain is dictated by the availability of observational data, and one may get the impression that the particular choice of the predictor region does not matter. These sensitivity experiments were therefore designed to test this assumption.

Table 5 shows the results from the sensitivity tests, both for the common EOF method and the projection method. It is evident that the common EOF estimates are relatively robust for January and April with respect to predictor domain, albeit with some differences that can be attributed to sampling fluctuations. The downscaled results for the grid point representing "Hordaland" tend to be lower in January than the actual value and those for northern Scandinavia

tend to be overestimated. The smaller predictor domain tends to be associated with the highest trend estimate. In July, on the other hand, there are substantial differences between the results based on the largest and smallest domain sizes. There is less systematic variation in the trend estimate with domain size for October.

These results must be seen in conjunction with the interpolated trends directly from the EOF filtered AOGCM shown in Table 2. The estimated tends for the AOGCM grid point temperatures are higher than the interpolated values after an EOF transformation. As the transform to EOFs tend to affect the local trend estimates, it will also affect the empirically downscaled results.

The conventional projection models tend to give higher trend estimates with larger predictor domain sizes. One explanation for the difference between the two approaches may be that the EOFs from the calibration period do not span the same space as those from the evaluation period. A regression with fewer data (grid) points may increasingly constrain the best-fit to near-zero values. Furthermore, the projection model results appear to be more sensitive to the choice of predictor domain.

These test results can be used to reject the hypothesis that the downscaled results are insensitive to the predictor domain size. Furthermore, the comparison between the two methods gives similar findings, and a remarkable feature for *both* methods is that they suggest zero or *negative* trends for the July month when the downscaling is based on the largest domain category. The corresponding grid point values indicate warming, which corresponds better with those results derived from predictors covering smaller area. There are also dramatic differences in the trend of the neighbouring grid points (Table 5), where "N. Trøndelag" suggests a warming of 0.32°C/decade whereas "Møre & Romsdal" and "N. Sweden" only indicate 0.13°C/decade and 0.19°C/decade respectively. This difference in grid-point response may suggest that the small-scale T(2m) field is changing, altering the relationship between the large-scale anomaly structures and local climate fluctuations (i.e. a non-stationary relationship).

An interesting observation is that there is greater spread in the warming between the adjacent model grid points during summer and winter months than in spring and autumn.

Hanssen-Bauer (2000) indicated that less than 75% of the projected long-term January warming over western Norway can be accounted for by the changes in the SLP, which is good agreement with the findings in this study (Table 6). Furthermore, the results for April in Table 6 are consistent with the findings in *Benestad* (2000c), who could not explain the long-term spring-time warming in the transient ECHAM4 *GHG* integration (greenhouse gases, but no aerosols) in terms of changes in the large-scale circulation (500hPa geopotential height, Φ_{500}). Figure 18 and the results in Table 6 show, however, that 55-77% of the winter-time warming in the AOGCM results is associated with changes in the large-scale atmospheric circulation pattern. The empirical model used by *Benestad* (2000c) was calibrated on historical observations, as opposed to AOGCM results used in this study, and adopted the projection strategy.

The two types of empirically downscaled results in Figure 17 and 18 are nevertheless similar. The temperature anomalies on the west coast of Norway are associated with the NAO dipole structures in both the T(2m) and SLP-based empirical models (Figure 17b,d and 18b,d). The predictor patterns for the common EOF model (b) and the conventional model (d) differ only in

4.2.1 Test of stationarity for linear relationship between large and small scales

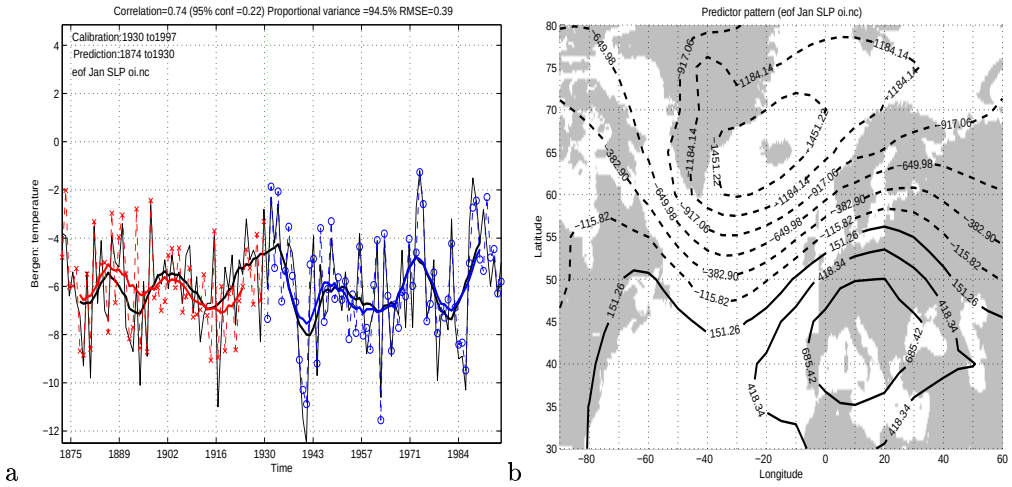

Figure 20: Investigation of the stationarity for the relation between large scale pressure patterns and local temperatures. This figure shows the predicted January temperature for Bergen-Florida over an independent period (red), and the best-fit for the calibration period (blue). The black curve shows the observations (corrected for inhomogeneities, Ø. Nordli, personal communication), and the thick lines give the 10-year low-passed values.

detail, and part of the differences between the two predictions may have been introduced at the pattern matching stage in applying the projection model.

The similarity between the results of the two downscaling approaches gives confidence to these downscaling methods. Furthermore, the presence of the NAO in predictor patterns of both the T(2m) and SLP fields (Figs 17b,d and 18b,d) suggests that the results are based on physically meaningful models.

4.1 Skill scores for common EOF downscaling models

In addition to assessing how well linear empirical models can reproduce the simulated local (grid box) climate variations from large-scale model circulation patterns, it is important to know how well these models can describe the variations in the *observed* local climate, given observed large-scale climatic anomalies. Such an assessment could be made in a similar fashion as for the AOGCM data, but due to short time series, a cross-validation analysis has been chosen here to test the skill of the empirical models.

4.2 Non-stationarity tests

Figure 20a shows the predictions of Bergen January temperatures from 1873-1930, based on a simple empirical regression model calibrated with the *Benestad* (2000a) SLP and Bergen temperatures over the period 1930-1997. Although this model is simpler than those employed in our study, the method is similar, and these results demonstrate that the empirical relationships have been approxi-

4.1.1 Downscaling temperature prediction scores for various locations in Norway

Location & experiment	Jan score r (%)	Apr score r (%)	Jul score r (%)	Oct score r (%)
T(2m)				
Oksøy	88,90,91	64,71,73	70,80,82	88,87,88
Ferder	87,90,91	63,72,73	74,86,87	87,86,86
Oslo	87,87,88	63,79,83	73,80,82	85,85,86
Nesbyen	81,80,83	59,71,74	71,76,79	73,74,74
Bergen	87,87,85	62,70,76	63,77,80	76,82,82
Ona	82,80,87	70,74,76	74,73,76	81,85,83
Dombås	79,80,82	64,76,84	72,81,83	80,87,88
Røros	75,76,78	64,74,81	80,85,89	80,87,88
Trondheim	82,83,86	74,80,85	76,78,85	84,87,88
Bodø	73,83,86	58,80,85	72,78,79	84,87,87
Tromsø	79,88,89	69,80,85	67,78,81	82,84,84
Karasjok	75,83,85	70,86,86	82,87,88	80,80,85
Vardø	77,77,80	78,85,83	68,82,77	82,84,84
SLP				
Oksøy	88,87,86	52,52,51	79,74,79	64,73,71
Ferder	86,85,85	49,49,49	78,71,73	69,75,74
Oslo	81,83,82	51,55,52	78,73,70	67,72,71
Nesbyen	76,79,79	61,55,56	74,73,72	54,62,59
Bergen	86,84,81	64,63,63	82,80,81	71,73,71
Ona	85,81,84	69,69,71	62,65,65	77,77,77
Dombås	83,79,80	62,57,59	78,74,75	66,71,73
Røros	81,75,76	57,57,60	81,77,78	67,72,75
Trondheim	85,80,84	53,68,68	82,82,84	74,79,79
Bodø	84,84,86	68,72,72	80,81,81	80,79,82
Tromsø	74,81,81	74,78,74	83,82,84	80,78,80
Karasjok	76,78,74	71,61,62	77,77,78	74,72,74
Vardø	59,58,54	73,70,73	60,60,63	71,69,73

Table 7: Cross-validation scores associated with empirical predictions for near-surface temperature based on analysis of historical data (*Benestad*, 2000a). The blank rows indicate which predictands (stations) were grouped together in the various regional models. The scores are for the *natl,nordic,scan* predictor domains.

4.1.2 Downscaling precipitation prediction scores for various locations in Norway

Location & experiment	Jan score r (%)	Apr score r (%)	Jul score r (%)	Oct score r (%)
Halden	72,72,75	65,65,65	59,64,63	74,76,77
Moss	69,74,76	62,60,64	57,61,66	68,73,73
Oslo	70,77,79	67,66,70	60,61,61	69,74,74
Røros	56,58,59	31,35,38	33,34,37	30,56,54
Skjåk	74,74,73	16,20,19	57,59,58	47,56,49
Norddal	85,85,85	73,78,77	30,22,46	77,81,80
Verma	81,81,82	69,76,76	37,43,48	71,72,73
Hemne	84,86,84	80,81,82	55,57,58	80,82,82
Namdalseid	84,89,87	74,74,74	44,47,56	78,80,81
Dunderlandsdal	81,80,85	62,68,71	40,47,46	73,77,78
Sulitjelma	80,84,78	53,59,56	66,66,73	66,60,66
Barkestad	71,77,77	63,71,69	68,73,74	67,72,77
Tromsø	79,84,84	54,73,75	50,51,59	71,78,75
Geilo	63,67,65	43,35,48	69,69,71	54,62,60
Bjåen	83,83,82	50,54,54	53,54,64	73,74,73
Sviland	80,86,85	76,75,80	54,65,70	87,89,89
Bergen	85,87,87	74,80,83	66,74,76	81,85,87
Lavik	87,86,85	72,78,80	69,73,74	77,79,82

Table 8: Cross-validation scores associated with empirical predictions for near-surface temperature based on common EOF analysis of historical data (*Benestad*, 2000a) and the GSDIO SLP fields. The horizontal lines indicate which predictands (stations) were grouped together in the various regional models. The scores are for the *natl,nordic,scan* predictor domains.

4.1.3 ANOVA statistics associated with the projection of model EOFs onto observed modes: ECHAM4 GSDIO and *Benestad* (2000a) data.

Location & experiment	Jan score R^2 (%)	Apr score R^2 (%)	Jul score R^2 (%)	Oct score R^2 (%)
T(2m)				
EOF 1	91,99,100	92,96,96	67,70,72	87,98,98
EOF 2	91,99,99	91,97,98	68,84,94	70,87,96
EOF 3	82,98,91	70,86,92	52,80,95	89,92,95
EOF 4	83,97,94	89,99,98	60,91,96	65,95,97
EOF 5	78,96,81	67,87,86	36,89,98	66,80,92
EOF 6	84,94,99	78,86,92	45,85,84	65,90,97
EOF 7	57,97,88	67,87,80	52,68,93	64,93,97
EOF 8	46,98,75	44,94,93	43,84,93	57,91,98
EOF 9	52,91,98	31,76,94	51,88,91	46,86,81
EOF 10	35,96,90	41,78,83	49,93,89	23,87,90
SLP				
EOF 1	99,99,98	98,97,98	98,98,99	98,98,99
EOF 2	96,99,99	96,100,99	95,100,100	98,99,99
EOF 3	96,98,98	97,99,98	98,99,100	98,99,100
EOF 4	90,97,99	91,95,96	93,99,98	96,98,99
EOF 5	81,96,98	87,99,100	92,97,98	90,96,96
EOF 6	91,94,96	90,94,99	89,97,99	84,95,99
EOF 7	86,97,100	90,97,100	80,100,98	84,97,96
EOF 8	87,98,99	84,96,93	77,99,97	86,99,99
EOF 9	83,91,94	74,94,99	54,94,85	80,98,94
EOF 10	70,96,96	82,92,96	81,96,100	76,95,96

Table 9: Statistics showing goodness-of-fit between anomalous model and observed spatial T(2m) distributions. The model data have been interpolated onto the observed grid using a cubic spline scheme. Data points with missing value have been ignored. The results are shown for the *natl,nordic,scan* domains.

4.1.4 The variance associated with the 4 leading common EOFs of the combined ECHAM4 GSDIO and *Benestad* (2000a) data.

Location & experiment	Jan score (%)	Apr score (%)	Jul score (%)	Oct score (%)
T(2m)				
cEOF 1	27,54,69	24,48,58	28,36,56	27,47,66
cEOF 2	22,18,15	20,18,22	10,16,13	15,18,15
cEOF 3	12,10,07	11,12,06	08,12,09	11,11,07
cEOF 4	08,05,03	10,06,05	07,08,07	09,08,05
sum	*69,87,94*	*65,84,91*	*54,72,85*	*62,84,93*
SLP				
cEOF 1	32,44,68	29,35,61	24,41,62	32,44,68
cEOF 2	22,31,22	19,30,24	18,24,23	22,31,22
cEOF 3	17,15,07	13,20,10	12,16,09	17,15,07
cEOF 4	10,04,01	11,06,02	10,06,02	10,04,01
sum	*81,94,98*	*72,91,97*	*64,87,96*	*52,94,98*

Table 10: The variance of the leading 4 common EOFs of *Benestad* (2000a) T(2m) and SLP and the corresponding ECHAM4 GSDIO results. The results are shown for the *natl,nordic,scan* domains.

4.2.2 Test of stationarity for linear relationship between large and small scales

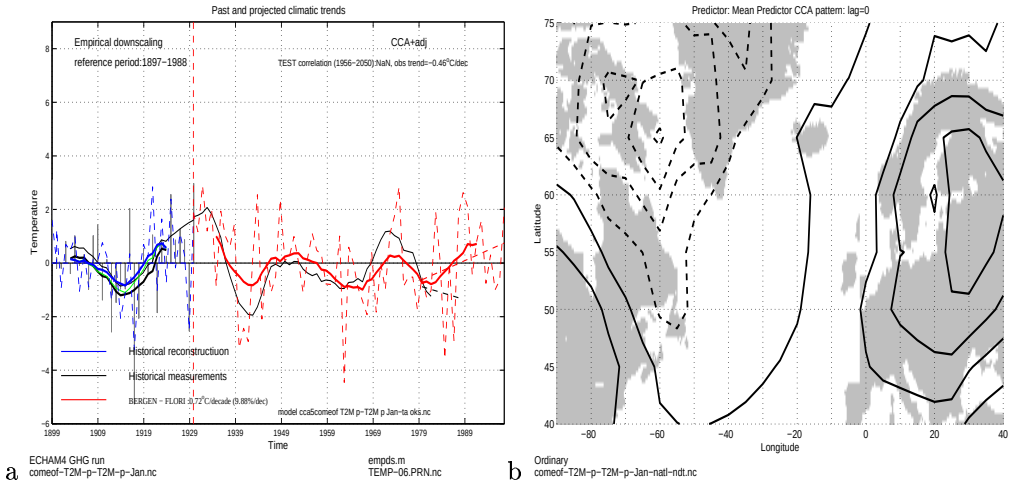

Figure 21: Investigation of the stationarity for the relation between large scale 2-meter temperature patterns and local temperatures. This figure shows the predicted January temperature for Bergen-Florida over an independent period (red), and the best-fit for the calibration period (blue). The black curve shows the observations (corrected for inhomogeneities, Ø. Nordli, personal communication), and the thick lines give the 10-year low-passed values.

mately stationary over the past 120 years. It is important to note that whereas the relationship between the large-scale circulation and Bergen temperature has been near-stationary, there is no guarantee that this is so for other locations.

The predictor pattern in Figure 20b is similar to the leading CCA patterns associated with the predictions described in this report, all which contain a strong signature of the NAO. *Benestad* (2000a) tested the empirical models discussed in this report and demonstrated that these also gave good results. Figure 21 shows the validation results of the same type of downscaling models using the T(2m) field as predictor.

Tables 7 and 8 show the cross-validation skill scores for these empirical models for three different domain sizes. The stations close together were grouped together as shown in the Tables (each group separated by blank line).

The scores of the downscaled temperature indicate high skill during January, July, and October, and slightly lower skill in April if the predictor is the large-scale temperature field. The spring time temperatures may be difficult to relate to large-scale anomalies if local snow-melting has a strong influence on the local climate. As expected, the skill scores tend to improve with smaller predictor size. Some exceptions to this rule can be seen for SLP-based downscaling models. The scores for Bergen and Ona tend to be higher in January when using the *natl* domain than the smaller domains, probably a consequence of the strong influence of the NAO. The models using larger domain sizes may possibly pick up the NAO signal better than those that focus more on Norway. The skill scores for the SLP models are highest in January, and lowest in April in southern Norway, but there is little difference between the seasons in the north.

The downscaling models for precipitation (Table 8) tend to be associated with lower scores than those predicting temperature, except for at the Norwegian west coast. The stations in the inland mountainous regions (Røros, Skjåk, Geilo) tend to have low scores, but stations Hemne, Namdalseid, Dunderlandsdal also have poor scores in July.

The stations Røros, Skjåk, Norddal, and Verma were grouped together in Table 8, but their scores are substantially different and may suggest that there should be separate regional models for Røros and Skjåk and for Norddal, and Verma.

As with the temperature downscaling models, the analysis for precipitation suggests that the models with smaller domains tend to give a better reproduction of the local climate variations. But, there is no clear systematic relationship between the domain size and the correlation score.

Table 9 shows the ANOVA type R^2 statistics for the regressional analysis between the simulated and observed T(2m) and SLP predictor fields. High values (100) indicate good match and that the model reproduces the observed geographical distribution of temperature or SLP. The regression for SLP fields indicate high AOGCM skill for all months, but the results for T(2m) suggest that ECHAM4 is less able to reproduce the observed temperature distribution. It is particularly in July that the R^2 scores are low, which is also the time when the downscaling models produce cooling when using the largest predictor domain. The smaller predictor domain tends to yield better match with the observations, but there are exceptions to this rule (eg T(2m): Jan EOF 3-5, SLP: Jan EOF 1). This shortcoming is partly related to the crude representation of the topography and land-sea mask in the model (Fig 1).

Another way of judging the skill of the model simulations is to check the

variance accounted for by the leading common EOFs (*Sengupta & Boyle*, 1993). If the spatial patterns are similar in the model simulations and the observations, then these can be described by a few common modes with high variance (assuming that most of the climate variability can be captured by a few normal modes). If, on the other hand, they are different, then twice as many EOFs are needed, and the variance is spread among more modes and the common EOFs are paired together with modes associated with similar variance.

Table 10 shows that the four leading EOFs account for more than 50% of the variance of the T(2m) and SLP fields in all seasons. The two leading T(2m) EOFs of the largest domain size (*natl*) account for similar amount of variance in April (24 and 20% of the variance), and are close to being degenerate according to *North* et al. (1982). Thus, there may be potential problems using the *natl* domain for downscaling based on T(2m) as this degeneracy may reflect differences between the simulated and observed spatial T(2m) structure. The variance of the common EOFs for the *natl* region is also spread over several modes in July for T(2m) and October for SLP. This again, may be a sign of a poor match between model and observed data, although there are no definite criteria for what is good and what is bad in terms of EOF variances. For the smallest domains, the EOFs are well separated, both for the T(2m) and SLP fields. It is clear that the model reproduces most of the observed spatial structure when the predictor domain is reduced to the *scan* region.

Grotch & MacCracken (1991) suggested that results from climate simulations tend to be uncertain on spatial scales smaller than sub-continental, which implies that downscaling models should aim at using as large domain sizes as possible. Thus, one should select the largest domain size that is associated with a high skill-score.

5 Temperature scenarios based on empirical downscaling of AOGCM results

5.1 Downscaling by common EOFs based on ECHAM4 GSDIO integrations

The sensitivity of the downscaled GSDIO scenarios on the domain size was investigated by making a series of downscaling experiments based on various domain sizes. The results of these tests are shown in Tables 11 to 14 for the January, April, July and October months respectively. The tests were carried out for both the common EOF method and the conventional projection approach.

Results from tests using both the common EOF and the projection method are shown in Table 11. The scenarios calculating the common EOF methods and the largest domain size (*eurasia*) are substantially smaller than those based on smaller domain size. There is much smaller difference between the scenarios of the largest domains when using the projection approach. Both model types give similar results for the *natl* domain size, but whereas the common EOF estimates tend to increase as the predictor domain is reduced, the projection systematically predicts lower trends as the analyses focuses on smaller predictor area. This result is problematic as the projection models do not seem to converge towards the grid-point values. The problem may be that with fewer degrees of freedom associated with the smaller domain size there is greater risk for the "model" EOFs not to span the "observed EOFs".

Figure 22a shows a downscaled January temperature scenario (red curve) for Oslo and panel b gives the large-scale temperature anomalies associate with variations in the Oslo temperature. The black line shows the observed January temperature in Oslo and the blue curve shows the cross-validation results for the empirical model. The blue and the black curves are similar, suggesting that the model can describe most of the variations in the Oslo January temperature in terms of the temperature anomaly shown in Figure 22b.

The maps in Figure 22b and d show T(2m) anomalies which are associated with high temperature in Oslo during January and July respectively. The projected winter warming is associated with temperature anomalies further east, whereas in July, the temperature anomalies in Oslo are more local. Figure 22 shows how the future climatic trends are estimated: least-squares fit over the 70-year period 1980-2049. The warming rate is estimated from the trend and is shown in the left panels.

There are substantial interannual and decadal variations in the temperature which result in high uncertainties in the trend estimates.

During January, the domain sizes smaller than 30°W-40°E, 50°N-70°N (*neur*, northern Europe) give similar estimates for Oslo, Nesbyen, Ferder, Oksøy Bodø Tromsø Karasjok and Vardø, indicating that these results are robust within this domain range. The downscaled temperature trends for the west coast have slightly lower estimates for the *neur* domain, but give robust answers for domain sizes smaller than 20°W-40°E, 50°N-75°N (*nord*, the Nordic countries). It is expected that the trend estimates will converge to the interpolated grid-point values (shown in column 8 of Tables 11 to 14) as the predictor area is reduced further.

Some of the difference between different warming rates associated with dif-

5.1.1 The influence of predictor domain size for downscaled January T(2m) scenarios

Location	euras	natl	neur	nord	scan	sscan	grid-point
cEOF							
OSLO	0.18	0.56	0.63	0.57	0.54	0.55	20-27
NESBYEN	0.18	0.71	0.90	0.84	0.75	0.79	19-27
FERDER	0.18	0.43	0.53	0.55	0.44	0.52	19-26
OKSØY	0.12	0.39	0.51	0.51	0.41	0.47	14-20
BERGEN	0.04	0.26	0.42	0.45	0.35	0.44	14-22
ONA	0.01	0.11	0.29	0.29	0.23	0.31	15-21
RØROS	0.42	0.74	0.74	0.62	0.63	0.75	21-30
DOMBÅS	0.33	0.62	0.63	0.53	0.54	0.61	19-26
VÆRNES	0.19	0.54	0.57	0.42	0.47	0.53	19-27
BODØ	-0.01	0.12	0.45	0.34	0.37	0.44	24-27
TROMSØ	0.04	0.17	0.42	0.36	0.37	0.38	29-30
KARASJOK	0.34	0.50	0.94	0.84	0.93	0.87	36-37
VARDØ	0.16	0.22	0.37	0.36	0.36	0.33	29-31
Projection							
OSLO	0.59	0.54	0.35	0.17	0.29	0.39	20-27
NESBYEN	1.02	0.74	0.44	0.12	0.38	0.68	19-27
FERDER	0.45	0.50	0.32	0.12	0.25	0.40	19-26
OKSØY	0.40	0.49	0.28	0.07	0.21	0.36	14-20
BERGEN	0.34	0.36	0.23	0.17	0.14	0.21	14-22
ONA	0.19	0.23	0.18	0.14	0.14	0.15	15-21
RØROS	0.58	0.58	0.49	0.19	0.48	0.71	21-30
DOMBÅS	0.50	0.52	0.41	0.17	0.40	0.57	19-26
VÆRNES	0.31	0.44	0.37	0.17	0.40	0.50	19-27
BODØ	0.23	0.34	0.37	0.34	0.36	0.20	24-27
TROMSØ	0.36	0.30	0.30	0.29	0.31	0.10	29-30
KARASJOK	0.93	0.70	0.80	0.83	0.72	0.09	36-37
VARDØ	0.33	0.30	0.23	0.35	0.24	-0.05	29-31

Table 11: Downscaled temperature scenario trends (°C/decade) using the domains: *euras* (90°W-90°E, 20°N-80°N), *natl* (90°W-40°E, 40°N-75°N), *neur* (30°W-40°E, 50°N-70°N), *nord* (20°W-40°E, 50°N-75°N),*scan* (0°W-30°E, 55°N-75°N), and *sscan* (0°W-20°E, 55°N-65°N). The results shown are for the common EOF method (cEOF) and the conventional projection method. The grid-point value range were estimated after filtering the AOGCM results through different sets of EOFs over the 3 domains: *scan*, *nordic*, and *natl* (Table 2). Length of interval= 70 years. Dates 15-Jan-1980 - 15-Jan-2049.

5.1.2 The influence of predictor domain size for downscaled April T(2m) scenarios

Location	euras	natl	neur	nord	scan	sscan	grid-point
cEOF							
OSLO	0.14	0.12	0.24	0.26	0.23	0.26	12-17
NESBYEN	0.17	0.10	0.20	0.23	0.20	0.22	12-16
FERDER	0.13	0.12	0.20	0.22	0.19	0.18	12-17
OKSØY	0.13	0.11	0.19	0.21	0.18	0.16	12-14
BERGEN	0.05	0.11	0.13	0.08	0.20	0.28	12-13
ONA	0.03	0.10	0.11	0.02	0.14	0.19	10-12
RØROS	0.09	0.14	0.05	0.10	0.30	0.29	10-16
DOMBÅS	0.07	0.12	0.05	0.10	0.27	0.29	11-14
VÆRNES	0.09	0.13	0.03	0.03	0.25	0.28	09-14
BODØ	0.13	0.12	-0.01	-0.01	0.19	0.19	10-13
TROMSØ	0.13	0.12	0.00	0.01	0.21	0.18	13-15
KARASJOK	0.09	0.16	0.26	0.00	0.21	0.22	14-16
VARDØ	0.08	0.11	0.18	0.06	0.14	0.11	17
Projection							
OSLO	0.07	-0.05	0.02	0.03	0.15	0.12	12-17
NESBYEN	0.08	-0.04	0.00	0.02	0.14	0.15	12-16
FERDER	0.13	-0.04	0.06	0.10	0.16	0.12	12-17
OKSØY	0.12	-0.03	0.05	0.08	0.15	0.12	12-14
BERGEN	-0.01	-0.14	-0.10	-0.15	-0.08	0.04	12-13
ONA	0.03	-0.14	-0.03	-0.06	-0.02	0.06	10-12
RØROS	0.14	-0.09	-0.00	-0.02	0.18	0.17	10-16
DOMBÅS	0.08	-0.07	-0.06	-0.08	0.13	0.17	11-14
VÆRNES	0.12	-0.08	0.00	-0.03	0.15	0.10	09-14
BODØ	0.16	-0.11	0.11	0.05	0.02	0.11	10-13
TROMSØ	0.23	-0.12	0.11	0.05	0.04	0.09	13-15
KARASJOK	0.34	-0.05	0.34	0.17	0.28	0.30	14-16
VARDØ	0.30	-0.02	0.25	0.15	0.16	0.15	17

Table 12: Downscaled temperature scenario trends (°C/decade) using the domains: *euras* (90°W-90°E, 20°N-80°N), *natl* (90°W-40°E, 40°N-75°N), *neur* (30°W-40°E, 50°N-70°N), *nord* (20°W-40°E, 50°N-75°N),*scan* (0°W-30°E, 55°N-75°N), and *sscan* (0°W-20°E, 55°N-65°N). The grid-point value range were estimated after filtering the AOGCM results through different sets of EOFs over the 3 domains: *scan*, *nordic*, and *natl* (Table 2). Length of interval= 70. Dates 15-Apr-1980 - 15-Apr-2049.

5.1.3 The influence of predictor domain size for downscaled July T(2m) scenarios

Location	euras	natl	neur	nord	scan	ssca	grid-point
cEOF							
OSLO	0.24	0.40	0.17	0.37	0.21	0.27	03-06
NESBYEN	0.21	0.32	0.15	0.30	0.18	0.21	02-06
FERDER	0.16	0.34	0.14	0.33	0.20	0.25	05-06
OKSØY	0.21	0.33	0.16	0.32	0.20	0.24	06
BERGEN	0.01	0.05	0.12	0.19	0.17	0.19	02-07
ONA	-0.01	0.04	0.04	0.14	0.13	0.12	06-10
RØROS	0.03	0.01	0.29	0.28	0.15	0.22	04-09
DOMBÅS	0.05	0.01	0.25	0.27	0.17	0.19	02-08
VÆRNES	0.01	-0.04	0.22	0.22	0.11	0.20	07-11
BODØ	-0.05	-0.02	0.02	0.08	0.20	0.32	07-11
TROMSØ	-0.01	-0.03	-0.03	0.02	0.21	0.29	07-13
KARASJOK	-0.07	0.00	0.02	0.27	0.12	0.17	11-18
VARDØ	-0.02	0.01	-0.02	0.22	0.05	0.05	16-20
Projection							
OSLO	-0.37	0.16	0.03	-0.07	0.08	0.12	03-06
NESBYEN	-0.24	0.17	0.03	-0.07	0.04	0.12	02-06
FERDER	-0.32	0.06	0.04	-0.04	0.08	0.08	05-06
OKSØY	-0.22	0.02	0.03	-0.02	0.09	0.05	06
BERGEN	-0.23	-0.29	0.21	-0.02	0.10	0.11	02-07
ONA	-0.31	-0.15	0.14	0.13	0.08	0.11	06-10
RØROS	-0.45	-0.12	0.18	0.20	0.22	0.22	04-09
DOMBÅS	-0.34	-0.06	0.09	0.05	0.15	0.20	02-08
VÆRNES	-0.48	-0.23	0.21	0.26	0.27	0.22	07-11
BODØ	-0.62	-0.36	0.36	0.54	0.17	0.28	07-11
TROMSØ	-0.64	-0.31	0.50	0.61	0.26	0.25	07-13
KARASJOK	-0.75	-0.38	0.59	0.73	0.37	0.30	11-18
VARDØ	-0.36	-0.21	0.47	0.48	0.16	0.18	

Table 13: Downscaled temperature scenario trends (°C/decade) using the domains: *euras* (90°W-90°E, 20°N-80°N), *natl* (90°W-40°E, 40°N-75°N), *nord* (20°W-40°E, 50°N-75°N),*scan* (0°W-30°E, 55°N-75°N), and *sscan* (0°W-20°E, 55°N-65°N). (cEOF predictors selected from 40 EOFs). The grid-point value range were estimated after filtering the AOGCM results through different sets of EOFs over the 3 domains: *scan*, *nordic*, and *natl* (Table 2). Length of interval= 70. Dates 15-Jul-1980 - 15-Jul-2049.

5.1.4 The influence of predictor domain size for downscaled October T(2m) scenarios

Location	euras	natl	neur	nord	scan	ssca	grid-point
cEOF							
OSLO	0.10	0.18	0.32	0.27	0.26	0.27	09-15
NESBYEN	0.05	0.16	0.30	0.26	0.25	0.25	08-15
FERDER	0.16	0.19	0.33	0.27	0.25	0.30	09-14
OKSØY	0.10	0.14	0.27	0.23	0.21	0.28	09-13
BERGEN	-0.07	-0.03	-0.03	-0.06	0.11	0.20	07-12
ONA	-0.06	-0.03	-0.04	-0.02	0.10	0.18	06-13
RØROS	0.09	0.13	0.20	0.21	0.31	0.33	07-17
DOMBÅS	0.05	0.09	0.18	0.15	0.27	0.29	07-16
VÆRNES	0.07	0.10	0.14	0.18	0.24	0.29	07-16
BODØ	0.00	0.04	0.07	0.08	0.28	0.09	08-13
TROMSØ	0.05	0.08	0.07	0.11	0.32	0.06	11-14
KARASJOK	0.00	0.20	0.15	0.28	0.36	0.23	16-20
VARDØ	0.11	0.17	0.11	0.17	0.23	0.15	19-24
Projection							
OSLO	0.26	0.64	0.22	0.16	0.23	0.26	09-15
NESBYEN	0.17	0.64	0.20	0.09	0.20	0.25	08-15
FERDER	0.33	0.58	0.19	0.15	0.21	0.22	09-14
OKSØY	0.15	0.47	0.14	0.06	0.16	0.05	09-13
BERGEN	-0.16	0.38	0.09	-0.12	0.05	0.07	07-12
ONA	-0.05	0.39	0.10	-0.06	0.12	0.28	06-13
RØROS	0.21	0.73	0.27	0.13	0.26	0.26	07-17
DOMBÅS	0.05	0.64	0.22	0.04	0.20	0.25	07-16
VÆRNES	0.14	0.62	0.23	0.08	0.24	0.25	07-16
BODØ	0.20	0.68	0.30	0.18	0.26	0.24	08-13
TROMSØ	0.20	0.66	0.29	0.25	0.26	0.57	11-14
KARASJOK	0.65	0.73	0.54	0.54	0.61	0.40	16-20
VARDØ							

Table 14: Downscaled temperature scenario trends (°C/decade) using the domains: *euras* (90°W-90°E, 20°N-80°N), *natl* (90°W-40°E, 40°N-75°N), *nord* (20°W-40°E, 50°N-75°N),*scan* (0°W-30°E, 55°N-75°N), and *sscan* (0°W-20°E, 55°N-65°N). The grid-point value range were estimated after filtering the AOGCM results through different sets of EOFs over the 3 domains: *scan*, *nordic*, and *natl* (Table 2). Length of interval= 70. Dates 15-Oct-1980 - 15-Oct-2049.

5.1.5 Downscaling by of ECHAM4 GSDIO common EOFs based on scan T(2m)

Location	Jan	Feb	Mar	Apr	May	Jun	Jul	Aug	Sep	Oct	Nov	Dec
OSLO	**54**	39	19	**23**	**25**	**18**	**21**	**40**	**20**	**26**	**36**	28
NESBYEN	**75**	47	16	**20**	**21**	**16**	**18**	**33**	**19**	**25**	**43**	34
FERDER	**44**	37	18	**19**	**21**	**19**	**20**	**34**	**19**	**25**	**31**	20
OKSØY	**41**	34	15	**18**	**16**	**15**	**20**	**32**	**19**	**21**	**28**	18
BERGEN	**35**	16	**24**	**20**	**14**	**22**	**17**	**22**	**23**	11	**24**	**20**
ONA	**23**	11	**19**	**14**	**13**	**19**	**13**	**20**	**20**	10	**20**	**21**
RØROS	**63**	36	24	**30**	**17**	**36**	15	**17**	**23**	**31**	**43**	20
DOMBÅS	**54**	31	18	**27**	**16**	**32**	**17**	**21**	**25**	**27**	**37**	15
VÆRNES	**47**	28	19	**25**	**16**	**33**	11	07	**24**	**24**	**35**	13
BODØ	**37**	24	**24**	**19**	06	**34**	20	**17**	**23**	**28**	**27**	22
TROMSØ	**37**	19	**28**	**21**	**16**	**36**	21	**17**	**24**	**32**	**25**	23
KARASJOK	**93**	52	38	**21**	15	**37**	12	**21**	**23**	**36**	**75**	**79**
VARDØ	**36**	**26**	19	**14**	**25**	**17**	05	**19**	**19**	**23**	**33**	**33**

Table 15: Downscaled temperature scenarios (×0.01°C/decade) of the GSDIO results using the common EOF method on the model and *Benestad* (2000b) T(2m). Length of interval= 70 years. Dates 15-Dec-1980 - 15-Dec-2049. The predictor domain was 0°W-30°E, 55°N-75°N. Entries shown in bold are significant at the 5% level.

5.1.6 Trend estimate uncertainties associated with common EOFs downscaling of local temperature based on scan T(2m) fields

Location	Jan	Feb	Mar	Apr	May	Jun	Jul	Aug	Sep	Oct	Nov	Dec
OSLO	93	140	84	50	36	54	46	53	39	46	58	106
NESBYEN	133	181	102	46	32	46	39	43	35	47	77	157
FERDER	94	136	80	43	29	42	42	44	35	43	55	84
OKSØY	83	118	75	40	25	33	38	43	34	39	55	84
BERGEN	82	75	50	46	33	42	40	34	43	38	59	75
ONA	58	57	40	36	23	28	34	33	42	37	48	48
RØROS	139	143	121	65	54	52	61	40	42	59	80	139
DOMBÅS	116	122	101	60	47	48	51	40	42	55	72	111
VÆRNES	107	105	90	54	51	48	67	43	40	52	62	101
BODØ	97	90	57	56	52	50	78	39	46	63	71	88
TROMSØ	82	77	52	51	50	64	89	40	47	64	67	74
KARASJOK	205	171	140	78	68	63	74	47	48	93	112	146
VARDØ	68	66	70	51	37	37	52	35	34	49	42	56

Table 16: Standard deviation of downscaled temperature scenario trends (×0.01°C/decade) of the GSDIO results using the common EOF method on the model and *Benestad* (2000b) T(2m). Length of interval= 70 years. Dates 15-Dec-1980 - 15-Dec-2049. The predictor domain was 0°W-30°E, 55°N-75°N.

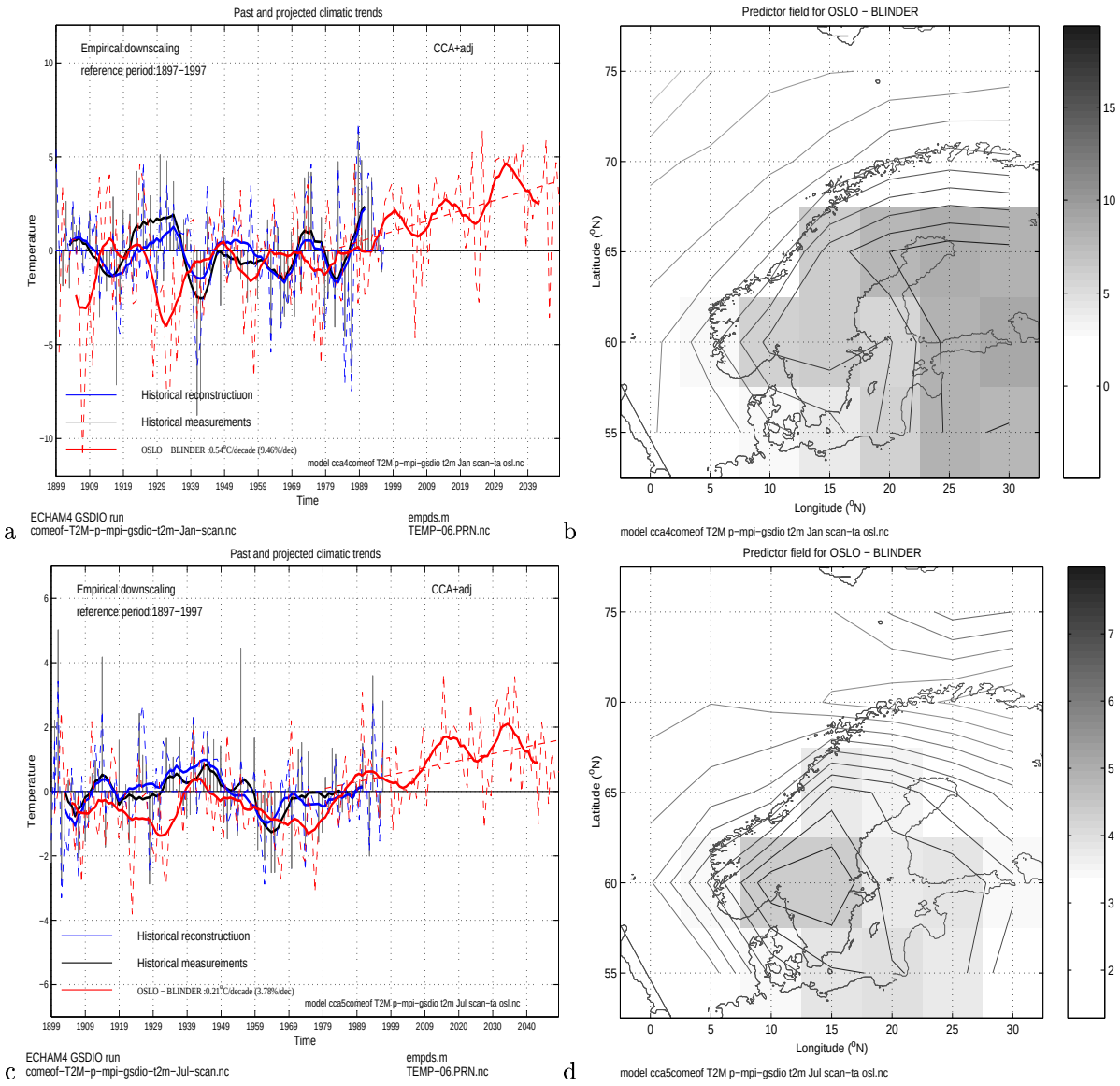

Figure 22: Left: local climate scenario for Oslo based on the ECHAM4 GSDIO integration. The red curve represents the scenario, the black shows the observations, and the blue line shows the results from a cross-validation analysis during model calibration. Right: the large-scale temperature anomaly structure associated with temperature fluctuations in Oslo. Upper panels show the results for January and the lower panels for July.

5.1.7 Evaluation of the spatial correlation during months when the downscaled trends suggest cooling

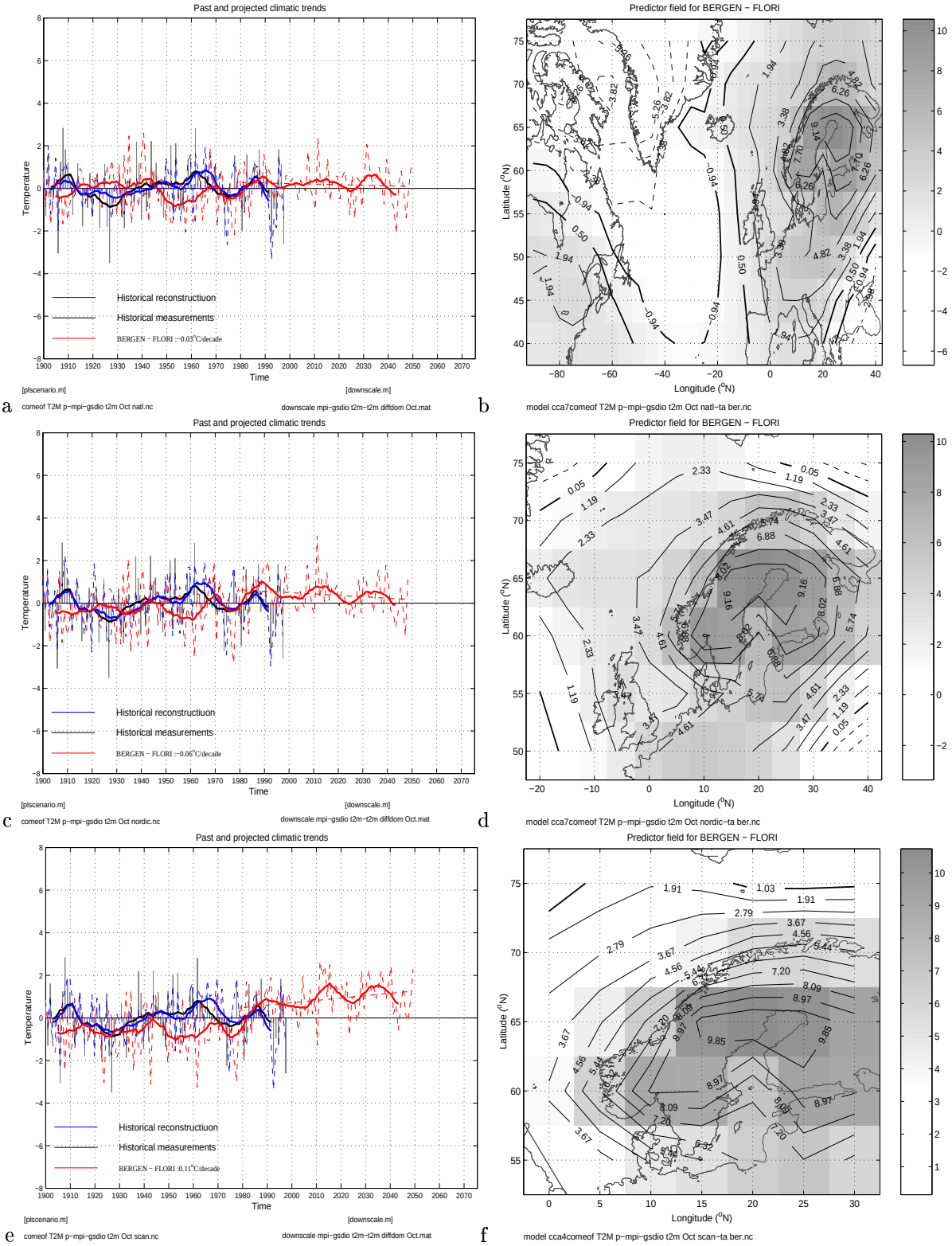

Figure 23: October T(2m) scenarios for Bergen (left) based on different predictor domains (left) from ECHAM4 GSDIO. The red line shows the the downscaled scenario, blue line represents cross-validation results, and the black shows the observations for Bergen.

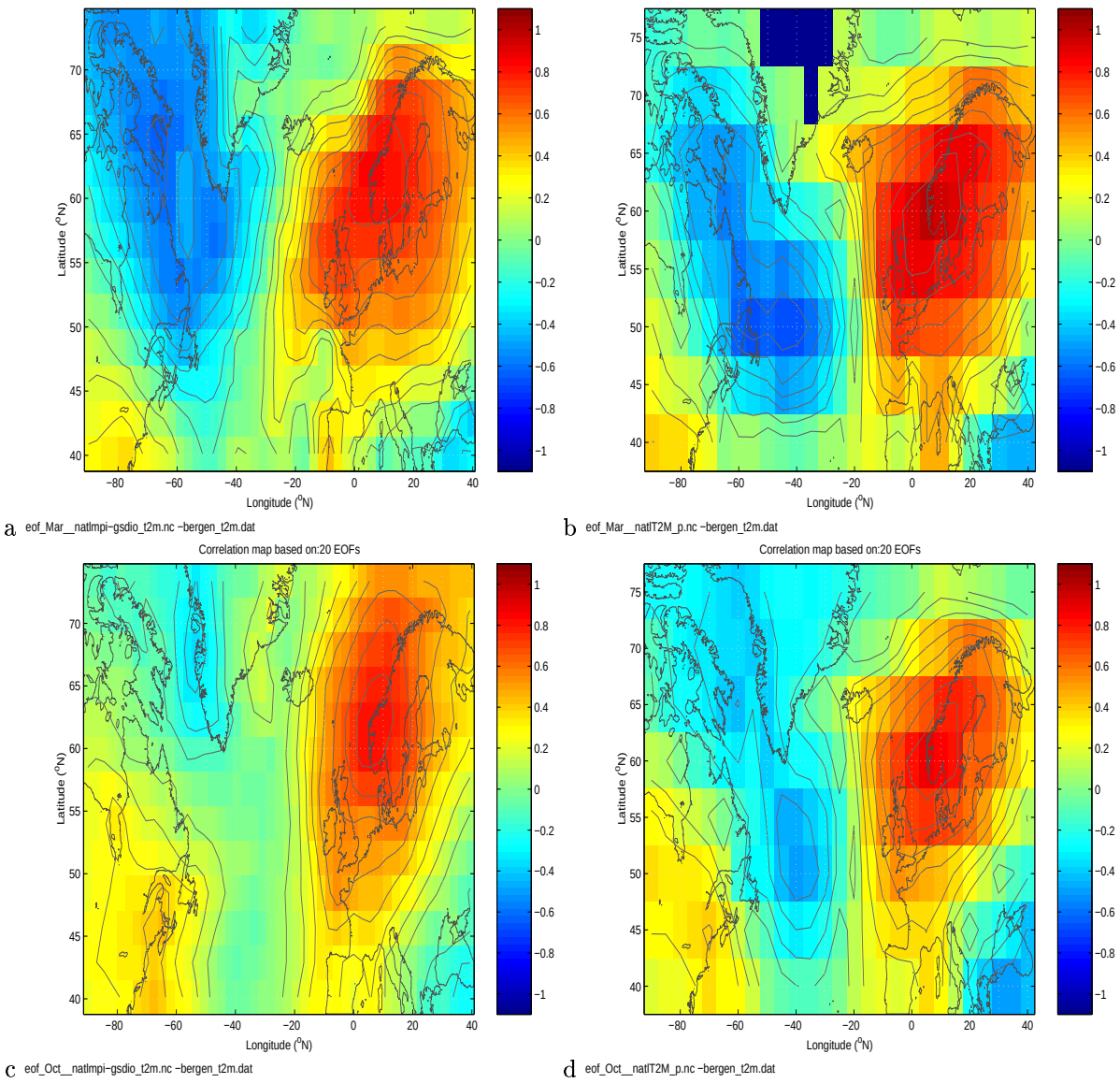

Figure 24: Correlation maps between the whole field and the closest grid box to 5°E-60°N using detrended EOF products for March (upper) and October (lower). The left panels show the analysis of the ECHAM GSDIO results whereas the right panels show the same results for the observations (*Benestad* (2000a) T(2m)).

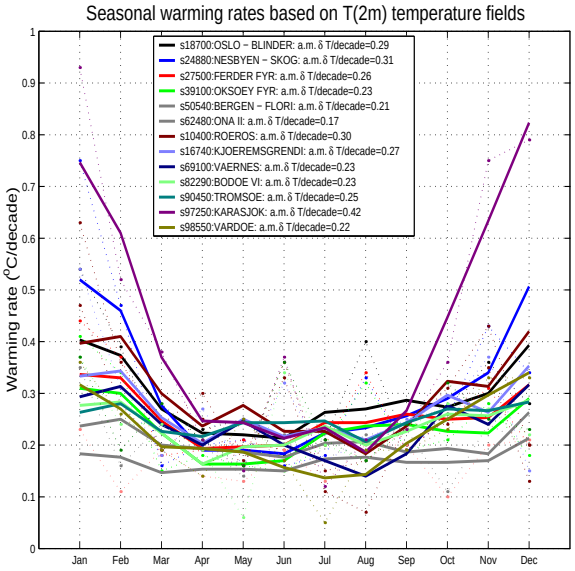

Figure 25: 3-month smoothed warming rate scenarios (curves) and estimates for the annual mean warming (after station names in the legend).

ferent predictor domains can be attributed to the fact that the EOF transform of the data affects the local climatic trends (Table 2).

Table for the April experiments (Table 12) suggests smaller domain ranges for which the trend estimates are robust. Experiments with an additional domain *weur* (40°W-30°E, 40°N-65°N, not shown) gave small trends, suggesting that data from north of 65°N must be included in the analysis in order to give realistic scenarios. The results are robust for a similar domain range as for January in southern Norway, but only two smallest regions gave robust results for Røros, Dombås, Værnes, Bodø and Tromsø. The estimates for Bergen, Ona, Karasjok and Vardø are highly uncertain, and for these locations the merits of downscaling are questionable. The projection method gives substantially smaller values than the common EOF approach during April. One interpretation of the April entries in Table 9 may be that the simulated spatial structure of T(2m) is not similar to the observed temperature distributions as in January. There is also a tendency in the 3rd column in Table 10 of the common EOFs coming in pairs associated with similar variance.

The July tests shown in Table 13 suggests smaller domain ranges over which the results are robust. The south Norwegian scenarios (Oslo, Nesbyen, Ferder and Oksøy) downscaled with T(2) fields using the *nord* domain tend to be higher than those computed with predictor fields with smaller and larger areas. The trend differences Bergen-Ona vary in the range 0.01 to 0.08, but domain sizes smaller than and equal to *nord* tend to give a consistent relationship between the two stations. Further north at Bodø and Tromsø the *scan* and *sscan* models yield higher trend estimates than both the larger domains, and the *nordic* gives the highest estimates at Karasjok, and Vardø. It is important to note that the *sscan* model domain may not be appropriate for northern Norway, as it excludes the region north of 65°N. Figure 22d shows the predictor pattern associated

with the July Oslo scenario, and the predictand is also associated with a local temperature anomaly. In this case, it is not clear which choice of domain is the most appropriate, and the merit of downscaling local climate scenarios in Norway is questionable as these seem to be less sensitive to large-scale anomalies than during winter.

Table 14 shows the test results from the domain size experiments for October month. The southern Norwegian estimates are robust with the 3 smallest predictor domains, giving some confidence in empirical downscaling for these regions at this time of the year. The west coast estimates, on the other hand, are not robust, and it is not clear whether the smallest domain *sscan* will give credible scenarios for this region. For Bodø and Tromsø the *scan* estimates give the highest trends. One may speculate as to whether the local climates in Bodø and Tromsø are influenced by local SSTs (near the coast and in the Norwegian Sea) which are not well described by the AOGCM. The estimates for Karasjok and Vardø, on the other hand, appear to be relatively robust with respect to predictor size, albeit with relatively large fluctuations.

The results from the projection model are roughly similar to those from the common EOF method, but have a greater scatter with respect to domain size. The largest domain gives high estimates and the small domains produce low trends in January. The results for April and July suggest small trends which are often negative. In October, the scenarios for Bergen and Ona suggest a slight cooling with the larger domain sizes. Thus, the estimates from the projection approach appear to be less robust than those derived using the common EOF method.

It is important to address the issue regarding the robustness of these estimates. Are they due to shortcomings of the empirical models, and the analysis or due to AOGCM errors or bad observations? Why do only a few downscaled scenarios give such "bad" results? From earlier analysis, it seems that part of the discrepancies can be explained by the EOF transformation and part is due to model-observation mismatch. Table 7 gives the cross-validation scores of the *natl* model for the various locations and the four months January, April, July, and October. Most of the correlation scores for T(2m) are around 0.80. The best model correlation skills associated with the T(2m) predictor field are found in January for locations in southern Norway. The model for Bergen gets low scores in April and July (r=62-81%), but the April month is also problematic many other locations. The correlation scores for Bergen and Ona are relatively high for all domain sizes in October.

Figure 23 shows Bergen's October temperature scenarios and the predictor patterns related to these scenarios. The predictor pattern has maximum weights over the northern Bothnian Sea in all of the three cases. The geographical weight distribution for the *natl* domain suggests that the Bergen temperature is influenced by the NAO. Both the *natl* and *nordic* domains gave negative temperature trends as opposed to a positive trend by the smaller *scan* domain, suggesting that the temperature somewhere outside the *scan* domain but within the *natl* and *nordic* domains affect the Bergen temperature in October. One potential area influencing the downscaled results may cover the Norwegian Sea and Iceland. The ECHAM4/OPYC3 AOGCM has a crude spatial resolution in the North Atlantic and the Nordic Seas, and a failure to give a good description of the conditions over this area may potentially influence the downscaling.

Figure 24 shows the correlation maps between the simulated (left) and ob-

served (right) temperature field and the grid point temperature at 5°E-60°N for March (upper) and October months (lower). These correlation scores were computed from the EOF products, retaining only the 20 leading EOFs and thus filtering out some of the small scale "noise". The contoured areas are significant at the 5% level or higher. Although both model and observations indicate a prominent west-east temperature dipole, there are some small-scale differences between the corresponding correlation patterns. But, the large-scale correlation weights are similar, suggesting that the spatial temperature consistency is realistic. In October the model describes too weak anti-correlation between the temperature over the Labrador Sea and Scandinavia. Hence, there are no indications that the failure of getting robust and credible results is due to strange AOGCM behaviour.

In summary, the downscaled results based on T(2m) are generally higher than the interpolated results, and do not show the enhanced winter warming at high latitudes as the AOGCM and the dynamically downscaled results from PT1 do (*Bjørge* et al., 2000). But, most of these scenarios are nevertheless in the same "ball park" as the AOGCM results. There are some downscaled projections which are not realistic, for which the estimates indicate slightly negative (but not statistically significant) trends.

Table 15 gives the scenarios for all of the calendar months. These estimates were based on the *scan* predictor domain, as this was found to be the most reliable in the earlier sensitivity experiments. The strongest warming according to this scenario is simulated during January, whereas the weakest trends are seen in June and July. The highest trend is prescribed for Karasjok in January (0.93°C/decade) and the slowest warming is projected for Vardø in July (0.05°C/decade).

A measure for the uncertainty associated with estimating the long-term linear trends can be based on the standard deviation, σ_m, of the slope estimate. Table 16 show estimates of σ_m computed according to *Press* et al. (1989) (Eq. 14.2.9 on p.555, and see p. 556 for dealing with unknown measurement errors):

$$\sigma_m = \sqrt{\frac{N\chi^2}{[N\sum_i x_i^2 - (\sum_i x_i)^2](N-2)}}.$$

The uncertainties in the slope are large due to strong interannual and decadal variations (e.g. Fig 22). There is a substantial scatter in the trend estimate from month to month, but one may expect a smooth variation in the warming rate with the seasonal cycle. This scatter therefore gives an indication of the uncertainties associated with the scenarios. Figure 25 shows 3-month smoothed values, as well as the annual mean warming rates (given in the legend). The seasonal difference in the downscaled warming rate is most pronounced at Karasjok. The highest annual mean warming is found at Karasjok and the slowest warming is simulated for Ona.

It is important to note that whereas the past observations (1876-1997) have indicated most significant warming during spring (*Hanssen-Bauer & Nordli*, 1998), the ECHAM4 model produces clearest warming trends during winter (*Benestad*, 2000c). Thus there is a systematic model error that results in a seasonal shift of the maximum warming rate. In other words, although ECHAM4 impressively reproduces many of the observed climatic features (*Machenhauer* et al., 1998; *Benestad* et al., 1999), it is not perfect.

5.2 Downscaled ECHAM4 GSDIO scenarios based on predictors other than the T(2m) field

Experiments with different predictor domains as with the T(2m) predictor were made with the SLP field, and the results from these experiments are given in Tables 17 to 20. In order to save space, a comparison with the projection approach is only shown for January. In general, the downscaled January results are more robust with respect to the domain size than those using T(2m) field as predictor. The SLP-based scenarios appear to be more robust than those based on the T(2m). The SLP field is not as strongly affected by the local SST in the North Atlantic and the Norwegian Sea as the T(2m) field, but these scenarios are also less sensitive to the Norwegian Sea and Icelandic region than the previous T(2m)-based scenarios. Another explanation for why the SLP-based scenarios are more robust may also be that the optimally interpolated SLP is believed to be of higher quality than the T(2m) (*Benestad*, 2000a).

The projection approach indicates less advective warming during January than the common EOF models do. There is little trend that can be attributed to long-term changes in the SLP during April and October, and a slight cooling simulated over southeastern Norway in July.

Table 21 lists the 1980-2050 scenario T(2m) trends based on the ECHAM4 GSDIO SLP for the *scan* domain size. In essence, most of the enhanced advective warming is seen during January. Note the large differences between December and January and February: the fact that these scenarios do not vary smoothly throughout the year makes these results somewhat suspect. Figure 26 shows the December, January, and February scenarios in addition to the predictor patterns. The large-scale SLP structures associated with these three months are roughly similar, implying southwesterly geostrophic winds and low pressure over Iceland. Thus, this SLP feature appears to strengthen more in January than in December and February.

The downscaled GSDIO results based on SLP (Table 21) indicate smaller trends than those based on temperatures (Table 15), which is in accordance to the expectations that the advective warming doesn't account for all the temperature changes. Changes in the circulation is responsible for much more of the winter-time warming than for the other seasons, and during summer, changes in the circulation may even have a cooling effect. Similar findings were reported by *Hanssen-Bauer* (2000).

Figure 27 shows some examples of downscaled temperature scenarios for Oslo, January and July temperatures respectively. The summer cooling in the model is due to a slight weakening of the summertime high-pressure systems over Scandinavia. Comparisons between the observations (black line in Figure 22 and model reproduction (blue curve) show impressive skill for the January model but moderate skill for the July predictions. The skill scores for all seasons and all regions are given in Table 7.

The January scenario for Oslo in Figure 27 suggests that on occasions (around "2005") violent temperatures may occur, but as the occurrence of this type of events is so rare it is not possible to estimate the significance of these (just a glitch?). However, a brief period of extreme cold conditions during the winters "1932" and "1933" in the vicinity of northern Norway was noted by *Hanssen-Bauer* et al. (2000) as these outliers gave unrealistic estimates for the standard deviation.

5.2.1 The influence of predictor domain size for downscaled January SLP scenarios

Location	euras	natl	neur	nord	scan	sscan
cEOF						
OSLO	0.12	0.18	0.27	0.25	0.25	0.28
NESBYEN	0.18	0.25	0.41	0.36	0.40	0.41
FERDER	0.10	0.13	0.24	0.20	0.20	0.23
OKSØY	0.10	0.14	0.25	0.20	0.19	0.23
BERGEN	0.16	0.10	0.25	0.17	0.17	0.24
ONA	0.11	0.07	0.17	0.13	0.11	0.15
RØROS	0.19	0.19	0.51	0.37	0.37	0.32
DOMBÅS	0.15	0.15	0.41	0.31	0.31	0.28
VÆRNES	0.18	0.20	0.38	0.30	0.28	0.26
BODØ	0.14	0.14	0.22	0.25	0.20	0.21
TROMSØ	0.15	0.11	0.19	0.21	0.15	0.18
KARASJOK	0.27	0.23	0.46	0.45	0.31	0.41
VARDØ	0.12	0.07	0.14	0.16	0.09	0.14
projection						
OSLO - BLINDER	0.09	0.15	0.09	0.06	0.05	0.04
NESBYEN - SKOG	0.14	0.17	0.11	0.06	0.07	0.05
FERDER FYR	0.09	0.13	0.09	0.06	0.05	0.03
OKSØY FYR	0.09	0.13	0.08	0.05	0.05	0.03
BERGEN - FLORI	0.03	0.09	0.05	0.03	0.03	0.02
ONA II	0.02	0.06	0.04	0.03	0.02	0.01
RØROS	0.02	0.11	0.15	0.09	0.10	0.05
DOMBÅS	0.03	0.11	0.12	0.08	0.07	0.04
VÆRNES	0.03	0.10	0.10	0.07	0.07	0.03
BODØ VI	0.00	0.09	0.07	0.07	0.05	0.02
TROMSØ	0.03	0.10	0.06	0.06	0.03	0.01
KARASJOK	0.10	0.17	0.08	0.09	0.05	0.01
VARDØ	0.05	0.08	0.03	0.03	0.02	0.01

Table 17: Downscaled scenario trends (°C/decade) using the domains: *euras* (90°W-90°E, 20°N-80°N), *natl* (90°W-40°E, 40°N-75°N), *neur* (30°W-40°E, 50°N-70°N), *nord* (20°W-40°E, 50°N-75°N),*scan* (0°W-30°E, 55°N-75°N), and *sscan* (0°W-20°E, 55°N-65°N). The results shown are for the common EOF method (cEOF) and the conventional projection method. Length of interval= 70 years. Dates 15-Jan-1980 - 15-Jan-2049. (cEOF predictors selected from 40 EOFs)

5.2.2 The influence of predictor domain size for downscaled April SLP scenarios

Location	euras	natl	neur	nord	scan	sscan
cEOF						
OSLO	0.03	0.07	0.05	0.04	-0.03	-0.01
NESBYEN	0.07	0.08	0.05	0.03	0.04	0.01
FERDER	0.02	0.05	0.04	0.03	-0.03	-0.01
OKSØY	0.02	0.06	0.04	0.04	-0.01	-0.01
BERGEN	0.02	0.06	0.01	0.02	0.05	0.01
ONA	0.04	0.02	-0.01	0.01	0.04	0.01
RØROS	0.08	0.09	0.00	-0.02	-0.05	0.02
DOMBÅS	0.07	0.10	0.01	-0.02	-0.05	0.04
VÆRNES	0.04	0.07	-0.02	-0.01	-0.04	0.02
BODØ	-0.01	-0.02	-0.07	0.00	-0.06	-0.06
TROMSØ	-0.01	-0.02	-0.05	-0.01	-0.07	-0.07
KARASJOK	-0.04	0.00	0.01	-0.03	-0.09	-0.12
VARDØ	0.01	0.01	0.00	-0.03	-0.05	-0.07

Table 18: Downscaled scenario trends (°C/decade) using the domains: *euras* (90°W-90°E, 20°N-80°N), *natl* (90°W-40°E, 40°N-75°N), *neur* (30°W-40°E, 50°N-70°N), *nord* (20°W-40°E, 50°N-75°N),*scan* (0°W-30°E, 55°N-75°N), and *sscan* (0°W-20°E, 55°N-65°N). The results shown are for the common EOF method (cEOF) and the conventional projection method. (cEOF predictors selected from 40 EOFs) Length of interval= 70 years. Dates 15-Jan-1980 - 15-Jan-2049.

5.2.3 The influence of predictor domain size for downscaled July SLP scenarios

Location	euras	natl	neur	nord	scan	sscan
cEOF						
OSLO	-0.01	-0.04	-0.11	-0.17	-0.16	-0.15
NESBYEN	-0.01	-0.03	-0.10	-0.15	-0.15	-0.19
FERDER	-0.02	-0.05	-0.10	-0.16	-0.14	-0.14
OKSØY	-0.02	-0.05	-0.10	-0.17	-0.15	-0.15
BERGEN	-0.03	-0.08	-0.12	-0.11	-0.15	-0.21
ONA	0.04	-0.04	-0.02	-0.02	-0.06	-0.06
RØROS	0.03	-0.06	-0.11	-0.09	-0.15	-0.17
DOMBÅS	0.03	-0.06	-0.11	-0.11	-0.17	-0.18
VÆRNES	0.01	-0.07	-0.09	-0.11	-0.14	-0.16
BODØ	-0.01	0.00	-0.01	0.02	0.02	0.10
TROMSØ	0.03	0.06	0.02	0.09	0.07	0.16
KARASJOK	0.00	0.04	0.05	0.01	0.07	0.10
VARDØ	0.00	0.03	0.06	0.04	0.08	0.03

Table 19: Downscaled scenario trends (°C/decade) using the domains: *euras* (90°W-90°E, 20°N-80°N), *natl* (90°W-40°E, 40°N-75°N), *neur* (30°W-40°E, 50°N-70°N), *nord* (20°W-40°E, 50°N-75°N),*scan* (0°W-30°E, 55°N-75°N), and *sscan* (0°W-20°E, 55°N-65°N). The results shown are for the common EOF method (cEOF) and the conventional projection method. Length of interval= 70 years. Dates 15-Jan-1980 - 15-Jan-2049. (cEOF predictors selected from 40 EOFs)

5.2.4 The influence of predictor domain size for downscaled October SLP scenarios

Location	euras	natl	neur	nord	scan	sscan
cEOF						
OSLO	-0.04	0.03	0.03	0.02	0.01	0.04
NESBYEN	-0.05	0.03	0.04	0.02	0.02	0.06
FERDER	-0.03	0.06	0.03	0.04	0.01	0.04
OKSØY	-0.04	0.03	0.00	0.03	0.01	0.03
BERGEN	-0.04	-0.06	-0.09	-0.01	-0.01	0.01
ONA	-0.04	-0.04	-0.09	-0.03	0.01	0.02
RØROS	-0.04	-0.03	0.05	-0.02	0.00	0.04
DOMBÅS	-0.05	-0.05	0.02	-0.02	-0.02	0.02
VÆRNES	-0.02	-0.01	0.01	-0.03	0.00	0.03
BODØ	0.06	-0.04	0.03	-0.03	0.01	0.13
TROMSØ	0.07	-0.01	0.07	0.03	0.06	0.18
KARASJOK	0.20	0.11	0.12	0.09	0.10	0.11
VARDØ	0.12	0.06	0.10	0.09	0.09	0.08

Table 20: Downscaled scenario trends (°C/decade) using the domains: *euras* (90°W-90°E, 20°N-80°N), *natl* (90°W-40°E, 40°N-75°N), *neur* (30°W-40°E, 50°N-70°N), *nord* (20°W-40°E, 50°N-75°N),*scan* (0°W-30°E, 55°N-75°N), and *sscan* (0°W-20°E, 55°N-65°N). The results shown are for the common EOF method (cEOF) and the conventional projection method. Length of interval= 70 years. Dates 15-Jan-1980 - 15-Jan-2049. (cEOF predictors selected from 40 EOFs)

5.2.5 Downscaling of ECHAM4 GSDIO scenarios by common EOFs based on *Benestad* (2000b) Scandinavian SLP

Location	Jan	Feb	Mar	Apr	May	Jun	Jul	Aug	Sep	Oct	Nov	Dec
OSLO	**29**	-06	02	00	07	-08	**-15**	-07	01	02	01	02
NESBYEN	**44**	-06	04	02	06	-08	**-14**	-06	01	03	06	02
FERDER	**23**	-05	03	-01	06	-06	**-13**	-05	03	01	02	05
OKSØY	**24**	-04	03	00	05	-06	**-14**	-06	00	01	02	06
BERGEN	**24**	-06	-06	06	01	-04	**-16**	-06	-09	-01	04	01
ONA	**16**	-04	-04	02	03	-01	-06	-05	-07	-03	03	-02
RØROS	**40**	-01	-04	02	06	-02	-14	-09	-01	01	04	07
DOMBÅS	**34**	00	-04	02	07	-01	**-16**	-10	-02	-01	04	07
VÆRNES	**31**	03	-04	00	05	-02	-13	-10	-06	00	02	03
BODØ	23	00	-03	-05	00	-04	00	-02	09	01	00	-03
TROMSØ	**19**	-01	-03	-06	04	01	05	02	-08	05	01	-04
KARASJOK	**43**	-14	-04	-05	08	05	02	-03	-04	09	00	-17
VARDØ	**13**	-06	-02	-03	06	02	02	00	-01	08	00	-03

Table 21: Downscaled scenarios (×0.01°C/decade) of the GHG results using the common EOF method on the model and *Benestad* (2000b) sea level pressure. Length of interval= 70 years. Dates 15-Dec-1980 - 15-Dec-2049. The predictor domain was 20°W-40°E, 50°N-75°N. Entries shown in bold are significant at the 5% level.

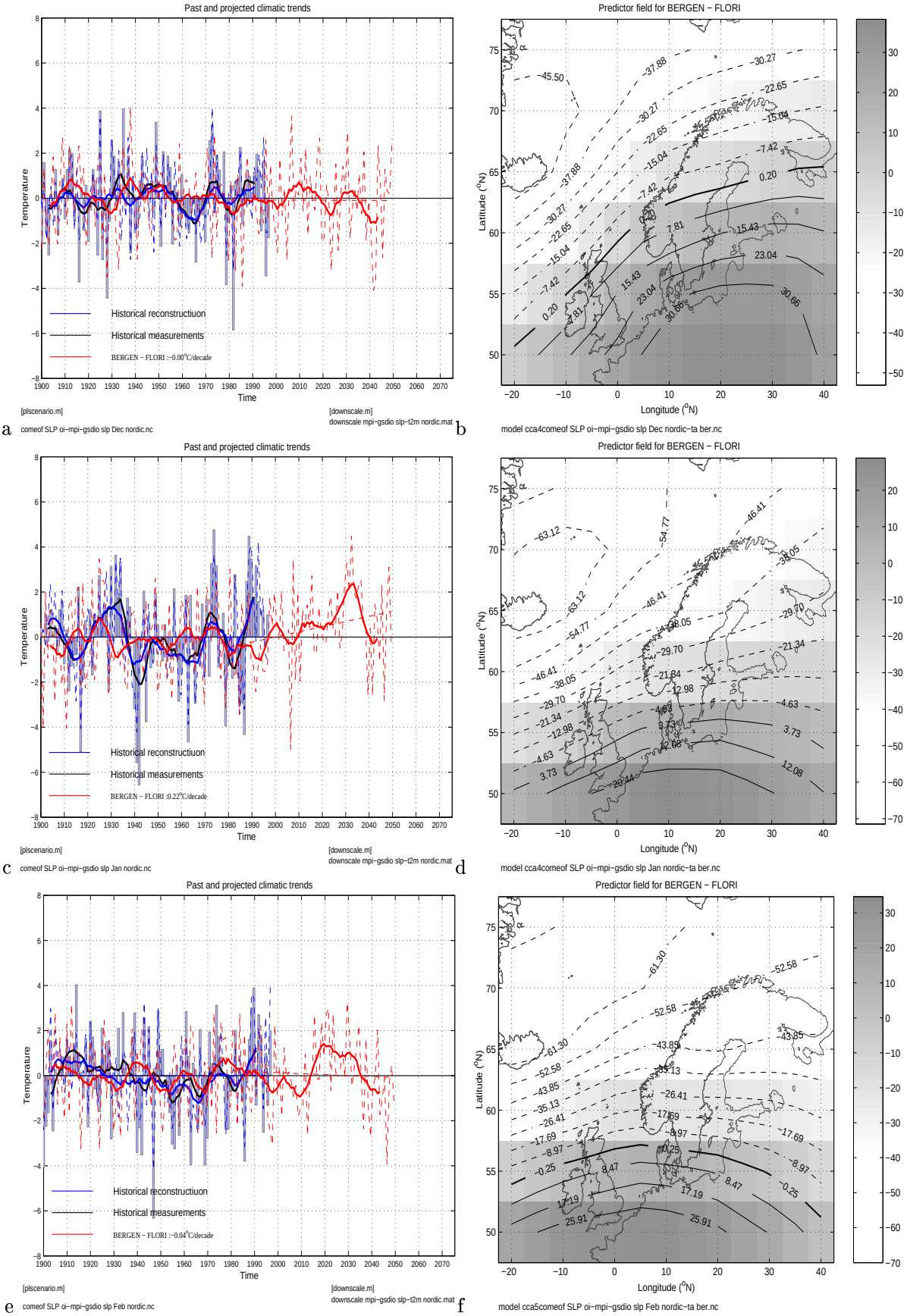

Figure 26: The downscaled scenarios from SLP and SLP predictor pattern for Bergen temperature during December (a,b), January (c,d), and February (e,f). The large-scale features in the predictor patterns are similar for these months.

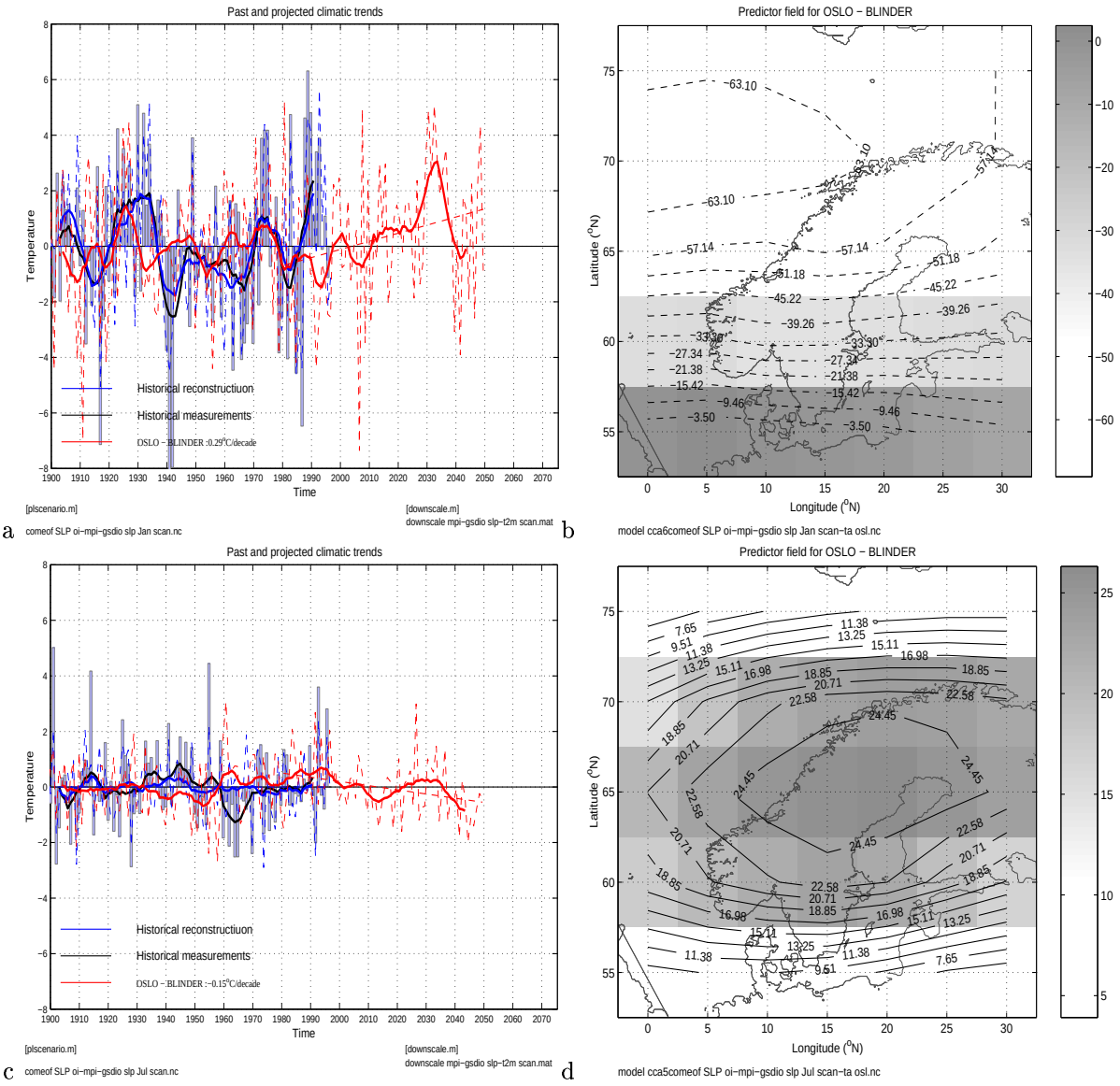

Figure 27: Downscaled scenarios for Oslo based on SLP for January (a,b) and July (c,d). Different circulation patterns are associated with the temperature variations in different seasons.

5.2.6 Downscaling by ECHAM4 GSDIO common EOFs based on 850hPa temperature scenarios natl.

Location	Jan	Apr	Jul	Oct
natl				
OSLO	**0.56**	**0.21**	**0.22**	0.12
NESBYEN	**0.70**	**0.14**	**0.23**	0.08
FERDER	**0.43**	**0.15**	**0.16**	**0.11**
OKSØY	**0.43**	**0.17**	**0.15**	0.09
BERGEN	**0.38**	-0.02	0.03	-0.08
ONA	**0.22**	-0.01	0.03	-0.06
RØROS	**0.28**	0.04	-0.01	0.16
DOMBÅS	**0.30**	0.03	0.00	0.09
VÆRNES	**0.31**	0.01	-0.03	**0.23**
BODØ	**0.25**	0.01	0.04	**0.25**
TROMSØ	**0.23**	0.00	0.06	**0.24**
KARASJOK	**0.48**	0.01	**0.21**	**0.33**
VARDØ	**0.15**	0.02	**0.20**	0.12
scan				
OSLO	**0.67**	**0.17**	0.10	**0.19**
NESBYEN	**0.97**	**0.15**	0.08	**0.18**
FERDER	**0.56**	**0.13**	0.09	**0.17**
OKSØY	**0.56**	**0.13**	0.11	**0.14**
BERGEN	**0.43**	**0.11**	0.04	**0.15**
ONA	**0.34**	**0.10**	**0.10**	**0.18**
RØROS	**0.71**	**0.19**	0.11	**0.28**
DOMBÅS	**0.62**	**0.19**	0.06	**0.26**
VÆRNES	**0.61**	**0.17**	0.10	**0.30**
BODØ	**0.49**	0.14	**0.22**	**0.27**
TROMSØ	**0.48**	0.11	**0.27**	**0.26**
KARASJOK	**1.03**	0.14	**0.28**	**0.47**
VARDØ	**0.31**	0.13	**0.17**	**0.28**

Table 22: Downscaled temperature scenario trends (°C/decade) using *natl* (90°W-40°E, 40°N-75°N) ECHAM4 GSDIO T_{850} scenarios as predictors. Length of interval= 70 years. Dates 15-Oct-1980 - 15-Oct-2049. Entries shown in bold are significant at the 5% level.

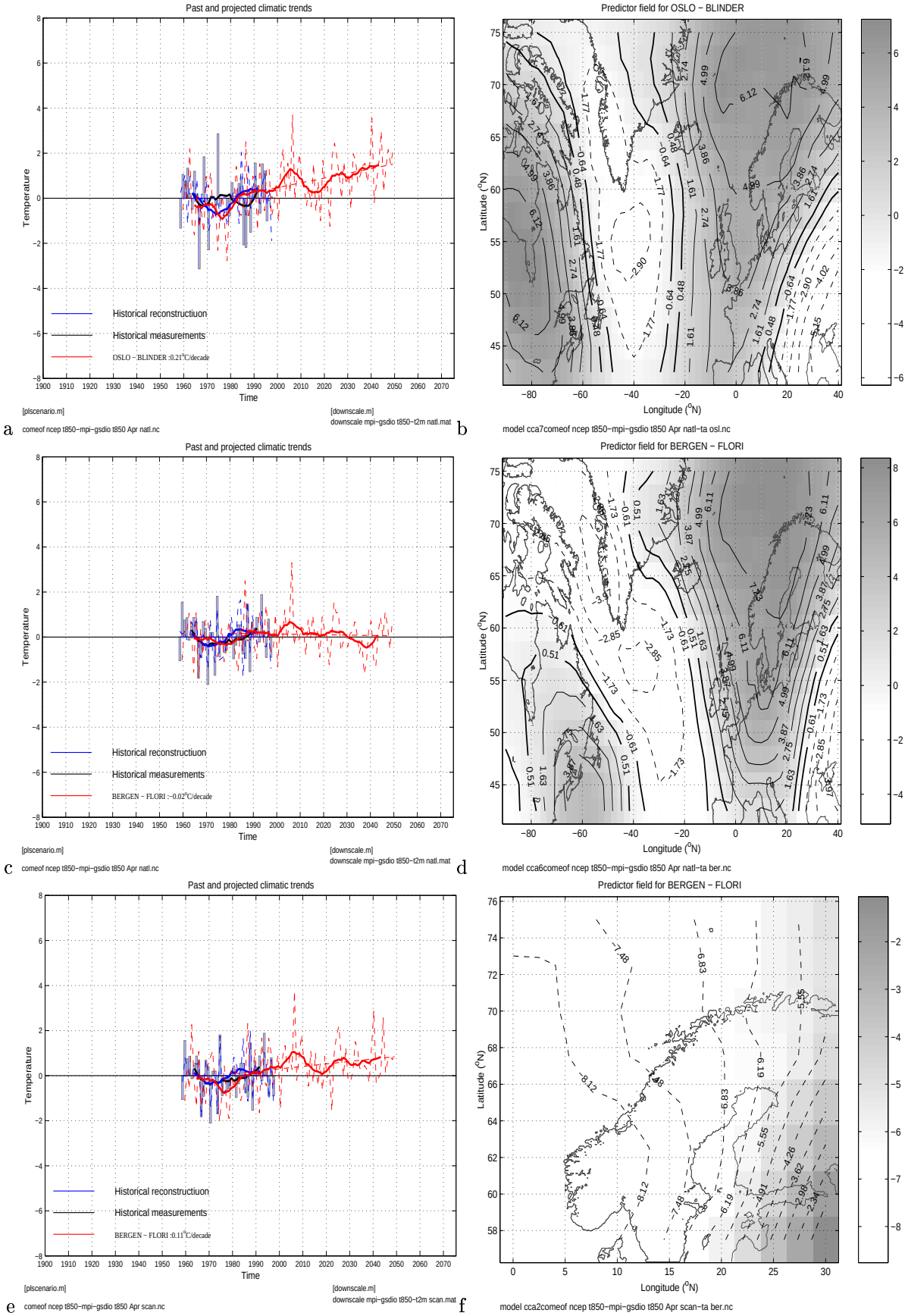

Figure 28: Downscaled temperature scenario trends (°C/decade) using *natl* (90°W-40°E, 40°N-75°N) ECHAM4 GSDIO T_{850} scenarios as predictors. Length of interval= 70 years. Dates 15-Oct-1980 - 15-Oct-2049.

5.2.7 Downscaling of ECHAM4 GSDIO by common EOFs based on 500 and 700 hPa geopotential height field.

Φ_{500} Location	Jan	Apr	Jul	Oct
OSLO	**0.45**	0.04	0.01	**0.14**
NESBYEN	**0.59**	0.05	0.03	**0.15**
FERDER	**0.36**	0.07	0.00	**0.16**
OKSØY	**0.36**	0.06	0.00	0.09
BERGEN	**0.31**	**0.08**	-0.06	0.00
ONA	**0.21**	**0.08**	-0.03	0.04
RØROS	**0.49**	0.03	0.07	0.13
DOMBÅS	**0.41**	0.03	0.11	0.11
VÆRNES	**0.37**	0.05	-0.06	0.13
BODØ	**0.26**	0.05	0.10	**0.23**
TROMSØ	**0.21**	0.05	0.13	**0.22**
KARASJOK	**0.59**	0.19	0.10	0.30
VARDØ	**0.13**	0.08	-0.02	0.15
Φ_{700}				
OSLO	**0.35**	0.05	-0.11	-0.02
NESBYEN	**0.48**	0.07	-0.07	-0.02
FERDER	**0.32**	0.04	-0.10	-0.02
OKSØY	**0.30**	0.05	**-0.11**	-0.01
BERGEN	**0.32**	0.03	**-0.10**	-0.05
ONA	**0.20**	0.02	**-0.06**	-0.02
RØROS	**0.52**	-0.01	**-0.17**	-0.07
DOMBÅS	**0.45**	0.01	**-0.18**	-0.08
VÆRNES	**0.40**	-0.01	**-0.19**	-0.04
BODØ	**0.19**	0.03	**0.15**	0.03
TROMSØ	**0.18**	0.02	**0.18**	0.08
KARASJOK	0.34	0.12	0.02	0.19
VARDØ	**0.10**	0.05	-0.03	0.14

Table 23: Downscaled temperature scenario trends (°C/decade) using *natl* (90°W-40°E, 40°N-75°N) ECHAM4 GSDIO Φ_{500} and Φ_{700} scenarios as predictors. Length of interval= 70 years. Dates 15-Oct-1980 - 15-Oct-2049. Entries shown in bold are significant at the 5% level.

5.2.8 Downscaling ECHAM4 GSDIO by common EOFs based on 500-700hPa thickness scenarios.

$\Phi_{500} - \Phi_{700}$ Location	Jan	Apr	Jul	Oct
natl				
OSLO	0.71	0.09	-0.02	0.21
NESBYEN	1.00	0.10	-0.00	0.20
FERDER	0.60	0.09	-0.04	0.16
OKSØY	0.60	0.09	-0.04	0.16
BERGEN	0.59	0.04	0.03	0.06
ONA	0.38	0.07	0.05	0.08
RØROS	0.69	0.25	0.16	0.20
DOMBÅS	0.61	0.24	0.13	0.14
VÆRNES	0.56	0.18	0.05	0.15
BODØ	0.18	0.02	0.06	0.14
TROMSØ	0.18	-0.00	0.06	0.18
KARASJOK	0.49	0.01	0.02	0.24
VARDØ	0.13	-0.02	0.00	0.15
nordic				
OSLO	0.52	-0.06	0.03	0.03
NESBYEN	0.77	-0.08	0.04	0.04
FERDER	0.43	-0.05	0.01	0.01
OKSØY	0.42	-0.05	0.02	0.02
BERGEN	0.34	-0.01	0.02	0.02
ONA	0.25	-0.00	0.01	0.01
RØROS	0.54	0.05	0.03	0.03
DOMBÅS	0.48	0.09	0.04	0.04
VÆRNES	0.45	0.05	0.00	0.00
BODØ	0.50	-0.00	-0.06	-0.06
TROMSØ	0.43	-0.05	-0.07	-0.07
KARASJOK	1.12	-0.07	0.08	0.08
VARDØ	0.34	-0.11	0.09	0.09
scan				
OSLO	0.57	0.09	0.21	0.21
NESBYEN	0.84	0.08	0.20	0.20
FERDER	0.46	0.03	0.16	0.16
OKSØY	0.47	0.03	0.16	0.16
BERGEN	0.45	0.14	0.06	0.06
ONA	0.33	0.10	0.08	0.08
RØROS	0.68	0.20	0.20	0.20
DOMBÅS	0.59	0.21	0.14	0.14
VÆRNES	0.60	0.15	0.15	0.15
BODØ	0.46	0.09	0.14	0.14
TROMSØ	0.42	0.05	0.18	0.18
KARASJOK	0.93	0.03	0.24	0.24
VARDØ	0.24	-0.00	0.15	0.15

Table 24: Downscaled temperature scenario trends (°C/decade) using *natl* (90°W-40°E, 40°N-75°N) ECHAM4 GSDIO $\Phi_{500} - \Phi_{700}$ scenarios as predictors. Length of interval= 70 years. Dates 15-Oct-1980 - 15-Oct-2049.

Table 22 shows downscaled results based on the 850 hPa temperature field. It is sometimes argued that upper air quantities are better reproduced by the climate models than the surface fields (*Huth & Kyselý*, 2000; *Goodess & Palutikof*, 1998; *Rummukainen*, 1997), and because these fields are less affected by the model topography the downscaled scenarios may potentially be less sensitive to domain size. Here, only scenarios using the *natl* and *scan* domains are shown, although a proper analysis ought to include similar sensitivity tests as for the T(2m) field. The T_{850hPa}-based analysis (*scan*, Table 22) gives slightly lower trend estimates for southern Norway during April and July, but higher July values in northern Norway than corresponding estimates derived using the T(2m) field as predictor (Table 15). There is an abrupt change between the spring and summer scenarios in the southeastern and the rest of Norway when the downscaling uses the *natl* domain, most probably reflecting a weakness in the analysis or the data. This feature is absent in the downscaled scenarios if derived from a smaller domain (*scan*). Figure 28 shows the scenarios (left) and the predictor patterns (right) for Oslo (upper panel) and Bergen (middle and lower panels). The different trends can be explained in terms of differences in the predictor patterns, and further scenario studies should be based on smaller domain size focused on Scandinavia. Table 12 indicates low trend estimates associated with the larger domain sizes, except for the 4 locations in southern Norway and possible Karasjok and Varø. A similar sensitivity of the downscaled scenarios to the domain choice as for the T(2m)-based models is evident from Table 22. Figure 28c,f shows the downscaled April temperature scenario for Bergen and associated predictor patter.

The fact that the T_{850} gives similar results to the near-surface temperature field gives increased confidence in the downscaling method and the AOGCM results, since the empirical models were developed using different data for the two sets of results. It is important to appreciate that the T_{850} from NCEP (*Kalnay* et al., 1996) only covers a brief period (1958-1998), whereas the *Benestad* (2000a) T(2m) stretches as far back as 1873. On the other hand, the re-analysed T_{850} is probably of higher quality than the T(2m) data.

Table 23 shows downscaled scenarios based on the ECHAM4 GSDIO 500hPa and 700hPa geopotential heights. The results for January are in good agreement with those based on T(2m), but the downscaled April, July and October trends are weaker than the T(2m) fields suggest. The downscaled October trends in Table 23 derived from the Φ_{500}-field are higher than corresponding results based on the T(2m) with similar predictor domain (*natl*) field, but still lower than the estimates listed in Table 15. Both the T(2m) and geopotential height based scenarios give small October warming in Bergen and Ona. It is remarkable that the higher level (Φ_{500}) gives stronger warming in October than the geopotential height changes at a lower altitude (Φ_{700}). The fact that the higher level yields slightly stronger warming in winter may suggest that the vertical temperature structure is relatively uniform.

The 700hPa-500hPa thickness field was tried as a predictor, and the results are given in Table 24 for 3 different predictor domains (*natl, nordic, scan*). The scenarios computed using the *scan* domain are similar to those calculated with the T(2m) field (Table 15), except for the April scenarios (weaker warming than the T(2m) based scenarios) and and in northern Norway during October (lower estimates than the T(2m) field). Once more, the downscaled results are sensitive to the domain size, particularly for April, July and October. The *natl* and *scan*

domains produce similar results, whereas the *nordic* domain gives substantially different scenarios. Thus, there is no systematic relationship between domain size and downscaled scenario.

The fact that the T_{850hPa}, ECHAM4 GSDIO T_{850}, and to some degree the 700hPa and 500hPa geopotential height give similar results to those derived using the T(2m) field suggests that these local scenarios are robust. There are some exceptions to this rule, particularly for April, and therefore less confidence can be attached to the empirically downscaled results for the spring months. The geopotential heights do not capture the July warming, but produce negative temperature trends similar to the SLP-based scenarios. Both the SLP and the geopotential heights can be used to describe the large-scale circulation pattern, and enhanced westerlies during summer is expected to produce lower summer temperatures.

5.3 Downscaled scenarios based on other global climate model scenarios

5.3.1 Downscaling by common EOFs based on NCAR-CSM *scan* T(2m) scenarios.

Location	Jan	Apr	Jul	Oct
natl				
OSLO	**0.31**	**0.16**	**0.50**	0.02
NESBYEN	**0.40**	**0.14**	**0.42**	0.01
FERDER	**0.20**	**0.14**	**0.49**	**0.04**
OKSØY	**0.18**	**0.11**	**0.49**	**0.04**
BERGEN	0.06	0.00	**0.38**	0.02
ONA	0.02	-0.01	**0.27**	0.02
RØROS	0.14	**0.24**	**0.41**	0.04
DOMBÅS	0.12	**0.17**	**0.37**	0.03
VÆRNES	0.08	**0.19**	**0.27**	0.03
BODØ	0.01	0.06	**0.19**	0.04
TROMSØ	0.02	0.07	**0.19**	0.06
KARASJOK	**0.24**	0.05	**0.01**	0.05
VARDØ	**0.09**	0.03	-0.00	0.04
scan				
OSLO	**0.68**	**0.42**	**0.40**	**0.31**
NESBYEN	**0.99**	**0.31**	**0.36**	**0.29**
FERDER	**0.59**	**0.29**	**0.38**	**0.31**
OKSØY	**0.58**	**0.26**	**0.32**	**0.30**
BERGEN	0.06	**0.19**	**0.42**	**0.18**
ONA	0.06	**0.18**	**0.27**	**0.22**
RØROS	**0.58**	**0.74**	**0.54**	**0.41**
DOMBÅS	**0.49**	**0.72**	**0.57**	**0.38**
VÆRNES	**0.40**	**0.62**	**0.47**	**0.42**
BODØ	**0.29**	**0.65**	0.03	**0.61**
TROMSØ	**0.32**	**0.59**	-0.03	**0.49**
KARASJOK	**1.16**	**0.61**	0.04	**0.64**
VARDØ	**0.45**	**0.42**	0.01	**0.37**

Table 25: Downscaled temperature scenario trends (°C/decade) using *natl* and *scan* NCAR-CSM (b006) T(2m) scenarios as predictors. Length of interval= 119. Dates 15-Oct-1990 - 15-Oct-2108. These results are substantially higher than the downscaled results based on the *natl* domain, with the exception of the July month. Entries shown in bold are significant at the 5% level.

5.3.2 Downscaling by common EOFs based on NCAR-CSM *scan* SLP scenarios.

Location	Jan	Apr	Jul	Oct
OSLO	-0.07	0.01	0.04	0.04
NESBYEN	-0.09	0.01	0.04	**0.05**
FERDER	-0.05	0.01	0.04	**0.04**
OKSØY	-0.05	0.01	0.03	**0.04**
BERGEN	-0.05	-0.03	0.00	**0.04**
ONA	-0.03	-0.01	-0.00	**0.06**
RØROS	-0.07	0.00	0.02	**0.06**
DOMBÅS	-0.06	-0.00	0.02	**0.06**
VÆRNES	-0.06	-0.00	0.01	**0.06**
BODØ	-0.05	0.00	0.01	**0.07**
TROMSØ	-0.03	0.01	0.04	**0.08**
KARASJOK	-0.05	0.03	0.06	**0.10**
VARDØ	-0.01	0.02	0.03	0.05

Table 26: Downscaled temperature scenario trends (°C/decade) using *scan* NCAR-CSM (b006) SLP scenarios as predictors. Length of interval= 119. Dates 15-Oct-1990 - 15-Oct-2108. The same analysis based on the *natl* domain gives similar results. Entries shown in bold are significant at the 5% level.

5.3.3 Downscaling by common EOFs based on HadCM3 T(2m) scenarios.

Location	Jan	Apr	Jul	Oct
nordic				
OSLO	**0.52**	**0.38**	**0.44**	**0.45**
NESBYEN	**0.72**	**0.32**	**0.39**	**0.45**
FERDER	**0.41**	**0.33**	**0.46**	**0.44**
OKSØY	**0.39**	**0.30**	**0.43**	**0.39**
BERGEN	**0.51**	**0.31**	**0.44**	**0.22**
ONA	**0.28**	**0.28**	**0.41**	**0.24**
RØROS	**0.60**	**0.38**	**0.69**	**0.65**
DOMBÅS	**0.53**	**0.31**	**0.56**	**0.60**
VÆRNES	**0.42**	**0.32**	**0.60**	**0.57**
BODØ	**0.43**	**0.43**	**0.11**	**0.11**
TROMSØ	**0.44**	**0.46**	0.07	**0.11**
KARASJOK	**1.14**	**0.62**	0.12	**0.16**
VARDØ	**0.52**	**0.43**	0.07	**0.10**
scan				
OSLO	**0.62**	**0.36**	**0.50**	**0.45**
NESBYEN	**0.92**	**0.30**	**0.45**	**0.46**
FERDER	**0.51**	**0.28**	**0.47**	**0.43**
OKSØY	**0.49**	**0.25**	**0.42**	**0.39**
BERGEN	**0.40**	**0.25**	**0.46**	**0.23**
ONA	**0.31**	**0.22**	**0.36**	**0.23**
RØROS	**0.79**	**0.23**	**0.64**	**0.63**
DOMBÅS	**0.65**	**0.23**	**0.58**	**0.59**
VÆRNES	**0.56**	**0.29**	**0.55**	**0.55**
BODØ	**0.45**	**0.39**	**0.36**	**0.29**
TROMSØ	**0.45**	**0.42**	**0.27**	**0.29**
KARASJOK	**0.86**	**0.19**	**0.19**	**0.41**
VARDØ	**0.35**	**0.17**	**0.11**	**0.25**

Table 27: Downscaled temperature scenario trends (°C/decade) using *nordic* and *scan* HadCM3 T(2m) scenarios as predictors. Length of interval= 119. Dates 15-Oct-1980 - 15-Oct-2098. Entries shown in bold are significant at the 5% level.

5.3.4 Downscaling by common EOFs based on HadCM3 *nordic* and *scan* SLP scenarios.

Location	Jan	Apr	Jul	Oct
nordic				
OSLO	**-0.45**	**0.11**	0.07	-0.01
NESBYEN	**-0.62**	**0.07**	0.07	-0.01
FERDER	**-0.36**	**0.08**	0.07	-0.01
OKSØY	**-0.36**	**0.08**	0.07	-0.02
BERGEN	**-0.16**	**0.12**	0.11	0.03
ONA	**-0.11**	**0.12**	0.05	0.04
RØROS	**-0.26**	**0.18**	0.05	0.04
DOMBÅS	**-0.24**	**0.15**	0.07	0.03
VÆRNES	**-0.24**	**0.14**	0.07	0.03
BODØ	**-0.22**	**0.10**	0.06	0.06
TROMSØ	**-0.18**	0.09	0.05	0.06
KARASJOK	-0.15	0.11	-0.01	0.06
VARDØ	-0.02	0.09	-0.02	0.04
scan				
OSLO	-0.05	0.05	-0.01	0.02
NESBYEN	-0.05	**0.05**	-0.01	0.03
FERDER	-0.04	**0.05**	-0.01	0.03
OKSØY	-0.04	**0.05**	-0.03	0.03
BERGEN	-0.01	0.02	-0.05	0.01
ONA	0.00	0.02	-0.01	-0.00
RØROS	-0.03	0.02	-0.04	0.02
DOMBÅS	-0.02	0.02	-0.05	0.03
VÆRNES	0.00	0.01	-0.05	0.02
BODØ	-0.01	-0.02	-0.03	0.00
TROMSØ	-0.00	-0.02	0.01	-0.00
KARASJOK	-0.03	0.03	0.04	0.05
VARDØ	0.01	0.03	0.04	0.02

Table 28: Downscaled temperature scenario trends (°C/decade) using *scan* HadCM3 SLP scenarios as predictors. Length of interval= 119. Dates 15-Oct-1980 - 15-Oct-2098. Entries shown in bold are significant at the 5% level.

5.3.5 Downscaling by common EOFs based on HadCM2 T(2m) scenarios.

Location	Jan	Apr	Jul	Oct
member 1				
OSLO	**0.39**	**0.28**	**0.35**	**0.32**
NESBYEN	**0.56**	**0.26**	**0.31**	**0.33**
FERDER	**0.34**	**0.21**	**0.33**	**0.34**
OKSØY	**0.35**	**0.20**	**0.29**	**0.33**
BERGEN	**0.36**	**0.24**	**0.31**	**0.14**
ONA	**0.18**	**0.19**	**0.25**	**0.13**
RØROS	**0.40**	**0.36**	**0.45**	**0.34**
DOMBÅS	**0.37**	**0.32**	**0.40**	**0.32**
VÆRNES	**0.29**	**0.30**	**0.39**	**0.28**
BODØ	**0.32**	**0.28**	**0.26**	**0.33**
TROMSØ	**0.28**	**0.27**	**0.16**	**0.35**
KARASJOK	**0.74**	**0.24**	**0.19**	**0.36**
VARDØ	**0.28**	**0.17**	**0.10**	**0.18**
member 2				
OSLO	**0.35**	**0.21**	**0.31**	**0.26**
NESBYEN	**0.49**	**0.19**	**0.27**	**0.26**
FERDER	**0.29**	**0.16**	**0.27**	**0.29**
OKSØY	**0.30**	**0.15**	**0.27**	**0.27**
BERGEN	**0.26**	**0.16**	**0.34**	**0.12**
ONA	**0.17**	**0.14**	**0.26**	**0.10**
RØROS	**0.29**	**0.29**	**0.30**	**0.26**
DOMBÅS	**0.27**	**0.26**	**0.22**	**0.27**
VÆRNES	**0.22**	**0.25**	**0.24**	**0.23**
BODØ	**0.29**	**0.25**	**0.33**	0.10
TROMSØ	**0.25**	**0.24**	**0.22**	**0.12**
KARASJOK	**0.52**	**0.32**	**0.34**	0.07
VARDØ	**0.16**	**0.21**	0.12	0.05
member 3				
OSLO	0.10	**0.35**	0.12	**0.23**
NESBYEN	0.14	**0.32**	0.11	**0.22**
FERDER	0.02	**0.26**	0.13	**0.26**
OKSØY	0.04	**0.25**	**0.14**	**0.26**
BERGEN	0.09	**0.32**	**0.16**	**0.21**
ONA	0.02	**0.24**	**0.17**	**0.23**
RØROS	-0.08	**0.45**	**0.29**	**0.31**
DOMBÅS	-0.03	**0.41**	**0.21**	**0.30**
VÆRNES	-0.09	**0.38**	**0.24**	**0.27**
BODØ	0.07	**0.32**	**0.40**	0.15
TROMSØ	0.12	**0.29**	**0.36**	**0.16**
KARASJOK	**0.55**	**0.31**	**0.42**	**0.05**
VARDØ	**0.21**	**0.26**	**0.21**	**0.04**
member 4				
OSLO	**0.78**	**0.37**	**0.57**	**0.40**
NESBYEN	**1.19**	**0.35**	**0.51**	**0.39**
FERDER	**0.73**	**0.28**	**0.53**	**0.41**
OKSØY	**0.73**	**0.27**	**0.47**	**0.38**
BERGEN	**0.51**	**0.25**	**0.50**	**0.31**
ONA	**0.31**	**0.20**	**0.36**	**0.31**
RØROS	**0.67**	**0.49**	**0.67**	**0.49**
DOMBÅS	**0.58**	**0.46**	**0.57**	**0.47**
VÆRNES	**0.51**	**0.41**	**0.55**	**0.43**
BODØ	**0.42**	**0.40**	**0.40**	**0.34**
TROMSØ	**0.36**	**0.33**	**0.23**	**0.35**
KARASJOK	**0.80**	**0.35**	**0.29**	**0.41**
VARDØ	**0.31**	**0.24**	0.16	**0.24**

Table 29: Downscaled temperature scenario trends (°C/decade) using *scan* HadCM2 T(2m) scenarios as predictors. Length of interval= 119. Dates 15-Oct-1980 - 15-Oct-2098. Entries shown in bold are significant at the 5% level.

5.3.6 Downscaling by common EOFs based on HadCM2 *scan* SLP scenarios.

Location	Jan	Apr	Jul	Oct
member 1				
OSLO	0.06	-0.01	0.05	0.01
NESBYEN	0.06	-0.02	0.05	0.01
FERDER	0.05	0.01	0.05	0.02
OKSØY	0.04	0.00	0.04	0.02
BERGEN	0.07	-0.03	0.05	0.02
ONA	0.03	-0.02	0.02	0.03
RØROS	0.05	-0.02	0.05	0.02
DOMBÅS	0.05	-0.02	0.05	0.03
VÆRNES	0.04	-0.02	0.04	0.02
BODØ	0.04	-0.03	0.01	0.02
TROMSØ	0.02	-0.02	0.00	0.02
KARASJOK	0.04	-0.05	0.05	0.01
VARDØ	0.02	-0.02	0.05	0.00
member 2				
OSLO	0.01	-0.01	0.09	**-0.08**
NESBYEN	0.02	-0.02	**0.08**	**-0.07**
FERDER	-0.00	-0.01	**0.09**	**-0.06**
OKSØY	-0.00	-0.01	0.07	**-0.06**
BERGEN	0.03	-0.03	0.06	**-0.06**
ONA	0.03	-0.04	0.02	**-0.07**
RØROS	0.08	-0.04	-0.02	**-0.11**
DOMBÅS	0.05	-0.03	0.00	**-0.10**
VÆRNES	0.06	-0.03	-0.04	**-0.10**
BODØ	0.05	-0.02	-0.06	**-0.10**
TROMSØ	0.05	-0.03	-0.04	**-0.10**
KARASJOK	0.10	-0.05	-0.03	**-0.12**
VARDØ	0.03	-0.03	-0.02	-0.06
member 3				
OSLO	**-0.20**	0.05	0.03	-0.02
NESBYEN	**-0.29**	0.05	0.03	-0.02
FERDER	**-0.18**	0.04	0.03	-0.02
OKSØY	**-0.18**	0.04	0.04	-0.02
BERGEN	**-0.13**	**0.07**	0.04	0.01
ONA	**-0.10**	**0.07**	-0.00	0.02
RØROS	**-0.19**	**0.10**	0.04	0.01
DOMBÅS	**-0.17**	**0.08**	0.05	0.00
VÆRNES	**-0.16**	**0.10**	0.05	0.01
BODØ	**-0.13**	0.06	0.03	0.03
TROMSØ	**-0.11**	0.07	0.04	0.05
KARASJOK	**-0.23**	0.05	0.03	0.03
VARDØ	**-0.06**	0.07	-0.01	0.02
member 4				
OSLO	0.16	-0.02	0.05	-0.02
NESBYEN	**0.24**	-0.03	0.06	-0.02
FERDER	0.13	-0.03	0.06	-0.03
OKSØY	0.13	-0.03	0.06	-0.02
BERGEN	**0.12**	0.01	0.08	-0.01
ONA	**0.09**	0.01	0.03	-0.00
RØROS	**0.19**	-0.03	-0.00	-0.02
DOMBÅS	**0.16**	-0.02	-0.02	-0.02
VÆRNES	**0.16**	0.00	0.03	-0.01
BODØ	**0.12**	0.00	0.05	0.01
TROMSØ	**0.09**	-0.01	0.06	0.02
KARASJOK	**0.21**	-0.05	0.02	-0.00
VARDØ	**0.06**	-0.03	-0.01	-0.00

Table 30: Downscaled temperature scenario trends (°C/decade) using *scan* HadCM2 SLP scenarios as predictors. Length of interval= 119. Dates 15-Oct-1980 - 15-Oct-2098. Entries shown in bold are significant at the 5% level.

5.3.7 Downscaling by common EOFs based on CCCma T(2m) scenarios.

Location	Jan	Apr	Jul	Oct
member 1				
OSLO	**0.44**	**0.26**	**0.43**	**0.28**
NESBYEN	**0.59**	**0.24**	**0.38**	**0.29**
FERDER	**0.30**	**0.22**	**0.40**	**0.24**
OKSØY	**0.36**	**0.21**	**0.36**	**0.23**
BERGEN	**0.39**	**0.20**	**0.32**	**0.31**
ONA	**0.24**	**0.16**	**0.26**	**0.27**
RØROS	**0.61**	**0.31**	**0.50**	**0.36**
DOMBÅS	**0.51**	**0.28**	**0.46**	**0.31**
VÆRNES	**0.44**	**0.26**	**0.46**	**0.30**
BODØ	**0.43**	**0.29**	**0.30**	**0.23**
TROMSØ	**0.38**	**0.29**	**0.24**	**0.22**
KARASJOK	**0.77**	**0.42**	**0.21**	**0.18**
VARDØ	**0.30**	**0.27**	**0.09**	**0.11**
member 2				
OSLO	**0.40**	**0.19**	**0.40**	**0.39**
NESBYEN	**0.55**	**0.13**	**0.35**	**0.41**
FERDER	**0.33**	**0.09**	**0.38**	**0.37**
OKSØY	**0.35**	**0.08**	**0.33**	**0.35**
BERGEN	**0.32**	**0.23**	**0.31**	**0.36**
ONA	**0.17**	**0.18**	**0.25**	**0.33**
RØROS	**0.31**	**0.35**	**0.48**	**0.55**
DOMBÅS	**0.28**	**0.31**	**0.44**	**0.54**
VÆRNES	**0.23**	**0.29**	**0.46**	**0.50**
BODØ	**0.27**	**0.22**	**0.17**	**0.37**
TROMSØ	**0.24**	**0.21**	**0.13**	**0.36**
KARASJOK	**0.47**	**0.29**	**0.17**	**0.56**
VARDØ	**0.19**	**0.19**	**0.07**	**0.33**
member 3				
OSLO	**0.43**	**0.23**	**0.35**	**0.35**
NESBYEN	**0.62**	**0.18**	**0.33**	**0.36**
FERDER	**0.31**	**0.12**	**0.34**	**0.35**
OKSØY	**0.39**	**0.10**	**0.30**	**0.33**
BERGEN	**0.43**	**0.26**	**0.31**	**0.27**
ONA	**0.24**	**0.22**	**0.25**	**0.22**
RØROS	**0.57**	**0.46**	**0.48**	**0.42**
DOMBÅS	**0.52**	**0.42**	**0.43**	**0.39**
VÆRNES	**0.39**	**0.39**	**0.43**	**0.39**
BODØ	**0.46**	**0.35**	**0.35**	**0.15**
TROMSØ	**0.45**	**0.33**	**0.26**	**0.14**
KARASJOK	**0.78**	**0.49**	**0.18**	**0.26**
VARDØ	**0.30**	**0.31**	**0.06**	**0.22**

Table 31: Downscaled temperature scenario trends (°C/decade) using *scan* CCCma T(2m) scenarios as predictors. Length of interval= 119. Dates 15-Oct-1980 - 15-Oct-2098.

5.3.8 Downscaling by common EOFs based on CCCma *scan* SLP scenarios.

Location	Jan	Apr	Jul	Oct
member 1				
OSLO	0.04	-0.03	-0.00	-0.00
NESBYEN	0.05	-0.03	0.02	0.00
FERDER	0.07	-0.01	0.00	-0.00
OKSØY	0.06	-0.01	0.00	-0.00
BERGEN	0.02	-0.03	0.03	-0.02
ONA	0.01	-0.03	0.02	-0.03
RØROS	0.03	-0.07	0.05	-0.02
DOMBÅS	0.03	-0.07	0.04	-0.02
VÆRNES	0.01	-0.07	0.05	-0.02
BODØ	-0.03	-0.06	0.06	-0.03
TROMSØ	-0.05	-0.05	0.06	-0.02
KARASJOK	-0.06	-0.07	0.03	-0.03
VARDØ	-0.00	-0.05	0.01	-0.01
member 2				
OSLO	-0.07	-0.03	-0.02	0.04
NESBYEN	-0.12	-0.03	-0.01	0.05
FERDER	-0.01	-0.00	-0.01	**0.05**
OKSØY	-0.02	-0.00	-0.02	**0.05**
BERGEN	-0.06	**-0.07**	0.00	0.01
ONA	-0.05	**-0.05**	0.00	0.00
RØROS	-0.08	**-0.11**	-0.01	0.03
DOMBÅS	-0.06	**-0.10**	-0.02	0.04
VÆRNES	-0.08	**-0.11**	0.01	0.03
BODØ	**-0.10**	**-0.11**	0.06	0.02
TROMSØ	**-0.12**	**-0.09**	0.07	0.02
KARASJOK	**-0.17**	**-0.13**	0.05	0.05
VARDØ	-0.03	-0.08	0.01	0.03
member 3				
OSLO	0.03	0.02	**-0.06**	-0.00
NESBYEN	0.02	0.03	-0.05	-0.00
FERDER	0.04	0.03	-0.05	-0.00
OKSØY	0.04	0.03	-0.05	-0.00
BERGEN	0.03	**-0.06**	-0.03	-0.02
ONA	0.01	**-0.07**	0.01	-0.02
RØROS	0.06	-0.06	-0.01	-0.02
DOMBÅS	0.06	-0.05	-0.04	-0.02
VÆRNES	0.04	**-0.09**	0.01	-0.02
BODØ	0.00	**-0.11**	**0.08**	-0.01
TROMSØ	-0.01	**-0.11**	**0.10**	0.00
KARASJOK	-0.06	**-0.16**	0.06	-0.00
VARDØ	-0.02	**-0.11**	0.02	0.00

Table 32: Downscaled temperature scenario trends (°C/decade) using *scan* CCCma SLP scenarios as predictors. Length of interval= 119 years. Dates 15-Oct-1980 - 15-Oct-2098. Entries shown in bold are significant at the 5% level.

5.3.9 Downscaling by common EOFs based on CSIRO T(2m) scenarios.

Location	Jan	Apr	Jul	Oct
nordic				
OSLO	**0.47**	**0.49**	**0.40**	**0.34**
NESBYEN	**0.60**	**0.45**	**0.36**	**0.35**
FERDER	**0.32**	**0.40**	**0.37**	**0.33**
OKSØY	**0.38**	**0.37**	**0.33**	**0.31**
BERGEN	**0.40**	**0.37**	**0.44**	**0.13**
ONA	**0.28**	**0.34**	**0.30**	**0.19**
RØROS	**0.59**	**0.65**	**0.46**	**0.45**
DOMBÅS	**0.49**	**0.55**	**0.45**	**0.43**
VÆRNES	**0.42**	**0.57**	**0.40**	**0.39**
BODØ	**0.22**	**0.60**	**0.14**	**0.21**
TROMSØ	**0.22**	**0.61**	**0.10**	**0.15**
KARASJOK	**0.63**	**0.89**	**0.10**	**0.17**
VARDØ	**0.26**	**0.58**	0.05	**0.09**

Table 33: Downscaled temperature scenario trends (°C/decade) using *scan* CSIRO T(2m) scenarios as predictors. Length of interval= 120. Dates 15-Oct-1980 - 15-Oct-2099. Entries shown in bold are significant at the 5% level.

5.3.10 Downscaling by common EOFs based on *scan* CSIRO SLP scenarios.

Location	Jan	Apr	Jul	Oct
OSLO	-0.05	**-0.03**	-0.01	**-0.07**
NESBYEN	-0.08	-0.03	-0.01	**-0.07**
FERDER	-0.04	-0.01	-0.01	**-0.07**
OKSØY	-0.04	-0.01	-0.01	**-0.06**
BERGEN	-0.04	**-0.03**	-0.01	**-0.05**
ONA	-0.03	**-0.03**	0.00	**-0.05**
RØROS	0.01	**-0.05**	-0.00	**-0.08**
DOMBÅS	-0.00	**-0.05**	-0.01	**-0.08**
VÆRNES	-0.02	**-0.05**	0.00	**-0.07**
BODØ	-0.04	**-0.06**	0.02	**-0.07**
TROMSØ	-0.04	**-0.05**	0.03	-0.05
KARASJOK	-0.05	**-0.09**	0.03	**-0.11**
VARDØ	0.00	-0.05	0.02	**-0.05**

Table 34: Downscaled temperature scenario trends (°C/decade) using *scan* SLP scenarios as predictors. Length of interval= 120. Dates 15-Oct-1980 - 15-Oct-2099. Entries shown in bold are significant at the 5% level.

5.3.11 Downscaling by common EOFs based on CCSR/NIES T(2m) scenarios.

Location	Jan	Apr	Jul	Oct
OSLO	**1.24**	**0.58**	**0.34**	**0.49**
NESBYEN	**1.76**	**0.50**	**0.31**	**0.50**
FERDER	**1.12**	**0.48**	**0.32**	**0.47**
OKSØY	**1.07**	**0.45**	**0.29**	**0.44**
BERGEN	**0.91**	**0.46**	**0.30**	**0.37**
ONA	**0.59**	**0.39**	**0.27**	**0.40**
RØROS	**1.47**	**0.80**	**0.41**	**0.60**
DOMBÅS	**1.23**	**0.70**	**0.32**	**0.55**
VÆRNES	**1.05**	**0.69**	**0.39**	**0.55**
BODØ	**0.44**	**0.75**	**0.34**	**0.63**
TROMSØ	**0.40**	**0.72**	**0.31**	**0.61**
KARASJOK	**0.89**	**0.62**	**0.41**	**0.31**
VARDØ	**0.36**	**0.40**	**0.25**	**0.18**

Table 35: Downscaled temperature scenario trends (°C/decade) using *scan* T(2m) CCSR/NIES scenarios as predictors. Length of interval= 119. Dates 15-Oct-1980 - 15-Oct-2098. Entries shown in bold are significant at the 5% level.

5.3.12 Downscaling by common EOFs based on *scan* CCSR/NIES SLP scenarios.

Location	Jan	Apr	Jul	Oct
OSLO	0.09	0.01	-0.01	0.01
NESBYEN	0.09	0.01	-0.00	0.01
FERDER	**0.09**	0.01	-0.00	0.03
OKSØY	0.08	0.01	-0.01	0.02
BERGEN	**0.08**	-0.02	-0.01	-0.01
ONA	0.03	-0.02	-0.01	-0.01
RØROS	0.07	-0.00	**-0.06**	0.01
DOMBÅS	0.06	-0.01	**-0.05**	0.01
VÆRNES	0.03	-0.01	**-0.06**	0.01
BODØ	0.00	0.00	**-0.05**	-0.02
TROMSØ	-0.02	0.00	-0.05	-0.01
KARASJOK	-0.04	0.01	**-0.09**	-0.00
VARDØ	0.00	0.00	**-0.06**	0.01

Table 36: Downscaled temperature scenario trends (°C/decade) using *scan* SLP scenarios as predictors. Length of interval= 119. Dates 15-Oct-1980 - 15-Oct-2098. Entries shown in bold are significant at the 5% level.

5.3.13 Downscaling by common EOFs based on ECHAM3 T(2m) scenarios.

Location	Jan	Apr	Jul	Oct
1				
OSLO	**0.56**	**0.37**	**0.30**	**0.34**
NESBYEN	**0.76**	**0.34**	**0.27**	**0.34**
FERDER	**0.50**	**0.30**	**0.28**	**0.30**
OKSØY	**0.48**	**0.28**	**0.26**	**0.28**
BERGEN	**0.25**	**0.35**	**0.11**	**0.30**
ONA	0.13	**0.28**	**0.19**	**0.29**
RØROS	**0.37**	**0.47**	**0.37**	**0.46**
DOMBÅS	**0.35**	**0.42**	**0.30**	**0.44**
VÆRNES	**0.27**	**0.39**	**0.35**	**0.42**
BODØ	0.25	**0.43**	**0.27**	**0.34**
TROMSØ	0.22	**0.42**	**0.28**	**0.33**
KARASJOK	0.21	**0.47**	**0.36**	**0.42**
VARDØ	0.12	**0.30**	**0.26**	**0.28**
2				
OSLO	**0.70**	**0.28**	**0.27**	**0.26**
NESBYEN	**0.93**	**0.26**	**0.23**	**0.26**
FERDER	**0.64**	**0.23**	**0.25**	**0.25**
OKSØY	**0.59**	**0.22**	**0.22**	**0.24**
BERGEN	**0.44**	**0.24**	**0.12**	**0.20**
ONA	**0.25**	**0.18**	**0.13**	**0.20**
RØROS	**0.58**	**0.25**	**0.31**	**0.28**
DOMBÅS	**0.53**	**0.23**	**0.26**	**0.26**
VÆRNES	**0.42**	**0.20**	**0.29**	**0.26**
BODØ	**0.36**	**0.26**	**0.23**	**0.31**
TROMSØ	**0.29**	**0.25**	0.23	**0.31**
KARASJOK	0.60	**0.23**	0.27	**0.38**
VARDØ	0.25	0.14	0.17	**0.22**

Table 37: Downscaled temperature scenario trends (°C/decade) using *scan* T(2m) scenarios as predictors. Length of interval= 70. Dates 15-Oct-1980 - 15-Oct-2049. Entries shown in bold are significant at the 5% level.

5.3.14 Downscaling by common EOFs based on *scan* ECHAM3 SLP scenarios.

Location	Jan	Apr	Jul	Oct
1				
OSLO	-0.10	0.02	0.06	-0.00
NESBYEN	-0.16	0.01	0.08	0.00
FERDER	-0.11	-0.01	0.05	-0.02
OKSØY	-0.10	0.00	0.06	-0.01
BERGEN	-0.04	0.09	0.07	-0.01
ONA	-0.04	0.03	0.04	-0.04
RØROS	-0.06	0.01	**0.24**	-0.03
DOMBÅS	-0.06	0.03	**0.21**	-0.04
VÆRNES	-0.05	0.01	**0.23**	-0.02
BODØ	-0.06	0.02	0.13	-0.02
TROMSØ	-0.06	-0.00	0.08	-0.01
KARASJOK	-0.31	-0.03	0.14	0.02
VARDØ	-0.09	-0.01	0.06	0.03

Table 38: Downscaled temperature scenario trends (°C/decade) using *scan* SLP scenarios as predictors. Length of interval= 69. Dates 15-Oct-1980 - 15-Oct-2048. Entries shown in bold are significant at the 5% level.

5.3.15 Downscaling by common EOFs based on ECHAM4 GSA T(2m) scenarios.

Location	Jan	Apr	Jul	Oct
OSLO	**0.45**	**0.33**	**0.24**	**0.21**
NESBYEN	**0.61**	**0.32**	**0.22**	**0.21**
FERDER	**0.38**	**0.25**	**0.21**	**0.21**
OKSØY	**0.37**	**0.24**	**0.18**	**0.18**
BERGEN	**0.36**	**0.35**	0.12	**0.12**
ONA	**0.22**	**0.26**	0.07	**0.12**
RØROS	**0.56**	**0.40**	0.14	**0.25**
DOMBÅS	**0.48**	**0.38**	0.13	**0.22**
VÆRNES	**0.41**	**0.31**	0.10	**0.22**
BODØ	**0.38**	**0.19**	-0.02	**0.18**
TROMSØ	**0.33**	**0.17**	-0.13	0.15
KARASJOK	**0.73**	**0.24**	-0.10	0.16
VARDØ	**0.28**	**0.16**	-0.17	0.10

Table 39: Downscaled temperature scenario trends (°C/decade) using *scan* ECHAM4-GSA T(2m) scenarios as predictors. Length of interval= 69. Dates 15-Oct-1980 - 15-Oct-2048. Entries shown in bold are significant at the 5% level.

5.3.16 Downscaling by common EOFs based on *scan* ECHAM4-GSA SLP scenarios.

Location	Jan	Apr	Jul	Oct
OSLO	0.07	0.10	**-0.15**	-0.01
NESBYEN	0.14	0.10	-0.14	-0.00
FERDER	0.10	**0.10**	**-0.13**	-0.00
OKSØY	0.10	0.09	**-0.13**	-0.00
BERGEN	-0.05	0.04	**-0.20**	-0.07
ONA	-0.00	0.05	**-0.11**	-0.06
RØROS	0.11	0.17	**-0.26**	-0.03
DOMBÅS	0.10	0.14	**-0.23**	-0.03
VÆRNES	0.07	0.12	**-0.26**	-0.03
BODØ	0.03	0.10	-0.19	-0.01
TROMSØ	0.01	0.09	-0.13	0.03
KARASJOK	0.10	0.14	-0.19	0.07
VARDØ	0.03	0.11	-0.11	0.07

Table 40: Downscaled temperature scenario trends (°C/decade) using *scan* ECHAM4 GSA SLP scenarios as predictors. Length of interval= 69. Dates 15-Oct-1980 - 15-Oct-2048. Entries shown in bold are significant at the 5% level.

5.3.17 Downscaling by common EOFs based on GFDL surface temperature scenarios.

Location	Jan	Apr	Jul	Oct
OSLO	**0.47**	**0.44**	**0.19**	**0.51**
NESBYEN	**0.63**	**0.39**	**0.17**	**0.51**
FERDER	**0.47**	**0.35**	**0.18**	**0.49**
OKSØY	**0.46**	**0.33**	**0.16**	**0.45**
BERGEN	**0.36**	**0.25**	**0.18**	**0.39**
ONA	**0.23**	**0.21**	**0.17**	**0.37**
RØROS	**0.53**	**0.51**	**0.32**	**0.65**
DOMBÅS	**0.45**	**0.46**	**0.24**	**0.60**
VÆRNES	**0.36**	**0.44**	**0.22**	**0.60**
BODØ	**0.22**	**0.42**	**0.22**	**0.32**
TROMSØ	**0.23**	**0.40**	**0.25**	**0.28**
KARASJOK	**0.41**	**0.40**	**0.30**	**0.57**
VARDØ	**0.20**	**0.27**	**0.22**	**0.39**

Table 41: Downscaled temperature scenario trends (°C/decade) using *nordic* and *scan* T(2m) scenarios as predictors. Length of interval= 85. Dates 15-Oct-1980 - 15-Oct-2064. Entries shown in bold are significant at the 5% level.

5.3.18 Downscaling by common EOFs based on *scan* GFDL surface pressure scenarios.

Location	Jan	Apr	Jul	Oct
OSLO	-0.10	**-0.09**	0.06	-0.04
NESBYEN	-0.15	**-0.11**	0.08	-0.03
FERDER	-0.09	**-0.08**	0.06	-0.04
OKSØY	-0.08	**-0.07**	0.04	-0.03
BERGEN	-0.12	**-0.08**	0.02	**-0.07**
ONA	-0.09	**-0.07**	0.03	-0.07
RØROS	-0.22	**-0.26**	0.09	-0.08
DOMBÅS	-0.19	**-0.24**	0.06	-0.07
VÆRNES	-0.18	**-0.20**	0.06	-0.07
BODØ	-0.13	**-0.08**	0.00	-0.05
TROMSØ	-0.10	**-0.08**	0.03	-0.04
KARASJOK	-0.21	**-0.15**	0.09	-0.01
VARDØ	-0.06	-0.09	0.09	0.02

Table 42: Downscaled temperature scenario trends (°C/decade) using *nordic* surface pressure scenarios as predictors. Length of interval= 85. Dates 15-Oct-1980 - 15-Oct-2064. Entries shown in bold are significant at the 5% level.

5.3.19 Downscaling by common EOFs based on NCAR-DOE surface temperature scenarios.

Location	Jan	Apr	Jul	Oct
OSLO	**1.37**	**0.85**	**0.83**	**0.58**
NESBYEN	**1.87**	**0.75**	**0.70**	**0.60**
FERDER	**0.96**	**0.54**	**0.76**	**0.43**
OKSØY	**1.13**	**0.47**	**0.68**	**0.44**
BERGEN	**0.92**	**0.49**	**0.59**	**0.57**
ONA	**0.69**	**0.45**	**0.43**	**0.58**
RØROS	**0.69**	**0.93**	**1.06**	**0.92**
DOMBÅS	**0.61**	**0.79**	**0.95**	**0.88**
VÆRNES	**0.47**	**0.82**	**0.92**	**0.85**
BODØ	**0.73**	**0.83**	**0.82**	**0.58**
TROMSØ	**0.75**	**0.91**	**0.57**	**0.61**
KARASJOK	**1.78**	**1.31**	**0.67**	**0.63**
VARDØ	**0.60**	**0.86**	0.35	**0.40**

Table 43: Downscaled temperature scenario trends (°C/decade) using *scan* NCAR-DOE T(2m) scenarios as predictors. Length of interval= 55. Dates 15-Oct-1980 - 15-Oct-2034. Entries shown in bold are significant at the 5% level.

5.3.20 Downscaling by common EOFs based on *scan* NCAR-DOE surface pressure scenarios.

Location	Jan	Apr	Jul	Oct
OSLO	0.23	-0.01	-0.17	-0.09
NESBYEN	0.30	-0.02	-0.17	-0.08
FERDER	0.22	-0.02	-0.10	-0.07
OKSØY	0.21	-0.02	-0.07	-0.06
BERGEN	0.17	0.01	-0.03	-0.15
ONA	0.07	-0.01	-0.03	-0.15
RØROS	0.22	-0.03	-0.12	-0.17
DOMBÅS	0.20	-0.02	-0.13	-0.16
VÆRNES	0.14	-0.01	-0.09	-0.16
BODØ	0.02	-0.06	0.02	-0.18
TROMSØ	-0.02	-0.06	0.04	-0.15
KARASJOK	0.01	0.01	-0.03	-0.22
VARDØ	0.02	-0.01	-0.02	-0.08

Table 44: Downscaled scenario trends (°C/decade) using *nordic* NCAR-DOE surface pressure scenarios as predictors. Length of interval= 55. Dates 15-Oct-1980 - 15-Oct-2034. Entries shown in bold are significant at the 5% level.

Table 25 shows trend estimates for the 1980-2108 from the NCAR-CSM model based on downscaling of the T(2m) field (*natl* and *scan* predictor domains). The scenarios derived using the predictor area *scan* are in rough agreement with the ECHAM4 GSDIO scenarios, albeit with higher estimates (Table 15). Note that the NCAR-CSM (*Meehl* et al., 2000) and the ECHAM4/OPYC3 (*Roeckner* et al., 1998) GSDIO integrations are based on slightly different scenarios: the former has a 1% annual increase in CO_2, but not sulfur cycle. The timing of the strongest warming in the NCAR-CSM scenario occurs in January, with the exception of Ona in July. Both scenarios indicate less warming for the west coast stations. Both scenarios give negligible summer-time trends for northernmost stations. Karasjok is the station which has highest predicted warming in January according to both model scenarios.

The fact that the downscaling gives such different estimates for the two different predictor domains suggests that the downscaled results based on the NCAR-CSM are not robust. In comparison, the GSDIO scenarios derived using the *natl* and *scan* predictor domains give more similar results for January, but less robust estimates for April, July, and October.

The downscaled results based on NCAR-CSM *scan* SLP scenario, shown in Table 26, suggest that a projected change in the large-scale circulation in January may reduce the local warming due to the increased CO_2 concentrations, but these trends are not statistically significant at the 5% level. These results disagree with the corresponding ECHAM4 GSDIO results (Table 21), which suggest that the atmospheric flow is likely to enhance the projected warming in January. In April, neither AOGCM give much trend. The weak July trends derived from the NCAR-CSM scenario stand in contrast to those of ECHAM4 GSDIO, which indicate enhanced advective cooling, and the NCAR model suggests a weak but significant warming trend in October whilst the corresponding downscaled GSDIO trends are not significantly different to zero.

Table 27 shows downscaled results based on HadCM3 T(2m) from two do-

mains (*nordic* and *scan*). The largest domain gives higher trend estimates in January, weaker warming in July, and relatively robust results in April and October. The highest warming rate is found in Nesbyen (Karasjok second) during January for the scenarios derived from the *scan* domain, but stronger warming is estimated for Karasjok if the *nordic* is used. Thus, there is a fairly good agreement between the GSDIO and the HadCM3 results on both the location and the seasonal timing of maximum warming. The HadCM3 results tend to be higher than those from the GSDIO run, but the two integrations are based on different scenarios, where the GSDIO includes both the direct and indirect effects of the aerosols and the HadCM3 (GSA) only includes the direct effect. The weakest warming is found in northern Norway during July, both in the downscaled results derived from the GSDIO and the HadCM3 results. The results appear to be robust with respect to the domain size smaller than *nordic*.

A comparison between the downscaled results based on the T(2m) and those derived from the SLP field can give an explanation for why the various scenarios differ. Table 28 suggests advective cooling during January but significant circulation driven warming in April. The *nordic* predictor domain gives more pronounced warming than the *scan*, and the downscaled HadCM3 results based on the SLP are therefore not robust. Furthermore, a reduction in the January warming rate due to the circulation patterns cannot explain the differences between the GSDIO and the HadCM3 based results. The explanation is more likely related to using different scenarios, different model formulations, and the fact that the HadCM3 doesn't utilize flux correction.

The downscaled results from a 4-member ensemble run with the HadCM2 model are shown in Table 29. This model is similar to the HadCM3 but with lower resolution in the ocean. The downscaled January estimates from the ensemble are both higher and lower than the GSDIO results, with 3 members giving smaller trends. The April and July trends derived from the HadCM2 model tend to be higher, with the exception of the third member July trends. The October trends have similar magnitude to those derived from the GSDIO scenario. The HadCM2 integrations included different physics to the GSDIO, as they did not include the indirect aerosol effects. This difference may explain the tendency to higher estimates in the results derived from the HadCM2 scenarios. However, the large scatter between the different ensemble run, suggests a great deal of uncertainty associated with the choice of initial condition, since the boundary conditions were the same for each ensemble member. All the downscaled scenarios in Table 29 indicate maximum warming in January near Nesbyen (4) or Karasjok (1,2,3), and three of the members indicate weak warming in northern Norway during July. The warming rate peaks in January for 3 of the ensemble members, but the last member does indicate maximum warming rate in January for Karasjok. The scenarios for Ona have a tendency of being associated with weaker warming rates than the other stations.

The same analysis derived using the *nordic* domain (not shown), gave stronger trends in the January results for member 1, stronger July trend for member 2, and weaker July warming for member 4. Roughly similar results were obtained for the two different domains in April, July and October for member 1, January, April and October for member 2, all months for member 3, and January, April and October for member 4. These downscaled results were therefore fairly robust, depending on the season and member.

The SLP-based scenarios in Table 30 indicate substantial advective cooling

in January for member 3, explaining the discrepancy between this member and the others. The scenarios derived from the SLP field were robust with respect to the domain size (*nordic* and *scan*), but a larger domain suggested more enhanced January warming for member 4. Thus, 3 out of the 4 HadCM3 scenarios suggest different climate regimes to the GSDIO integration, suggesting that the SLP field is very sensitive to the initial conditions.

The downscaling of the 3 member ensemble integration with the CCCma model gave less intra-ensemble spread than the HadCM2 experiment (Table 31). The CCCma-based results indicate slightly weaker trends over southeastern Norway in January than those derived from the GSDIO scenario, but stronger warming in July and October. The CCCma scenarios for the west coast and middle Norway similar to the results derived from the GSDIO integration, and the CCCma scenarios associated with relatively small January trends in Karasjok. In April, Table 31 suggests weaker trends in southern Norway but more pronounced warming in the north. The maximum warming tends to be in Karasjok during January, but the second ensemble member suggests greater warming in Karasjok during October. Similar analysis on the CCCma results derived with the *nordic* domain (not shown) doesn't alter this picture significantly, except for the October temperature at Bodø, Tromsø, Karasjok and Vardø derived from the ensemble member number three.

The downscaling of the CCCma SLP field (Table 32) produced mostly weak trends, suggesting that the circulation driven climate change in these scenarios is of less importance then in the HadCM2 experiments. Again, there is little sign of a strengthening of the NAO and enhanced westerlies over the Norwegian Sea bringing milder climate in January. The same analysis applied to the data using the *nordic* domain (not shown) suggests that these findings are relatively robust.

The results from the downscaling analysis applied to the CSIRO model are shown in Table 33, and the results are in good agreement with those from the GSDIO integration for the January month. The January trends are slightly lower in northern Norway, but the April estimates are systematically higher than the results in Table 15. In fact, the CSIRO model was the only one of these AOGCMs that gave maximum warming during springtime, in line with the past trends seen in the observations (*Benestad*, 2000c), possibly associated with substantial springtime reduction in the snow-cover (*Brown*, 2000). The strongest warming in the results derived from the CSIRO model is found in Karasjok during April, and the weakest warming is located in Vardø in July. In July and October, the CSIRO based results tend to suggest strongest warming in the south and more modest warming in the north. These results are robust with respect to the predictor domain smaller than *nordic*.

The temperature changes associated with shifts in the large-scale circulation (Table 34) are small compared with the trends estimated using the T(2m) field as predictor (Table 33). The CSIRO scenarios give no sign of pronounced wintertime warming due to a strengthening of the westerlies over the Norwegian Sea. The same analysis on the results calculated using the *nordic* domain gives similar conclusions (not shown).

Table 35 shows the downscaled results based on the Japanese CCSR/NIES model. The analysis of this scenario gives substantially higher trend estimates than the GSDIO results in Table 21, with the maximum warming as high as 1.76°C/decade for January in Nesbyen. The weakest warming trend is seen in

Vardø during October. The CCSR/NIES results give greatest warming rates in southern Norway and less warming further north. The analysis with the *nordic* domain produces similar results (not shown).

The downscaled CCSR/NIES SLP scenarios, shown in Table 36, give only moderate winter-time warming associated with circulationary changes. Thus, the CCSR/NIES scenario does not reproduce the systematic strengthening of the NAO as seen in the GSDIO results. The downscaling model based on the *nordic* domain (not shown) gives stronger January temperature trends in the south.

Table 37 shows downscaled results from two scenarios with the ECHAM3 model. This AOGCM is similar to the ECHAM4 model used in the GSDIO run, but with different ocean model (LSG) and parameterisation. The results from the ECHAM3 experiments are similar to the ECHAM4 GSDIO results, except for more modest warming rates in northern Norway during January. The differences between the two ensemble members are of similar magnitude to the differences between the two runs and the GSDIO results. The *nordic* downscaling models give similar results (not shown).

The SLP field was available for only one of the ECHAM3 ensemble members, and the downscaling analysis of this scenario suggests that the January warming is partially offset by advective cooling (Table 38). Thus, these results are contradictory to the strengthening of the NAO as seen in the GSDIO SLP. Only the July trend in Bergen is statistically significant at the 5% level if the same analysis is done with a *nordic* model (not shown).

Table 39 shows downscaled results from the GSA integration with the ECHAM4 model. These results were computed with the same model as in the ECHAM4 GSDIO experiment, except for not taking the aerosols' *indirect* effect (on the cloud drops and life times) into account. The results in Table 39 are in good agreement with the results in Table 15, except for the hints of cooling (not statistically significant at the 5% level) seen in northern Norway in July. The highest trend estimate is seen in Karasjok during January, as in many of the other AOGCM results. These results are relatively robust regarding the predictor domain.

The downscaled results from the ECHAM4 GSA SLP scenarios are shown in Table 40, and with the exception of Bergen and Ona, the wintertime circulation changes may enhance the warming rate slightly (not statistically significant at the 5% level), in agreement with the ECHAM4 GSDIO results (Table 21). Furthermore, the July scenarios suggest a cooling effect of the shifts in the atmospheric flow. These findings are similar in the analysis with the *nordic* domain (not shown).

The downscaled analysis of the GFDL scenarios (Table 41) are in fairly good agreement with the ECHAM4 GSDIO results. The discrepancies between these two experiments include less warming in the north during January in the GFDL results, but stronger warming in July. The strongest warming estimate is seen in Røros during October, and the highest seasonal warming rates for many locations are estimated for the October month. If the analysis is done with the *nordic* model, then the strongest seasonal warming rate is seen in January and April (highest rate of 0.82°C/decade in Nesbyen during January, not shown). The SLP changes in the GFDL experiment suggest that the winter and spring-time warming rates are reduced by advective cooling due to long-term changes in the circulation patterns. Thus, the GFDL scenario disagrees with the ECHAM4

GSDIO experiment on the issue of strengthened NAO. The GFDL results are relatively robust with respect to the domain size.

The last AOGCM scenario examined here is from the NCAR-DOE model. It is evident from Table 43 that this model gives high estimates for the temperature trend, and these scenarios are extreme on the high end. Since this AOGCM does not use flux correction, it is possible that the high estimates are partly due to an artificial climate drift. However, in a comparison between the NCAR-CSM and NCAR-DOE, *Meehl* et al. (2000) explained the differences between the two models in terms of different cloud representation and different oceanic heat transport.

Table 43 suggests equal or faster increase in the January temperature in Bergen and Ona than for the inland stations Røros and Dombås, which doesn't make sense. The NCAR-DOE results also indicate maximum warming during January, except for at Røros, Dombås and Værnes for which the strongest warming rates are estimated during July and Bodø and Tromsø, with most pronounced warming in April. The highest trend estimate is found in Karasjok during January: 1.78°C/decade, and is substantially higher than other estimates. The analysis based on the *nordic* domain (not shown) reduces the estimates in the south, but increases the January estimate for Karasjok: 2.10°C/decade. The spring and summer-time warming for southern Norway is reduced with larger predictor area, but increased in northern Norway. Hence, these estimates are not robust with respect to the predictor domain.

The NCAR-DOE SLP scenarios suggest (not statistically significant at the 5% level due to strong short-term variations) advective warming over southern Norway in January, and some cooling during July and October. The same analysis with the *nordic* domain does not reproduce the July cooling.

6 Precipitation scenarios based on SLP

The precipitation stations were in this report selected according the data record length and continuity of the records. The criteria in this case was that they must cover the period 1891-1990. Figure 29 shows the locations of the stations that qualified in this test.

6.1 ECHAM4/OPYC3 GSDIO

Downscaled precipitation scenarios for the January and July months based on SLP patterns are shown in Figure 30. These trends are related to the shifts in the circulation patterns. Such circulation changes may be due to global warming, but may also occur naturally. Here, long-term changes which in the AOGCM scenarios are caused by a global warming are examined. The results from the ECHAM4 GSDIO experiment suggests a strengthening of the westerlies for all seasons, enhancing the advective warming in the winter and reducing the warming in the summer (Table 21).

Table 45 shows how the downscaled precipitation scenarios vary with the domain size. Although there are some scatter among the various estimates, the results seem to be relatively robust with respect to the domain choice. In general, the results suggest an increase in the precipitation on the west coast in summer and autumn which is associated with enhanced mean westerly winds.

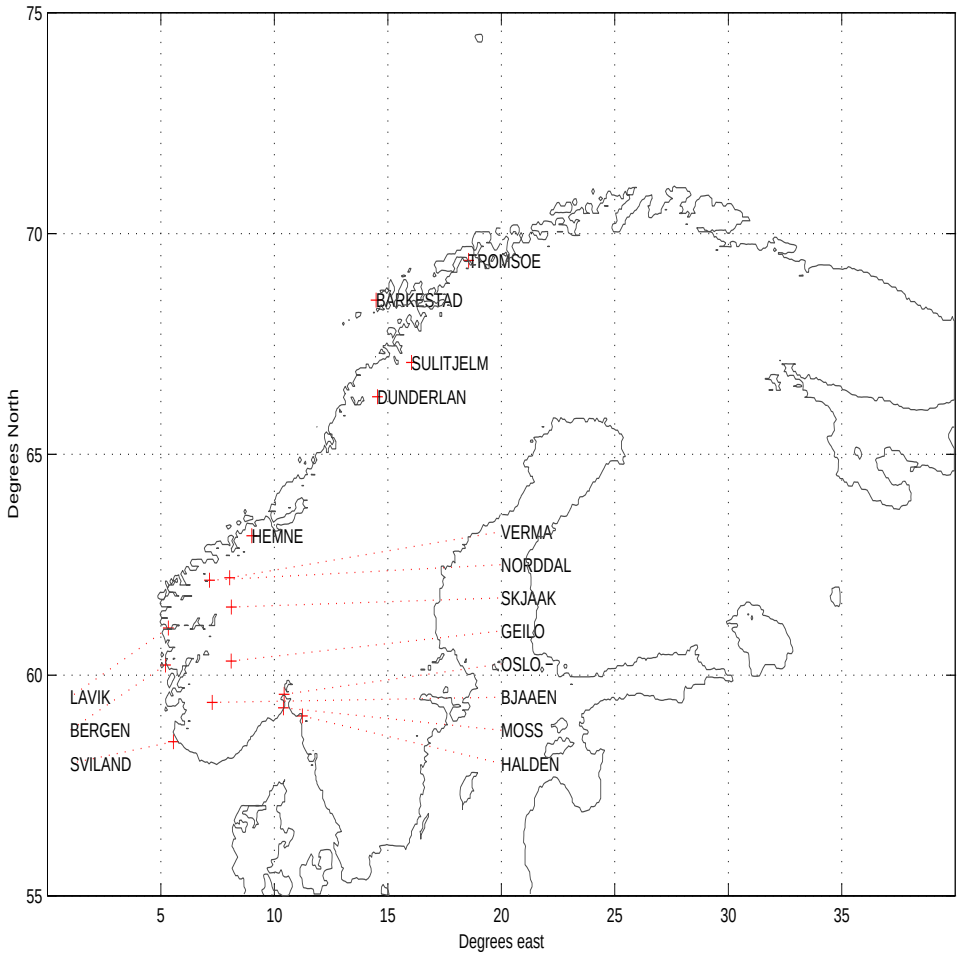

Figure 29: Map showing the location of the rainfall stations used in this study.

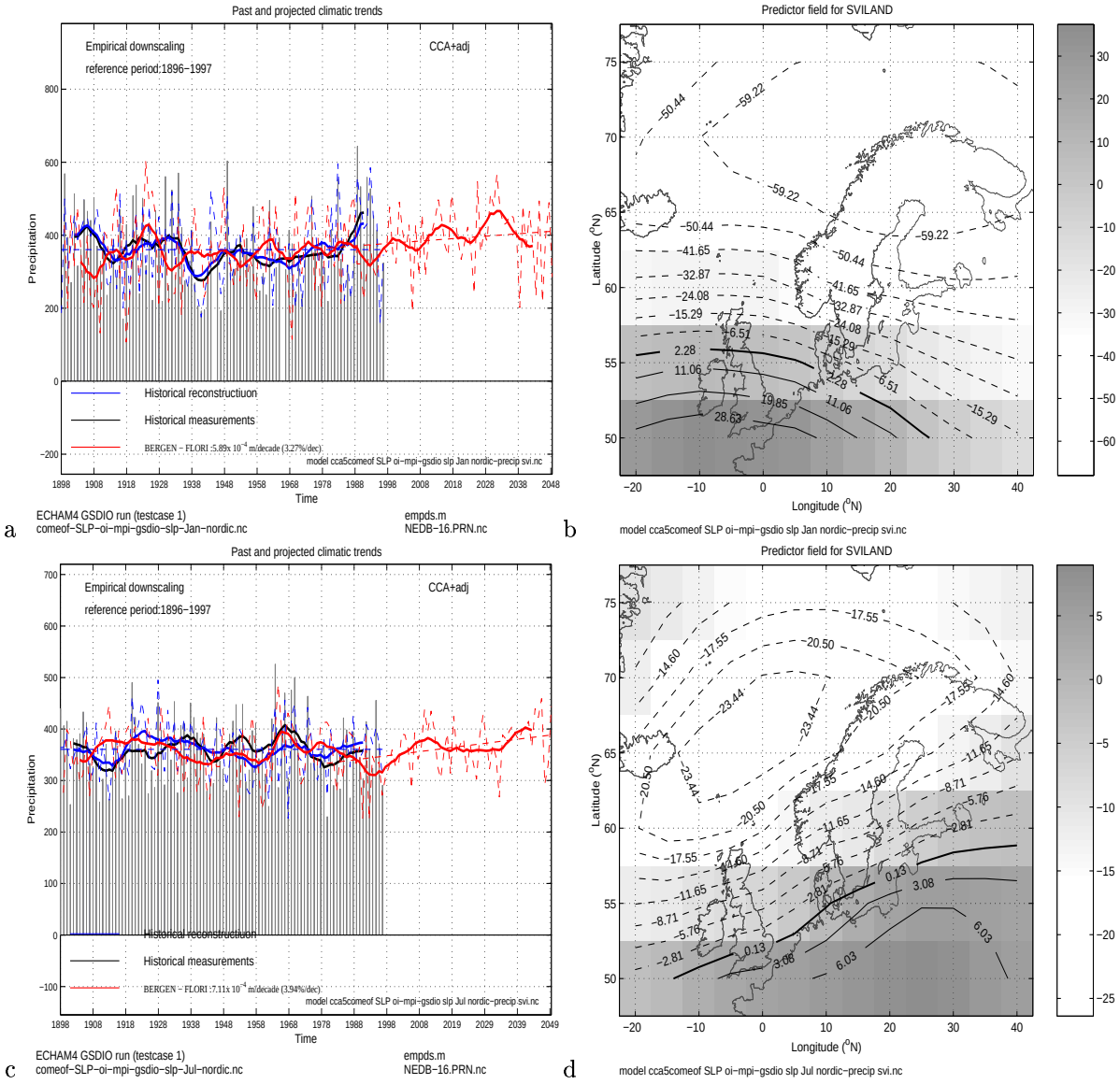

Figure 30: The precipitation scenarios (red), observations (black), and cross-validation results (blue) for Bergen (left) and the leading CCA pattern for Sviland, Bergen, and Lavik precipitation series (right).

6.1.1 The influence of predictor domain size for downscaled ECHAM4 GSDIO SLP rainfall scenarios

Location	natl	nord	scan	natl	nord	scan
commonEOF						
	January			*April*		
HALDEN	1.4/2	1.6/3	1.5/2	**-1.9/-3**	-1.9/-3	-1.4/-2
MOSS	0.8/1	1.1/2	0.8/1	**-2.0/-3**	-1.9/-3	-1.6/-2
OSLO	0.7/1	1.1/2	1.0/2	**-1.8/-3**	-1.9/-3	-1.6/-3
RØROS	-0.4/-1	-0.2/0	-0.5/-1	-0.1/-0	-0.1/-0	-0.4/-1
SKJÅK	0.7/3	1.0/4	1.0/4	-0.1/-0	0.1/0	0.0/0
NORDDAL	0.7/1	2.1/3	1.9/2	0.4/0	0.6/1	0.2/0
VERMA	-0.1/0	0.8/1	0.8/1	0.3/0	0.5/1	0.0/0
HEMNE	0.4/0	2.9/2	0.7/1	2.2/2	1.6/1	1.7/1
NAMDALSEID	-0.4/-0	1.6/1	0.3/0	2.0/2	1.8/2	2.2/2
DUNDERLANDSDAL	1.9/2	4.9/4	7.1/6	0.3/0	2.7/2	2.6/2
SULITJELMA	-1.9/-2	-1.2/-1	4.0/5	1.4/2	3.0/4	1.3/1
BARKESTAD	-1.4/-1	-0.2/-0	0.2/0	1.5/1	3.2/3	2.9/2
TROMSØ	-1.8/-2	-0.1/0	-1.0/-1	0.2/0	2.2/3	2.0/3
GEILO	2.0/3	1.6/3	2.0/3	-0.4/-1	-0.3/-1	-0.6/-1
BJÅEN	4.5/6	**5.1/7**	**5.9/8**	-0.2/0	-0.3/0	0.0/0
SVILAND	3.4/2	4.9/3	4.7/3	-0.8/-1	0.3/0	-0.4/0
BERGEN	4.3/2	6.5/4	6.0/3	-0.3/0	1.1/1	-0.1/0
LAVIK	4.8/3	6.6/4	5.7/3	0.4/0	1.5/1	1.0/1
	July			*October*		
HALDEN	0.0/0	-0.1/0	1.5/2	**4.4/7**	2.9/5	**4.1/7**
MOSS	-0.6/-1	0.4/1	2.0/3	4.5/7	2.9/4	4.6/7
OSLO	-0.5/-1	0.6/1	2.0/3	3.5/6	2.2/4	3.6/6
RØROS	0.6/2	0.7/2	**2.5/6**	-0.1/-0	0.3/1	0.5/1
SKJÅK	-0.3/-1	1.0/4	1.6/6	-1.0/-4	-0.2/-1	0.3/1
NORDDAL	0.9/1	0.8/1	**3.0/4**	-1.6/-2	-0.9/-1	0.7/1
VERMA	0.7/1	0.9/1	**2.0/3**	-0.7/-1	-0.5/-1	0.5/1
HEMNE	2.4/2	**3.9/3**	**3.7/3**	-3.0/-2	-2.7/-2	-2.1/-2
NAMDALSEID	1.6/1	**3.2/3**	**2.9/3**	-2.7/-3	-2.2/-2	-1.5/-1
DUNDERLANDSDAL	**2.9/3**	**2.4/2**	1.5/1	-2.8/-3	1.3/1	-0.7/-1
SULITJELMA	3.0/3	1.6/2	1.2/1	**-7.0/-8**	-2.5/-3	-3.6/-4
BARKESTAD	2.4/2	1.3/1	1.6/1	-5.9/-5	-4.2/-4	-6.0/-5
TROMSØ	1.0/1	0.4/0	0.9/1	**-5.9/-8**	-5.3/-7	-4.7/-6
GEILO	-0.3/0	-0.9/-1	1.1/2	2.6/4	1.3/2	2.2/4
BJÅEN	-0.8/-1	-0.1/0	1.8/2	3.6/5	3.1/4	3.6/5
SVILAND	4.0/3	**6.0/4**	**5.0/3**	7.4/5	6.3/4	8.6/6
BERGEN	**7.5/4**	**7.9/4**	**7.1/4**	4.7/3	5.8/3	6.5/4
LAVIK	**8.4/5**	**8.0/5**	**7.3/4**	0.3/0	4.8/3	2.5/1

Table 45: Downscaled precipitation scenario trends (mm/(month decade) and %/decade) using the domains: *natl* (90°W-40°E, 40°N-75°N), *nord* (20°W-40°E, 50°N-75°N), and *scan* (0°W-30°E, 55°N-75°N). The results shown are for the common EOF method (cEOF). Length of interval= 70 years. Dates 15-Jan-1980 - 15-Jan-2049. Entries shown in bold are significant at the 5% level.

6.1.2 Downscaling precipitation by common EOFs based on *Benestad* (2000b) Scandinavian ECHAM4 GSDIO SLP

Location	Jan	Feb	Mar	Apr	May	Jun	Jul	Aug	Sep	Oct	Nov	Dec
HALDEN	1.5/2	-0.8/1	-0.8/1	-1.4/2	-0.9/1	-0.4/1	1.5/2	-0.4/1	-0.4/1	**4.1/7**	-1.7/-3	0.4/ 1
MOSS	0.8/1	-1.2/2	-1.0/2	-1.6/2	-0.5/1	0.1/0	2.0/3	-0.4/1	-1.8/3	4.6/7	-2.5/4	-0.2/0
OSLO	1.0/2	-0.7/1	-0.8/1	-1.6/3	-0.5/1	0.0/0	2.0/3	-0.5/1	-1.1/2	3.6/6	-1.5/2	0.1/0
RØROS	-0.5/1	0.9/2	0.3/1	-0.4/1	-0.2/0	-0.1/0	**2.5/6**	1.4/3	0.9/2	0.5/1	-0.1/0	0.2/1
SKJÅK	1.0/4	0.9/3	-0.0/0	0.0/0	-0.2/1	0.0/0	1.6/6	0.8/3	**1.3/5**	0.3/1	0.4/2	0.4/1
NORDDAL	1.9/2	3.6/5	1.3/2	0.2/0	0.3/0	0.7/1	**3.0/4**	2.2/3	**8.8/11**	0.6/1	3.0/4	1.5/2
VERMA	0.8/1	4.4/7	1.5/2	0.0/0	0.1/0	0.6/1	**2.0/3**	1.6/3	**6.8/11**	0.5/1	2.7/4	1.6/3
HEMNE	0.7/1	5.3/4	1.1/1	1.7/1	0.1/0	0.7/1	**3.7/3**	**5.6/4**	**10.4/8**	-2.1/2	2.2/2	2.1/2
NAMDAL'	0.3/0	2.2/2	0.8/1	2.2/2	0.4/0	0.2/0	**2.9/3**	3.2/3	**9.3/9**	-1.5/1	1.5/1	1.6/2
DUNDER'	7.1/6	-0.9/1	0.6/0	2.6/2	2.0/2	1.3/1	1.5/1	1.0/1	**8.7/8**	-0.7/1	4.0/4	-3.3/3
SULITJ'	4.0/5	-0.4/1	0.2/0	1.3/1	1.0/1	1.4/2	1.2/1	-1.6/2	4.8/6	-3.5/4	3.4/4	0.5/1
BARKEST'	0.2/0	-0.1/0	0.9/1	2.9/2	2.3/2	1.4/1	1.6/1	-2.7/2	6.1/5	-6.0/5	4.5/4	0.7/1
TROMSØ	-1.0/1	0.4/0	-0.3/0	2.0/3	1.4/2	0.8/1	0.9/1	-2.0/3	3.4/4	-4.7/6	3.4/4	0.9/1
GEILO	1.9/3	-0.2/0	-0.4/1	-0.6/1	-1.2/2	-0.1/0	1.1/2	-0.4/1	0.0/0	2.2/4	0.1/0	0.3/0
BJÅEN	**5.9/8**	0.9/1	-0.8/1	0.0/0	-0.7/1	-0.5/1	1.8/2	-0.9/1	0.4/1	3.6/5	0.9/1	1.7/2
SVILAND	4.7/3	1.2/1	1.8/1	-0.4/0	0.1/0	1.4/1	**5.0/3**	3.0/2	5.0/3	8.6/6	0.9/1	1.4/1
BERGEN	6.0/3	1.6/1	1.9/1	-0.1/0	2.0/1	3.9/2	**7.1/4**	6.1/3	11.3/6	6.5/4	4.9/3	-0.6/0
LAVIK	5.7/3	1.9/1	2.8/2	1.0/1	2.4/1	4.4/2	**7.3/4**	**6.9/4**	**14.3/8**	2.5/1	6.7/4	2.2/1

Table 46: Downscaled precipitation scenarios (mm/(month decade) and %/decade) of the GSDIO results using the common EOF method *Benestad* (2001). Length of interval= 70 years. Dates 15-Dec-1980 - 15-Dec-2049. The predictor domain was 90°W-40°E, 40°N-75°N. Entries shown in bold are significant at the 5% level.

These results are in close agreements with the dynamically downscaled results from RegClim's principal task 1 (*Bjørge* et al., 2000). The southeastern part of Norway will get slightly dryer spring and summer according to these scenarios (not all of these are statistically significant), but these summer projections contrasts with the dynamically downscaled ones. During winter and autumn, the north may get reduced precipitation whereas the south may get more, which again is different to the dynamically downscaled projections. It is important to note that the empirically and dynamically downscaled results are not directly comparable as *a)* the empirical scenarios represent a single location whereas the latter describe mean changes over larger areas, and *b)* because the former are estimated from best-fit linear trends fitted to the 1970-2050 period (70 years) whereas the latter are estimated from two time slice experiments (1980-2000 and 2030-2050), so that there will be differences due to natural (decadal) fluctuations. The diverging results may be regarded as a result of uncertainties where the (empirical or dynamical) models do not give robust answers. The highest rate of precipitation change estimated for the empirical downscaled scenarios is 11%/decade for Nordal and Verma (September, Table 46) which is not extraordinary as the observed change in the winter precipitation on the western coast of Norway over the past 4 decades has been around 10%/decade (Hanssen-Bauer private communication).

Common EOFs of the SLP was used to downscale SLP to make precipitation scenarios. Such scenarios will only capture the "large-scale" component of the precipitation, and are not expected to describe much of "convective" (cumulus) type convection.The empirical downscaling was done the same way as for the temperature using a step-wise CCA approach where each common principal component was tested in a cross-validation analysis for their contribution towards the model skill . The "skill" of these empirical precipitation models can be inferred from Table 8, which gives the cross-correlation scores for the empirical predictions using the (*Benestad*, 2000a) SLP as a basis. The actual values were computed for the common EOFs of (*Benestad*, 2000a) and ECHAM4 GSDIO

6.1.3 Downscaling of ECHAM4 GSDIO by common EOFs based on NCEP 700hPa geopotential height.

Location	Jan	Apr	Jul	Oct
HALDEN	1.6/ 3	-1.0/ -2	-0.5/ -1	**5.8/ 9**
MOSS	0.4/ 1	-0.6/ -1	0.9/ 1	4.8/ 7
OSLO	0.6/ 1	-0.5/ -1	0.3/ 1	3.3/ 5
RØROS	-0.6/ -1	**-0.7/ -2**	1.5/ 4	0.4/ 1
SKJÅK	0.3/ 1	0.2/ 1	**1.9/ 7**	-0.3/ -1
NORDDAL	-0.2/ 0	0.6/ 1	**1.6/ 2**	0.9/ 1
VERMA	0.0/ 0	0.2/ 0	1.3/ 2	0.6/ 1
HEMNE	-1.0/ -1	-0.3/ 0	1.9/ 1	-1.1/ -1
NAMDALSEID	0.2/ 0	0.8/ 1	2.6/ 3	-2.6/ -3
DUNDERLANDSDAL	3.9/ 3	3.4/ 3	-1.3/ -1	4.2/ 4
SULITJELMA	1.0/ 1	-1.7/ -2	**-4.0/ -5**	1.5/ 2
BARKESTAD	1.1/ 1	1.2/ 1	-2.9/ -3	**-10.1/ -9**
TROMSØ	-0.9/ -1	0.4/ 1	0.6/ 1	**-6.4/ -8**
GEILO	1.6/ 3	-0.47/ -1	0.5/ 1	1.3/ 2
BJÅEN	**5.5/ 7**	-0.9/ -1	0.8/ 1	**5.2/ 7**
SVILAND	**6.1/ 4**	-1.1/ -1	**4.4/ 3**	5.3/ 4
BERGEN	**7.4/ 4**	2.4/ 1	*5.4/ 3*	6.3/ 3
LAVIK	7.5/ 4	2.56/ 1	**6.4/ 4**	3.4/ 2

Table 47: Downscaled precipitation scenarios (mm/(month decade) and %/decade) of the ECHAM4 GSDIO results using the common EOF method on the model and NCEP z700. Length of interval= 119 years. Dates 15-Oct-1990 - 15-Oct-2108. The predictor domain was *natl*. Entries shown in bold are significant at the 5% level.

SLP, but since these results only relate to the observational part and the same observations are used in the computation of the common EOFs for all model scenarios, it is expected that these results are valid for all AOGCM scenarios.

Table 8 indicates that the precipitation based models cannot capture as much of the signal as the models predicting the temperature (Table 7). The lowest cross-validation correlation scores are seen in April and July. The empirical model skill is considered good in winter and autumn for the locations on the west coast, and (Norddal, Verma, Hemne, Namdalseid, Tromsø, Bjåen, Sviland, Bergen, Lavik, see Figure 29).

Figure 30 shows one precipitation scenario for Bergen for January and July. The figure illustrates how the long-term linear trends in the precipitation is calculated. A linear least squares method against time after 1980 was used to infer the most likely linear trend. The right hand panels show the predictor patterns associated with the rainfall anomalies.

The sensitivity of the downscaled results with respect to domain size was examined for the ECHAM4 GSDIO results, and some of these results are shown in Table 45. There is some uncertainty associated with these results, as they are not entirely robust with respect to predictor domain. But, the scenarios based on different predictor domains for the west coast and mid Norway tend to give similar trends in January and October. In many cases the trends are small and not statistically significant, and their sign may fluctuate between being positive and negative. In those cases where statistically significant trends are found, the sign of the slope doesn't change with predictor domain. Thus, these estimates are reasonably robust.

Table 46 gives the estimated trends from the ECHAM4 GSDIO for each of the 12 calendar months. These results were based on the *scan* domain, and show significant in July and September. Positive estimates denote trends towards a wetter climate, whereas negative values indicate a change towards drier conditions. Most of the increased rainfall is estimated for the west coast and mid-Norway (Figure 29). The cross-validation scores in Table 8 are lowest for these seasons (correlation of 0.4-0.8), and the empirical models only capture 16%-60% of the rainfall. Thus, these estimates are not the whole story.

The results from a downscaling test using the Φ_{700hPa}-field are shown in Table 47. This test suggested wetter autumn in the south and drier spring in souther n Norway. Furthermore, the west coast can expect more rainfall during winter according to these estimates. The test results from the Φ_{700hPa}-experiments are roughly similar to those based on the SLP, exception for the drier Φ_{700hPa}-scenarios for Sulitjelma in July.

6.2 A super-ensemble scenario based on 33 estimations and 15 global climate model scenarios

A simple multiple regressional analysis (not stepwise in this case) between the 10 leading common principal components between *Benestad* (2000b) SLP and 15 AOGCMs was carried out with the analytical package called `R`. Table 48 shows the ANOVA F-statistics and p-value associated with the regression between the observational part of the principal component (*Benestad* (2000b)). Only for a few locations (the West coast in January, Troms/ø= in July, and Bergen in October) were the regressions considered as good, and only a poor relationship was found for the majority of the stations. The results associated

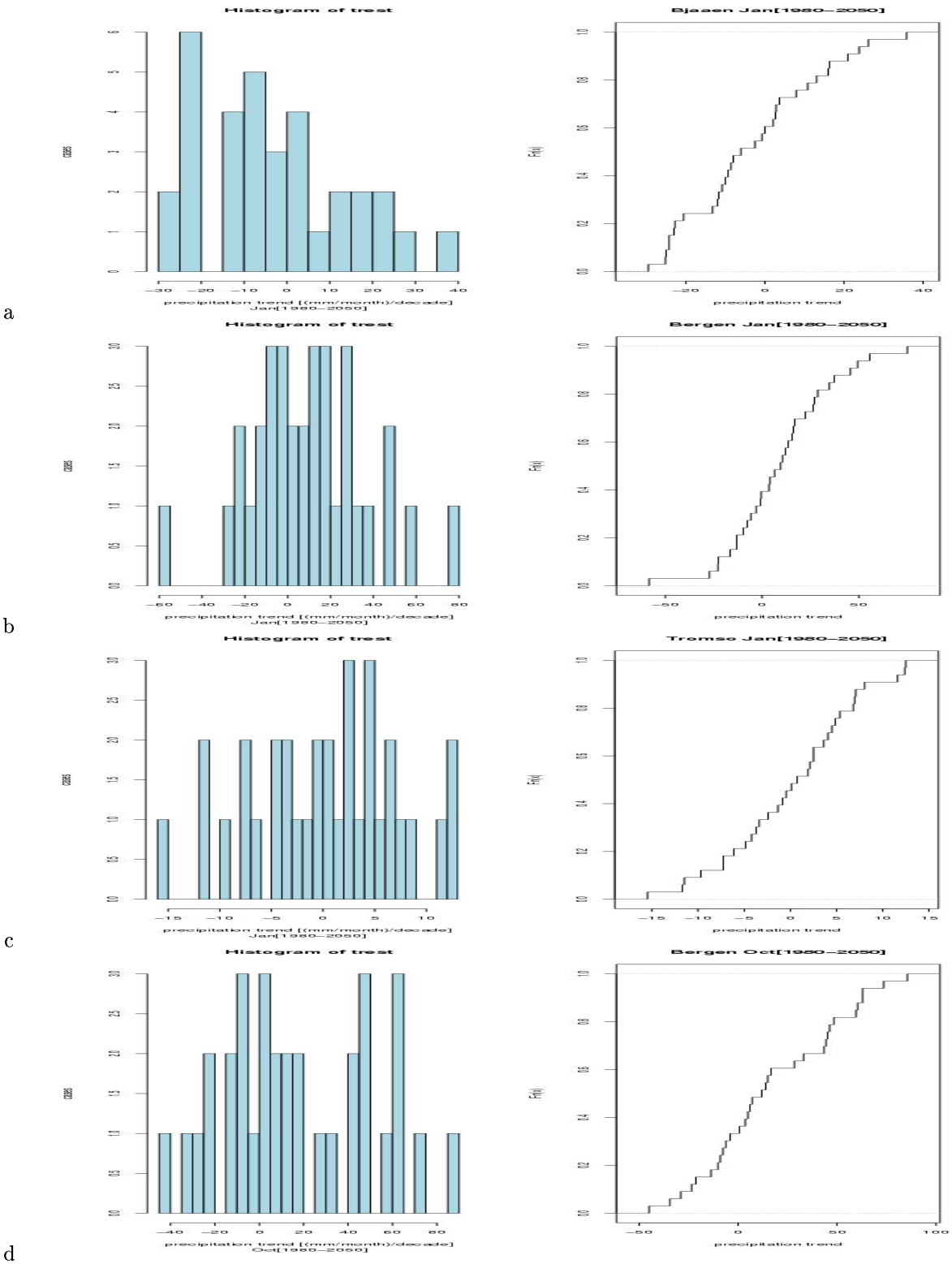

Figure 31: Plots showing the histogram and e.d.f. of linear precipitation trend estimates for various locations and calendar months computed using an R code employing ordinary linear multiple regression (no step-wise screening). The ANOVA statistics associated with these results can be found in Table 48.

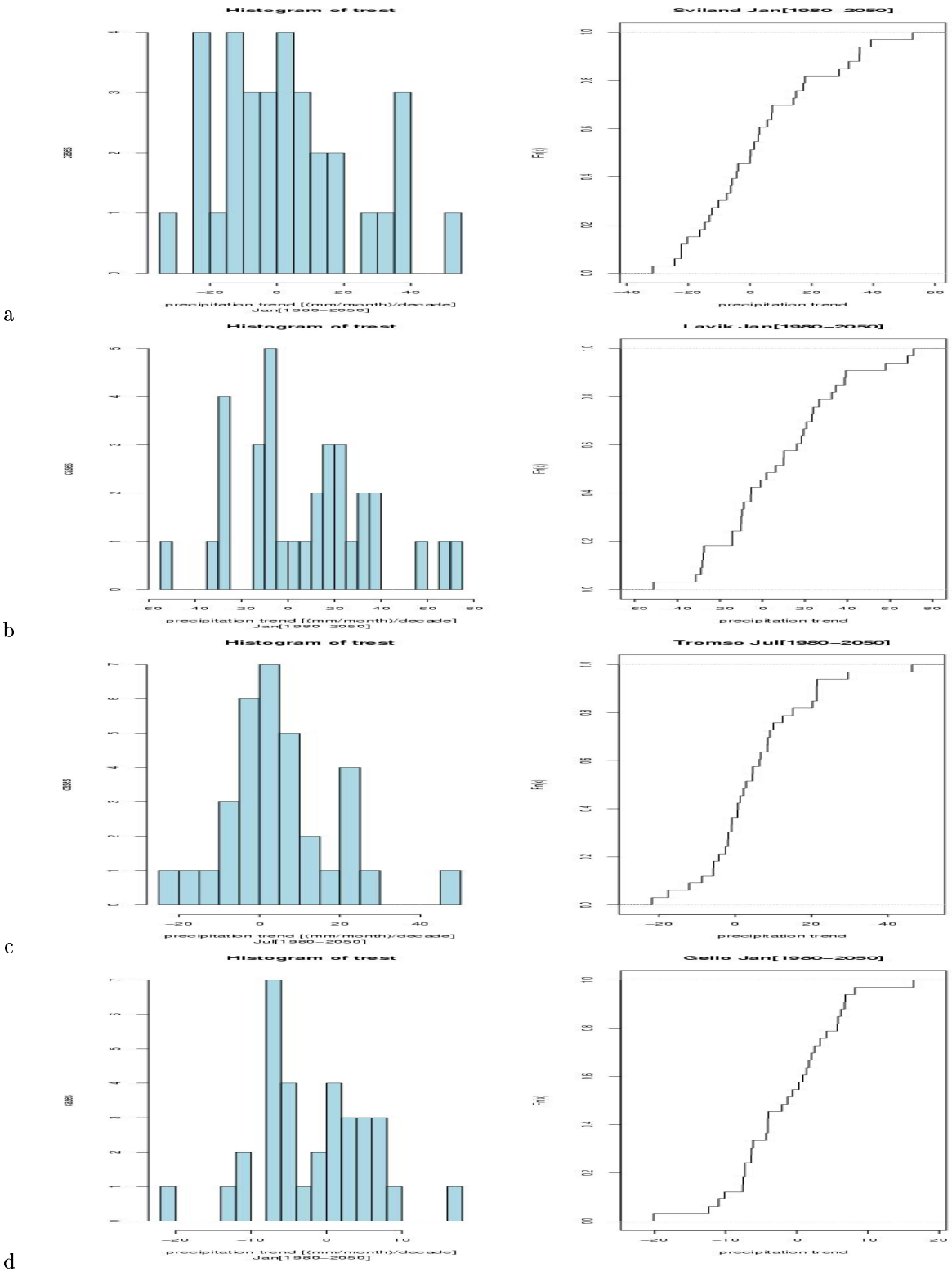

a

b

c

d

Figure 32: Plots showing the histogram and e.d.f. of linear precipitation trend estimates for various locations and calendar months computed using an R code employing ordinary linear multiple regression (no step-wise screening). The ANOVA statistics associated with these results can be found in Table 48.

6.2.1 F-statistics and P-value for the regression between SLP and precipitation.

Location	Jan	Apr	Jul	Oct
HALDEN	1.55 /0.14	0.98 /0.46	0.77 /0.66	1.44 /0.18
OSLO	0.94 /0.50	1.10 /0.37	0.66 /0.76	1.44 /0.18
GEILO	1.87 /0.06	1.47 /0.16	0.76 /0.66	1.04 /0.41
RØROS	1.66 /0.10	1.43 /0.18	0.79 /0.64	1.62 /0.11
BJÅEN	3.27 /0.00	0.80 /0.62	1.08 /0.38	1.41 /0.19
SVILAND	2.28 /0.02	1.67 /0.10	0.77 /0.66	1.40 /0.19
BERGEN	2.19 /0.03	0.57 /0.83	0.77 /0.66	2.20 /0.02
LAVIK	2.10 /0.03	0.47 /0.90	1.51 /0.15	1.54 /0.13
TROMSØ	1.94 /0.05	1.23 /0.28	2.98 /0.00	1.55 /0.13

Table 48: Estimated goodness of model fit (ANOVA F-test / P-value). The higher F-test estimate and the lower P-value indicate better fit. P-values lower than 0.05 indicate a confidence limit on the 5% level. All the results with a p-value of 0.06 or less are shown graphically in Figures 31 and 32.

with the highest skill are shown in Figures 31 and 32 as histograms and empirical distribution functions (e.d.f) of the trend estimates ((mm/month)/decade). A large spread is evident from these results, suggesting that there is little agreement between the models as whether to expect dryer or wetter conditions. It is nevertheless possible to get a rough probability estimate from the e.d.f.s, by reading off the probability associated with a precipitation rate equal to or smaller than zero.

6.2.2 Scenarios based on step-wise screening CCA of various AOGCMs scenarios

Table 49 shows downscaled scenarios based on the HadCM3 SLP scenarios. Both the trend in (mm/month)/decade and in %/decade are given, and the numbers in parentheses indicate the p-value associated with the trend-estimates (0.05 and smaller indicate significance at the 5% level. The trend-test score is taken as the mean of Mann-Kendall statistics and T-test estimate of differences). The uncertainties associated with these results are fairly large, as the two estimates shown based on different predictor domains indicate substantial differences.

Statistical significant trends at the 5% level are seen in: Halden, Moss, Oslo, Namdalseid, Dunderlandsdal, Barkestad and Tromsø in January; Hemne, Namdalseid, Sviland, Bergen, Skjåk, Bjåen and Lavik in April,; Dunderlandsdal, Sulitjelma, Sviland, Røros, Skjåk, Sulitjelma, Barkestad, Tromsø, and Bjåen in July; and Bjåen in October.

The estimates using the smaller (*nordic*) domain suggest an increase in the winter-time rainfall in Sviland and Bergen, but the *natl* predictor domain suggests drier conditions. In southern Norway, the smaller domain suggests drier conditions in the future whereas the larger predictor area gives more rain in April. The results for Røros and Hemne in July and Halden, Oslo, Barkestad, Tromsø, and Geilo in October also are not robust. Most of the places with trends "significantly different" to zero have the same sign when using the two different predictor domains, except for the July trend at Røros. Table 8 suggests

6.2.3 Downscaling of HadCM3 by common EOFs based on *Benestad* (2000b) SLP.

Location	Jan	Apr	Jul	Oct
nordic				
HALDEN	0.6/ 1 (30)	-0.09/ -0 (56)	-1.27/ -2 (6)	-0.39/ -1 (46)
MOSS	0.7/ 1 (17)	-0.1/ -0 (76)	-0.6/ -1 (23)	-0.9/ -1 (26)
OSLO	0.5/ 1 (18)	-0.3/ -0 (37)	-0.4/ -1 (55)	-0.8/ -1 (22)
RØROS	-0.3/ -1 (22)	0.1/ 0 (44)	-0.1/ -0 (37)	0.0/ 0 (82)
SKJÅK	-0.2/ -1 (64)	0.1/ 1 (6)	-0.1/ -0 (38)	0.4/ 2 (23)
NORDDAL	-1.5/ -2 (42)	0.9/ 1 (37)	-0.0/ -0 (42)	1.9/ 2 (29)
VERMA	-1.7/ -3 (32)	0.5/ 1 (66)	0.1/ 0 (70)	1.1/ 2 (37)
HEMNE	-3.3/ -3 (19)	2.6/ 2 (5)	0.8/ 1 (46)	3.4/ 3 (17)
NAMDALSEID	-2.2/ -2 (21)	2.0/ 2 (5)	1.1/ 1 (7)	2.4/ 2 (17)
DUNDERLANDSDAL	-2.0/ -2 (35)	1.2/ 1 (11)	1.2/ 1 (4)	3.6/ 3 (11)
SULITJELMA	-2.0/ -2 (14)	0.8/ 1 (23)	1.4/ 2 (2)	0.4/ 0 (78)
BARKESTAD	-1.4/ -1 (27)	0.7/ 1 (38)	0.7/ 1 (26)	2.6/ 2 (14)
TROMSØ	-0.7/ -1 (47)	0.7/ 1 (23)	0.1/ 0 (59)	1.0/ 1 (32)
GEILO	0.6/ 1 (23)	0.0/ 0 (76)	-0.8/ -1 (26)	-0.1/ -0 (64)
BJÅEN	0.7/ 1 (82)	0.5/ 1 (10)	-0.1/ -0 (83)	1.3/ 2 (33)
SVILAND	0.7/ 0 (86)	2.7/ 2 (0)	2.0/ 1 (5)	3.7/ 3 (16)
BERGEN	0.2/ 0 (90)	4.1/ 2 (1)	2.0/ 1 (17)	4.6/ 3 (10)
LAVIK	-0.6/ -0 (65)	4.1/ 2 (1)	2.4/ 1 (15)	5.0/ 3 (12)
natl				
HALDEN	1.1/ 2 (3)	0.6/ 1 (10)	-0.1/ -0 (72)	1.3/ 2 (42)
MOSS	1.6/ 2 (2)	0.6/ 1 (25)	-0.8/ -1 (12)	-0.2/ -0 (67)
OSLO	1.1/ 2 (2)	0.5/ 1 (31)	-0.7/ -1 (19)	0.1/ 0 (85)
RØROS	-0.3/ -1 (23)	0.2/ 1 (9)	0.8/ 2 (1)	0.2/ 1 (29)
SKJÅK	-0.1/ -0 (68)	0.1/ 0 (3)	-1.2/ -5 (0)	0.2/ 1 (46)
NORDDAL	-1.2/ -2 (38)	0.7/ 1 (39)	-0.1/ -0 (39)	0.4/ 1 (87)
VERMA	-1.5/ -2 (33)	0.6/ 1 (57)	0.1/ 0 (51)	0.3/ 0 (71)
HEMNE	-3.9/ -3 (12)	1.6/ 1 (26)	-0.7/ -1 (15)	0.2/ 0 (92)
NAMDALSEID	-3.1/ -3 (6)	1.1/ 1 (29)	0.0/ 0 (91)	0.3/ 0 (79)
DUNDERLANDSDAL	-4.7/ -4 (3)	1.4/ 1 (9)	4.1/ 4 (0)	2.0/ 2 (26)
SULITJELMA	-2.8/ -3 (6)	0.7/ 1 (31)	4.6/ 5 (0)	0.4/ 0 (77)
BARKESTAD	-3.1/ -3 (2)	0.1/ 0 (92)	3.3/ 3 (0)	-2.3/ -2 (16)
TROMSØ	-2.3/ -3 (2)	0.1/ 0 (92)	1.7/ 2 (0)	-1.3/ -2 (31)
GEILO	0.6/ 1 (32)	0.3/ 0 (26)	-1.1/ -2 (12)	1.5/ 3 (6)
BJÅEN	0.4/ 0 (99)	0.6/ 1 (2)	-1.2/ -2 (2)	2.3/ 3 (5)
SVILAND	-0.2/ -0 (76)	1.9/ 1 (2)	0.3/ 0 (87)	2.7/ 2 (21)
BERGEN	-0.5/ -0 (77)	2.9/ 2 (3)	1.1/ 1 (43)	2.4/ 1 (39)
LAVIK	-0.5/ -0 (78)	3.3/ 2 (2)	1.3/ 1 (28)	2.6/ 1 (32)

Table 49: Downscaled precipitation scenarios of the HadCM3 results using the common EOF method. Both the units of mm/(month decade) and %/decade are given (after the "/"), and the parentheses give the p-value according to a trend test. Length of interval= 119. Dates 15-Oct-1980 - 15-Oct-2098

6.2.4 Downscaling NCAR-CSM by common EOFs based on *Benestad* (2000b) SLP.

Location	Jan	Apr	Jul	Oct
nordic				
HALDEN	-0.4/ -1 (57)	0.6/ 1 (18)	-1.2/ -2 (19)	-0.9/ -2 (26)
MOSS	-0.3/ -0 (81)	0.5/ 1 (21)	-0.9/ -1 (21)	-1.1/ -2 (29)
OSLO	-0.4/ -1 (42)	0.4/ 1 (39)	-0.9/ -2 (24)	-0.8/ -1 (33)
RØROS	0.1/ 0 (76)	0.2/ 0 (31)	-0.5/ -1 (22)	-0.3/ -1 (7)
SKJÅK	0.1/ 0 (87)	0.1/ 0 (22)	-0.8/ -3 (11)	-0.1/ -1 (76)
NORDDAL	0.1/ 0 (88)	1.0/ 1 (29)	-0.7/ -1 (11)	-0.7/ -1 (62)
VERMA	0.01/ 0 (88)	0.8/ 1 (39)	-0.6/ -1 (14)	-0.8/ -1 (36)
HEMNE	-0.3/ -0 (79)	0.8/ 1 (60)	0.3/ 0 (77)	0.1/ 0 (97)
NAMDALSEID	-0.3/ -0 (63)	0.6/ 1 (51)	0.3/ 0 (62)	-0.0/ -0 (98)
DUNDERLANDSDAL	-1.8/ -2 (53)	0.8/ 1 (36)	0.3/ 0 (55)	2.3/ 2 (12)
SULITJELMA	-0.6/ -1 (81)	0.2/ 0 (62)	0.4/ 1 (61)	1.2/ 1 (24)
BARKESTAD	-0.5/ -0 (72)	-0.1/ -0 (92)	0.8/ 1 (38)	2.3/ 2 (14)
TROMSØ	-0.3/ -0 (74)	-0.0/ -0 (78)	0.3/ 0 (47)	0.6/ 1 (51)
GEILO	0.1/ 0 (75)	0.3/ 1 (21)	-1.0/ -2 (12)	-0.4/ -1 (46)
BJÅEN	0.0/ 0 (91)	0.6/ 1 (12)	-0.4/ -1 (31)	-0.2/ -0 (99)
SVILAND	-1.2/ -1 (62)	2.1/ 1 (10)	-0.9/ -1 (30)	-1.5/ -1 (47)
BERGEN	-1.5/ -1 (59)	3.2/ 2 (13)	-0.4/ -0 (91)	-1.1/ -1 (69)
LAVIK	-1.5/ -1 (64)	3.1/ 2 (19)	0.3/ 0 (65)	-0.0/ -0 (76)
natl				
HALDEN	-0.0/ -0 (88)	0.1/ 0 (86)	-1.0/ -2 (23)	-1.1/ -2 (21)
MOSS	0.2/ 0 (74)	-0.0/ -0 (92)	-1.4/ -2 (11)	-1.6/ -2 (11)
OSLO	-0.1/ -0 (80)	-0.1/ -0 (82)	-1.4/ -2 (10)	-1.1/ -2 (11)
RØROS	-0.2/ -0 (42)	-0.0/ -0 (90)	-0.4/ -1 (26)	-0.3/ -1 (26)
SKJÅK	-0.1/ -1 (71)	0.0/ 0 (25)	-1.3/ -5 (2)	-0.1/ -0 (92)
NORDDAL	-0.6/ -1 (74)	0.6/ 1 (51)	-0.3/ -0 (26)	0.1/ 0 (90)
VERMA	-0.6/ -1 (76)	0.5/ 1 (63)	-0.7/ -1 (6)	-0.3/ -0 (61)
HEMNE	-2.2/ -2 (32)	1.2/ 1 (43)	0.0/ 0 (93)	0.2/ 0 (97)
NAMDALSEID	-1.4/ -1 (26)	0.9/ 1 (41)	0.3/ 0 (52)	0.2/ 0 (86)
DUNDERLANDSDAL	-2.7/ -2 (21)	1.3/ 1 (26)	0.2/ 0 (88)	1.5/ 1 (30)
SULITJELMA	0.1/ 0 (68)	0.7/ 1 (35)	0.5/ 1 (76)	0.6/ 1 (92)
BARKESTAD	-1.0/ -1 (42)	0.1/ 0 (63)	1.0/ 1 (35)	1.8/ 2 (20)
TROMSØ	-0.7/ -1 (26)	0.1/ 0 (62)	0.3/ 0 (57)	0.5/ 1 (51)
GEILO	-0.2/ -0 (94)	0.3/ 0 (21)	-1.2/ -2 (7)	-0.4/ -1 (47)
BJÅEN	-1.0/ -1 (59)	0.7/ 1 (9)	-0.9/ -1 (7)	-0.2/ -0 (100)
SVILAND	-1.4/ -1 (46)	1.9/ 1 (13)	-1.0/ -1 (26)	-0.3/ -0 (86)
BERGEN	-2.0/ -1 (35)	2.7/ 2 (20)	-0.7/ -0 (70)	-0.4/ -0 (82)
LAVIK	-2.3/ -1 (28)	2.9/ 2 (17)	-0.2/ -0 (97)	0.5/ 0 (53)

Table 50: Downscaled precipitation scenarios of the NCAR-CSM results using the common EOF method. Both the units of mm/(month decade) and %/decade are given (after the "/"), and the parentheses give the p-value according to a trend test. Length of interval= 119. Dates 15-Oct-1980 - 15-Oct-2098

6.2.5 Downscaling HadCM2 by common EOFs based on *Benestad* (2000b) SLP.

Location	Jan	Apr	Jul	Oct
nordic				
HALDEN	1.6/ 2 (2)	-0.1/ -0 (66)	-0.4/ -1 (68)	-2.3/ -4 (4)
MOSS	1.2/ 2 (22)	-0.1/ -0 (67)	-1.3/ -2 (26)	-2.8/ -4 (1)
OSLO	0.5/ 1 (36)	-0.3/ -1 (52)	-1.0/ -2 (41)	-2.2/ -4 (1)
RØROS	-0.5/ -1 (3)	0.3/ 1 (3)	-1.3/ -3 (2)	-0.3/ -1 (28)
SKJÅK	-0.4/ -1 (19)	0.2/ 1 (1)	-1.4/ -6 (1)	0.1/ 0 (69)
NORDDAL	-2.8/ -4 (4)	1.7/ 2 (8)	-1.3/ -2 (2)	0.9/ 1 (49)
VERMA	-3.6/ -6 (1)	1.6/ 3 (8)	-1.1/ -2 (3)	0.4/ 1 (76)
HEMNE	-1.3/ -1 (43)	2.5/ 2 (8)	-1.4/ -1 (19)	2.3/ 2 (25)
NAMDALSEID	-0.3/ -0 (84)	1.8/ 2 (6)	-0.8/ -1 (42)	1.9/ 2 (18)
DUNDERLANDSDAL	0.2/ 0 (60)	1.6/ 1 (31)	0.3/ 0 (70)	2.3/ 2 (28)
SULITJELMA	-0.9/ -1 (59)	0.8/ 1 (46)	1.3/ 2 (13)	1.9/ 2 (17)
BARKESTAD	-0.0/ -0 (78)	-0.1/ -0 (66)	1.6/ 1 (16)	3.0/ 3 (20)
TROMSØ	0.4/ 1 (62)	-0.3/ -0 (30)	0.4/ 0 (49)	2.0/ 3 (16)
GEILO	0.8/ 1 (12)	0.1/ 0 (81)	-0.4/ -1 (75)	-0.9/ -2 (16)
BJÅEN	1.0/ 1 (53)	0.5/ 1 (18)	-0.6/ -1 (50)	-0.7/ -1 (54)
SVILAND	1.0/ 1 (66)	1.8/ 1 (7)	-1.3/ -1 (30)	-0.2/ -0 (96)
BERGEN	-0.1/ -0 (89)	2.9/ 2 (11)	-1.7/ -1 (37)	1.0/ 1 (91)
LAVIK	-2.2/ -1 (36)	3.6/ 2 (10)	-1.6/ -1 (53)	2.0/ 1 (67)
natl				
HALDEN	0.6/ 1 (38)	0.5/ 1 (27)	-0.1/ -0 (94)	-1.9/ -3 (3)
MOSS	1.0/ 1 (24)	0.3/ 0 (52)	-0.7/ -1 (51)	-2.9/ -4 (0)
OSLO	0.4/ 1 (50)	0.1/ 0 (82)	-0.7/ -1 (55)	-2.4/ -4 (0)
RØROS	-0.7/ -2 (0)	0.4/ 1 (1)	-0.3/ -1 (61)	0.0/ 0 (92)
SKJÅK	-0.5/ -2 (9)	0.1/ 1 (8)	-1.0/ -4 (8)	0.4/ 1 (26)
NORDDAL	-3.3/ -4 (1)	2.4/ 3 (0)	-0.7/ -1 (15)	1.4/ 2 (33)
VERMA	-4.0/ -6 (0)	2.1/ 3 (0)	-0.6/ -1 (16)	0.8/ 1 (46)
HEMNE	-3.3/ -3 (3)	4.0/ 3 (0)	-1.7/ -1 (5)	2.6/ 2 (27)
NAMDALSEID	-0.8/ -1 (46)	2.7/ 3 (0)	-1.2/ -1 (15)	2.0/ 2 (21)
DUNDERLANDSDAL	-0.1/ -0 (97)	2.0/ 2 (2)	0.6/ 1 (26)	2.3/ 2 (33)
SULITJELMA	1.7/ 2 (14)	1.5/ 2 (4)	0.9/ 1 (36)	2.1/ 2 (15)
BARKESTAD	-0.7/ -1 (66)	0.6/ 1 (44)	0.7/ 1 (53)	2.3/ 2 (15)
TROMSØ	0.1/ 0 (90)	0.3/ 0 (56)	0.2/ 0 (68)	1.2/ 2 (27)
GEILO	0.5/ 1 (39)	0.2/ 0 (42)	-0.8/ -1 (35)	-0.5/ -1 (47)
BJÅEN	-0.9/ -1 (46)	0.7/ 1 (1)	-1.0/ -1 (9)	-0.4/ -1 (70)
SVILAND	-0.8/ -1 (63)	1.6/ 1 (10)	-1.1/ -1 (33)	-1.0/ -1 (53)
BERGEN	-2.2/ -1 (26)	1.7/ 1 (31)	-2.4/ -1 (22)	-0.0/ -0 (87)
LAVIK	-3.6/ -2 (16)	2.0/ 1 (39)	-2.7/ -2 (28)	2.4/ 1 (52)

Table 51: Downscaled precipitation scenarios of the HadCM2 member 1 results using the common EOF method. Both the units of mm/(month decade) and %/decade are given (after the "/"), and the parentheses give the p-value according to a trend test. Length of interval= 119. Dates 15-Oct-1980 - 15-Oct-2098

6.2.6 Downscaling HadCM2 by common EOFs based on *Benestad* (2000b) SLP.

Location	Jan	Apr	Jul	Oct
nordic				
HALDEN	-0.6/ -1 (34)	-1.2/ -2 (5)	-2.0/ -3 (6)	-1.1/ -2 (14)
MOSS	-1.1/ -2 (25)	-1.1/ -2 (6)	-2.8/ -4 (2)	-1.4/ -2 (27)
OSLO	-0.8/ -1 (30)	-1.1/ -2 (7)	-2.2/ -4 (4)	-1.2/ -2 (26)
RØROS	-0.1/ -0 (75)	0.0/ 0 (72)	-1.0/ -3 (1)	-0.1/ -0 (93)
SKJÅK	-0.3/ -1 (50)	0.1/ 0 (80)	-1.5/ -6 (1)	-0.3/ -1 (68)
NORDDAL	-0.7/ -1 (98)	0.1/ 0 (96)	-0.7/ -1 (2)	1.2/ 1 (48)
VERMA	-0.8/ -1 (81)	0.2/ 0 (81)	-1.0/ -2 (2)	1.2/ 2 (30)
HEMNE	-0.9/ -1 (89)	1.2/ 1 (44)	0.7/ 1 (46)	2.2/ 2 (46)
NAMDALSEID	-0.4/ -0 (69)	0.9/ 1 (65)	0.5/ 0 (46)	1.5/ 1 (47)
DUNDERLANDSDAL	1.6/ 1 (26)	1.1/ 1 (33)	0.3/ 0 (59)	-0.0/ -0 (96)
SULITJELMA	1.1/ 1 (31)	1.0/ 1 (19)	1.3/ 2 (7)	0.5/ 1 (66)
BARKESTAD	0.8/ 1 (37)	0.5/ 0 (51)	1.9/ 2 (7)	-0.4/ -0 (84)
TROMSØ	1.1/ 1 (28)	0.5/ 1 (41)	0.3/ 0 (47)	0.1/ 0 (74)
GEILO	-0.5/ -1 (33)	-0.2/ -0 (32)	-2.9/ -5 (1)	-0.8/ -1 (9)
BJÅEN	-0.9/ -1 (63)	-0.9/ -1 (3)	-2.0/ -3 (1)	-1.5/ -2 (12)
SVILAND	-1.9/ -1 (24)	-1.4/ -1 (17)	0.8/ 1 (47)	-1.1/ -1 (61)
BERGEN	-2.0/ -1 (38)	-2.3/ -1 (20)	1.2/ 1 (52)	-2.0/ -1 (66)
LAVIK	-2.1/ -1 (55)	-2.5/ -1 (31)	1.4/ 1 (52)	-1.5/ -1 (71)
natl				
HALDEN	-1.2/ -2 (5)	-0.4/ -1 (59)	-1.6/ -3 (2)	-2.0/ -3 (5)
MOSS	-1.3/ -2 (9)	-0.4/ -1 (60)	-1.6/ -2 (3)	-1.4/ -3 (22)
OSLO	-1.0/ -2 (7)	-0.5/ -1 (42)	-1.8/ -3 (3)	-1.6/ -3 (16)
RØROS	-0.3/ -1 (58)	0.1/ 0 (69)	-0.4/ -1 (55)	0.1/ 0 (49)
SKJÅK	-0.6/ -2 (15)	0.0/ 0 (72)	-0.9/ -3 (13)	-0.3/ -1 (47)
NORDDAL	-2.2/ -3 (23)	1.1/ 1 (28)	0.2/ 0 (50)	0.7/ 1 (62)
VERMA	-2.2/ -4 (21)	0.9/ 1 (31)	-0.1/ -0 (96)	1.2/ 2 (34)
HEMNE	-1.1/ -1 (56)	1.4/ 1 (39)	-0.7/ -1 (47)	1.7/ 1 (53)
NAMDALSEID	0.0/ 0 (82)	0.8/ 1 (40)	-0.4/ -0 (70)	1.1/ 1 (55)
DUNDERLANDSDAL	0.4/ 0 (55)	-1.8/ -2 (15)	0.4/ 0 (56)	2.4/2 (34)
SULITJELMA	2.5/ 3 (10)	0.4/ 0 (72)	1.5/ 2 (10)	1.3/ 2 (37)
BARKESTAD	1.1/ 1 (29)	0.2/ 0 (81)	2.1/ 2 (7)	-0.7/ -1 (87)
TROMSØ	1.7/ 2 (15)	0.3/ 0 (62)	0.7/ 1 (26)	0.1/ 0 (83)
GEILO	-0.8/ -1 (7)	-0.1/ -0 (54)	-1.7/ -3 (4)	-0.6/ -1 (24)
BJÅEN	-2.1/ -3 (8)	-0.0/ -0 (99)	-0.8/ -1 (13)	-1.4/ -2 (22)
SVILAND	-2.6/ -2 (5)	0.1/ 0 (83)	-0.5/ -0 (88)	-1.9/ -1 (44)
BERGEN	-3.0/ -2 (12)	-0.5/ -0 (93)	0.3/ 0 (86)	-2.6/ -1 (56)
LAVIK	-3.1/ -2 (22)	-0.8/ -0 (61)	1.2/ 1 (55)	-2.0/ -1 (80)

Table 52: Downscaled precipitation scenarios of the HadCM2 member 2 results using the common EOF method. Both the units of mm/(month decade) and %/decade are given (after the "/"), and the parentheses give the p-value according to a trend test. Length of interval= 101. Dates 15-Oct-1980 - 15-Oct-2089

6.2.7 Downscaling HadCM2 by common EOFs based on *Benestad* (2000b) SLP.

Location	Jan	Apr	Jul	Oct
nordic				
HALDEN	-0.3/ -0 (70)	-0.6/ -1 (49)	-0.2/ -0 (98)	-0.6/ -1 (66)
MOSS	0.2/ 0 (86)	-0.1/ -0 (100)	-0.5/ -1 (75)	-0.5/ -1 (86)
OSLO	-0.2/ -0 (88)	-0.3/ -0 (73)	-0.6/ -1 (72)	-0.3/ -1 (89)
RØROS	-0.6/ -1 (6)	-0.1/ -0 (43)	-0.4/ -1 (51)	-0.4/ -1 (38)
SKJÅK	-0.7/ -3 (4)	0.1/ 0 (38)	-0.6/ -2 (56)	-0.5/ -2 (27)
NORDDAL	-2.4/ -3 (7)	-1.2/ -1 (23)	-0.4/ -0 (51)	-2.7/ -3 (27)
VERMA	-2.7/ -4 (10)	-1.4/ -2 (18)	-0.3/ -1 (69)	-1.7/ -3 (27)
HEMNE	-4.1/ -3 (3)	-1.0/ -1 (60)	-1.5/ -1 (29)	-3.8/ -3 (22)
NAMDALSEID	-3.2/ -3 (4)	-0.4/ -0 (77)	-1.6/ -2 (12)	-2.8/ -3 (24)
DUNDERLANDSDAL	-7.8/ -7 (0)	1.4/ 1 (14)	-1.5/-1 (21)	-2.8/-2 (61)
SULITJELMA	-4.7/ -6 (1)	0.3/ 0 (70)	-1.9/ -2 (21)	-0.7/ -1 (90)
BARKESTAD	-3.4/ -3 (3)	0.2/ 0 (72)	-1.1/ -1 (86)	-2.6/ -2 (63)
TROMSØ	-1.2/ -2 (38)	-0.4/ -1 (67)	-0.9/ -1 (53)	-2.3/ -3 (64)
GEILO	-0.5/ -1 (18)	0.3/ 1 (39)	0.5/ 1 (73)	-0.0/ -0 (98)
BJÅEN	-3.2/ -4 (2)	0.2/ 0 (53)	-0.1/ -0 (92)	-1.2/ -2 (45)
SVILAND	-4.2/ -3 (1)	0.3/ 0 (65)	-1.7/ -1 (26)	-2.6/ -2 (43)
BERGEN	-6.7/ -4 (1)	0.9/ 1 (72)	-3.6/ -2 (12)	-3.6/ -2 (40)
LAVIK	-8.7/ -5 (0)	0.4/ 0 (94)	-4.0/ -2 (18)	-4.5/ -3 (44)
natl				
HALDEN	-1.0/ -2 (14)	0.2/ 0 (87)	-0.5/ -1 (81)	-1.1/ -2 (77)
MOSS	-0.2/ -0 (62)	0.3/ 0 (88)	-1.0/ -2 (40)	-0.4/ -1 (98)
OSLO	-0.9/ -1 (11)	0.1/ 0 (96)	-0.8/ -1 (51)	-0.4/ -1 (97)
RØROS	-0.7/ -2 (4)	0.0/ 0 (75)	-0.9/ -2 (14)	-0.4/ -1 (30)
SKJÅK	-1.3/ -5 (0)	0.1/ 0 (26)	-0.5/ -2 (55)	-0.6/ -2 (13)
NORDDAL	-5.2/ -7 (0)	-0.2/ -0 (82)	-1.0/ -1 (7)	-2.6/ -3 (21)
VERMA	-4.9/ -8 (1)	-0.3/ -0 (83)	-0.6/ -1 (46)	-1.5/ -2 (26)
HEMNE	-4.6/ -4 (7)	1.1/ 1 (59)	-2.4/ -2 (4)	-2.9/ -2 (34)
NAMDALSEID	-3.8/ -4 (7)	1.1/ 1 (47)	-1.9/ -2 (11)	-2.0/ -2 (34)
DUNDERLANDSDAL	-4.3/ -4 (4)	1.4/ 1 (21)	-0.9/ -1 (26)	-1.5/-1 (86)
SULITJELMA	-3.0/ -3 (10)	0.8/ 1 (48)	-0.7/ -1 (66)	-1.1/ -1 (65)
BARKESTAD	-2.4/ -2 (10)	0.3/ 0 (78)	0.7/ 1 (72)	-1.0/ -1 (70)
TROMSØ	-0.6/ -1 (61)	0.0/ 0 (93)	0.4/ 1 (63)	-1.1/ -1 (60)
GEILO	-1.1/ -2 (3)	-0.0/ -0 (86)	-0.7/ -1 (71)	-0.1/ -0 (92)
BJÅEN	-6.0/ -8 (0)	0.3/ 0 (24)	-1.0/ -1 (31)	-1.2/ -2 (78)
SVILAND	-7.4/ -5 (0)	0.5/ 0 (81)	-3.4/ -2 (3)	-2.1/ -1 (44)
BERGEN	-10.6/ -6 (0)	0.6/ 0 (75)	-5.7/ -3 (1)	-2.8/ -2 (43)
LAVIK	-12.6/ -7 (0)	0.4/ 0 (85)	-6.2/ -4 (3)	-4.4/ -3 (39)

Table 53: Downscaled precipitation scenarios of the HadCM2 member 3 results using the common EOF method. Both the units of mm/(month decade) and %/decade are given (after the "/"), and the parentheses give the p-value according to a trend test. Length of interval= 101. Dates 15-Oct-1980 - 15-Oct-2089

6.2.8 Downscaling HadCM2 by common EOFs based on *Benestad* (2000b) SLP.

Location	Jan	Apr	Jul	Oct
nordic				
HALDEN	0.3/ 0 (76)	-0.1/ -0 (89)	0.2/ 0 (92)	0.0/ 0 (97)
MOSS	0.2/ 0 (75)	0.3/ 0 (55)	-0.8/ -1 (24)	0.6/ 1 (76)
OSLO	0.0/ 0 (96)	0.1/ 0 (78)	-0.2/ -0 (54)	0.4/ 1 (79)
RØROS	-0.2/ -0 (79)	-0.2/ -0 (35)	-0.5/ -1 (11)	-0.8/ -2 (1)
SKJÅK	-0.0/ -0 (98)	-0.1/ -0 (75)	-0.7/ -3 (16)	-0.7/ -3 (3)
NORDDAL	-0.6/ -1 (94)	-1.6/ -2 (23)	-0.5/ -1 (6)	-3.6/ -5 (4)
VERMA	-1.2/ -2 (63)	-1.7/ -3 (13)	-0.3/ -0 (26)	-2.5/ -4 (4)
HEMNE	1.3/ 1 (55)	-2.6/ -2 (22)	-1.7/ -1 (19)	-4.9/ -4 (4)
NAMDALSEID	2.4/ 2 (14)	-1.7/ -2 (25)	-0.8/ -1 (35)	-3.5/ -3 (3)
DUNDERLANDSDAL	2.4/ 2 (12)	-1.5/ -1 (14)	0.2/ 0 (86)	-4.2/-4 (12)
SULITJELMA	0.9/ 1 (50)	-1.7/ -2 (5)	1.1/ 1 (28)	-2.9/ -3 (14)
BARKESTAD	0.7/ 1 (44)	-2.7/ -2 (3)	0.9/ 1 (56)	-2.8/ -2 (20)
TROMSØ	0.6/ 1 (66)	-1.7/ -2 (5)	-0.1/ -0 (94)	-1.9/ -3 (21)
GEILO	0.6/ 1 (45)	-0.0/ -0 (100)	-0.1/ -0 (64)	0.5/ 1 (60)
BJÅEN	2.0/ 3 (25)	-0.6/ -1 (15)	-0.4/ -1 (34)	-0.9/ -1 (22)
SVILAND	2.0/ 1 (44)	-0.0/ -0 (99)	-1.0/ -1 (42)	-2.3/ -2 (22)
BERGEN	2.3/ 1 (44)	-0.6/ -0 (81)	-1.8/ -1 (31)	-4.1/ -2 (16)
LAVIK	1.5/ 1 (65)	-1.7/ -1 (37)	-1.8/ -1 (35)	-5.2/ -3 (18)
natl				
HALDEN	0.1/ 0 (100)	0.9/ 1 (9)	1.3/ 2 (38)	0.7/ 1 (66)
MOSS	-0.2/ -0 (96)	0.9/ 1 (11)	0.9/ 1 (51)	1.4/ 2 (35)
OSLO	-0.0/ -0 (76)	0.7/ 1 (16)	0.9/ 2 (51)	1.1/ 2 (37)
RØROS	-0.2/ -0 (50)	-0.1/ -0 (92)	-0.1/ -0 (83)	-0.4/ -1 (12)
SKJÅK	0.1/ 0 (90)	-0.0/ -0 (81)	-0.3/ -1 (49)	-0.7/ -3 (7)
NORDDAL	-0.8/ -1 (72)	-0.7/ -1 (31)	-0.1/ -0 (80)	-3.4/ -4 (3)
VERMA	-1.8/ -3 (35)	-0.9/ -1 (21)	0.6/ 1 (41)	-1.9/ -3 (9)
HEMNE	-0.2/ -0 (83)	-1.0/ -1 (47)	-1.1/ -1 (23)	-4.3/ -3 (5)
NAMDALSEID	2.8/ 3 (12)	-0.5/ -0 (65)	-0.7/ -1 (20)	-2.7/ -3 (9)
DUNDERLANDSDAL	2.9/ 3 (19)	-0.4/ -0 (57)	0.8/ 1 (40)	-3.8/ -3 (10)
SULITJELMA	4.3/ 5 (3)	-0.3/ -0 (73)	0.7/ 1 (56)	-2.4/ -3 (14)
BARKESTAD	2.0/ 2 (27)	-1.5/ -1 (15)	0.1/ 0 (100)	-3.3/ -3 (8)
TROMSØ	2.3/ 3 (11)	-0.3/ -0 (47)	-0.4/ -1 (67)	-2.4/ -3 (6)
GEILO	0.4/ 1 (57)	0.2/ 0 (53)	1.4/ 2 (28)	0.2/ 0 (93)
BJÅEN	1.6/ 2 (31)	-0.3/ -0 (59)	0.8/ 1 (51)	-0.9/ -1 (26)
SVILAND	2.9/ 2 (21)	-0.9/ -1 (57)	0.6/ 0 (69)	-1.5/ -1 (44)
BERGEN	3.0/ 2 (32)	-2.0/ -1 (42)	-1.4/ -1 (48)	-3.0/ -2 (25)
LAVIK	2.3/ 1 (52)	-2.4/ -1 (36)	-2.3/ -1 (32)	-3.4/ -2 (26)

Table 54: Downscaled precipitation scenarios of the HadCM2 member 4 results using the common EOF method. Both the units of mm/(month decade) and %/decade are given (after the "/"), and the parentheses give the p-value according to a trend test. Length of interval= 91. Dates 15-Oct-1980 - 15-Oct-2084

6.2.9 Downscaling CCCma by common EOFs based on *Benestad* (2000b) SLP.

Location	Jan	Apr	Jul	Oct
nordic				
HALDEN	0.5/ 1 (35)	-0.1/ -0 (92)	-0.1/ -0 (85)	-0.14/ -0 (78)
MOSS	0.1/ 0 (96)	-0.3/ -0 (72)	-0.3/ -0 (67)	-0.13/ -0 (67)
OSLO	0.1/ 0 (86)	-0.4/ -1 (69)	-0.3/ -0 (61)	-0.16/ -0 (70)
RØROS	0.5/ 1 (1)	0.4/ 1 (0)	-0.2/ -1 (51)	0.1/ 0 (92)
SKJÅK	0.7/ 3 (2)	0.2/ 1 (1)	0.2/ 1 (54)	0.0/ 0 (75)
NORDDAL	2.8/ 3 (2)	1.4/ 2 (5)	-0.1/ -0 (77)	0.9/ 1 (13)
VERMA	2.7/ 4 (2)	1.2/ 2 (9)	0.1/ 0 (81)	0.7/ 1 (12)
HEMNE	3.6/ 3 (2)	2.3/ 2 (11)	-0.1/ -0 (66)	1.1/ 1 (19)
NAMDALSEID	1.8/ 2 (14)	1.4/ 1 (38)	-0.5/ -0 (22)	0.7/ 1 (25)
DUNDERLANDSDAL	2.3/ 2 (19)	0.4/ 0 (78)	-0.7/ -1 (25)	1.5/ 1 (35)
SULITJELMA	0.9/ 1 (37)	0.8/ 1 (16)	-0.7/ -1 (22)	-0.0/ -0 (94)
BARKESTAD	0.6/ 1 (44)	0.1/ 0 (96)	-1.2/ -1 (16)	0.5/ 0 (60)
TROMSØ	-0.2/ -0 (73)	0.2/ 0 (92)	-1.0/ -1 (2)	0.1/ 0 (95)
GEILO	0.6/ 1 (16)	0.0/ 0 (93)	-0.4/ -1 (61)	-0.21/ -0 (43)
BJÅEN	1.8/ 2 (8)	0.3/ 0 (26)	-0.3/ -0 (42)	0.1/ 0 (85)
SVILAND	2.9/ 2 (6)	1.1/ 1 (27)	0.0/ 0 (84)	0.9/ 1 (40)
BERGEN	3.6/ 2 (6)	0.7/ 0 (54)	-0.7/ -0 (77)	0.5/ 0 (72)
LAVIK	4.6/ 3 (4)	1.3/ 1 (46)	-1.0/ -1 (42)	-0.0/ -0 (96)
natl				
HALDEN	0.2/ 0 (78)	-0.3/ -0 (33)	0.8/ 1 (10)	-0.3/ -1 (55)
MOSS	0.0/ 0 (78)	-0.5/ -1 (14)	0.6/ 1 (22)	-0.2/ -0 (59)
OSLO	-0.1/ -0 (51)	-0.4/ -1 (24)	0.6/ 1 (24)	-0.3/ -1 (51)
RØROS	0.5/ 1 (1)	0.3/ 1 (4)	0.3/ 1 (28)	0.1/ 0 (13)
SKJÅK	0.7/ 3 (1)	0.1/ 1 (6)	-0.7/ -3 (4)	-0.0/ -0 (91)
NORDDAL	2.9/ 4 (0)	1.1/ 1 (9)	-0.2/ -0 (61)	0.6/ 1 (21)
VERMA	2.7/ 4 (0)	1.1/ 2 (9)	-0.1/ -0 (100)	0.6/ 1 (11)
HEMNE	3.3/ 3 (2)	2.5/ 2 (6)	-1.6/ -1 (0)	0.8/ 1 (27)
NAMDALSEID	1.9/ 2 (7)	1.7/ 2 (9)	-1.0/ -1 (2)	0.5/ 0 (30)
DUNDERLANDSDAL	1.8/ 2 (22)	0.7/ 1 (52)	0.7/ 1 (26)	0.4/ 0 (58)
SULITJELMA	1.3/ 2 (12)	0.5/ 1 (53)	0.3/ 0 (53)	0.3/ 0 (61)
BARKESTAD	1.1/ 1 (10)	0.2/ 0 (70)	0.2/ 0 (66)	-0.8/ -1 (51)
TROMSØ	0.4/ 0 (64)	0.3/ 0 (44)	-0.3/ -0 (58)	-0.6/ -1 (47)
GEILO	0.3/ 1 (26)	0.4/ 1 (8)	0.4/ 1 (46)	-0.4/ -1 (26)
BJÅEN	0.9/ 1 (31)	0.6/ 1 (12)	0.8/ 1 (2)	-0.5/ -1 (39)
SVILAND	1.8/ 1 (15)	1.3/ 1 (15)	0.3/ 0 (88)	1.1/ 1 (32)
BERGEN	2.1/ 1 (20)	1.6/ 1 (14)	-0.4/ -0 (72)	0.9/ 0 (53)
LAVIK	3.4/ 2 (12)	1.6/ 1 (15)	-0.9/ -1 (48)	0.7/ 0 (75)

Table 55: Downscaled scenarios of the CCCma member 1 results using the common EOF method. Both the units of mm/(month decade) and %/decade are given (after the "/"), and the parentheses give the p-value according to a trend test. Length of interval= 119. Dates 15-Oct-1980 - 15-Oct-2098

6.2.10 Downscaling CCCma by common EOFs based on *Benestad* (2000b) SLP.

Location	Jan	Apr	Jul	Oct
nordic				
HALDEN	0.7/ 1 (32)	-0.3/ -0 (43)	0.4/ 1 (43)	-1.08/ -2 (10)
MOSS	0.6/ 1 (42)	-0.6/ -1 (17)	-0.0/ -0 (97)	-1.56/ -2 (6)
OSLO	-0.0/ -0 (53)	-0.6/ -1 (14)	0.2/ 0 (69)	-1.25/ -2 (6)
RØROS	0.6/ 1 (0)	0.5/ 1 (1)	-0.4/ -1 (15)	0.0/ 0 (79)
SKJÅK	0.5/ 2 (9)	0.2/ 1 (3)	-0.3/ -1 (50)	0.3/ 1 (8)
NORDDAL	2.5/ 3 (4)	2.2/ 3 (1)	-0.3/ -0 (22)	2.8/ 3 (1)
VERMA	2.6/ 4 (3)	2.0/ 3 (1)	-0.1/ -0 (78)	1.6/ 3 (2)
HEMNE	2.5/ 2 (16)	2.5/ 2 (3)	-0.1/ -0 (67)	3.8/ 3 (1)
NAMDALSEID	1.8/ 2 (18)	1.7/ 2 (3)	-0.1/ -0 (73)	2.9/ 3 (1)
DUNDERLANDSDAL	0.7/ 1 (67)	1.2/ 1 (29)	-0.0/ -0 (91)	7.4/ 7 (0)
SULITJELMA	0.7/ 1 (53)	1.1/ 1 (4)	-0.4/ -0 (40)	3.0/ 3 (2)
BARKESTAD	0.1/ 0 (94)	-0.9/ -1 (43)	-0.6/ -1 (35)	4.9/ 4 (0)
TROMSØ	-0.1/ -0 (70)	-0.5/ -1 (54)	-0.8/ -1 (4)	2.6/ 3 (1)
GEILO	0.8/ 1 (10)	-0.2/ -0 (53)	0.0/ 0 (88)	-1.0/ -2 (4)
BJÅEN	1.6/ 2 (20)	0.2/ 0 (54)	0.1/ 0 (87)	0.0/ 0 (91)
SVILAND	1.6/ 1 (31)	2.2/ 1 (5)	-0.6/ -0 (47)	0.7/ 0 (57)
BERGEN	1.6/ 1 (40)	2.1/ 1 (10)	-0.1/ -0 (30)	0.7/ 0 (57)
LAVIK	2.1/ 1 (34)	2.8/ 2 (4)	-0.5/ -0 (44)	0.6/ 0 (67)
natl				
HALDEN	0.3/ 1 (59)	0.9/ 1 (17)	1.3/ 2 (2)	-1.1/ -2 (7)
MOSS	0.6/ 1 (26)	0.7/ 1 (35)	0.9/ 1 (8)	-1.3/ -2 (6)
OSLO	0.3/ 0 (72)	0.7/ 1 (27)	1.0/ 2 (6)	-1.0/ -2 (9)
RØROS	0.5/ 1 (0)	0.5/ 1 (0)	-0.2/ -1 (63)	0.2/ 1 (6)
SKJÅK	0.5/ 2 (10)	0.2/ 1 (1)	-0.6/ -2 (18)	0.4/ 2 (6)
NORDDAL	2.4/ 3 (5)	1.9/ 2 (1)	-0.5/ -1 (20)	2.2/ 3 (4)
VERMA	2.2/ 4 (5)	1.8/ 3 (1)	-0.3/ -1 (57)	1.4/ 2 (5)
HEMNE	2.7/ 2 (12)	2.7/ 2 (4)	-1.3/ -1 (1)	3.7/ 3 (2)
NAMDALSEID	2.0/ 2 (9)	1.6/ 2 (9)	-1.0/ -1 (4)	2.9/ 3 (1)
DUNDERLANDSDAL	0.2/ 0 (81)	-0.9/ -1 (30)	0.1/ 0 (97)	4.4/ 4 (1)
SULITJELMA	0.2/ 0 (82)	0.1/ 0 (82)	0.3/ 0 (89)	3.0/ 3 (1)
BARKESTAD	0.3/ 0 (94)	0.1/ 0 (77)	0.8/ 1 (49)	2.9/ 2 (3)
TROMSØ	0.3/ 0 (60)	0.3/ 0 (44)	0.5/ 1 (39)	1.4/ 2 (8)
GEILO	0.4/ 1 (46)	0.6/ 1 (0)	0.1/ 0 (69)	-0.7/ -1 (16)
BJÅEN	1.2/ 2 (24)	1.2/ 2 (0)	0.2/ 0 (57)	-0.1/ -0 (79)
SVILAND	2.2/ 2 (9)	1.0/ 1 (47)	-0.0/ -0 (78)	2.4/ 2 (3)
BERGEN	2.9/ 2 (8)	1.5/ 1 (47)	-1.0/ -1 (46)	3.1/ 2 (4)
LAVIK	4.9/ 3 (3)	2.4/ 1 (26)	-1.5/ -1 (18)	3.9/ 2 (3)

Table 56: Downscaled precipitation scenarios of the CCCma member 2 results using the common EOF method. Both the units of mm/(month decade) and %/decade are given (after the "/"), and the parentheses give the p-value according to a trend test. Length of interval= 119. Dates 15-Oct-1980 - 15-Oct-2098

6.2.11 Downscaling CCCma by common EOFs based on *Benestad* (2000b) SLP.

Location	Jan	Apr	Jul	Oct
nordic				
HALDEN	0.4/ 1 (43)	-0.3/ -0 (55)	1.4/ 2 (2)	0.1/ 0 (80)
MOSS	0.2/ 0 (68)	-1.1/ -2 (3)	1.2/ 2 (4)	0.2/ 0 (86)
OSLO	0.1/ 0 (69)	-1.3/ -2 (1)	1.3/ 2 (2)	0.1/ 0 (90)
RØROS	0.2/ 0 (39)	0.4/ 1 (1)	0.1/ 0 (61)	-0.3/ -1 (12)
SKJÅK	0.3/ 1 (52)	0.2/ 1 (2)	0.2/ 1 (45)	-0.2/ -1 (19)
NORDDAL	1.6/ 2 (12)	2.8/ 4 (0)	0.0/ 0 (70)	-0.4/ -0 (61)
VERMA	1.4/ 2 (19)	2.1/ 4 (0)	0.2/ 0 (37)	-0.2/ -0 (77)
HEMNE	1.6/ 1 (32)	4.8/ 4 (0)	-0.3/ -0 (91)	-0.3/ -0 (76)
NAMDALSEID	1.4/ 1 (21)	3.4/ 3 (0)	-0.4/ -0 (81)	-0.2/ -0 (78)
DUNDERLANDSDAL	1.9/ 2 (51)	3.3/ 3 (0)	0.6/ 1 (30)	1.0/ 1 (78)
SULITJELMA	0.6/ 1 (61)	2.5/ 3 (0)	1.0/ 1 (17)	-0.4/ -1 (56)
BARKESTAD	0.7/ 1 (61)	1.7/ 1 (6)	0.1/ 0 (88)	-0.2/ -0 (76)
TROMSØ	0.5/ 1 (63)	1.4/ 2 (2)	-0.1/ -0 (76)	-0.3/ -0 (63)
GEILO	0.6/ 1 (23)	-0.6/ -1 (6)	1.2/ 2 (3)	-0.1/ -0 (97)
BJÅEN	1.4/ 2 (32)	0.1/ 0 (64)	1.2/ 2 (1)	-0.2/ -0 (67)
SVILAND	1.9/ 1 (46)	2.9/ 2 (2)	1.6/ 1 (8)	0.1/ 0 (92)
BERGEN	2.2/ 1 (45)	4.0/ 2 (2)	1.1/ 1 (36)	-0.8/ -0 (47)
LAVIK	2.4/ 1 (53)	5.7/ 3 (0)	0.5/ 0 (61)	-1.0/ -1 (37)
natl				
HALDEN	0.1/ 0 (88)	-0.1/ -0 (98)	1.8/ 3 (0)	-0.1/ -0 (96)
MOSS	0.3/ 0 (56)	-0.4/ -1 (31)	1.3/ 2 (1)	0.4/ 1 (53)
OSLO	0.1/ 0 (88)	-0.3/ -1 (35)	1.8/ 3 (0)	0.2/ 0 (79)
RØROS	0.2/ 1 (20)	0.4/ 1 (1)	-0.1/ -0 (72)	0.0/ 0 (99)
SKJÅK	0.3/ 1 (45)	0.1/ 1 (4)	-0.4/ -2 (39)	-0.1/ -0 (66)
NORDDAL	1.3/ 2 (38)	2.9/ 4 (0)	-0.5/ -1 (20)	-0.5/ -1 (41)
VERMA	1.0/ 2 (46)	2.9/ 5 (0)	-0.3/ -1 (29)	-0.2/ -0 (76)
HEMNE	0.8/ 1 (94)	4.8/ 4 (0)	-1.8/ -1 (0)	-0.3/ -0 (70)
NAMDALSEID	0.9/ 1 (69)	2.9/ 3 (0)	-1.1/ -1 (2)	-0.2/ -0 (75)
DUNDERLANDSDAL	-0.6/ -1 (49)	1.7/ 2 (12)	1.5/ 1 (1)	-1.1/ -1 (29)
SULITJELMA	0.0/ 0 (98)	1.8/ 2 (1)	2.2/ 3 (1)	-0.3/ -0 (64)
BARKESTAD	0.5/ 0 (66)	2.3/ 2 (1)	1.6/ 1 (12)	-0.4/ -0 (57)
TROMSØ	-0.2/ -0 (76)	1.4/ 2 (0)	0.5/ 1 (28)	-0.8/ -1 (27)
GEILO	0.1/ 0 (82)	0.1/ 0 (59)	1.3/ 2 (1)	-0.1/ -0 (76)
BJÅEN	0.5/ 1 (81)	0.1/ 0 (56)	0.9/ 1 (1)	-0.6/ -1 (31)
SVILAND	1.1/ 1 (92)	1.1/ 1 (31)	2.6/ 2 (2)	0.0/ 0 (72)
BERGEN	1.2/ 1 (94)	1.2/ 1 (31)	1.9/ 1 (21)	-1.0/ -1 (33)
LAVIK	1.9/ 1 (80)	1.6/ 1 (16)	0.0/ 0 (82)	-1.2/ -1 (42)

Table 57: Downscaled precipitation scenarios of the CCCma member 3 results using the common EOF method. Both the units of mm/(month decade) and %/decade are given (after the "/"), and the parentheses give the p-value according to a trend test. Length of interval= 119. Dates 15-Oct-1980 - 15-Oct-2098

6.2.12 Downscaling CSIRO by common EOFs based on *Benestad* (2000b) SLP.

Location	Jan	Apr	Jul	Oct
nordic				
HALDEN	-0.3/ -0 (66)	-0.3/ -0 (41)	0.3/ 0 (44)	-1.0/ -2 (29)
MOSS	0.0/ 0 (87)	-0.3/ -0 (64)	0.3/ 0 (53)	-1.1/ -2 (40)
OSLO	-0.4/ -1 (50)	-0.4/ -1 (41)	0.3/ 1 (60)	-1.0/ -2 (30)
RØROS	-0.1/ -0 (54)	0.2/ 0 (21)	0.2/ 0 (53)	-0.3/ -1 (15)
SKJÅK	-0.1/ -0 (93)	0.0/ 0 (100)	0.2/ 1 (47)	-0.4/ -2 (9)
NORDDAL	-0.4/ -1 (76)	0.6/ 1 (34)	0.1/ 0 (53)	-0.3/ -0 (92)
VERMA	-0.5/ -1 (78)	0.6/ 1 (38)	0.2/ 0 (58)	0.1/ 0 (72)
HEMNE	-0.6/ -0 (80)	1.3/ 1 (16)	0.2/ 0 (73)	0.0/ 0 (81)
NAMDALSEID	-0.1/ -0 (78)	1.1/ 1 (7)	0.2/ 0 (49)	-0.2/ -0 (92)
DUNDERLANDSDAL	-0.3/ -0 (63)	0.4/ 0 (51)	0.6/ 1 (7)	-2.3/ -2 (18)
SULITJELMA	0.6/ 1 (72)	0.4/ 1 (31)	0.4/ 1 (28)	-1.3/ -2 (28)
BARKESTAD	0.7/ 1 (59)	0.1/ 0 (97)	0.4/ 0 (31)	-0.4/ -0 (93)
TROMSØ	0.8/ 1 (24)	0.1/ 0 (80)	0.1/ 0 (78)	-0.3/ -0 (80)
GEILO	0.1/ 0 (76)	-0.2/ -0 (52)	0.1/ 0 (62)	-0.6/ -1 (53)
BJÅEN	0.1/ 0 (81)	0.1/ 0 (60)	0.2/ 0 (59)	-1.1/ -1 (26)
SVILAND	-0.4/ -0 (73)	0.6/ 0 (37)	0.7/ 1 (10)	-1.9/ -1 (33)
BERGEN	-0.6/ -0 (66)	0.2/ 0 (83)	0.8/ 0 (24)	-2.6/ -1 (20)
LAVIK	-0.6/ -0 (70)	0.7/ 0 (59)	0.7/ 0 (30)	-1.5/ -1 (43)
natl				
HALDEN	-0.5/ -1 (28)	-0.2/ -0 (75)	0.5/ 1 (32)	-1.1/ -2 (26)
MOSS	-0.5/ -1 (49)	-0.3/ -0 (69)	0.0/ 0 (99)	-1.2/ -2 (31)
OSLO	-0.5/ -1 (33)	-0.3/ -0 (66)	0.0/ 0 (93)	-1.1/ -2 (21)
RØROS	-0.1/ -0 (96)	0.2/ 0 (2)	-0.2/ -1 (30)	-0.0/ -0 (72)
SKJÅK	0.1/ 0 (57)	0.1/ 0 (18)	-0.2/ -1 (26)	-0.3/ -1 (14)
NORDDAL	0.3/ 0 (48)	1.1/ 1 (5)	0.0/ 0 (81)	-0.2/ -0 (80)
VERMA	0.1/ 0 (65)	1.2/ 2 (3)	-0.0/ -0 (92)	0.4/ 1 (47)
HEMNE	-1.5/ -1 (36)	1.6/ 1 (9)	0.1/ 0 (63)	0.4/ 0 (74)
NAMDALSEID	-0.9/ -1 (35)	1.2/ 1 (9)	0.1/ 0 (69)	0.3/ 0 (82)
DUNDERLANDSDAL	-3.0/ -3 (4)	1.0/ 1 (18)	0.8/ 1 (2)	-0.8/ -1 (66)
SULITJELMA	-0.8/ -1 (33)	0.7/ 1 (18)	0.9/ 1 (6)	0.2/ 0 (61)
BARKESTAD	-0.2/ -0 (78)	0.5/ 0 (58)	0.9/ 1 (5)	-1.7/ -1 (27)
TROMSØ	0.1/ 0 (93)	0.5/ 1 (35)	0.4/ 0 (23)	-0.7/ -1 (75)
GEILO	-0.0/ -0 (98)	0.1/ 0 (61)	-0.1/ -0 (80)	-0.1/ -0 (92)
BJÅEN	-0.7/ -1 (56)	0.2/ 0 (26)	-0.4/ -0 (19)	-1.5/ -2 (14)
SVILAND	-0.5/ -0 (75)	0.6/ 0 (29)	0.9/ 1 (20)	-1.5/ -1 (42)
BERGEN	-1.3/ -1 (49)	0.4/ 0 (72)	0.6/ 0 (37)	-2.7/ -2 (19)
LAVIK	-1.8/ -1 (42)	1.0/ 1 (44)	0.3/ 0 (58)	-2.1/ -1 (22)

Table 58: Downscaled precipitation scenarios of the CSIRO results using the common EOF method. Both the units of mm/(month decade) and %/decade are given (after the "/"), and the parentheses give the p-value according to a trend test. Length of interval= 120. Dates 15-Oct-1980 - 15-Oct-2099

6.2.13 Downscaling ECHAM3 by common EOFs based on *Benestad* (2000b) SLP.

Location	Jan	Apr	Jul	Oct
nordic				
HALDEN	1.7/ 3 (27)	-2.0/ -3 (14)	2.9/ 5 (1)	5.1/ 8 (1)
MOSS	2.8/ 4 (18)	-2.1/ -3 (18)	1.7/ 3 (11)	5.8/ 9 (2)
OSLO	1.9/ 3 (23)	-2.0/ -3 (18)	2.0/ 3 (5)	4.5/ 7 (2)
RØROS	-0.6/ -2 (31)	-0.5/ -1 (37)	0.0/ 0 (82)	-0.4/ -1 (52)
SKJÅK	-0.7/ -3 (51)	-0.1/ -0 (65)	0.7/ 3 (29)	0.1/ 0 (86)
NORDDAL	-3.1/ -4 (57)	-0.1/ -0 (84)	0.7/ 1 (8)	-2.6/ -3 (37)
VERMA	-2.5/ -4 (51)	-0.4/ -1 (79)	0.4/ 1 (42)	-1.8/ -3 (36)
HEMNE	-7.8/ -6 (37)	-1.4/ -1 (78)	-2.7/ -2 (3)	-1.0/ -1 (75)
NAMDALSEID	-3.6/ -3 (68)	-0.3/ -0 (91)	-1.6/ -2 (8)	-1.1/ -1 (72)
DUNDERLANDSDAL	-4.0/ -4 (89)	-0.6/-1 (81)	-0.1/-0 (83)	-2.6/-2 (72)
SULITJELMA	-1.4/ -2 (94)	2.3/ 3 (20)	-0.2/ -0 (92)	-3.9/ -5 (16)
BARKESTAD	-1.2/ -1 (97)	1.3/ 1 (67)	-0.1/ -0 (90)	-4.6/ -4 (53)
TROMSØ	-1.3/ -2 (54)	1.5/ 2 (46)	0.4/ 0 (94)	-3.5/ -5 (19)
GEILO	0.8/ 1 (55)	-0.8/ -1 (31)	1.8/ 3 (11)	3.0/ 5 (1)
BJÅEN	-1.5/ -2 (79)	-1.5/ -2 (9)	0.7/ 1 (40)	3.4/ 4 (5)
SVILAND	0.0/ 0 (83)	-4.1/ -3 (12)	1.5/ 1 (31)	6.0/ 4 (15)
BERGEN	-2.3/ -1 (96)	-5.0/ -3 (27)	-0.4/ -0 (90)	2.8/ 2 (67)
LAVIK	-5.8/ -3 (65)	-5.0/ -3 (31)	-2.8/ -2 (18)	-2.0/ -1 (63)
natl				
HALDEN	2.3/ 4 (22)	-1.1/ -2 (34)	1.5/ 2 (24)	2.6/ 4 (20)
MOSS	4.1/ 6 (3)	-1.1/ -2 (43)	0.8/ 1 (45)	3.0/ 5 (27)
OSLO	3.1/ 5 (5)	-1.0/ -2 (50)	0.7/ 1 (66)	2.4/ 4 (24)
RØROS	-0.5/ -1 (53)	-0.2/ -0 (57)	-1.3/ -3 (18)	0.1/ 0 (73)
SKJÅK	-1.4/ -6 (22)	-0.3/ -1 (12)	-1.1/ -4 (31)	0.1/ 0 (92)
NORDDAL	-6.3/ -8 (16)	-0.3/ -0 (85)	-1.6/ -2 (8)	-1.4/ -2 (70)
VERMA	-6.1/-10 (14)	-0.2/ -0 (92)	-1.3/ -2 (14)	-0.5/ -1 (87)
HEMNE	-10.0/ -8 (9)	0.4/ 0 (84)	-1.9/ -2 (4)	-2.8/ -2 (51)
NAMDALSEID	-5.6/ -5 (30)	0.6/ 1 (64)	-1.7/ -2 (3)	-1.7/ -2 (68)
DUNDERLANDSDAL	-4.1/ -4 (51)	0.5/ 0 (75)	-0.7/-1 (62)	-2.2/-2 (46)
SULITJELMA	-2.5/ -3 (57)	2.5/ 3 (6)	-0.5/ -1 (92)	-3.0/ -3 (48)
BARKESTAD	-1.0/ -1 (86)	2.3/ 2 (30)	-0.1/ -0 (85)	-6.6/ -6 (10)
TROMSØ	-1.5/ -2 (51)	1.9/ 3 (13)	-0.2/ -0 (75)	-2.6/ -3 (36)
GEILO	0.8/ 1 (69)	-0.8/ -1 (26)	1.2/ 2 (37)	3.8/ 7 (0)
BJÅEN	-0.5/ -1 (86)	-1.1/ -1 (14)	0.9/ 1 (35)	2.9/ 4 (6)
SVILAND	-2.8/ -2 (51)	-3.5/ -2 (13)	-0.2/ -0 (87)	5.0/ 3 (14)
BERGEN	-2.8/ -2 (63)	-4.9/ -3 (20)	-0.9/ -0 (66)	4.4/ 2 (35)
LAVIK	-3.3/ -2 (72)	-4.1/ -2 (40)	-2.5/ -1 (30)	1.6/ 1 (71)

Table 59: Downscaled precipitation scenarios of the ECHAM3 results using the common EOF method. Both the units of mm/(month decade) and %/decade are given (after the "/"), and the parentheses give the p-value according to a trend test. Length of interval= 69. Dates 15-Oct-1980 - 15-Oct-2048

6.2.14 Downscaling ECHAM4 GSA by common EOFs based on *Benestad* (2000b) SLP.

Location	Jan	Apr	Jul	Oct
nordic				
HALDEN	-1.1/ -2 (37)	0.7/ 1 (52)	-0.1/ -0 (95)	-0.0/ -0 (90)
MOSS	-2.4/ -4 (15)	0.8/ 1 (57)	-0.0/ -0 (97)	-0.4/ -1 (90)
OSLO	-1.5/ -2 (20)	0.4/ 1 (88)	0.5/ 1 (72)	-0.3/ -0 (97)
RØROS	0.7/ 2 (44)	0.0/ 0 (54)	0.0/ 0 (92)	0.5/ 1 (41)
SKJÅK	1.1/ 4 (26)	0.3/ 1 (4)	-0.1/ -0 (69)	0.1/ 0 (96)
NORDDAL	6.0/ 8 (17)	0.6/ 1 (55)	-0.2/ -0 (60)	2.3/ 3 (53)
VERMA	5.7/ 9 (22)	0.1/ 0 (69)	0.1/ 0 (96)	1.7/ 3 (53)
HEMNE	10.1/ 8 (10)	2.8/ 2 (24)	2.5/ 2 (6)	1.1/ 1 (72)
NAMDALSEID	5.6/ 5 (13)	2.7/ 3 (18)	1.5/ 1 (22)	0.6/ 1 (84)
DUNDERLANDSDAL	4.1/ 4 (36)	3.6/ 3 (11)	0.4/ 0 (88)	4.4/ 4 (38)
SULITJELMA	2.1/ 3 (48)	2.5/ 3 (20)	1.6/ 2 (35)	-1.1/ -1 (53)
BARKESTAD	1.4/ 1 (46)	1.2/ 1 (59)	2.4/ 2 (34)	-1.8/ -2 (59)
TROMSØ	1.1/ 1 (72)	1.1/ 1 (32)	0.8/ 1 (50)	-3.2/ -4 (24)
GEILO	0.3/ 1 (87)	0.5/ 1 (31)	-0.7/ -1 (100)	0.1/ 0 (74)
BJÅEN	2.3/ 3 (54)	1.2/ 2 (6)	0.3/ 0 (72)	1.6/ 2 (32)
SVILAND	2.2/ 1 (57)	4.5/ 3 (2)	2.0/ 1 (33)	3.9/ 3 (29)
BERGEN	4.2/ 2 (52)	7.3/ 4 (2)	1.7/ 1 (72)	2.9/ 2 (46)
LAVIK	7.3/ 4 (29)	6.7/ 4 (4)	1.8/ 1 (64)	1.2/ 1 (66)
natl				
HALDEN	-1.0/ -2 (39)	0.8/ 1 (39)	0.3/ 0 (80)	0.3/ 1 (58)
MOSS	-1.6/ -2 (25)	1.2/ 2 (19)	-0.1/ -0 (84)	0.0/ 0 (54)
OSLO	-1.3/ -2 (26)	1.1/ 2 (25)	0.1/ 0 (100)	0.0/ 0 (48)
RØROS	0.3/ 1 (51)	0.0/ 0 (75)	-0.0/ -0 (89)	0.5/ 1 (30)
SKJÅK	0.9/ 4 (27)	0.0/ 0 (68)	-1.0/ -4 (7)	0.4/ 1 (55)
NORDDAL	4.0/ 5 (19)	0.2/ 0 (78)	-0.2/ -0 (85)	2.2/ 3 (39)
VERMA	3.8/ 6 (23)	-0.2/ -0 (92)	0.1/ 0 (89)	1.4/ 2 (41)
HEMNE	7.1/ 6 (28)	2.8/ 2 (26)	0.4/ 0 (88)	1.5/ 1 (64)
NAMDALSEID	4.1/ 4 (29)	2.6/ 2 (15)	-0.0/ -0 (88)	0.9/ 1 (69)
DUNDERLANDSDAL	-1.7/ -1 (63)	2.1/ 2 (37)	1.6/ 1 (13)	2.1/ 2 (95)
SULITJELMA	-0.3/ -0 (80)	0.5/ 1 (79)	2.7/ 3 (7)	-0.9/ -1 (56)
BARKESTAD	-0.1/ -0 (90)	-0.2/ -0 (96)	2.7/ 2 (16)	0.4/ 0 (89)
TROMSØ	0.8/ 1 (59)	-0.5/ -1 (81)	1.3/ 2 (19)	-1.8/ -2 (32)
GEILO	-0.1/ -0 (94)	0.7/ 1 (15)	-0.2/ -0 (90)	-0.8/ -1 (53)
BJÅEN	0.4/ 0 (90)	1.0/ 1 (7)	-0.8/ -1 (43)	0.7/ 1 (94)
SVILAND	1.0/ 1 (66)	2.9/ 2 (9)	1.5/ 1 (35)	3.8/ 3 (30)
BERGEN	1.4/ 1 (86)	4.1/ 2 (7)	2.3/ 1 (73)	3.6/ 2 (49)
LAVIK	2.8/ 2 (84)	4.0/ 2 (13)	2.0/ 1 (80)	3.9/ 2 (51)

Table 60: Downscaled precipitation scenarios of the ECHAM4-GSA results using the common EOF method. Both the units of mm/(month decade) and %/decade are given (after the "/"), and the parentheses give the p-value according to a trend test. Length of interval= 69. Dates 15-Oct-1980 - 15-Oct-2048

6.2.15 Downscaling GFDL by common EOFs based on *Benestad* (2000b) SLP.

Location	Jan	Apr	Jul	Oct
nordic				
HALDEN	0.3/ 1 (52)	0.8/ 1 (6)	-0.0/ -0 (85)	1.3/ 2 (26)
MOSS	1.0/ 2 (13)	0.3/ 0 (21)	0.1/ 0 (87)	1.7/ 3 (18)
OSLO	0.6/ 1 (30)	0.1/ 0 (27)	0.2/ 0 (81)	1.1/ 2 (25)
RØROS	-0.1/ -0 (71)	0.5/ 1 (4)	0.2/ 0 (61)	-0.2/ -0 (51)
SKJÅK	-0.3/ -1 (31)	0.1/ 0 (23)	0.3/ 1 (29)	-0.1/ -0 (33)
NORDDAL	-2.2/ -3 (14)	1.2/ 1 (24)	0.3/ 0 (16)	0.7/ 1 (85)
VERMA	-2.2/ -4 (16)	1.2/ 2 (22)	0.3/ 0 (28)	0.8/ 1 (68)
HEMNE	-3.5/ -3 (21)	1.5/ 1 (39)	-0.2/ -0 (86)	1.7/ 1 (44)
NAMDALSEID	-2.3/ -2 (22)	1.0/ 1 (47)	0.4/ 0 (28)	1.2/ 1 (63)
DUNDERLANDSDAL	-4.6/ -4 (16)	-1.8/ -2 (30)	1.8/ 2 (3)	3.0/ 3 (16)
SULITJELMA	-2.1/ -2 (22)	-1.3/ -2 (24)	1.9/ 2 (13)	-0.9/ -1 (49)
BARKESTAD	-1.8/ -2 (24)	-4.6/ -4 (1)	2.0/ 2 (26)	-0.3/ -0 (98)
TROMSØ	-1.9/ -2 (25)	-2.1/ -3 (6)	0.6/ 1 (49)	-0.2/ -0 (92)
GEILO	-0.3/ -1 (66)	0.3/ 1 (11)	-0.3/ -0 (93)	0.3/ 0 (62)
BJÅEN	-1.7/ -2 (31)	0.2/ 0 (53)	0.5/ 1 (40)	1.1/ 1 (39)
SVILAND	-2.0/ -1 (34)	0.6/ 0 (88)	2.2/ 2 (11)	3.0/ 2 (30)
BERGEN	-3.3/ -2 (20)	-1.7/ -1 (46)	2.5/ 1 (13)	2.4/ 1 (46)
LAVIK	-4.4/ -2 (21)	-1.4/ -1 (47)	2.1/ 1 (13)	1.8/ 1 (70)
natl				
HALDEN	0.8/ 1 (22)	0.0/ 0 (55)	-0.7/ -1 (22)	1.1/ 2 (22)
MOSS	1.4/ 2 (16)	-0.1/ -0 (88)	-1.3/ -2 (3)	1.4/ 2 (17)
OSLO	1.2/ 2 (8)	-0.3/ -0 (78)	-1.0/ -2 (11)	0.9/ 1 (24)
RØROS	-0.0/ -0 (99)	0.1/ 0 (53)	-0.6/ -2 (40)	0.4/ 1 (17)
SKJÅK	-0.3/ -1 (51)	0.0/ 0 (96)	-0.2/ -1 (58)	0.2/ 1 (68)
NORDDAL	-1.6/ -2 (27)	0.5/ 1 (54)	0.2/ 0 (28)	1.5/ 2 (38)
VERMA	-1.3/ -2 (52)	0.4/ 1 (63)	0.3/ 0 (22)	1.3/ 2 (20)
HEMNE	-3.2/ -3 (21)	0.5/ 0 (65)	0.5/ 0 (34)	1.1/ 1 (72)
NAMDALSEID	-2.0/ -2 (32)	-0.1/ -0 (88)	0.1/ 0 (70)	1.0/ 1 (70)
DUNDERLANDSDAL	-4.6/ -4 (13)	-1.9/ -2 (26)	1.0/ 1 (11)	0.7/ 1 (61)
SULITJELMA	-2.9/ -3 (11)	-0.6/ -1 (62)	1.2/ 1 (18)	-0.4/ -1 (58)
BARKESTAD	-2.2/ -2 (18)	-2.7/ -2 (6)	0.6/ 0 (55)	-2.4/ -2 (20)
TROMSØ	-1.9/ -3 (18)	-0.6/ -1 (44)	0.3/ 0 (46)	-1.3/ -2 (24)
GEILO	0.2/ 0 (82)	0.4/ 1 (19)	-0.5/ -1 (39)	1.0/ 2 (16)
BJÅEN	-0.9/ -1 (53)	0.3/ 0 (49)	-0.6/ -1 (24)	1.4/ 2 (24)
SVILAND	-2.5/ -2 (16)	1.0/ 1 (50)	3.3/ 2 (2)	4.2/ 3 (11)
BERGEN	-3.3/ -2 (15)	-1.0/ -1 (93)	2.6/ 1 (10)	2.7/ 1 (30)
LAVIK	-4.2/ -2 (19)	-1.2/ -1 (83)	1.8/ 1 (19)	0.1/ 0 (96)

Table 61: Downscaled precipitation scenarios of the GFDL results using the common EOF method. Both the units of mm/(month decade) and %/decade are given (after the "/"), and the parentheses give the p-value according to a trend test. Length of interval= 85. Dates 15-Oct-1980 - 15-Oct-2064

that the correlation between the large-scale circulation and the local rainfall is weak ($r = 0.33 \cdot 0.37$), and the discrepancy between the two estimates may be due to the poorly defined relationship between the large and the local scales, but the trend test may also be affected by smaller fluctuations.

Corresponding downscaled results from the NCAR CSM are presented in Table 50. These results suggest only one statistically significant trend: Skjåk in July. Also this estimate is associated with low correlation ($r = 0.57 \cdot 0.58$). There are uncertainties as to what type of climate the model predicts for Moss, Røro, Norddal, Verma, Sulitjelma, Geilo and Bjåen in January as the *nordic* and the *natl* predictors indicate trends of opposite sign. The April scenarios for southern Norway suggest a wetter climate if the smaller domain is used and marginally drier spring-time conditions if based on the larger domain size. In July, it is only the Skjåk scenario that indicates a real trend, but this scenario is not based on a model with a clear and strong relationship between the large and small scale variability. The slope of the precipitation curve nevertheless have the same sign for both estimates. As these are not statistically significant from zero at the 5% level, it is concluded that the NCAR-CSM scenarios do not indicate any significant shifts in the rainfall statistics.

Tables 51 to 54 give the downscaled results fro the 4 members of the HadCM2 ensemble integrations and Table 55 to 57. In these two groups of scenarios, the respective boundary conditions are the same for each member, but the initial conditions are different. Thus, the difference between the intra-ensemble members yields a rough representation of the uncertainty associated with the unknown initial conditions for 1860.

The statistically significant entries for member 1 HadCM2 in Table 51 (Jan: Halden, Røros, Norddal, Verma, Hemne; April: Røros, Skjåk, Norddal, Verma, Hemne; Jul: Røros, Skjåk, Norddal, Verma, Hemne; Oct: Halden, Moss, Oslo) are of same sign for the two estimates shown. Similar tendencies can be seen for the second (exception: Jul: Norddal), third and fourth members. In general, the HadCM2 experiments give drier winters, although most of these trends are small and not all these estimates are statistically significant. All the January estimates indicate dryer conditions for Verma, Hemne and Lavik, but a substantial scatter for the locations Namdalseid-Bergen (the stations listed between these in Table 51). In April, there are no common trend in the precipitation, thus there are substantial uncertainties associated with the spring-time results. The downscaled July scenarios tend towards drier conditions, with the exception of Sulitjelma and Barkestad, and in October, the Sviland and Bjåen scenarios are all towards drier climates.

The CCCma scenarios (Table 55 to 57) are associated with smaller intra-ensemble spread than the HadCM2 results. But, in contrary to the HadCM2 results, the Canadian model gives more precipitation in January. It is only for Barkestad, Tromsø and Oslo that have a spread in estimates that cover both negative and positive values. The spring-time scenarios in general also indicate more precipitation, except for Halden, Moss, and Oslo. In July, the estimates give wetter climate in southern Norway, although with substantial spread. Røros, Skjåk, Verma, Norddal and Lavik, according to these results, may get drier summers. The general impression for October is that of more rainfall, but the scatter is large, and the uncertainties are high. A good portion of the January estimates qualify as "statistically significant".

The downscaled CSIRO scenarios are shown in Table 58. Only the scenario

for Dunderdalsland (*natl*, drier) qualifies as "statistically significant" in January, and a trend towards wetter condition in Røros, Norddal, Verma in April, and in Dunderdalsland in July.

The downscaled scenarios from the ECHAM3 model are given in Table 59, and these estimates suggest more January precipitation in Moss and Oslo. None of the trends estimated in April qualified as statistically significant at the 5% level, but in July the model produced wetter future climate in Halden and Oslo. In Hemne and Namdalseid, on the other hand, some of the estimates gave statistically significant trends towards drier climates for July. The clearest trends can be found in October, suggesting wetter future climates in southern Norway.

The downscaled ECHAM4-GSA scenarios (Table 60) only suggest statistically significant changes in April (Skjåk). In contrast, the corresponding ECHAM4-GSDIO results (Table 46) indicate statistically significant trends in January (Bjåen: wetter), April (Halden, Moss, Oslo: drier), July (Hemne, Namdalseid, Dunderlandsdal, Sviland, Bergen, Lavik: wetter) and October (Halden: wetter; Sulitjelma, Tromsø: drier). These two experiments differ in their boundary conditions and physical representation of aerosols and their effects on clouds and radiation, but have the same initial conditions (?)CHECK!. One may therefore, by contrasting these results, conclude that the uncertainties associated with the aerosols or the representation of clouds will influence the estimation of future rainfall patterns.

Table 61 lists the downscaled results from the GFDL model. Of all the trend estimates, only the April value at Røros (wetter), Barkestad (drier), July slope at Dunderlandsdal, Sviland (wetter) and Moss (drier) could be considered as statistically significant at the 5% level.

7 Climate scenarios based on several AOGCMs

7.1 An objective comparison of AOGCM model skill

It was established in section 5.2 that the different global climate models tend to produce different climate scenarios. Most notable were the American NCAR-DOE and the Japanese CCSR/NIES models which give substantially higher trend estimates than the other models. It is important to ask why two of these scenarios produced such extreme results. Are these models less representative of the real world? One hypotheses could be that these models do not give an adequate representation of the real world because of too low spatial resolution. Table 1 lists the model resolution of the various models, and both NCAR-DOE and CCSR/NIES belong to the model group with the lowest horizontal resolution (40×48 and 32×64 respectively), but the GFDL-19 also have similar grid box sizes and still gives estimates more in line with the other models.

To examine whether there are substantial differences in the models' capability of reproducing the observed spatial T(2m) structure, the variance of the leading 6 common EOFs were compared in Figure 33. Table 10 also lists the variance associated with the 4 leading common EOFs from the ECHAM4 GSDIO results for the *natl*, *nordic*, and the *scan* domains. According to *Sengupta & Boyle* (1993), if the most significant common principal components account for a 'large' portion (75-95%) of the variance, then the simulated and observed fields can be considered 'similar'. The leading common EOF from the ECHAM4 GSDIO scenario described 69% and the 4 leading modes account for 94% of the variance, which suggests that these results are in good agreement with the observations. A comparison can be made between these values and the variance of ordinary EOFs from the ECHAM4 GSDIO results: 80%, 8%, 4% and 3% (95% in total). On the other hand, the EOFs computed from the observed T(2m) (*Benestad*, 2000a) suggest variances of 58%, 28%, 7%, and 2%. Hence, the models tend to produce anomalies with too high spatial coherence, thereby giving too much power in the leading mode. But, different eigenvalues do not necessarily imply that the spatial patterns are different. It is therefore not clear if the criterion for model observation inter-comparison suggested by *Sengupta & Boyle* (1993) is of any use here. The eigenvalues associated with the common EOFs are similar for the various AOGCM scenaries, with lowest variance associated with the leading modes from the HadCM3, ECHAM3 and GFDL-R19 results.

A comparison between the leading common EOF patterns is provided by *Benestad* (2000b), who shows that while all model results describe a NAO-like SLP dipole in their leading mode, the ECHAM3, GFDL and CCSR/NIES results have stronger meridional SLP gradients and the CSIRO, ECHAM3, GFDL and members 2-4 of the HadCM2 ensemble suggest a more prominent southerly component in the geostrophic wind.

Benestad (2000b) compared the coupling between the SLP and T(2m) fields of the various AOGCMs, and found that most of the models could reproduce the main NAO feature. There were nevertheless some models which did not reproduce the observed coupling as well as others, and it was found that the NCAR-DOE and GFDL-R19 results[11] were suspect and that there may poten-

[11] Here the GFDL *surface* pressure was assumed to be similar to the pressure at the sea level, but this is not the case everywhere.

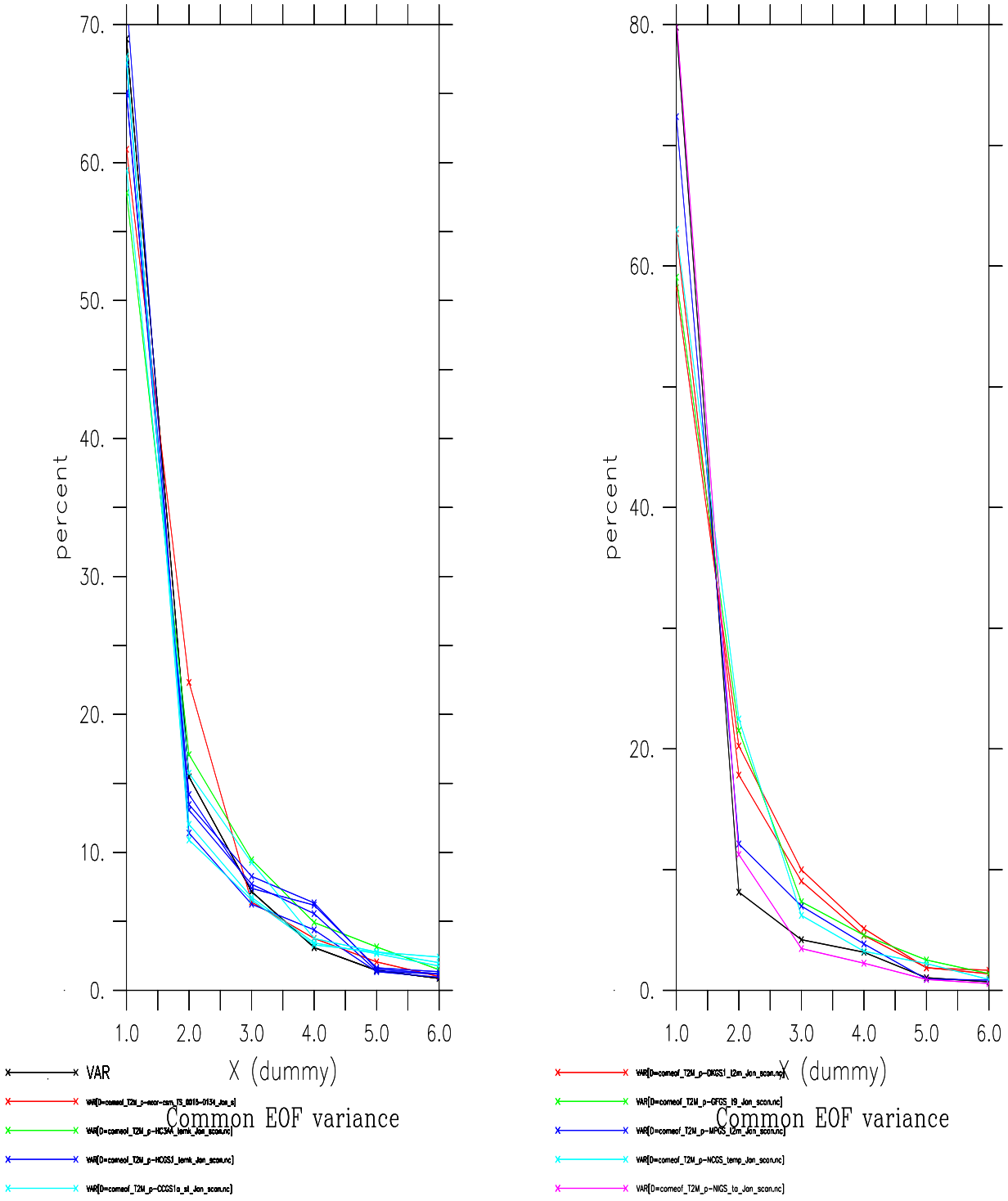

Figure 33: The variance associated with the 6 leading EOFs.

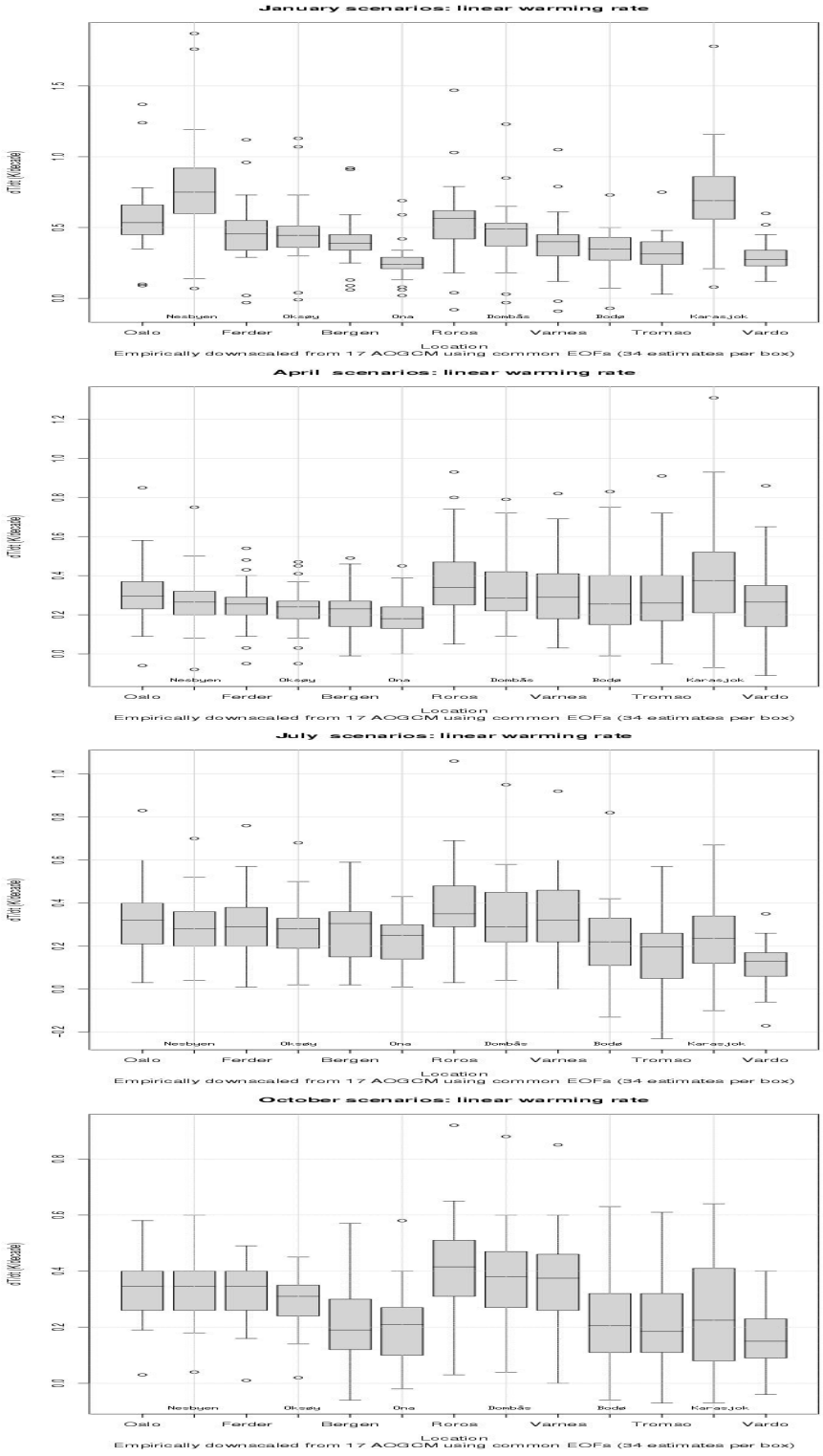

Figure 34: Box-plot presentation of 34 warming trend estimates based on 17 different AOGCM scenarios using the T(2m) fields in addition to the ECHAM4-GSDIO T_{850hPa}, and $\Phi_{500hPa} - \Phi_{700hPa}$ thickness. The linear trend estimates were calculated from model date 1980 to the end of the transient run (2050-2100), and these estimates were derived using both the *scan* and *nordic* domains, with the exception for the ECHAM4-GSDIO T_{850hPa}, CCSR/NIES T(2m) and NCAR-DOE T(2m) results, for which only the *scan* domain was used. The whiskers extend to the most extreme data point which is no more than 1.5 times the interquartile range from the box. The outliers are given as circles. The boxes represent the interquartile range and the horizontal line gives the median.

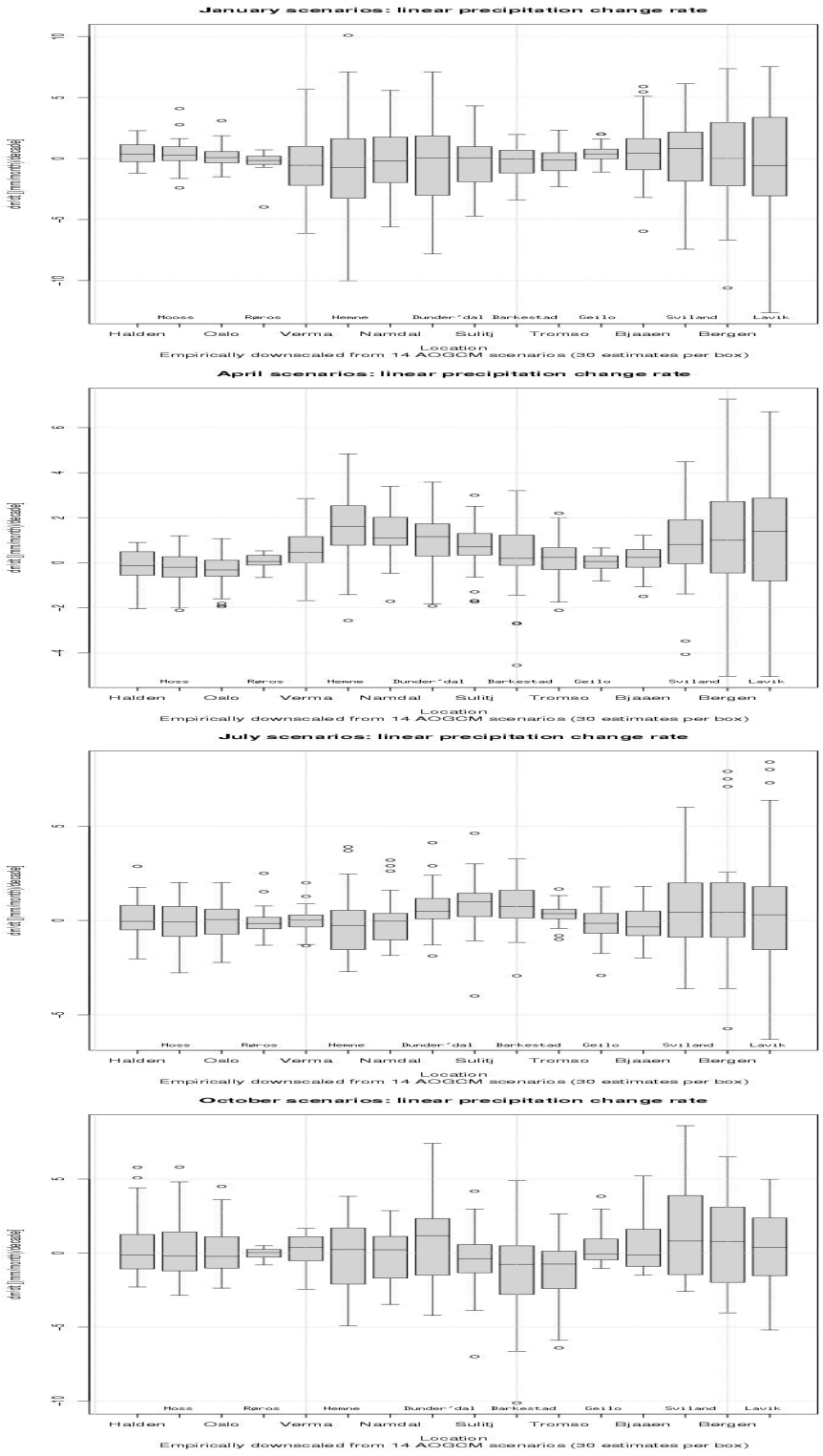

Figure 35: Box-plot presentation of 30 warming trend estimates based on 15 different AOGCM scenarios using the SLP fields in addition to the ECHAM4-GSDIO Φ_{700hPa} field. The linear trend estimates were calculated from model date 1980 to the end of the transient run (2050-2100), and these estimates were derived using the *scan*, *nordic* and *natl* domains. The whiskers extend to the most extreme data point which is no more than 1.5 times the interquartile range from the box. The outliers are given as circles. The boxes represent the interquartile range and the horizontal line gives the median.

7.1.1 Details on the box-plot scenarios.

n	Model	domain	field	Integration
T(2m)				
1	ECHAM4/OPYC3	nordic	T(2m)	GSDIO
1	ECHAM4/OPYC3	scan	T(2m)	GSDIO
1	ECHAM4/OPYC3	nordic	H(700hPa-500hPa)	GSDIO
1	ECHAM4/OPYC3	scan	H(700hPa-500hPa)	GSDIO
1	ECHAM4/OPYC3	scan	T at 850 hPa	GSDIO
1	ECHAM4/OPYC3	scan	T(2m)	GSA
1	ECHAM4/OPYC3	nordic	T(2m)	GSA
2	ECHAM3/LSG	scan	T(2m)	GSA
2	ECHAM3/LSG	nordic	T(2m)	GSA
1	HadCM3	scan	T(2m)	GSA
1	HadCM3	nordic	T(2m)	GSA
4	HadCM2	scan	T(2m)	GSA
4	HadCM2	nordic	T(2m)	GSA
3	CCCma	scan	T(2m)	GSA
3	CCCma	nordic	T(2m)	GSA
1	CSIRO	scan	T(2m)	GSA
1	CSIRO	nordic	T(2m)	GSA
1	NCAR-CSM	scan	T(2m)	GSA
1	NCAR-DOE	scan	T(2m)	GSA
1	CCSR/NIES	scan	T(2m)	GSA
1	GFDL	scan	T(2m)	GSA
1	GFDL	nordic	T(2m)	GSA
Precipitation				
1	ECHAM4/OPYC3	natl	SLP	GSDIO
1	ECHAM4/OPYC3	nordic	SLP	GSDIO
1	ECHAM4/OPYC3	scan	SLP	GSDIO
1	ECHAM4/OPYC3	natl	700hPa height	GSDIO
1	ECHAM4/OPYC3	natl	SLP	GSA
1	ECHAM4/OPYC3	nordic	SLP	GSA
1	ECHAM3/LSG	natl	SLP	GSA
1	ECHAM3/LSG	nordic	SLP	GSA
1	HadCM3	natl	SLP	GSA
1	HadCM3	nordic	SLP	GSA
4	HadCM2	natl	SLP	GSA
4	HadCM2	nordic	SLP	GSA
3	CCCma	natl	SLP	GSA
3	CCCma	nordic	SLP	GSA
1	CSIRO	natl	SLP	GSA
1	CSIRO	nordic	SLP	GSA
1	NCAR-CSM	natl	SLP	GSA
1	NCAR-CSM	nordic	SLP	GSA
1	GFDL	natl	SLP	GSA
1	GFDL	nordic	SLP	GSA

Table 62: Details of the estimates made to produce the box-plots in Figures 34 and 35.

tially also be some systematic errors in the CCCma, CSIRO and the ECHAM3 results.

Figures 34 and 35 show box-plots of a number (34 for T(2m) and 30 for precipitation) of "future" ("1980" and onward, except for NCAR-CSM whose integration starts in "1990") T(2m) and precipitation trend estimates from the different AOGCM scenarios. A list of the calculation detail is given in Table 62. It is assumed here (as first-order approximation) that each estimate is "equally reliable", although it is reality more probable that the most recent scenarios (i.e. HadCM3, ECHAM4 GSDIO) are more representative than the older scenarios (i.e. NCAR-DOE). Some degree of subjectivity is nevertheless present, as these results were inferred using more estimates based on the ECHAM4 and the HadCM*X* model results than the older models scenarios. In many cases, extreme values from the NCAR-DOE are shown as outliers in the box-plot diagrams.

The spread in the data evident from Figures 34 and 35 give a rough indication of the uncertainty associated with these scenarios. All the temperature scenarios indicate a future warming, but there is a small spread in these values. It was remarkable how well the various model estimates agreed with each other, much the differences being attributed to different circulation patterns. On the other hand, since the empirical models associate the temperature at a given place with a spatial temperature structure, the various temperature predictions for the different locations given by these models tend to follow the same pattern. One may regard the common EOF method as imposing empirical relationships onto the scenarios.

The downscaled super-ensemble precipitation scenarios (Figure 35) have in general large spread. The box-plot span both positive and negative values in January, and there are no clear common signal for the winter. In April, on the other hand, most of the estimates indicate a trend towards wetter conditions at Hemne, Namdalseid, Dunderlandsdal and Sulitjelma. The downscaled model results also suggest wetter conditions for Dunderlandsdal and Sulitjelma in July, but the scatter in October is too great and include both polarities so that the autumn scenarios are associated with too high uncertainties to make any statement about a model "consensus".

In these estimates, there are many different types of uncertainties:

i Uncertainty in the AOGCM initial conditions: a crude estimate can be obtained using ensemble integrations such as done for the HadCM2 model.

ii Uncertainty in the boundary conditions (e.g. CO_2 concentrations and total solar irradiance): a crude measure from comparing a given model integrated using different greenhouse gas scenarios. Eg. ECHAM4-GSA and ECHAM4-GSDIO.

iii Uncertainty in the model description of the climate system (e.g. cloud feedback mechanisms, ocean transport, sea ice, topography): unknown, but a crude idea can be obtained by comparing a number of different AOGCMs. Eg. ECHAM3 and ECHAM4-GSA.

iv Uncertainty in the linear modeling of large-scale to small-scale variations (e.g. observational errors, linear approximation, short time series, predictor domain) - can be quantified to some extent through test experiments.

v Uncertainty in trend estimate: σ_m - can be quantified.

Categories *i*, *ii* and *iii* are to some extent taken into account in the super-ensemble approach, as the different AOGCM scenarios tend to have different initial states, different parameterisation schemes and different forcing scenarios have been used. Nevertheless, more work is required for a better assessment of these sources of uncertainty. Point *iv* has also been addressed in a simple way by including different predictor domains, but again the work ought to be expanded by large number of different downscaling model approaches and configurations. The question about the uncertainty in the trend estimate has been mentioned in isolation with the respective models, where trend test based on Mann-Kendall and t-test of tendencies $(y_{n+1} - y_n)$ were applied. The standard deviation associated with the slope estimate can also be calculated according to standard procedure, but since the approach of super-ensemble was adopted were, the spread of the various estimates was found to be more appropriate by into account all the above mentioned sources of uncertainties.

8 Summary

Comparisons between the simulated "past" *local* trends by the ECHAM4 (GSDIO) climate model and those inferred from actual observations indicate serious differences. Some of these are due to sampling fluctuations, but there may also be other explanations for these "discrepancies". Global atmospheric oceanic climate models are not capable of describing local climatic features such as those in valleys and alpine regions. This shortcoming can partly be explained by the crude model topographies and grids (Figure 1), but, the details of the representation of the various climatic processes (by parameterisation schemes) are also important, as simulations with different AOGCMs give different results for the local climates. The AOGCMs project a future warming for most locations, but the various scenarios for SLP and precipitation are associated with large spread. An investigation of the different AOGCM scenarios of the NAO suggests serious model differences, and it is not possible to say whether the future will bring a strengthening or weakening trend in the NAO.

In order to investigate the implications of the given global climate scenarios for Norway, the AOGCM results were downscaled using empirical/statistical methods. A new method, based on common EOFs, was adopted, and this method was compared with a more conventional approach. The common EOF method involves a quality control, as the exact spatial patterns associated with actual climate variations are identified in the model results and the time evolution of these are used to infer the projected local climate changes. The empirical downscaling models for the local temperature used large-scale temperature fields, SLP, geopotential heights, and layer thickness as predictors. The empirical models based on the temperature field were associated with higher skill than the more circulation based models. Downscaling models for precipitation used SLP and geopotential height as predictor. The models for downscaling temperature obtained higher skill scores in cross-validation analyses than the models predicting precipitation. A series of tests were conducted to assess the skill of the two methods, and the test results suggest that the common EOF method is more suitable than the conventional method. A number of sensitivity tests were also conducted to investigate the influence of the predictor domain choice on the final results. The predictor domain does affect the downscaled

results, but the results tend to be robust within a range of predictor domains. This range varies, depending on the predictand and predictor variables, season and location.

Uncertainties associated with the local climate scenarios can be estimated in a crude fashion by comparing different calculations based on different AOGCM scenarios and different downscaling model configurations. The spread in these estimates gives an indication of a minimum error associated with an assessment of the future climatic trends.

8.1 Discussion

The fact that climate models do not reproduce the past local climate trends (Figure 2) raises the question of whether the simulation of the future local climates is credible: *How can the model predict the future if it does not describe the past future trends?*. This discrepancy may have one or more explanations: *i)* Sampling uncertainties (statistical fluctuations); *ii)* Model errors or shortcomings; *iii)* Uncertainties in the initial conditions or inappropriate spin-up history; *iv)* Errors in the forcing term; *v)* Natural variations; *vi)* Other forcings than the greenhouse gases and aerosols specified in the GSDIO experiment; and/or *vii)* The model dates do not correspond with the real dates.

The last point is important, because the choice of model date is to some extent arbitrary, and the only "time stamp" on the model results are given by the forcing term estimates (which are themselves crude). The HadCM2 ensemble results in Figure 7 demonstrate that the choice of initial conditions makes a difference for the climatic trend estimates because different initial states give different evolution of the natural variations. We don't know the right and exact initial conditions for 1860 and therefore the climate models may not give a represenative description of the 1860 climate. If the models were linear, this wouldn't matter since we use the linear trend for making scenarios, but because the models are nonlinear, the initial model climate seems to matter. It was furthermore shown (Figures 2)a and 4a) that the observed past climate trends appear to be in closer agreement with the model simulations of the "future" climate. The difference between the simulated "past" and the "future" should therefore be interpreted with care. Furthermore, it is the accumulation of the forcing terms (i.e. greenhouse gases, oceanic heat) that is most important, not the rate of change, and if the model scenarios start with incorrect concentrations, then the model dates do not correspond to the actual dates.

One question these results raise is whether the local scenarios are useful. Even though there is a substantial spread about zero, the estimates may give useful information about the odds for the future. The empirical distribution functions (e.d.f., the cumulative probabilities) given in the right hand panels of Figures 31 and 32 can give an indication of whether the ensemble of AOGCM results favour wetter or drier conditions. The location (i.e. mean value) and range of estimates also give some information about possible climate change magnitudes.

In order to use these ensemble results, one must make some assumptions about the various ensemble members: Are they equally representative or are some models "better" than others? Both Figure 6 and the downscaled results for temperature suggest that the NCAR-DOE and the CCSR/NIES models give substantially stronger warming than the others. Are these outliers equally

representative as the other AOGCM results? These AOGCMs are older and have coarser model grid than for instance the HadCM3 model. *Benestad* (2000b) suggested that HadCM3, HadCM2, ECHAM4, and NCAR CSM give a more realistic description of the present day climate than the others and that the NCAR-DOE, CCSR/NIES, CCCma and ECHAM3 may potentially have some shortcomings. Here, the issue of different model credibility was solved by using more estimates based on the "better" models and maximum one based on the NCAR-DOE, CCSR/NIES results (see Table 62).

One important question is whether these climate models are adequate for making good climate scenarios. There will always be a risk that not all of the important climate processes are taken into account. Furthermore, due to the large complexity of the real climate system and the limited computation capacity, the climate models can only give an approximate representation of the climate system and a simplified description of the actual world. Comparisons between the AOGCM results and climate observations have nevertheless suggested that the climate models capture the essential features of the climate with a high degree of realism (*Benestad*, 2000b).

It is also assumed that the empirical relationships employed in the "physical" parameterisation schemes and the empirical downscaling really hold for the actual future world. It was shown in this study that the relationship between the large and small scales in the ECHAM4 GSDIO results are approximately stationary throughout the scenario integration, although test results suggest that the empirical models do not capture all of the projected warming (Figure 17). It is well possible that the individual scenario estimates are associated with systematic errors due to this small non-stationarity, and it has not been investigated further whether this systematic error is the same for the different AOGCM results[12] or if there is no inter-model dependency of this error term.

One important finding of this study is that there is a high degree of uncertainty in the estimation of local climatic trends. Downscaling using different predictors and predictor domains can give different results. It was shown that in some cases the downscaling "failed" for a few locations and seasons, where the estimated trends were zero or even negative (Tables 5, 12, and 13). The failure of producing a representative trend in the test results is due to the employment of a T(2m) field representing an inappropriate area as a predictor. The range of results from the downscaling of various AOGCMs also can be interpreted as measure for the uncertainty associated with these estimates. The range in the estimates obtained here demonstrate need for extensive sampling of estimates by systematically going through a range of various empirical downscaling choices and climate scenarios. It is dubious to base any local scenario on just one empirical model and one AOGCM scenario.

8.2 Conclusions

Different AOGCMs tend to give different local climate scenarios, although all produce strongest warming near the poles. In spite of these differences, there is a reasonably good agreement among the downscaled temperature from the various transient integrations for all Norwegian locations examined in this study. The

[12] If this is the case, then the estimates produced here will tend to underestimate the warming projected by the AOGCMs.

warming tends to be strongest in winter at places with continental type climates like Nesbyen and Karasjok. The northern Norway may get marginally smaller temperature increase in July and the coast is projected to get the least warming.

The various AOGCMs give diverging scenarios for the precipitation, due to different trends in the atmospheric circulation and the NAO. There is only a weak model consensus suggesting wetter future conditions for a few locations in April and July.

The downscaled estimates are sensitive to the choice of predictor region, but may nevertheless be relatively robust for a small range of predictor domains. Empirical downscaling based on common EOFs appear to be more appropriate than strategies where the model results are projected onto the EOFs of the observations.

It is important to assess the uncertainties associated with the AOGCM scenario and the downscaling models. The use of only *one* AOGCM scenario for extrapolating the climatic trends may not give a representative picture of the future, and it is not even certain whether an ensemble of many AOGCM scenarios will give a good representation for the future. But the use of many AOGCM scenarios gives some idea about the uncertainty and ranges of values to expect.

References

Arrhenius. 1896. On the Influence of Carbonic Acid in the Air upon the Temperature of the Ground. *Philosophical Magazine and Journal of Science*, 236–276.

Barnett, T.P. 1999. Comparison of Near-Surface Air Temperature Variability in 11 Coupled Global Climate Models. *Journal of Climate*, **12**, 511–518.

Benestad, R. E. 2000a. *Analysis of gridded sea level pressure and 2-meter temperature for 1873-1998 based on UEA and NCEP re-analysis II.* KLIMA 03/00. DNMI, PO Box 43 Blindern, 0313 Oslo, Norway.

Benestad, R. E. 2000b. *Fifteen Global Climate Scenarios: The conversion to netCDF and quality control.* KLIMA 16/00. DNMI, PO Box 43 Blindern, 0313 Oslo, Norway.

Benestad, R.E. 1998. *CCA applied to Statistical Downscaling for Prediction of Monthly Mean Land Surface Temperatures: Model Documentation.* Klima 28/98. DNMI, PO Box 43 Blindern, 0313 Oslo, Norway.

Benestad, R.E. 1999a. *Evaluation of the common EOF approach in linear Empirical Downscaling of Future ECHAM4/OPYC3 GSDIO Climate Scenarios.* KLIMA 35/99. DNMI, PO Box 43 Blindern, 0313 Oslo, Norway.

Benestad, R.E. 1999b. *MVR applied to Statistical Downscaling for Prediction of Monthly Mean Land Surface Temperatures: Model Documentation.* Klima 2/99. DNMI, PO Box 43 Blindern, 0313 Oslo, Norway.

Benestad, R.E. 1999c. *Pilot Studies of Enhanced Greenhouse Gas Scenarios for Norwegian Temperature and Precipitation from Empirical Downscaling.* Klima 16/99. DNMI, PO Box 43 Blindern, 0313 Oslo, Norway.

Benestad, R.E. 1999d. *S-mode and T-mode EOFs from a GCM modeller's perspective: Notes on the linear algebra.* Klima 24/99. DNMI, PO Box 43 Blindern, 0313 Oslo, Norway.

Benestad, R.E. 2000c. The cause of warming over Norway in the ECHAM4/OPYC3 *GHG* integration. *International Journal of Climatology*, Accepted.

Benestad, R.E. 2001. A comparison between two empirical downscaling strategies. *Climate Research*, **submitted to Int. J. Climatology**.

Benestad, R.E., Hanssen-Bauer, I., Førland, E.J., Tveito, O.E., & Iden, K. 1999. *Evaluation of monthly mean data fields from the ECHAM4/OPYC3 control integration.* Klima 14/99. DNMI, PO Box 43 Blindern, 0313 Oslo, Norway.

Benestad, R.E., Sutton, R.T., Allen, M., & Anderson, D.L.T. 2000. Interaction between Intraseasonal Kelvin waves and Tropical Instability waves in the Tropical Pacific. *submitted to JPO.*

Bjørge, D., Haugen, J.E., & Nordeng, T.E. 2000. *Future Climate in Norway.* Research Reoprt 103. DNMI, PO Box 43 Blindern, 0313 Oslo, Norway.

Boer, G.J., Flato, G.M., Reader, M.C., & Ramsden, D. 1998a. A transient climate change simulation with historical and projected greenhouse gas and aerosol forcing: experimental design and comparison with the instrumental record for the 20th century. *Climate Dynamics.*

Boer, G.J., Flato, G.M., Reader, M.C., & Ramsden, D. 1998b. A transient climate change simulation with historical and projected greenhouse gas and aerosol forcing: projected climate for the 20th century. *Climate Dynamics.*

Brown, R.D. 2000. Northern Hemipshere Snow Cover Variability and Change, 1915-97. *Journal of Climate*, **13**(July), 2339–2355.

Crane, R.G., & Hewitson, B.C. 1998. Doubled CO_2 Precipitation Changes for the Susquehanna Basin: Downscaling from the Genesis General Circulation Model. *International Journal of Climatology*, **18**, 65–76.

Cullen, M.J.P. 1993. The unified forecast/climate model. *Meteor. Mag.*, 81–94.

Deliang, C., & Hellström, C. 1999. The influence of the North Atlantic Oscillation on the regional temperature variability in Sweden: spatial and temporal variations. *Tellus*, **51A**(4), 505–516.

Delworth, T.L., Broccoli, A.J., Dixon, K., Held, I., Knutson, T.R., Kushner, P.J., Spelman, M.J., Stouffer, R.J., Vinnikov, K.Y., & Wetherald, R.E. 1999. Coupled Climate Modelling at GFDL: Recent Accomplishment and Future Plans. *Pages 15–20 of: Clivar Exchanges*, vol. 4.

Deser, C., & Blackmon, M.L. 1993. Surface climate variations over the North Atlantic ocean during winter: 1900-1989. *Journal of Climate*, **6**, 1743–1753.

Emori, S., Nozawa, T., Abe-Ouchi, A., Numaguti, A., Kimoto, M., & Nakajima, T. 1999. Coupled ocean-atmosphere model experiments of future climate change with an explicit representation of sulfate aerosol scattering. *Journal of the Meteorological Society of Japan*, **77**(6), 1299 –1307.

Flato, G.M., Boer, G.J., Lee, W.G., McFarlane, N.A., Ramsden, D., Reader, M.C., & Weaver, A.J. 2000. The Canadian Centre for Climate Modelling and Analysis Global Coupled Model and its Climate. *Climate Dynamics*, 16,451–16,467.

Flury, B. 1988. *Common Principal Components and Related Multivariate Models.* Wiley Series in Probability and Mathematical Statistics. New York: Wiley.

Fu, C., Diaz, H.F., Dong, D., & Fletcher, J.O. 1999. Changes in atmospheric circulation over northern hempisphere oceans associated with the rapid warming of the 1920s. *International Journal of Climatology*, **19**, 581–606.

Goodess, C.M., & Palutikof, J.P. 1998. Development of daily rainfall scenarios for southeast Spain using a circulation-type approach to downscaling. *International Journal of Climatology*, **10**, 1051–1083.

Gordon, C., Cooper, C., Senior, C.A., Banks, H., Gregory, J.M., Johns, T.C., Mitchell, J.F.B., & Wood, R.A. 2000. The simulation of SST, sea ice extents and ocean heat transports in a version of the Hadley Centre coupled model without flux adjustments. *Climate Dynamics*, **16**, 147–168.

Gordon, H. B., & O'Farrell, S. P. 1997. Transient climate change in the CSIRO coupled model with dynamic sea ice. *Monthly Weather Review.*

Grotch, S., & MacCracken, M. 1991. The use of general circulation models to predict regional climate change. *Journal of Climate*, **4**, 286–303.

Hanssen-Bauer, I. 2000. *Evaluation and analysis of the ECHAM4/OPYC3 GSDIO temperature- and SLP-fields over Norway and Svalbard.* KLIMA 06/00. DNMI, PO Box 43 Blindern, 0313 Oslo, Norway.

Hanssen-Bauer, I., & Førland, E.J. 1998. Long-term trends in precipitation and temperature in the Norwegian Arctic: can they be explained by changes in the atmospheric circulation patterns? *Climate Research*, **10**, 143–153.

Hanssen-Bauer, I., & Nordli, P.Ø. 1998. *Annual and seasonal temperature variations in Norway 1896-1997.* Klima 25/98. DNMI.

Hanssen-Bauer, I., Tveito, O.E., & Førland, E.J. 2000. *Temperature Scenarios for Norway.* KLIMA 24/00. DNMI, PO Box 43 Blindern, 0313 Oslo, Norway.

Heyen, H., Zorita, E., & von Storch, H. 1996. Statistical downscaling of monthly mean North Atlantic air-pressure to sea level anomalies in the Baltic Sea. *Tellus*, **48A**, 312–323.

Higuchi, K, Huang, J., & Shabbar, A. 1999. A wavelet characterization of the North Atlantic oscillation variation and its relationship to the North Atlantic sea surface temperature. *International Journal of Climatology*, **19**, 1119–1129.

Huth, R., & Kyselý, J. 2000. Constructing Site-Specific Climate Change Scenarios on a Monthly Scale. *Theor. Appl. Climatol.*

IPCC. 1995. *The Second Assessment Report.* Technical Summary. WMO & UNEP.

Johannessen, O.M., Shalina, E.V., & Miles, M.W. 1999. Satellite Evidence for an Arctic Sea Ice Cover in Transformation. *Science*, **286**(December), 1937–1939.

Kalnay, E., Kanamitsu, M., Kistler, R., Collins, W., Deaven, D., Gandin, L., Iredell, M., Saha, S., White, G., Wollen, J., Zhu, Y., Chelliah, M., Ebisuzaki, W., Higgins, W., Janowiak, J., Mo, K.C., Ropelewski, C., Wang, J., Leetmaa, A., Reynolds, R., Jenne, R., & Joseph, D. 1996. The NCEP/NCAR 40-Year Reanalysis Project. *Bull. Amer. Meteor. Soc.*, **77**(3), 437–471.

Kapala, A., Mächel, H., & Flohn, H. 1998. Behaviour of the centres of action above the Atlantic since 1881. Part II: Associateion with regional climate anomalies. *International Journal of Climatology*, **18**, 22–36.

Kidson, J.W., & Thompson, C.S. 1998. A Comparison of Statistical and Model-Based Downscaling Techniques for Estimating Local Climate Variations. *Journal of Climate*, **11**, 735–753.

Mächel, H., Kapala, A., & Flohn, H. 1998. Behaviour of the centres of action above the Atlantic since 1881. Part I: Charactersitics of seasonal and interannual variability. *International Journal of Climatology*, **18**, 1–22.

Machenhauer, B., Windelband, M., Botzet, M., Christensen, J.H., Déqué, M., Jones, R.G., Ruti, P.M., & Visconti, G. 1998. *Validation and Analysis of Regional Present-day Climate and Climate Change Simulations over Europe.* Tech. rept. 275. Max Planck-Institute für Meteorologie.

McFarlane, N.A., Boer, G.J., Blanchet, J.-P., & Lazare, M., J. 1992. *Climate.*

Meehl, G.A., Collins, W.D., Boville, B.A., Kiehl, J.T., Wigley, T.M.L., & Arblaster, J.M. 2000. Response of the NCAR Climate System Model to Increased CO_2 abd the Role of Physical Processes. *Journal of Climate*, **13**(June), 1879–1898.

Murphy, J. 1999. An Evaluation of Statistical and Dynamical Techniques for Downscaling Local Climate. *Journal of Climate*, **12**, 2256–2284.

Murphy, J. 2000. Predictions of climate change over Europe using statistical and dynamical downscaling techniques. *International Journal of Climatology*, **20**, 489–501.

North, G.R., Bell, T.L., & Cahalan, R.F. 1982. Sampling Errors in the Estimation of Empirical Orthogonal Functions. *Monthly Weather Review*, **110**, 699–706.

Oberhuber, J.M. 1993. Simulation of the Atlantic circulation with a coupled sea ice-mixed layer isopycnal general circulation model. Part 1: Model description. *Journal of Physical Oceanography*, **22**, 808–829.

Palmer, T.N., Branckovic, C., & Richardson, D.S. 1998. *A Probability and Decsision-Model Analysis of PROVOST Seasonal Multi-Model Ensemble Integrations.* Technical Memarandum 265. ECMWF, Reading, UK. Also submitted to Q.J.R.Met.Soc.

Press, W.H., Flannery, B.P., Teukolsky, S.A., & Vetterling, W.T. 1989. *Numerical Recipes in Pascal.* Cambridge University Press.

Roeckner, E., Arpe, K., Bengtsson, L., Dümenil, L., Esch, M., Kirk, E., Lunkeit, F., Ponater, M., Rockel, B., Sausen, B., Schlese, U., Schubert, S., & Windelband, M. 1992. *Simulation of present-day climate with the ECHAM model: impact of model physics and resolution.* Tech. rept. Max Planck-Institute für Meteorologie.

Roeckner, E., Arpe, K., Bengtsson, L., Christof, M., Claussen, M., Dümenil, L., Esch, M., Giorgetta, M., Schlese, U., & Schulzweida, U. 1996. *The atmospheric general circulation model ECHAM4: model description and simulation of present-day climate.* Tech. rept. 218. Max Planck-Institute für Meteorologie, Hamburg.

Roeckner, E., Bengtsson, L., Feichter, J., Lelieveld, J., & Rode, H. 1998. *Transient climate change simulations with a coupled atmosphere-ocean GCM including the tropospheric sulfur cycle.* Tech. rept. Max Planck-Institute für Meteorologie.

Rummukainen, M. 1997. *Methods for Statistical downscaling of GCM simulations.* SWECLIM 80. SMHI.

Schubert, S. 1998. Downscaling local extreme temperature change in south-eastern Australia from the CSIRO MARK2 GCM. *International Journal of Climatology*, **18**, 1419–1438.

Sengupta, S. K., & Boyle, J. S. 1993 (November). *Statistical Intercomparison of Global Climate Models: A Common Principal Component Approach.* Tech. rept. 13. PCMDI, Lawrence Livermore National Laboratory, California, USA, [http://www-pcmdi.llnl.gov/pcmdi/pubs/pdf/13.pdf].

S.Hankin, & Denham, M. 1994. *Ferret Users Guide.* NOAA/PMEL/TMAP.

Stephenson, D.B., Pavan, V, & Bojariu, R. 2000. Is the North Atlantic Oscillation a random walk? *International Journal of Climatology*, **20**, 1–18.

Thompson, W.J., & Wallace, J.W. 1998. ? *Geophys. Res. Lett.*, **25**, 1297–1300.

Tourre, Y.M., Rajagoplan, B., & Kushnir, Y. 1999. Dominant Patterns of Climate Variability in the Atlantic Ocean during the last 136 Years. *Journal of Climate*, **12**(August), 2285–2299.

Tziperman, E. 2000. Uncertainties in thermohaline circulation response to greenhouse warming. *Geophys. Res. Lett.*, **27**(19), 3077–3080.

Vinnikov, K.Y., Robock, A., Stouffer, R.J., Walsh, J.E., Parkinson, C.L., Cavalieri, D.J., Mitchell, J.F.B., Garrett, D., & Zakharov, V. F. 1999. Global Warming and Northern Hemisphere Sea Ice Extent. *Science.*

von Storch, H., Zorita, E., & Cubasch, U. 1993. Downscaling of Global Climate Change Estimates to Regional Scales: An Application to Iberian Rainfall in Wintertime. *Journal of Climate*, **6**, 1161–1171.

Wilks, D.S. 1995. *Statistical Methods in the Atmospheric Sciences.* Orlando, Florida, USA: Academic Press.

Zorita, E., & von Storch, H. 1999. The Analog Method as a Simple Statistical Downscaling Technique: Comparison with More Complicated Methods. *Journal of Climate*, **12**, 2474–2489.

Zorita, E., Hughes, J.P., Lettermaier, D.P., & von Storch, H. 1995. Stochastic Characterization of Regional Circulation Patterns for Climate Model Diagnosis and Estimation of Local Precipitation. *Journal of Climate*, **8**(May), 1023–1042.

Index

Symbols

500 hPa field 63
700 hPa field 63
700hPa geopotential height 91
850 hPa 61
850hPa temperature 65

A

AO 4
Arctic oscillation 4
Arctic warming 7
Arrhenius 1
atmospheric circulation 2

B

Barents Sea 12
Bergen 52, 53, 65, 85
bias warm 7
Bodø 52, 53, 84, 86

C

CCCma 11, 12, 73, 74, 84, 102–104
CCSR/NIES 11, 76, 84, 111
climate local 2
climate local types 2
climate maritime 2
climate regional 1
climatic outlook 7
common EOF method 24
common EOFs 3, 111
correlation maps 53
CSIRO 11, 12, 75, 84, 105

D

Dombås 22, 52, 86
downscaling geopotential heights 65
downscaling method comparison 24
downscaling methods 24
downscaling models 2
downscaling rainfall from SLP 86
downscaling sea level pressure 55, 82, 83, 86
downscaling skill scores 41
downscaling T(2m) 55, 82
downscaling thickness fields 65
dynamical downscaling 2

E

early 20th century warming 21
ECHAM GSDIO 16
ECHAM3 11, 77, 78, 85, 106
ECHAM4 11
ECHAM4 GSA 11, 12, 79, 85, 107
ECHAM4 GSDIO 14, 43, 48, 61, 63, 64, 89–91
ECHAM4GSA 79
ECMAH4 GSDIO 58
El Niño Southern Oscillation 1
empirical downscaling 2, 14
ensemble integration 84
ensemble prediction 3
ensemble scenarios 12
ENSO 1
EOF 14
EOF analysis 27
EOF calculation 27

F

f-statistics ANOVA 95
Ferder 52
flux adjustment 11
flux correction 11

G

geopotential height 35
geostrophic wind 111
GFDL 11, 80, 85, 108
global climate models 1
GSA 12

H

HadCM2 11, 12, 71, 83, 98–101
HadCM3 11, 14, 69, 70, 82, 96

I

interpolation simple 16
intertropical convergence zone 12
IPCC 1
ITCZ 12

K

Karasjok 52, 54, 82–84, 86
Kjøremsgrende 22

L

LSG 85

M
Max-Planck-Institute 2
Model results comparison with observations 4

N
NAO 1, 19, 86, 111
NCAR-CSM 11, 67, 68, 82, 97
NCAR-DOE 11, 12, 81, 82, 86, 111
NCEP reanalysis 4
Nesbyen 52, 83, 84
Nordal 90
North Atlantic Oscillation 1, 19
Norwegian Sea 84

O
Oksøy 52
Ona 52, 53, 65, 83, 85
Oslo 52, 55

P
p-value ANOVA 95
precipitation 41, 90
precipitation global scenarios 12
principal components 27
projection models 35, 55

R
RegClim PT1 54
Røros 52, 86

S
scenario uncertainty 3
sea level pressure warming 35
sea-ice 1
sensitivity studies 43
SLP 58
stratified models 24

T
testing empirical downscale models 34
thickness 500-700 hPa 64
trend uncertainties 48
trend uncertainty 54
Tromsø 52, 53, 84, 86

V
Vardø 52, 54, 84
variance 111
Verma 90
Værnes 52, 86

W
warming continents 12
warming polar regions 12